POWER GENERATION AND CONTROL OF MECHATRONICS SYSTEMS — THEORY AND TEST

A Thesis
Presented to
the Graduate School of
Clemson University

In Partial Fulfillment
of the Requirements for the Degree
Master of Science
Mechanical Engineering

by
Kelly R. Austin
May 2012

Accepted by:
Dr. John Wagner, Committee Chair
Dr. Ardalan Vahidi
Dr. Todd Schweisinger

UMI Number: 1512661

UMI 1512661

Copyright 2012 by ProQuest LLC.

ProQuest LLC.
789 East Eisenhower Parkway
P.O. Box 1346
Ann Arbor, MI 48106 - 1346

www.manaraa.com

Abstract

An integrated, multi-disciplined approach to engineering design is a broad definition of mechatronics. Though some mechatronics proponents differ in their definitions of the topic, an interdisciplinary approach to engineering is taken by many industries which should be reflected on campus in the approach to engineering education. In this thesis, two mechatronics systems are investigated. A laboratory experiment is developed for use in the mechanical engineering program at Clemson University, and thermoelectric power generation from diesel engine exhaust heat is investigated as an automotive industry application.

An electromagnet excited mass–pendulum system with attached spring and damper elements is introduced as an undergraduate/graduate laboratory experiment for engineering courses. This laboratory offers mechanical, electrical, and control engineering challenges to the students. The non-linear coupled equations of motion are derived using both Newtonian and Lagrangian approaches. The dynamic system is pendulum actuated by a 38W electromagnet for which the magnetic force is modeled by a magnetostatic forcing function. By accounting for the characteristics of a fluctuating magnetic field, the forcing function is useful in simulating the system response for the experimentally determined system parameters. Representative numerical and experimental results are presented which validate the mathematical model. Overall, the percent difference between the numerical and experimental results range from 2% to 47% for positions of the electromagnet within ±7.5cm of the system's equilibrium position. Further, the bench top experiment offers hands-on

opportunities for the students to explore science and classical engineering concepts.

In the transportation industry, the need to improve powertrain efficiency and provide additional power to the many amenities in today's vehicles has encouraged research on engine waste heat recovery. Approximately one-third of the gasoline or diesel fuel energy passes through the exhaust system. With ongoing development in materials and module design, thermoelectric generation, used since the 1960s for its reliable power output in space applications, has potential for use in bulk applications of engine heat recovery. In this study, the capability of generating usable power from thermoelectric generation from the exhaust heat of a 3-cylinder, 4-cycle, 697 cubic-centimeter diesel engine was investigated. It was found that the maximum surface temperature of the exhaust thermoelectric generation system was approximately 204°C. However, to ensure that the maximum temperature of the module's cold side was not exceeded, forced air was applied across the module's finned heat sinks. From laboratory testing, the maximum power outputs for a single module and four modules connected in series were 0.47W and 2.81W, with predicted maximum power outputs of 0.49W and 2.91W, respectively. Comparing the experimental values to numerically calculated values from the manufacturer's supplied data, it was observed that such calculations present an ideal outcome. The feasibility of the proposed alternative energy source merits further study and field testing but electric power can be generated in small quantities.

Dedication

This thesis is dedicated to my family for their ongoing encouragement and support.

Acknowledgments

The author would like to thank all the friends and colleagues who helped and encouraged me in the research and writing of this thesis. I am grateful to the Mechanical Engineering shop technicians Michael Justice, Jamie Cole, and Stephen Bass for all of their help in machining parts, setting up test systems, and assisting with equipment. Their help and advice were invaluable. I would also like to thank Mr. Dave Moline for his help and suggestions in setting up several of the electrical systems contained in my experimental systems. Also, thank you to the many classmates, coworkers, and friends who offered their insight on many subject areas and computer programs.

For my thesis committee members, Dr. Vahidi and Dr. Schweisinger, thank you for your role in evaluating my thesis work. I would especially like to thank my advisor Dr. Wagner for the many opportunities he has given me to obtain some valuable experience. I am very appreciative of his assistance and advice.

Table of Contents

List of Tables

List of Figures

Nomenclature

Chapter 2 Nomenclature

A	Cross sectional area magnetic flux lines pass through, m^2
A_C	Cross sectional area of magnet core, m^2
A_g	Air gap cross sectional area, neglecting fringing, m^2
A_{g_F}	Air gap cross sectional area, considering fringing, m^2
A_L	Load cross sectional area, m^2
b	Torsional damping from pendulum's rotary bearings, N·m·s
B	Magnetic flux density, T
D	Horizontal distance between M_2 and the electromagnet, m
c	Damping coefficient of M_1, N·s/m
$\vec{F}_b$	Friction force from torsional damping in pendulum, N
$\vec{F}_c$	Damping force acting on M_1, N
$\vec{F}_f$	Sliding friction force acting on M_1, N
$\vec{F}_k$	Spring force acting on M_1, N
$\vec{F}_N$	Normal force acting on M_1, N
$\vec{F}_T$	Tension, N
$\vec{F}_{M_1}$	Weight of M_1, N
$\vec{F}_{M_2}$	Weight of M_2, including pendulum rod, N
$\vec{F}_\theta$	Magnetic force vector applied to M_2, N
$f(x_g)$	magnetic force magnitude, neglecting fringing, N
$f_F(x_g)$	Magnetic force magnitude, considering fringing, N
$\mathcal{F}$	Magnetomotive force (mmf), A-turns
g	Gravity, m/s^2
i	Current through the electromagnet, A
k	Spring constant, N/m
L	Lagrangian function
l_C	Mean flux path through the electromagnet core, m
l_L	Mean flux path through the load (M_2), m
M_1	Mass of main mass, kg
M_2	Mass of pendulum, including pendulum rod, kg

N	Number of wire turns around the electromagnet core
Q_θ	Generalized force (torque) acting on M_2, N·m
R	Pendulum rod length, m
$\mathcal{R}_C$	Magnetic reluctance of the electromagnet core, A-turns/Wb
$\mathcal{R}_L$	Magnetic reluctance of the load (pendulum mass),A-turns/Wb
$\mathcal{R}_{x_g}$	Magnetic reluctance of air gap, A-turns/Wb
$\mathcal{R}(x_g)$	Function of total magnetic reluctance,A-turns/Wb
W	Total weight acting on M_1, N
x	Displacement of M_1 from equilibrium, m
x_g	Air gap length from electromagnet to M_2, m
x_m	Displacement of electromagnet from equilibrium, m
δ	Log decrement
μ	Magnetic permeability, H/m
μ_r	Relative permeability, dimensionless
μ_{r_C}	Relative permeability of electromagnet core
μ_{r_g}	Relative permeability of air gap
μ_{r_L}	Relative permeability of load (M_2)
μ_0	Absolute permeability, H/m
μ_k	Coefficient of sliding friction
ω_{d_P}	Damped natural frequency of M_2, rad/s
ω_{n_P}	Natural frequency of M_2, rad/s
ω_d	Damped natural frequency M_1, rad/s
ω_n	Natural frequency of M_1, rad/s
ϕ	Magnetic flux, Wb
ϕ_C	Magnetic flux in the electromagnet core, Wb
ψ	Angular displacement between M_2 and $\vec{f}(x_g)$, rad
τ_b	Torque from torsional damping in pendulum, N·m
θ	Angular displacement of M_2 from equilibrium, m
ζ	Damping ratio of M_1
ζ_p	Damping ratio of M_2

Chapter 3 Nomenclature

A	Cross sectional area of single element, m^2
A_c	Combustion cylinder surface area, m^2
c_v	Specific heat at constant volume, J/kg·K
h_c	Convective heat transfer coefficient, W/m^2·K
h_i	Enthalpy of combustion volume, J/kg
I	Current in TEG, A
I_{P_max}	Current at maximum power, A

J	Current density, $\frac{I}{A}$, in a TE element
K_C	Thermal conductance of a couple, W/K
K_M	Thermal conductance of TEM, W/K
l	Length of single element, mm
m_c	Mass of cylinder charge, kg
m_i	Mass flow in combustion volume, kg
n	Number of TE couples in a module
p	Pressure of combustion cylinder, N/m^2
P_O	TEM output power, W
$P_{\max}$	Maximum output power, W
q_{C_C}	Heat transfer rate out of a TE couple, W
q_{H_C}	Heat transfer rate into a TE couple, W
q_{C_E}	Heat transfer rate out of individual element, W
q_{H_E}	Heat transfer rate into individual element, W
q_C	Heat transfer rate out of TEM, W
q_H	Heat transfer rate into TEM, W
q_{in}	Heat transfer rate into element's cross sectional area, W
q_{out}	Heat transfer rate out of element's cross sectional area, W
Q_C	Heat transferred into combustion volume, J
Q_L	Heat transferred out of combustion volume, J
R	Universal gas constant, 8.315 kJ/kmol·K
R_C	Electrical Resistance of a couple, Ω
R_L	TEG resistive load, Ω
R_M	Electrical Resistance of TEM, Ω
R_{M_4}	Total Electrical Resistance of four modules connected in series, Ω
T	Temperature, °C
TE	Thermoelectric
TEM	Thermoelectric module
TEG	Thermoelectric Generator
TWHS	Thermoelectric Waste Heat System
T_C	Cold reservoir temperature, °C
T_H	Hot reservoir temperature, °C
T_{E_1}	Exhaust temperature 7.6cm after exhaust manifold, °C
T_{E_2}	Exhaust temperature 56.4cm after exhaust manifold, °C
T_{R_1}	Coolant temperature exiting engine, °C
T_{R_2}	Coolant temperature after exiting radiator, °C
T_∞	Ambient Temperature, °C
ΔT	Temperature gradient, $T_H - T_C$, °C
T_w	Combustion cylinder wall temperature, °C
U	Internal energy of combustion volume, J
v_0	Open circuit voltage of a single TEM, V
V_0	Open circuit voltage, V

$V_{P_{\max}}$	Voltage at maximum power, V
W	Work done by engine's combustion volume, J
x	Ratio of TWHS load resistance to TEM internal resistance
Z	Thermoelectric figure of merit, K^{-1}
ZT	Nondimensional figure of merit
α	Seebeck coefficient, V/K
$n\alpha$	Seebeck coefficient of a module of n couples, V/K
$n\alpha_4$	Seebeck coefficient for 4 modules in series, V/K
η_t	TEG thermal efficiency
$\eta_{t(P_{O\max})}$	TEG thermal efficiency at maximum output power
γ	Ratio of cross sectional area A to length l of TE element
λ	Thermal conductivity of TE material, W/m·K
ρ	Electrical resistivity of TE material, $\Omega \cdot$ m

xvi

Chapter 1

Introduction

A mechatronics system can be defined as the integration of mechanical, electrical, control, and information technologies into a smart product or process. However, a cursory overview of articles on the topic reveals a lack of consensus among professionals on the exact definition. A list published by Colorado State University provides over twenty definitions from a variety of publications and educational institutions [1]. Although many of the definitions specify mechatronics as the integration or fusion of core engineering disciplines throughout a system's entire design process, the varying emphasis on different disciplines reveals the lack of a unified structure in mechatronics education among universities.

Even without a universally accepted definition, the importance of mechatronics in education is evidenced by the number of papers, journals, and conferences dedicated to the topic. This growing interest in mechatronics also extends to industry where a competitive market, with the need for cost and time efficiencies, has driven many companies to develop an interdisciplinary approach to product development and manufacture [2].

1.1 Mechatronics Definition

The two questions that arise from the conglomeration of definitions are then, 'Is there a single definition of mechatronics?' and 'Should there be a single definition of mechatronics?' For the purpose of discussion, David Bradley from the University of Abertay Dundee (Dundee, Scotland) poses such questions in [3]. Bradley asks if a specific, encompassing definition of mechatronics is a source of confusion, and instead of attempting to conform to this definition, would it be better for mechatronics practitioners to form their own definitions according to the context of their work. Other mechatronics practitioners desire a specific definition and an overarching structure of mechatronics courses among universities. This is suggested in [4], where the author desires to restrict the definition of controls in mechatronics systems. Still other practitioners desire a common base for a mechatronics educational discipline without being bounded by a specific definition [5, 6].

1.1.1 Basic Definition

An overview of mechatronics technology presented in [6], from the creation of the term credited to Tetsuro Mori in 1969 to present, shows that mechatronics has evolved since its inception. Originally the term identified the integration of electrical and mechanical disciplines in a system, also referred to as an electro-mechanical system. Now mechatronics has been applied to areas such as automation and robotics, automotive systems, optoelectronics, industrial machinery, material handling technologies, composite materials, medical systems, and sensing and control systems [3, 6]. This list is not exhaustive and only serves to illustrate the difficulty in providing a single definition of a mechatronics system. However, for the purpose of clear communication, a usable definition is required.

The integration of mechanical, electrical, computer, and control engineering in the design and production of a product or process is a basic definition. A general mechatronics

2
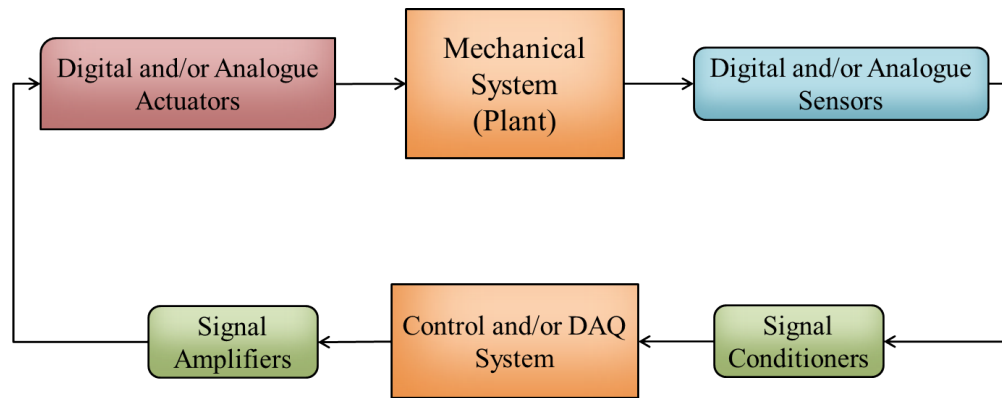
Figure 1.1: A typical mechatronics system integrates technology from mechanical, electrical, control, and computer engineering

system can be viewed in Fig. 1.1, in which the dynamics of a mechanical system or plant is monitored by a sensor or set of sensors. This may require signal conditioners to linearize, filter, or amplify the sensors' signals before sending the signals to a control and/or data acquisition (DAQ) system. The control system, generally containing a type of microcomputer, determines the desired output signals based on the input signals. With the use of a DAQ system, an associated computer program is used to collect and analyze sensor data and determine the output signal. After amplification, the output signal is sent to the actuator which alters the dynamics of the mechanical system by either electrical or mechanical means, and so continues the system's operation.

From Fig. 1.1, it can be clearly seen that designing a system with these components requires knowledge in all of the engineering fields listed in the basic definition. This definition goes beyond the sequential integration of the engineering disciplines to encompass the integration of the disciplines beginning at the design stage. For instance, consideration may be given to correct sensor operation and possible arrangements in the mechanical design to extend sensor life. Concurrent development of the control and mechanical components allows for changes in one component to be quickly adjusted for in the other component. Designing the system with knowledge of the necessary electrical components could en-

3

courage the creation of a compact, energy efficient application.

1.1.2 Mechatronics Design Philosophy

The basic definition of mechatronics has not limited its growth as some proponents consider mechatronics to be an interdisciplinary engineering philosophy which adjusts to the needs of technology [3, 7]. In [6], the author promotes mechatronics as a way for engineers to think about the design process that leads them to integrate disciplines necessary to most effectively solve the problem at hand.

The scope of mechatronics can be expanded to include disciplines outside of the core in the above definition [3, 6]. These may include integrating aspects of economics, manufacturing, and industrial design. Bradley warns in [3] that failure to see the importance of the overall system in the product's design, of which mechatronics design is a part, may result in the failure of the part and negative views of the mechatronics discipline.

1.2 Significance of Mechatronics Design Philosophy

Mechatronics systems are prevalent in society: in automotive systems as active suspension, braking control, adaptive cruise control, and engine management; in health care as operating room instrumentation, intelligent prostheses, and improved surgical aids; in home appliances as washing machines, coffee makers, and bread makers. Manufacturing and aerospace applications also feature many mechatronics systems. There is some debate on the difference between automated systems and mechatronics systems which depends mainly on the controller's complexity. Regardless of the debate, a system with the basic interaction shown in Fig. 1.1 is enhanced when an interdisciplinary approach is taken in its design and development. Because companies must remain competitive to economically survive, mechatronics may be important to their design approach, which reinforces the need

4

for entry level engineers trained in mechatronics at educational institutions.

1.2.1   Mechatronics Design Philosophy in Academics

The increase in industrial emphasis on interdisciplinary design and mechatronics systems has fostered an interest in mechatronics within the academic community. Many engineering programs offer a mechatronics course with a few schools offering degreed programs. Since mechatronics does not have a unique technology, the emphasis and structure between mechatronics programs can vary greatly depending on the arrangement of the program as independent, embedded, or cross discipline.

1.2.1.1   Mechatronics as An Independent Discipline

The lack of a set structure has prompted some mechatronics practitioners to propose objectives and suggestions for developing a basic course structure to promote mechatronics as a specific discipline [4, 6]. The core disciplines of mechanical, electrical, computer, and control engineering are given as the minimum requirement for a mechatronics course. Though some course content between the core disciplines would overlap, developing in-depth knowledge of the fundamental concepts while obtaining the necessary practical experience to integrate the content would require a considerable amount of time. The expected product of an independent mechatronics discipline would then be an engineer graduate with a broad foundation of the core fundamentals who is not specialized in any particular discipline. Consequently the student may need to receive depth in at least one core discipline to make the mechatronics engineer an asset [3].

5

1.2.1.2 Mechatronics as An Embedded Course

As an embedded (single department) course, mechatronics would be offered within an existing engineering department. In this arrangement, the focus of the course greatly depends on which department the mechatronics class is organized under. Control theory and robotics would likely receive more emphasis in an electrical and/or systems engineering department [2, 8], whereas sensor and actuator integration in a dynamic system would likely receive more emphasis in a mechanical engineering department.

The absence of an overarching structure for mechatronics and the fact that it is not industry specific allows engineering departments to define mechatronics in terms of their own discipline. This approach may reduce some confusion when trying to reconcile courses among different departments [3]. It is then the department's and the instructor's responsibility to ensure that the course is developed to offer the most benefit to students graduating from the given department. This approach ideally requires academia to be in close contact with local industries that hire their graduates to insure that students are equipped with the expected interdisciplinary skills and knowledge. A concern may be that an instructor holds to a restrictive definition of mechatronics, as in [4], and creates too narrow a course which hinders students by not giving them the knowledge breadth needed in multi-disciplined engineering.

1.2.1.3 Mechatronics as An Interdisciplinary Course

The most direct approach to properly prepare students for interdisciplinary engineering may be to offer interdisciplinary courses. This approach may include courses which combine students from different disciplines, courses taught by different departments, and/or courses which are team taught by various departments. With interdisciplinary courses, both departments and students can benefit from combined department re-

6

sources, department shared workload and course development, and increased collaboration and respect among disciplines [9]. Although this approach to interdisciplinary engineering requires significant cooperation and communication between the departments, it offers significant benefits to the students.

1.2.2 Mechatronics Design Philosophy in Mechanical Engineering

Mechanical engineering is perhaps the broadest engineering discipline. The diversity built into most mechanical engineering programs may be why some mechatronics proponents believe mechanical engineers should be the leaders in mechatronics design. [2].

1.2.2.1 Interdisciplinary Approach in Mechanical Engineering

An education in mechanical engineering is by nature a multi-disciplined effort. A concern in adding more diversity to an already broad program would be that an understanding of existing course content would be diminished. It can be argued that mechanical engineering, as it stands, is sufficiently distributed among core concepts and fundamentals that no mechanical engineer can be an expert in every mechanical engineering topic [10]. Adding more topics to this field may then be viewed to be a frustration to students and educators.

It can also be argued that the increased complexity of integrated systems leads to the natural division of system components among the integrated disciplines, since no individual can readily manage all aspects of complexity. This may seem to imply that interdisciplinary education is not necessary. However, it can also imply that individuals must be able to develop proficiency in the design of their specific component while understanding how all components are integrated to form the overall system [3]. An engineering education which offers a strong foundation in one discipline while introducing students to the application

7

and usefulness of other disciplines would appear to offer the best education to the student. This type of education may also help students develop respect for disciplines outside of their own and prepare them to enter an industry emphasizing an interdisciplinary approach to engineering.

An introduction to the other core disciplines is already included in most mechanical engineering degree programs which require students to take basic electrical engineering, control theory, and computer programming courses. In an interdisciplinary approach to mechanical engineering, students would then benefit from experience integrating these disciplines in a mechanical system.

1.2.2.2 Interdisciplinary Approach in Mechanical Systems

A practical means of gaining experience integrating disciplines in a mechanical system is through the development and use of an experimental system to verify a mathematical model or theoretical analysis. In developing an experimental system, the mechanical engineer should learn of the various sensors available for measuring a desired physical phenomenon. Integrating the sensors into the design of the physical plant requires knowledge of sensor operation and accompanying circuitry. Interpreting the sensor signal will likely require signal processing and knowledge of the electrical requirements and limitations of the DAQ system. Obtaining the desired system information may require the use of digital circuits or computer code. The engineer may need to have knowledge of the available controllers and the accompanying code or circuit design.

An experimental system, such as a mechatronics system, provides those students in mechanical engineering the opportunity to be introduced to multiple disciplines outside of mechanical engineering and see their usefulness in evaluating system behavior. Even when using a previously developed experimental system, evaluating the operation of the individual components and their integration into the overall system provides insight into

8

other disciplines as well as practical knowledge in mechanical engineering. This interdisciplinary approach to mechanical engineering can equip the engineer with useful skills in multiple disciplines as needed for mechatronics system design.

1.2.3 Mechatronics Design Philosophy in Industry

Many companies take an interdisciplinary approach to engineering design to reduce cost, while increasing the functionality of the part and decreasing the time it requires to bring the part to market [2].

1.2.3.1 Interdisciplinary Approach in Industry

By multiple disciplines working closely together, designs become more complex and design changes can be quickly implemented. The different subsystems can also be adjusted to account for design changes in another subsystem, such as altering the controller to account for any mechanical system changes that alter the weight or size of a part. The increased communication between the disciplines is also beneficial in generating product ideas or optimizing a product's size or performance [3].

An integrated approach to the design of new products is already the norm for many industries, such as the automotive industry [2]. Many of these industries have gone beyond the general scope of the core mechatronics disciplines to implement additional disciplines and processes in product design. This may include designing product tests, which are implemented during the design process, or product life cycle, which considers servicing, upgrading, and recycling the part [3, 6]. The collaboration of multiple disciplines is imperative for today's highly integrated designs.

9

1.2.3.2 Mechatronics Applications in Industry

The modern vehicle is the perfect example of a very complex mechatronics system requiring the collaboration of multiple disciplines to improve its operation. With an increased emphasis on vehicle amenities and driver assistance, the necessity of integrating the electrical, computer, and mechanical systems in the vehicle's design is readily apparent. With the increase in government policies reducing fuel consumption and exhaust emissions, the engineers have to consider other disciplines to meet regulations. The operation and the aesthetics of the designs also have to be considered concurrently. Incorporated into the entire design and production process are the business considerations of the company which keeps the company competitive.

To increase fuel economy, many automobile manufacturers are reducing vehicle weight by replacing previously used mechanically operated components with electrically operated components activated by an on-board controller. The replacement of mechanical processes with electrical subsystems can reduce the weight and size of the component, thereby decreasing the overall vehicle weight while offering popular electronic features, such as the shift-by-wire gear selector design described in [11]. This increased use of electrical systems and controllers in vehicles has increased the vehicle's electrical load demand. Providing additional electrical power to the vehicle while increasing the vehicle's fuel efficiency is a continual challenge in integrated vehicle design.

1.3 Research Objectives

Two different experimental systems, a mass-pendulum system and a thermoelectric generator for waste heat recovery in a diesel engine, were developed and are discussed in this thesis. Mathematical models for each system are proposed and verified using exper-

imental systems. These experimental systems incorporate sensor integration, calibration, data acquisition, and data analysis.

The mass-pendulum system was developed as a laboratory experiment for senior and graduate mechanical engineering students. The experimental system was created to offer a practical bench-top system for analyzing a classic coupled dynamics problem while providing hands on experience in the multiple disciplines inherent in an experimental system. The experimental plant is pendulum actuated by an electromagnet which is modeled and verified.

The thermoelectric generator was developed to test the efficiency of thermoelectric generator modules in producing power from the heat of diesel engine exhaust. The experiment is offered as an initial system design for waste heat recovery without adding additional demands or reducing the efficiency of the engine. Theoretical evaluations of thermoelectric power generation and diesel engine combustion analysis are discussed and compared to test data to evaluate the proposed electrical generation source.

1.4   Thesis Organization

This thesis is organized into four chapters with Appendices. Chapter 2 covers the theory and test of a mass-pendulum bench top experiment actuated by an electromagnet. Chapter 3 presents the theory and test of thermoelectric generation from the waste heat of a diesel engine. Chapter 4 contains concluding remarks and suggestions. The Matlab and Simulink files, AutoCAD part drawings, and additional figures and graphs for Chapter 2 and Chapter 3 are contained in the Appendices.

Chapter 2

An Electromagnet Excited Mass–Pendulum System Laboratory Experiment — Theory And Test

The mass–pendulum system with spring and damper elements is a classical coupled dynamics problem that may be posed to senior and graduate engineering students. The dynamics of the mass-pendulum system, somewhat similar to the suspension spring pendulum interfaces on tower clock mechanisms, offers the challenge of working with a coupled system subject to non-linear motion. The system shares some similarities with the underactuated cart driven inverted pendulum and pendulum driven cart mechanical systems with respective swing-up stabilizing and tracking problems [12, 13]. In each case, the challenge is controlling a system which is sensitive to disturbances.

Due to the inertial coupling of the masses, the mass–pendulum system also offers an optimization problem in vibration reduction. As a passive tuned mass damper, the pendulum was found to be useful in reducing steady state and low seismic motion [14]. The pendulum has also been researched as an active mass damper against wind and low seismic

12

motion [15]. Both of these have the challenge of working with a system that is subject to non-linear and chaotic motion depending on system damping and forcing frequency [16].

This laboratory experiment incorporates fundamental engineering concepts while working with a physical system to verify a nonlinear dynamic model. In this experiment, students mathematically model the system by either a direct application of Newton's second law or by use of Lagrange's equations. The model is then verified by numerical simulation of the free response of the coupled system which requires analyzing the motions of the individual as well as the coupled masses to determine the system parameter values. Calculating the system parameters from the physical system incorporates sensor integration and calibration, data acquisition, signal processing, and data analysis.

The actuator used in the physical laboratory system is a powerful electromagnet which must be incorporated into the physical system to drive the pendulum based on the real time motion of the coupled system. By mathematically modeling the magnitude of the electromagnet's magnetic force, the forced response of the mass-pendulum mathematical model can be simulated and compared to the forced response of the physical system. With the physical system and validated model, the linear and nonlinear motion of the coupled system can be experimentally and analytically evaluated to control the system response.

Understanding the behavior of the coupled system is necessary for minimizing oscillations and/or controlling the mass–pendulum system to meet prescribed motion. This system is a simplified model in which the point of rotation of a mass is not stationary, but actually has some flexibility or horizontal displacement.

2.1 Mathematical Models

The coupled mass–pendulum experimental system can be represented by the diagram shown in Fig. **??** where the origin is at point O. The mass M_1 provides a sturdy

13

support assembly for the pendulum of mass M_2. Attached to M_1 is a compression spring with stiffness k. The linear damping coefficient c lumps the damping from the translational spring and the linear bearings acting on M_1. The torsional damping coefficient b results from two rotary bearings that attach the pendulum rod of length R to M_1. The motion of the masses is defined by the horizontal displacement x and the angular displacement θ in terms of the unit vectors $\hat{i}$, $\hat{j}$ and $\hat{k}$, with $\hat{k}$ directed out of the page. The two dimensional motion of the system is confined to the $\hat{i}$-$\hat{j}$ plane.
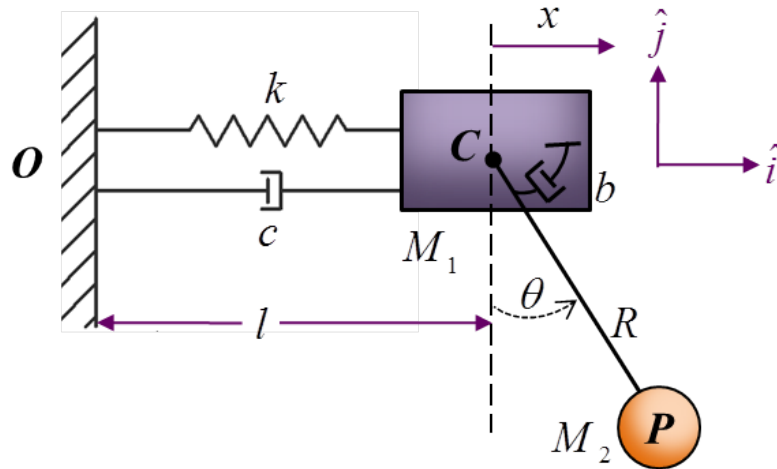
Figure 2.1: A mass-pendulum system model with spring and damper elements

To simplify the model, M_1 and M_2 are treated as point masses, at points C and P respectively. The air resistance acting on the masses is neglected. The spring and rod are considered to be massless. In this arrangement, when the spring is un-stretched ($x = 0$) M_1 is at equilibrium. In its equilibrium position where $\theta = 0$, the pendulum is hanging straight down.

2.1.1 Direct Method

A direct application of Newton's second law requires defining the accelerations of both masses and identifying the forces associated with their motion.

14

2.1.1.1 Kinematics of Masses M_1 and M_2

The kinematic equations of M_1 are

$$\vec{r}_c = x\hat{i} \tag{2.1}$$

$$\vec{v}_c = \dot{\vec{r}}_c = \dot{x}\hat{i} \tag{2.2}$$

$$\vec{a}_c = \dot{\vec{v}}_c = \ddot{\vec{r}}_c = \ddot{x}\hat{i} \tag{2.3}$$

where position $\vec{r}_c$, velocity $\vec{v}_c$, and acceleration $\vec{a}_c$ describe the motion of the mass which is constrained to move horizontally. The actual position of C is $\vec{r}_c = (l+x)\hat{i}$ where l is the distance from the origin to C when M_1 is in its equilibrium position. This constant does not appear in the derivatives and therefore is left out of the position vectors.

The kinematic equations of M_2, which has combined rotational and translational motion, are

$$\vec{r}_p = x\hat{i} + R\sin\theta\hat{i} - R\cos\theta\hat{j} \tag{2.4}$$

$$\vec{v}_p = \dot{\vec{r}}_p = \dot{x}\hat{i} + R\dot{\theta}\cos\theta\hat{i} + R\dot{\theta}\sin\theta\hat{j} \tag{2.5}$$

$$\vec{a}_p = \dot{\vec{v}}_p = \ddot{\vec{r}}_p = \ddot{x}\hat{i} + R\left(\ddot{\theta}\cos\theta - \dot{\theta}^2\sin\theta\right)\hat{i} + R\left(\ddot{\theta}\sin\theta + \dot{\theta}^2\cos\theta\right)\hat{j}. \tag{2.6}$$

2.1.1.2 System Forces

To apply Newton's law to the masses, the system forces must be written as vectors. As the pendulum swings, torsional damping acts on the pendulum. It is assumed that the torsional damping torque is caused by a linear rotary bearing friction force $\vec{F}_b$ which must be derived.

15

Rotary Bearing Friction   The two rotary bearings were modeled as a single torsional damper with dissipative torque $\vec{\tau}_b = b\dot{\theta}\hat{k}$ [17]. The vector representation of the torque is shown in Fig. 2.2(a). The direction of the force vectors were chosen so that a negative torque caused the magnitude of θ to decrease. The derived force $\vec{F}_b$ acting on M_2 can be found by equating the expression $\vec{\tau}_b = \vec{R} \times \vec{F}_b = RF_b\hat{k}$ to the dissipative damping acting on M_2, $\vec{\tau}_b = -b\dot{\theta}\hat{k}$, so that $F_b = -\frac{b}{R}\dot{\theta}$.
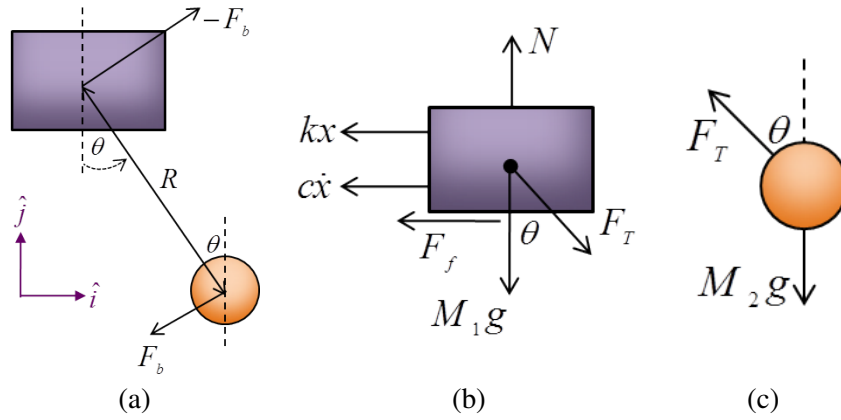
Figure 2.2: Mass-pendulum system with (a) torsional damping τ_b from friction force $\vec{F}_b$ and remaining forces acting on (b) M_1, and (c) M_2

Forces Acting on M_1 and M_2   The free body diagram (FBD) of M_1 is shown in Fig. 2.2(b). The total forces F_{M_1} acting on M_1 are the normal force N, sliding friction F_f, weight, spring force, damping force, tension T, and rotary bearing friction so that

$$\sum \vec{F}_{M_1} = \vec{F}_N + \vec{F}_f + \vec{F}_{M_1} + \vec{F}_k + \vec{F}_c + \vec{F}_T + \vec{F}_b. \tag{2.7}$$

It is assumed that the sliding friction acting on M_1 is negligible. The FBD of M_2 is shown in Fig. 2.2(c). The total forces F_{M_2} acting on M_2 are tension, weight, and rotary bearing friction such that

$$\sum \vec{F}_{M_2} = \vec{F}_T + \vec{F}_{M_2} + \vec{F}_b. \tag{2.8}$$

16

The force vectors listed in Table 2.1 have been resolved into $\hat{i}$ and $\hat{j}$ components. Checking the signs of $\vec{F}_b$ given in Table 2.1, the friction in the rotary bearings opposes the motion of M_2, while its reaction force acts on M_1.

Table 2.1: Force Vectors in Coupled System

	Forces on M_1		Forces on M_2
$\vec{F}_N$	$N\hat{j}$	$\vec{F}_T$	$T\left(-\sin\theta\hat{i} + \cos\theta\hat{j}\right)$
$\vec{F}_{M_1}$	$-M_1 g\hat{j}$	$\vec{F}_{M_2}$	$-M_2 g\hat{j}$
$\vec{F}_k$	$-kx\hat{i}$	$\vec{F}_b$	$-\frac{b}{R}\dot{\theta}\left(\cos\theta\hat{i} + \sin\theta\hat{j}\right)$
$\vec{F}_c$	$-c\dot{x}\hat{i}$		
$\vec{F}_T$	$T\left(\sin\theta\hat{i} - \cos\theta\hat{j}\right)$		
$\vec{F}_b$	$\frac{b}{R}\dot{\theta}\left(\cos\theta\hat{i} + \sin\theta\hat{j}\right)$		

2.1.1.3 Equations of Motion

Applying Newton's second law of motion to M_1 and M_2 for the external forces given in Table 2.1 and the accelerations from Eq. (2.3) and Eq. (2.6) gives the equations

$$N\hat{j} - M_1 g\hat{j} - kx\hat{i} - c\dot{x}\hat{i} + T\left(\sin\theta\hat{i} - \cos\theta\hat{j}\right) + \frac{b}{R}\dot{\theta}\left(\cos\theta\hat{i} + \sin\theta\hat{j}\right) = M_1\ddot{x}\hat{i} \quad (2.9)$$

and

$$-M_2 g\hat{j} + T\left(-\sin\theta\hat{i} + \cos\theta\hat{j}\right) - \frac{b}{R}\dot{\theta}\left(\cos\theta\hat{i} + \sin\theta\hat{j}\right)$$
$$= M_2\left(\ddot{x}\hat{i} + R\left(\ddot{\theta}\cos\theta - \dot{\theta}^2\sin\theta\right)\hat{i} + R\left(\ddot{\theta}\sin\theta + \dot{\theta}^2\cos\theta\right)\hat{j}\right). \quad (2.10)$$

17

Considering the $\hat{i}$ and $\hat{j}$ components of these two equations provides the four simultaneous equations

$$-kx - c\dot{x} + T\sin\theta + \frac{b}{R}\dot{\theta}\cos\theta = M_1\ddot{x} \tag{2.11}$$

$$N - M_1g - T\cos\theta + \frac{b}{R}\dot{\theta}\sin\theta = 0 \tag{2.12}$$

$$-T\sin\theta - \frac{b}{R}\dot{\theta}\cos\theta = M_2\ddot{x} + M_2R\ddot{\theta}\cos\theta - M_2R\dot{\theta}^2\sin\theta \tag{2.13}$$

$$-M_2g + T\cos\theta - \frac{b}{R}\dot{\theta}\sin\theta = M_2R\ddot{\theta}\sin\theta + M_2R\dot{\theta}^2\cos\theta \tag{2.14}$$

of which Eq. (2.11), Eq. (2.13), and Eq. (2.14) are used to find the EOM for M_1 and M_2. Solving Eq. (2.13) for $T\sin\theta$ and substituting the result into Eq. (2.11) yields the M_1 dynamics

$$(M_1 + M_2)\ddot{x} = M_2R\dot{\theta}^2\sin\theta - M_2R\ddot{\theta}\cos\theta - c\dot{x} - kx. \tag{2.15}$$

Multiplying Eq. (2.13) and Eq. (2.14) by $\cos\theta$ and $\sin\theta$, respectively, and adding the results gives the EOM for M_2,

$$M_2R\ddot{\theta} = -M_2\ddot{x}\cos\theta - \frac{b}{R}\dot{\theta} - M_2g\sin\theta. \tag{2.16}$$

2.1.2 Lagrangian Method

Deriving the equations of motion by Lagrange's method requires finding the Lagrangian function L, which is a function of the system's total kinetic energy T and potential energy V, the energy dissipated due to damping, and any nonconservative forces acting on the system.

2.1.2.1   Lagrangian Function

The motion of each mass can be described in an inertial frame which has an origin at O. In the inertial frame, the position and velocity vectors from O are the same as those given in Eq. (2.1) and Eq. (2.2) for M_1 and Eq. (2.4) and Eq. (2.5) for M_2. The total kinetic energy of the system, which is the sum of the kinetic energies of M_1 and M_2, is found by the expression $T = \frac{1}{2} M_1 \left(\vec{v}_c\right)^2 + \frac{1}{2} M_2 \left(\vec{v}_p\right)^2$. After substituting Eq. (2.2) and Eq. (2.5), and squaring the velocity vectors, the kinetic energy is

$$T = \frac{1}{2} M_1 \dot{x}^2 + \frac{1}{2} M_2 \left(\dot{x}^2 + 2R\dot{x}\dot{\theta}\cos\theta + R^2\dot{\theta}^2 \right). \tag{2.17}$$

The sum of the potential energies due to the position of the spring and the position of M_2 gives the total potential energy in the system,

$$V = \frac{1}{2}kx^2 - M_2 gR\cos\theta. \tag{2.18}$$

Subtracting Eq. (2.18) from Eq. (2.17) gives the Lagrangian function

$$\begin{aligned} L = T - V = \frac{1}{2} M_1 \dot{x}^2 + \frac{1}{2} M_2 \dot{x}^2 + M_2 R\dot{x}\dot{\theta}\cos\theta + \\ \frac{1}{2} M_2 R^2 \dot{\theta}^2 - \frac{1}{2}kx^2 + M_2 Rg\cos\theta. \end{aligned} \tag{2.19}$$

2.1.2.2   Lagrange's Equations

The equation describing the motion of a generalized coordinate q_i is determined by evaluating Lagrange's equation

$$\frac{d}{dt}\left(\frac{\partial L}{\partial \dot{q}_i}\right) - \frac{\partial L}{\partial q_i} + \frac{\partial D}{\partial \dot{q}_i} = Q_i \quad (i = 1, 2, \cdots) \tag{2.20}$$

19

where the Lagrangian L is given in Eq. (2.19), the energy dissipated due to damping is given for the damping coefficient c_i at velocity $\dot{q}_i$ by Rayleigh's dissipation function $D = \frac{1}{2}c_i\dot{q}_i^2$, and the generalized force Q_i encompasses the applied force and any non conservative force such as sliding friction [18].

The EOM for M_1 is found by evaluating Eq. (2.20) for the coordinate $q_1 = x$, where the partial derivatives of Eq. (2.19) are taken with respect to $\dot{x}$ and x, and Rayleigh's dissipation function for the damping of x is $D = \frac{1}{2}c\dot{x}^2$. This gives the M_1 dynamics

$$(M_1 + M_2)\ddot{x} - M_2 R\dot{\theta}^2 \sin\theta + M_2 R\ddot{\theta}\cos\theta + c\dot{x} + kx = 0. \tag{2.21}$$

Evaluating Eq. (2.20) for the coordinate $q_2 = \theta$ gives the dynamics for M_2. For this, the partial derivatives in Eq. (2.19) are taken with respect to $\dot{\theta}$ and θ, and $D = \frac{1}{2}b\dot{\theta}^2$ is Rayleigh's dissipation function for the damping in θ. The EOM for M_2 is then

$$M_2 R\ddot{x}\cos\theta - M_2 R\dot{x}\dot{\theta}\sin\theta + M_2 R^2\ddot{\theta} + M_2 R\dot{x}\dot{\theta}\sin\theta + b\dot{\theta} + M_2 gR\sin\theta = 0, \tag{2.22}$$

which simplifies to give

$$M_2 R^2\ddot{\theta} + M_2 R\ddot{x}\cos\theta + b\dot{\theta} + M_2 gR\sin\theta = 0. \tag{2.23}$$

The EOM for M_1 and M_2 found from Lagrange's method are the same as those given in Eq. (2.15) and Eq. (2.16), which can be solved for $\ddot{x}$ and $\ddot{\theta}$ respectively to give the EOM for the mass-pendulum system [14, 19]

$$\ddot{x} = \frac{1}{M_1 + M_2} \left(M_2 R \dot{\theta}^2 \sin\theta - M_2 R \ddot{\theta} \cos\theta - c\dot{x} - kx \right) \qquad (2.24)$$

$$\ddot{\theta} = \frac{1}{M_2 R} \left(-M_2 \ddot{x} \cos\theta - M_2 g \sin\theta - \frac{b}{R} \dot{\theta} \right). \qquad (2.25)$$

2.1.3   Model of Magnetic Force

The magnetic effect of the electromagnet is conveniently characterized in terms of magnetic flux density $\vec{B}$, measured in webers per square meter (Wb/m^2) or teslas (T) in SI units. Integrating the flux density over the surface area the flux lines pass through gives the magnetic flux ϕ. The vector field properties of the electromagnet can be treated as scalars by viewing the electromagnet and the attracted load, M_2, as a "magnetic circuit" analogous to a resistive electric circuit [20]. The parallel magnetic and electric properties used to model the magnetic force acting on M_2 are given in Table 2.2. Relating the magnetic and the electric properties in this way requires several assumptions and simplifications.

It is assumed that the electromagnet is in an electrostatic state powered by the direct current i, and the N coil turns on the tightly wound electromagnet core are linked by the generated magnetic field lines. In effect, this increases the current N times, as stated by the magnetomotive force (mmf) of the electromagnet $\mathcal{F} = Ni$. The magnetic flux ϕ produced by the mmf is assumed to follow a mean closed path of length l through each material comprising the magnetic circuit and be entirely confined in the circuit. It is also assumed that the flux density is constant over the cross sectional area A of each material.

The reluctance $\mathcal{R}$ is a material property defined as l through the material divided by the product of the material's permeability μ and cross sectional area, $\mathcal{R} = l/(\mu A)$. The μ of the material can be factored into the permeability of free space μ_0 and the material's dimensionless relative permeability μ_r. For a magnetostatic measurement, μ is also referred

21

Table 2.2: Analogy Between Electric and Magnetic Circuits

	Electric Property	Symbol	Units
1)	Voltage	V	V
2)	Current	i	A
3)	Current density	J	A/m^2
4)	Resistance	R	Ω
5)	Conductivity	Σ	$1/(\Omega \cdot \text{m})$
	Magnetic Property	**Symbol**	**Units**
1)	Magnetomotive force	$\mathcal{F}$	A-turns
2)	Magnetic flux	ϕ	Wb
3)	Magnetic flux density	B	Wb/m^2 or T
4)	Reluctance	$\mathcal{R}$	A-turns/Wb
5)	Permeability	μ	H/m

to as the absolute permeability or DC permeability. While μ_0 is a magnetic constant, the relative permeability of a ferromagnetic material depends on the degree to which the material is magnetized [21]. By the analogy in Table 2.2 and the definition of $\mathcal{R}$, the mmf can be written as

$$\mathcal{F} = Ni = \phi\mathcal{R} = \phi\frac{l}{\mu A} = \phi\frac{l}{\mu_0\mu_r A}. \tag{2.26}$$

For this approximation of the magnetic force, the magnetic circuit includes a solid core electromagnet and movable load M_2 separated on both sides by equal sized air gaps. In the magnetic circuit shown in Fig. 2.3, the mean path of the flux is considered to be through the core, a length of l_C, across the air gap, a length of x_g, through the load, a length of l_L, and back across the air gap to the core. The total reluctance is a function of x_g, which
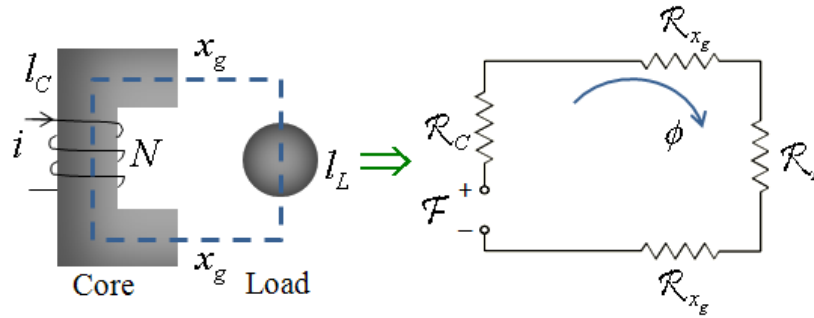
Figure 2.3: The electromagnet's magnetic force, following a mean flux path (- - -) through the attracted load, is approximated as a magnetic circuit, analogous to a resistive series circuit

varies as the load moves, and is found by adding the reluctance of each section to give

$$\mathcal{R}(x_g) = \frac{l_C}{\mu_0 \mu_{r_C} A_C} + 2\frac{x_g}{\mu_0 \mu_{r_g} A_g} + \frac{l_L}{\mu_0 \mu_{r_L} A_L} \tag{2.27}$$

where μ_{r_C}, μ_{r_g}, and μ_{r_L} are the relative permeabilities of the core, the air gap, and the load respectively, and A_C, A_g, and A_L are the cross sectional areas of the core, the air gap, and the load, respectively.

The magnetic force f acting on M_2 can be approximated by considering the work done by the current in the coil and the work required to move M_2 from a position x_g meters away. The derived forcing function is $|f(x_g)| = -\frac{1}{2}\phi^2 \frac{d\mathcal{R}(x_g)}{dx_g}$ [20]. The derivative of the reluctance in Eq. (2.27) with respect to x_g is $\frac{d\mathcal{R}(x_g)}{dx_g} = \frac{2}{\mu_0 \mu_{r_g} A_g}$, and the flux from Eq. (2.26) is $\phi = \frac{Ni}{\mathcal{R}(x_g)}$. The magnetic force, in Newtons, is calculated from the function

$$|f(x_g)| = -\frac{(Ni)^2}{\mathcal{R}^2(x_g)\mu_0 \mu_{r_g} A_g} \tag{2.28}$$

where $\mathcal{R}(x_g)$ is calculated from Eq. (2.27) for x_g in meters. This forcing function assumes that no fringing of the magnetic flux lines occurs in the air gap, in which the flux lines leaving the core bow out and then come back into the load. Fringing can be accounted for

23

by considering that fringing increases the cross sectional area of the air gap with respect to the distance between the electromagnet and the load. The air gap cross sectional area considering fringing A_{g_F} was assumed to be a function of x_g, where $A_{g_F}(x_g) = (\sqrt{A_g} + x_g)^2$ and A_g is the air gap cross sectional area neglecting fringing. Considering this term in Eq. (2.27) and the derivative of this expression with respect to x_g, gives the magnetic force function $|f_F(x_g)|$, which approximates for the fringing of the magnetic flux lines in the air gap, as

$$|f_F(x_g)| = \frac{-(Ni)^2 \left(x_g - A_g^{\frac{1}{2}}\right) \left(x_g + A_g^{\frac{1}{2}}\right)^{-3}}{\left(\frac{\frac{2x_g}{\sqrt{\mu_0}}}{\left(x_g + A_g^{\frac{1}{2}}\right)^2} + \frac{l_C \mu_{r_L} A_L + l_L \mu_{r_C} A_C}{\sqrt{\mu_0} \mu_{r_C} A_C A_L}\right)^2}. \tag{2.29}$$
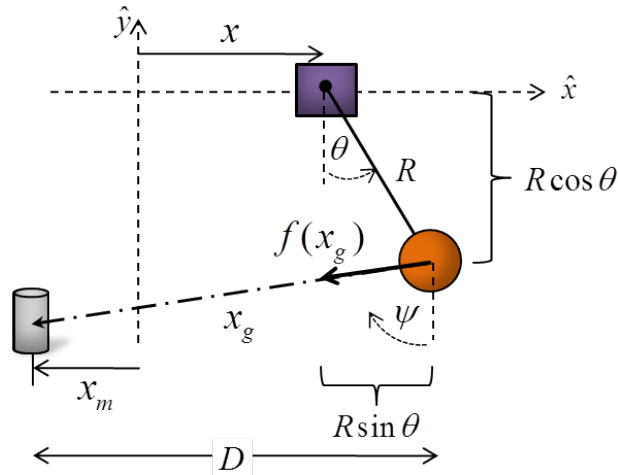
Figure 2.4: The magnetic force $f(x_g)$ of the electromagnet, positioned $\pm x_m$ from the equilibrium, acts at angle ψ on the pendulum mass located at a horizontal distance D over the air gap displacement x_g

The displacement x_g of M_2 from the electromagnet and the approximated magnetic force $f(x_g)$ are illustrated in Fig. 2.4, where the equilibrium position of the system is at the $\hat{x}, \hat{y}$ axes, and the electromagnet is positioned $\pm x_m$ with respect to the $\hat{y}$-axis. The positive or negative horizontal distance D of M_2 from the electromagnet is found by $D =$

$x + R\sin\theta - x_m$, where the sign of D indicates to which side of the electromagnet M_2 is. From Fig. 2.4, the magnitude of the displacement x_g is calculated by

$$|x_g| = \sqrt{(x + R\sin\theta - x_m)^2 + (R - R\cos\theta)^2}. \tag{2.30}$$

For small angle motion, x_g and D have approximately the same magnitude.

The magnetic force produces a torque on the pendulum. This torque is represented as a generalized force in Eq. (2.20) for the coordinate θ as $Q_\theta = \vec{F}_\theta \cdot \frac{\partial \vec{r}_\theta}{\partial \theta}$, where $\vec{r}_\theta$ is given in Eq. (2.4). The magnetic force vector applied to M_2 at an angle ψ from the vertical is $\vec{F}_\theta = -f(x_g)\sin\psi\hat{i} - f(x_g)\cos\psi\hat{j}$. The dot product of the force vector and the partial derivative of Eq. (2.4) with respect to θ gives the generalized force acting on M_2 as

$$\begin{aligned} Q_\theta &= \vec{F}_\theta \cdot \left(R\cos\theta\hat{i} + R\sin\theta\hat{j} \right) \\ &= -f(x_g)R\sin(\theta + \psi), \end{aligned} \tag{2.31}$$

where $\psi = \tan^{-1}\left(\frac{D}{R - R\cos\theta} \right)$.

2.2 Analysis of System Parameters

By decoupling the motions of M_1 and M_2, the system constants can be analytically and experimentally estimated. The log decrement method was used to estimate the damping ratios of M_1 and M_2, which are assumed to be underdamped. The remaining parameters can then be calculated from the variable definitions.

25

2.2.1 Model of Uncoupled M_1

Uncoupled from the pendulum, the main mass M_1 and its attached spring form a mass–spring–damper system which has the EOM

$$M_1\ddot{x} + c\dot{x} + kx = 0, \tag{2.32}$$

also written as

$$\ddot{x} + 2\zeta\omega_n\dot{x} + \omega_n^2 x = 0 \tag{2.33}$$

by defining the undamped natural frequency ω_n and the damping ratio ζ of M_1 as $\omega_n = \sqrt{\frac{k}{M_1}}$ and $\zeta = \frac{c}{2M_1\omega_n} = \frac{c}{2\sqrt{M_1 k}}$, respectively. The general solution for the underdamped motion of M_1 is

$$x(t) = Ae^{-\zeta\omega_n t}\sin\left(\omega_n\sqrt{1 - \zeta^2}\, t + \beta\right), \tag{2.34}$$

with damped natural frequency $\omega_d = \omega_n\sqrt{1 - \zeta^2}$ [22].

2.2.2 Model of Uncoupled M_2

The uncoupled M_2 is acted on by the moments M from the weight, $M_2 gR\sin\theta$, and the torsional damping, $b\dot{\theta}$, shown in Fig. 2.5. Newton's second law $I\ddot{\theta} = \sum M$ gives the EOM of M_2, with moment of inertia $I = M_2 R^2$, as

$$M_2 R^2\ddot{\theta} = -b\dot{\theta} - M_2 gR\sin\theta. \tag{2.35}$$

Assuming small angle motion, this equation can be linearized by setting $\sin\theta \approx \theta$. Defining an underdamped natural frequency ω_{n_p} and damping ratio ζ_p for M_2, the dynamics can be rewritten as

$$\ddot{\theta} + 2\zeta_p\omega_{n_p}\dot{\theta} + \omega_{n_p}^2\theta = 0, \tag{2.36}$$

26
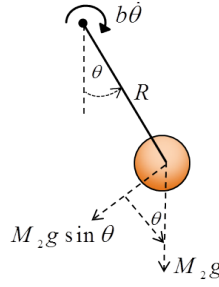
Figure 2.5: Forces acting on uncoupled M_2 include weight and torsional damping $b\dot{\theta}$ due to rotary bearing friction

where $\omega_{n_p} = \sqrt{\frac{g}{R}}$ and $\zeta_p = \frac{b/(2M_2 R^2)}{\sqrt{g/R}}$ [23]. Relating Eq. (2.36) to Eq. (2.33), the general solution becomes [22]

$$\theta(t) = B e^{\zeta_p \omega_{n_p} t} \sin\left(\omega_{n_p} \sqrt{1 - \zeta_p^2}\, t + \beta_p\right). \tag{2.37}$$

The torsional damping in the pivot point at C causes M_2 to oscillate at a damped natural frequency $\omega_{d_p} = \omega_{n_p} \sqrt{1 - \zeta_p^2}$.

2.2.3 Logarithmic Decrement Method

For the free response of underdamped M_1 described by Eq. (2.34), the logarithmic decrement δ is defined as the natural logarithm of the ratio of successive amplitudes separated by period P, $\delta = \ln \frac{x(t)}{x(t+P)}$. Since the experimental data of $x(t)$ will contain some noise or measurement error, δ can be modified to account for this by using two amplitudes separated by n periods [17],

$$\delta = \frac{1}{n} \ln \frac{x(t)}{x(t + nP)}. \tag{2.38}$$

Using Eq. (2.34), this equation can be simplified to $\delta = \zeta \omega_n P$, where $P = \frac{2\pi}{\omega_d} = \frac{2\pi \zeta}{\omega_n \sqrt{1-\zeta^2}}$

27

so that

$$\zeta = \frac{\delta}{\sqrt{4\pi^2 + \delta^2}}. \tag{2.39}$$

The value of ω_d, estimated from P, and the value of ζ can be used to calculate the remaining system variables. The values for k and the mass of M_1 can also be determined from static tests. The equations, given here in terms of M_1 motion, can be applied directly to the motion of M_2. The damping coefficient b can then be calculated from the estimated value of ζ_p.

2.3 Experimental System

The bench top laboratory experiment shown in Fig. 2.6 was designed to encourage student interactions with the physical system.

2.3.1 Characteristics of Physical Structure

Mass M_1, made of an aluminum alloy, is equipped with six linear bearings to allow the mass to slide with low friction on three parallel shafts. A compression spring is connected to M_1 over the middle shaft to prevent possible buckling in the spring when it is compressed. The other end of the spring is connected to a beam load cell by means of a connection assembly which is constrained to move horizontally on the middle shaft. The connection assembly and attached sensor are shown in Fig. 2.7(a). The attachments of this sensor to the stationary support and the connection block were designed to provide the mounting arrangement designated by the sensor manufacturers to create the double bend in the beam load cell necessary for accurate sensor performance [24].

A bracket attached to the base of M_1 supports a 6.35mm diameter shaft which sup-

28
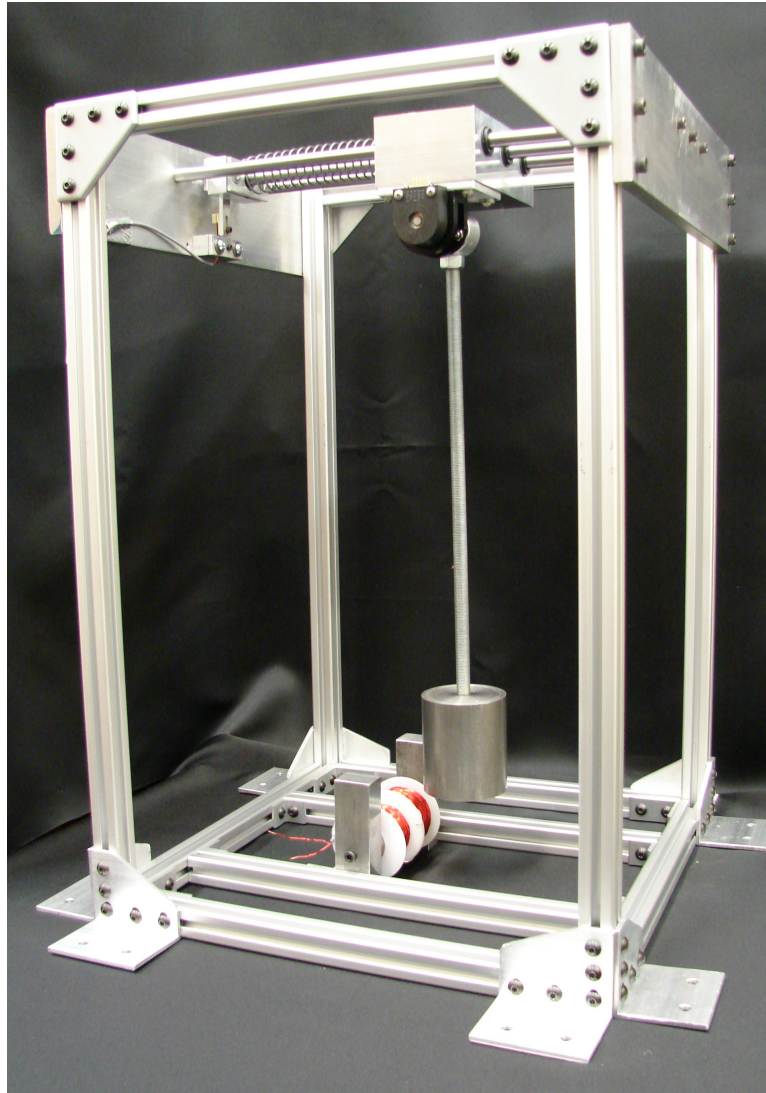
Figure 2.6: Mass-pendulum system with integrated sensors and electromagnet

ports the pendulum. The pendulum rod is attached to the shaft by a threaded collar. When the pendulum swings, the entire shaft rotates which rotates an optical encoder attached to the end of the shaft. The pendulum attachment can be seen in Fig. 2.7(b) with the encoder housing attached to the outside of the bracket. The pendulum bob is made of 1018 low carbon steel and is threaded to attach to the threaded pendulum rod. Additional weights may be added along the pendulum rod to alter the weight and inertia of the pendulum.

29
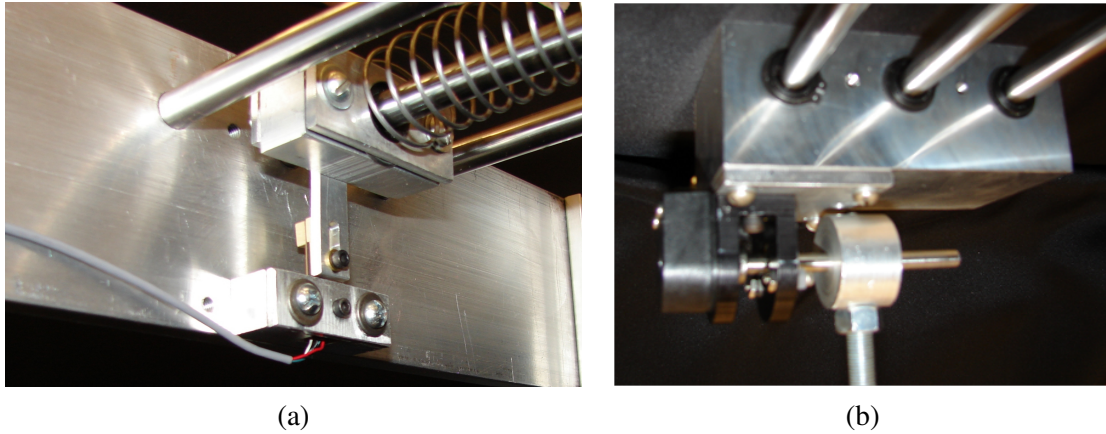
Figure 2.7: In the physical system, the location of M_1 and M_2 are measured by (a) a beam load cell, mounted to move horizontally with M_1 and (b) an optical encoder, mounted to the base of M_1 and moving radially with M_2

The structure of the experimental system is made of 20mm extruded aluminum and is designed to remain stationary on a level counter top under the expected motion of M_1 and M_2. The pendulum length is determined so that M_2 may swing between the poles of the U-shaped electromagnet which is attached to the base of the structure and may be moved horizontally. The measurements of the physical system are listed in Table 2.4.

2.3.2   Instrumentation and Control

The sensors interfaced in the lab system are a full bridge beam load cell manufactured by Omega Engineering with part number LCL-010 and a quadrature optical encoder kit manufactured by US Digital with part number E2-1024-N-DD-B. The load cell, which is subject to the spring force, is used to identify the displacement x of M_1. The output signal of the load cell is amplified by a strain gage amplifier manufactured by Omega Engineering, part number DRC-4710 which also supplies the sensor's (5-12)VDC bridge supply.

The optical encoder kit consists of a 1-inch rotary code wheel with 1024 counts per revolution (CPR) per channel, which is read by a HEDS-9100 optical encoder module, and

the manufacturer's default base and cover. The pin connections on the encoder module are the 5VDC, ground, and two output channels, A and B. The optional third output channel which gives an index signal was not used in this experiment. Channels A and B output two TTL square waves, 90 degrees out of phase, which must be decoded to give θ and $\dot{\theta}$ for the given CPR of the code wheel. The CPR of the encoder, also called the encoder lines, determines the sensitivity of the encoder to tracking motion.

The electromagnet is made of 1018 low carbon steel and is wound with 22-AWG magnet wire. The current i is supplied by a 15VDC power supply. The parameters of the electromagnet are given in Table 2.4.

The DAQ system used is a dSpace controller board DS1103 and a CLP1103 connector panel which work with ControlDesk version 3.2.2 and Matlab/Simulink. The analog output of the amplified load cell signal and the encoder are wired directly to the connector panel which supplies the required 5VDC supply to the encoder and contains an embedded encoder to counter interface. The up and down counts and time between counts from the counter interface are determined by embedded code in Simulink and used to determine the encoder motion. The maximum data sampling step size specified in the Simulink model is limited by the CPR of the encoder disk and the angular velocity of the pendulum. For the overall motion of the experimental system, the maximum possible step size was 0.05sec.

2.4   Electromagnet Control

Using the electromagnet as an actuator requires identifying the direction of motion and position of M_2 with respect to the electromagnet. In the physical system, the displacement of the electromagnet from the equilibrium position x_m can have a maximum value of 11.4cm measured from the center of the electromagnet. To activate motion, the electromagnet should turn on when M_2 is swinging toward it and turn off the moment the pendulum

31

swings past it so that the magnetic field does not slow the pendulum's motion.

The magnetic field lines of the electromagnet are directed across the poles of the electromagnet in the opposite direction of the current flow [21]. As the pendulum swings between the poles of the U-shaped electromagnet, M_2 attempts to follow the field lines, causing the pendulum to jerk in the $\pm\hat{k}$ direction. The sensors do not directly show this additional dimension of motion, however the motion results in an overall reduction in amplitude of the oscillating system. The motion also produces jitter in the encoder, causing miscounts of the encoder signal which appear as the zero of the pendulum's equilibrium position being shifted. From Fig. 2.4 it can be seen that x_g is measured from the center of M_2 to the center of the electromagnet. Physically, it should be measured to the edge of each mass. To account for this in the simulated system and to prevent the undesired motion in the pendulum, the signal to the electromagnet is turned off when x_g is within 1cm of the electromagnet's center.

In the physical system, the control logic is incorporated in the Simulink model that is used with dSpace and ControlDesk. The model identifies the input connector terminals of the sensors and gives the analogue voltage value of the load cell and the line count and delta line count of the encoder. Because of the internal resistance in the dSpace connector panel, the supplied voltage signal must be multiplied by 10. After sending the scaled voltage signal through a low pass filter, an embedded function is used to calibrate the voltage signal to give the displacement, x. For the motion of M_2, the line count and line velocity must be dividing by the CPR of the code wheel and multiplied by 2π to give θ and $\dot{\theta}$ in radians and radians per second. Simulink block functions and a series of if-else conditions were then used to send the logic signal to the digital bit output terminal of the connector panel. The bit output pin supplies ground and 5VDC or 0VDC depending on the high or low logic signal. The 5VDC signal was used to supply the required (2–4)VDC gate threshold voltage to the MOSFET switch controlling the external voltage supply to the electromagnet.

32

In the simulation, Eq. (2.24) and Eq. (2.25) were coded as a subsystem in Simulink. The torque acting on M_2, calculated from Eq. (2.28) and Eq. (2.31), was implemented as embedding functions in a series of if-else conditions activated by the control logic. To account for the varying strength of the electromagnet because of the rapid on/off switching, positive and negative torque were coded as separate functions.

In the physical system it is assumed that for larger x_m values, the magnetic force will have little influence on M_2 and the position of the pendulum will govern when the electromagnet is powered rather than the value of x_g. The goal of the logic is to produce periodic motion, determine the extent to which the magnetic field influences the motion of the pendulum, and determine the effectiveness of Eq. (2.28) and Eq. (2.29) at representing the magnetic force acting on M_2.

The control logic for the experimental and the simulated systems is listed in Table 2.3. The logic inputs of the experimental system identify the sets of conditions that must be true for the electromagnet to be activated. The logic inputs of the simulated system identify the conditions that must be true for the positive or negative torque to be calculated for the value of x_g and applied to the system. If the first set of conditions listed for both the experimental and simulated systems is true, the pendulum is approaching the right side of the electromagnet, as shown in Fig. 2.4. The second set of conditions listed for both systems then signals that the pendulum is approaching the left side of the electromagnet.

The time derivative of x_g gives the change in the displacement between M_2 and the electromagnet with respect to time. The logic condition u_1 checks for a negative value of $\frac{d|x_g|}{dt}$ which signals that M_2 is approaching the electromagnet. The sign of D, shown in Fig. 2.4, identifies whether the pendulum is to the left or right of the electromagnet. This position is checked by logic condition u_2. Condition u_3 checks the direction of the pendulum's swing which is determined by the sign of $\dot{\theta}$. Condition u_4 is used in the experimental system to turn the electromagnet off when the pendulum comes within 0.01m

33

Table 2.3: System Logic Conditions for Output Signal Activation

	Logic Conditions	
u_1	$\text{sgn}\left(\frac{d|x_g|}{dt}\right)$	
u_2	$\text{sgn}(D)$	
u_3	$\text{sgn}(\dot{\theta})$	
u_4	Interval Test, $x_g > |0.01\text{m}|$	
u_5	Interval Test, $0.01\text{m} < x_g < 0.10\text{m}$	
Logic Inputs Experimental System		Output
$u_1 < 0$, $u_2 > 0$, $u_3 < 0$, and $u_4{=}1$		On
$u_1 < 0$, $u_2 < 0$, $u_3 > 0$, and $u_4{=}1$		On
Logic Inputs Simulated System		Output
$u_1 < 0$, $u_2 > 0$, $u_3 < 0$, and $u_5{=}1$		$-Q_\theta$
$u_1 < 0$, $u_2 < 0$, $u_3 > 0$, and $u_5{=}1$		$+Q_\theta$

of the electromagnet to prevent the interference of the magnetic flux lines on the motion of the pendulum. In the simulated system, the control condition u_5 is an interval test to limit the values of x_g for which the magnetic force is calculated. The lower limit of this interval is also the lower limit used in the experimental system. The upper limit was determined by comparing the simulated forced response with the physical system response. A boolean logic signal of 1 indicated that an interval test is true.

2.5 Numerical and Experimental Results

The free and forced responses of the experimental and simulated systems were compared by first determining the system parameters of the experimental system to be used in the simulation. This also required estimating the uncertain electromagnet parameters to derive the magnetic forcing function.

34

2.5.1 System Parameters

The uncoupled free responses of M_1 and M_2 were evaluated using Eq. (2.38) and Eq. (2.39) to determine the parameters of each mass. All system parameters are listed in Table 2.4. A spring constant of (87.9 ± 9.67)N/m was calculated by a static force fest to verify the listed k which was calculated by experimentally determined parameter values. Checking the natural frequency of the pendulum mass by the definition of natural frequency for a simple pendulum for small angle oscillations, $\omega_n^2 = \frac{g}{R}$, gives 5.36rad/s for M_2, which falls in the range of experimentally calculated measurements.

2.5.2 Magnetic Forcing Function

In calculating the magnetic force function $f(x_g)$, the uncertain parameters were the cross sectional area of the air gap, the relative permeability of the steel used in the electromagnet core and the load, and the presence of fringing. The analogy used to derive the magnetic force function assumes that the flux is confined in the core and only exits through the poles. This assumption may be more accurate for a core made of a single piece of material, although any electromagnet will have some flux leakage from the sides. In the experimental system, the core is made up of three pieces, and the presence of joints affects the strength of the electromagnet [21]. The magnetic force in the experimental system is strongest across the polls and the windings.

Since the relative permeability of a ferromagnetic material is a function of the degree of magnetization, the exact relative permeability of the steel used in this experiment is not known. To reduce the number of uncertain parameters, the relative permeability of the core and the load were assumed to be equal, where $\mu_r = \mu_{r_C} = \mu_{r_L}$.

The static magnetic force acting on M_2 was experimentally found for a small range of x_g displacements and compared with the calculated forcing function to determine the

35

Table 2.4: System Parameters

Parameter, Variable	Value
Electromagnet Parameters	
Magnetic Permeability of free space, μ_0	$4\pi \times 10^{-7}$ H/m
Magnetic Permeability of steel, μ_r	70 ± 10
Magnetic Permeability of air, μ_{r_g}	1
Mean flux path through core, l_C	0.203m
Mean flux path through load, l_L	5.71×10^{-2}m
Core cross sectional area, A_C	5.07×10^{-4}m^2
Load cross sectional area, A_L	2.74×10^{-3}m^2
Air gap cross sectional area, A_g	1.27×10^{-3}m^2
Turns on electromagnet, N	864turns
Current, i	2.67A
M_1 Parameters	
Mass (including encoder)	0.950kg
Damped natural frequency, ω_d	(9.70 ± 0.35)rad/s
Damping ratio, ζ	0.0904 ± 0.0363
Damping coefficient, c	(1.67 ± 0.71)N·s/m
Spring constant, k	(90.1 ± 13.4)N/m
Natural frequency, ω_n	(9.74 ± 0.35)rad/s
Friction coefficient, μ_k	(0.015 ± 0.004)
M_2 Parameters	
Mass (includes rod mass)	1.363 kg
Rod length, R	0.341 m
Damped natural frequency, ω_{d_p}	(5.32 ± 0.01)rad/s
Damping ratio, ζ_p	$(1.89\pm0.89)\cdot10^{-4}$
Damping coefficient, b	$(3.18\pm1.54)\cdot10^{-4}$N·m·s
Natural frequency, ω_{n_p}	(5.32 ± 0.01)rad/s
Structure Parameters	
Structure Dimensions	
Length	0.34m
Width	0.33m
Height	0.51m
Allowable M_1 motion	±0.13m
Allowable M_2 rotation	±1.51rad

36

uncertain parameters. The displacement x_g is taken from the center of the electromagnet. Since the signal to the electromagnet is switched off when M_2 is within 0.01m of the electromagnet, the magnetic force of concern is for $x_g > 0.01$m. The relative permeability of the electromagnet core and the pendulum mass was approximated to range from 60 to 80.

As M_2 does not approach the electromagnet as depicted in Fig. 2.3 and the flux is not exiting the electromagnet only through the poles, an approximate air gap cross sectional area had to be determined. From the basic assumptions, the smallest air gap cross sectional area considered is equal to the core cross sectional area, $A_g = A_C$. The largest air gap cross sectional area is equal to the load cross sectional area, $A_g = A_L$. A larger A_g value offers a lower force value at $x_g = 0$, however, it gives higher values for the range $x_g > 0.01$m.

The magnetic force at $x_g = 0$ is the estimated holding force for the given load, which assumes that the load closes the air gap, forming a completely closed magnetic circuit with the poles of the electromagnet. The magnetic holding forces calculated for M_2 at $\mu_r = 70$ for the smallest and the largest air gap cross sectional areas were 363N and 67.3N, respectively. The calculated magnetic forces from Eq. (2.28) which neglects fringing and Eq. (2.29) which considers fringing are equal at $x_g = 0$. In the physical system, the calculated holding force could not be experimentally verified for the pendulum mass since the distance between the electromagnet poles is greater than the diameter of the pendulum mass. It is assumed, from checking the holding force on larger steel pieces, that the theoretical holding force on M_2 should be between 100N and 200N.

After comparing the forced response of the experimental system with the simulated response for varying values of A_g, the air gap cross sectional area is considered to be 2.0 and 2.5 times the value of the core cross sectional area. The calculated magnetic forces for $A_g = A_C$ and $A_g = 2.5A_C$ are shown in Fig. 2.8, neglecting and considering fringing for both cases. The calculated holding force for $A_g = 2.5A_C$ is 145N which is thought to be

37

reasonable.
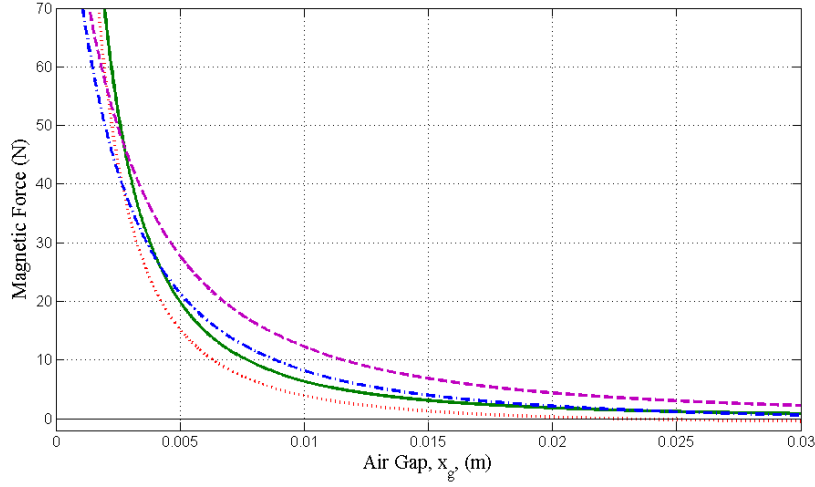
Figure 2.8: Calculated magnitude of magnetic force acting on M_2 located at x_g for $A_g = A_C$, considering fringing ($\cdots$) and neglecting fringing (—), and for $A_g = 2.5A_C$, considering fringing ($\cdot-\cdot$) and neglecting fringing (- - -)

Although the experimentally determined data points fit more closely with the plots for $A_g = A_C$, the force values corresponding to $x_g > 0.01$m for this air gap cross sectional area were too low in the simulation. This may be attributed to the magnetic field not being uniform around the electromagnet, and the experimentally determined data points found for only a linear orientation of M_2 with the electromagnet.

The magnetic forcing functions (N) acting on M_2, x_g meters away, calculated from Eq. (2.28) and Eq. (2.29) for $A_g = 2.5A_C$, are

$$|f(x_g)| = \frac{1.74 \times 10^{-5}}{(x_g + 3.46 \times 10^{-4})^2} \tag{2.40}$$

in which fringing is neglected, and

$$|f_F(x_g)| = \frac{-(0.184x_g^2 - 2.33 \times 10^{-4})}{(x_g^2 + 0.403x_g + 1.27 \times 10^{-3})^2} \tag{2.41}$$

in which fringing is considered. Considering fringing of the flux lines gives a more ac-

38

curate account of the effect of the electromagnet on M_2 at a distance x_g. After a certain distance, the magnetic force acting on M_2 will be negligible. In the physical system, the electromagnet weakly attracts M_2 up to $x_g = 0.12$m. However, Eq. (2.41) which considers fringing can only be applied for $x_g < 0.0356$m since the graph crosses the x_g axis at this point, after which the magnetic force must be considered to be zero if using this function. Therefore Eq. (2.40) was restricted to the interval $x_g = [0.01, 0.10]$m for use in Eq. (2.31) which gives the torque acting on M_2 at the corresponding θ and ψ.

Using the parameters from Table 2.4 in Eq. (2.26), the magnetomotive force $\mathcal{F}$ and the magnetic flux in the core ϕ_C, disregarding the load and the air gap, were calculated to be 2307A-turns and 5.06×10^{-4}Wb, respectively. The magnitude of the flux density of the core, calculated by dividing the core flux by the cross sectional area of the core, $B = \frac{\phi_C}{A_C}$, was found to be 0.999T. This value is in the range of expected values given that powerful permanent magnets have a flux density of $(0.1 - 0.5)$T and powerful laboratory electromagnets produce fields of $(1 - 2)$T [21, 25].

2.5.3 Free Response

The free response of the mass-pendulum system was analyzed for various combinations of initial conditions and compared to the free response of the system motion simulated in Matlab/Simulink from Eq. (2.24) and Eq. (2.25) for the same initial conditions. In comparing the free response of the experimental system and the simulated system, it was determined that the experimentally determined damping coefficient c of M_1 did not sufficiently characterize the response of M_1. This was resolved by considering the differing response of the experimental system to be due to a friction force $F_f = \mu_k W \operatorname{sgn}(\dot{x})$ from the linear bearings in M_1, where μ_k is the kinetic friction coefficient and W is the weight. In the coupled system, the weight was considered to be the sum of the weights of

39

www.manaraa.com

both masses. The damping coefficients c and b were calculated from the uncoupled free responses of M_1 and M_2, respectively, using Eq. (2.38) and Eq. (2.39), while the friction coefficient was estimated by comparing the simulated and experimental responses.

The free response of the system for which the initial positions of M_1 and M_2 are opposed to each other is shown in Fig. 2.9(a)–(d). Due to friction, the oscillations in the physical system quickly decrease with all perceptible motion in M_1 ceasing approximately 15sec before M_2 stops oscillating. As can be seen from the plots, the simulated response gives a good representation of the motion in the system for the parameters listed in Table 2.4.

The motion of M_1 and M_2 relative to each other for similar initial conditions is shown in Fig. 2.10. As can be seen from the plots, the simulated response of the system is close to the response of the physical system. The simulated response shows the motion of M_1 having a higher positive amplitude for the extent of its motion. This can be observed by comparing the upper x amplitudes of the physical response with the simulated response. This can also be viewed in Fig. 2.9(c) and (d) after the initial transient motion dies out. The lower relative maximums in the physical system may be a result of the type of spring used in the physical system. The simulation assumes a spring which would function as both an extension and a compression spring oscillating equally about its equilibrium point. In the physical system, a compression spring is used. The linear range of the spring does not extend as far in the positive x direction, for the orientation given in Fig. **??**. For a hardened spring, a larger force in this direction would then be required to extend the spring [26].

For all the combinations of initial conditions tested, after approximately (3–4) seconds, the initial transient motion of the masses dies out and the motion of the masses appears to synchronize briefly with M_1 and M_2 oscillating at the same frequency, 4.499rad/s in the physical system and 4.295rad/s in the simulated system. Due to friction, M_1 motion ceases approximately 15sec before M_2.

40
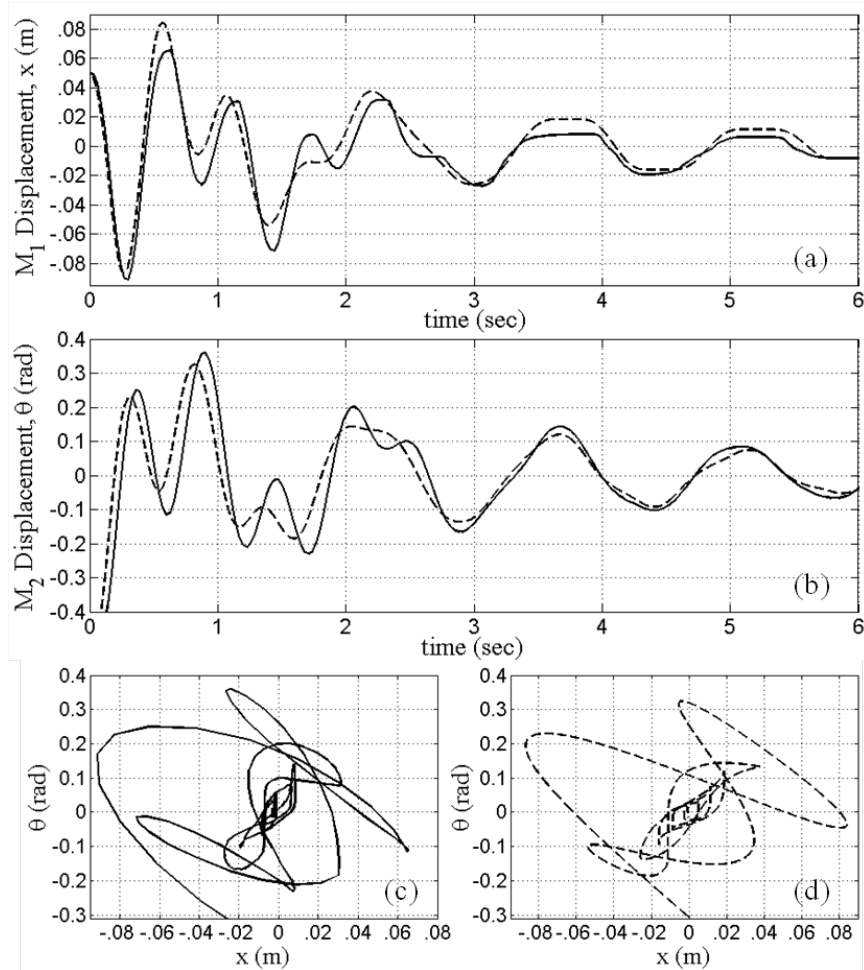
Figure 2.9: Comparison of the physical (—) and simulated (- - -) system free responses due to initial conditions $\theta_0 = -\pi/6$rad and $x_0 = 0.05$m for (a) M_1, (b) M_2, and (c and d) motion of M_2 with respect to M_1
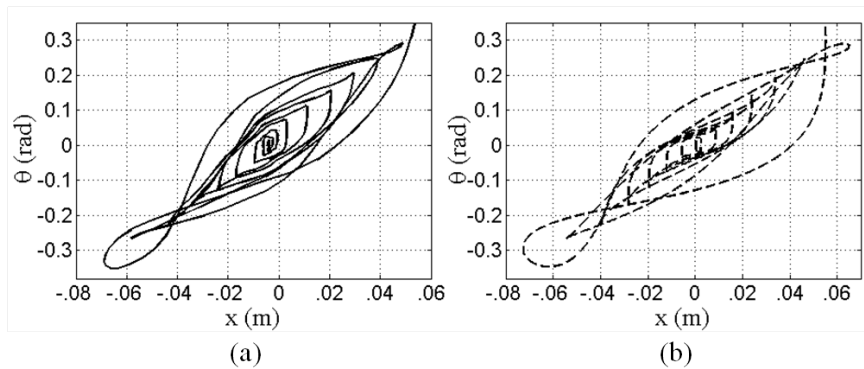
Figure 2.10: Free response motion of M_2 with respect to M_1 for (a) experimental and (b) simulated systems using initial conditions $\theta_0 = \pi/6$rad and $x_0 = 0.05$m

41

2.5.4 Forced Response

In the experimental system, the forced response was investigated for three positions of the electromagnet, $x_m = (1) -4$cm, (2) -7.5cm, and (3) -11.4cm (the response of the system for positive values of x_m placements was found to be similar). The negative x_m position indicates that the electromagnet was positioned in the negative $\hat{i}$ direction from the equilibrium position of the main mass and pendulum. Since the control to the electromagnet is a logic high or low, the strength of the magnetic force in the physical system is altered by the position of the electromagnet. The position of the electromagnet with respect to M_2 determines the angle ψ, shown in Fig. 2.4, which influences the torque calculated from Eq. (2.31) for a magnetic force of $f(x_g)$, which is also dependent on the displacement of the electromagnet .

In comparing the forced response in the physical system with the simulated response, it was determined that the magnetostatic forcing function did not account for the varying strength of the magnetic field due to the rapid on/off switching of the electromagnet. To account for this in the simulation, the relative permeability μ_r, which is dependent on the magnetization of the material, was adjusted from 50 to 70, in increments of 10, depending on the length of time the electromagnet was on in the physical system. For the rapid switching in Fig. 2.11(a) when the pendulum swings from left to right, the magnetic force was assumed to be 80% of the calculated forcing function for the reduced μ_r value. It was also found that the insulating effect of the air gap which surrounds M_2 because the mass is smaller in diameter than the distance between the poles of the electromagnet had to be accounted for. This was done by adding 0.004m to x_g at each iteration of the simulation before calculating the magnetic force corresponding to the distance between M_2 and the electromagnet. This considers M_2 to be farther away from the electromagnet than the calculated x_g value.

The forced response was found for two scenarios to compare the effect of the interaction between the masses and the application of the magnetic force. The electromagnet induced motion of M_2 was found, keeping M_1 fixed, and the coupled response of the system was found in which M_1 was unconstrained. A summary of the forced system response for the experimental and simulated systems is shown in Tables 2.5 and 2.6, respectively. A snapshot of the oscillations of M_1 and M_2 for the scenario in which M_1 has allowable motion is shown for the experimental system and the simulated system in Figs. 2.11 and 2.12, respectively, for the three locations of x_m. The on/off switching of the electromagnet is shown for the experimental system for each test, and the applied positive and negative torque is shown for the simulated system for each test.

For the case in which M_1 was held stationary, the RMS amplitude, and minimum and maximum amplitudes of M_2 are given with its oscillating frequency for the first 100 seconds of motion. Since the motion of M_2 for this case was dependent on the initial conditions, the simulated response for each test was determined at the same initial conditions as the corresponding experimental responses.

For the case in which M_1 is not constrained, the RMS amplitude, and the minimum and maximum amplitudes of both M_1 and M_2 were determined for a 10sec sample time, after the initial transients of the system died out. Only the oscillating frequency of M_2 is listed since the masses oscillate at the same frequency. For the electromagnet positioned furthest away, the oscillating frequency of M_1 could not be determined. Since the initial conditions of the system did not influence the motion of the system after the initial transients died out, the experimental data listed in Table 2.5 is the average values of related tests.

Keeping M_1 constrained, the simulated M_2 response is representative of the response of the physical system up to approximately $\theta = \frac{\pi}{4}$rad for all tests. For Test 1, in which the electromagnet is positioned at -4cm, the physical and the simulated system

43

Table 2.5: Experimental System Forced Response

M_1 Held Stationary			
[0–100]sec			
x_m	θ_{rms} (rad)	θ_{min} (rad)	θ_{max} (rad)	ω_{M_2} (rad/s)
1	0.407	−0.825	0.822	5.27
2	0.383	−0.755	0.755	5.27
3	0.237	−0.542	0.542	5.32

M_1 Free to Move						
[90–100]sec						
x_m	x_{rms} (cm)	x_{min} (cm)	x_{max} (cm)	θ_{rms} (rad)	θ_{min} (rad)	θ_{max} (rad)	ω_{M_2} (rad/s)
1	1.62	−2.94	1.90	0.113	−0.158	0.164	4.50
2	1.22	−1.99	1.32	0.086	−0.144	0.123	4.16
3	0.267	−0.497	−0.155	0.009	−0.017	0.015	5.26

Table 2.6: Simulated System Forced Response

M_1 Held Stationary			
[0–100]sec			
x_m	θ_{rms} (rad)	θ_{min} (rad)	θ_{max} (rad)	ω_{M_2} (rad/s)
1	0.400	−0.809	0.806	5.23
2	0.369	−0.766	0.768	5.27
3	0.244	−0.528	0.525	5.32

M_1 Free to Move						
[90–100]sec						
x_m	x_{rms} (cm)	x_{min} (cm)	x_{max} (cm)	θ_{rms} (rad)	θ_{min} (rad)	θ_{max} (rad)	ω_{M_2} (rad/s)
1	1.88	−3.05	1.99	0.0883	−0.139	0.132	4.22
2	1.42	−2.20	2.13	0.0943	−0.179	0.105	3.84
3	0.0228	−0.0195	0.0312	0.0202	−0.0293	0.0278	5.37

reach a maximum amplitude of $\frac{\pi}{4}$ in approximately 90sec. The average percent difference between the amplitudes of the two plots for $[0-90]$sec is 3.1% with a maximum percent difference of 6.2%. For Test 2, the physical and simulated system reach $\frac{\pi}{4}$ in approximately 100sec, with an average percent difference in their amplitudes of 11.0% and a maximum of 13.3%. For the electromagnet positioned furthest away, Test 3, M_2 reaches $\frac{\pi}{4}$ in approximately 215sec in the physical response and 230sec in the simulated. The percent difference between the plots for the first 100sec of motion is 7.7% with a maximum percent difference of 17.6%. For the time interval $[100-230]$sec, the difference between the simulated and experimental response increases to an average percent difference of 11.4% with a maximum percent difference of 17.5%.

In the physical system the oscillations of the pendulum, with M_1 held stationary, appear to keep increasing. After 30 minutes of motion, for ever tested position of x_m, the average peak amplitude of a 10sec test interval was approximately $\frac{5\pi}{12}$rad, increasing at approximately 1.7×10^{-3}rad/min, with oscillating frequency 4.91rad/s. The forced response was not tested for longer since the pendulum's peak amplitude was approaching the maximum allowed motion. In the simulated system response, the amplitude of M_2, after reaching $\frac{\pi}{4}$rad, increases at a much faster rate than in the physical system. In the simulation, M_2 reaching $\frac{5\pi}{12}$rad in approximately 5min for Tests 1 and 2 and 15min for Test 3, implying that the system model is only representative of the physical system for smaller angle motion.

When M_1 is not fixed, as seen in Tables 2.5 and 2.6, the motion of M_1 greatly reduces the amplitude of the pendulum's oscillations for the same force. Starting with a small initial condition, each mass reaches steady state oscillation within five seconds. Compared to the motion of the pendulum when M_1 is held stationary, when the pivot point of an oscillating mass has allowable motion, the influence of the driving force on the mass is damped. The motion of M_1, which is constrained by the attached spring, effectively

45

limits the motion of M_2. Therefore a much larger force would be required to increase the oscillating amplitudes of the masses.

As can be viewed in Figs. 2.11 and 2.12, the offset electromagnet from the equilibrium position of the system attracts the pendulum in the direction of the offset, causing the pendulum have a higher amplitude in that direction. The closer the electromagnet is located to the equilibrium position, the more symmetric the oscillations of M_2 are about zero since the magnetic force acts on M_2 as it swings in both the positive and the negative directions.

The strength of the magnetic field as well as the angle at which it acts on M_2 determines the oscillating amplitudes of the system. When the electromagnet is positioned at $x_m = 0$, the minimum and maximum amplitudes of M_2 are approximately equal, however the amplitudes are lower than when the electromagnet is positioned at $x_m = -4$cm. In both the physical and the simulated systems, a small increase in the displacement of the electromagnet from $x_m = -7.5$cm produces approximately 70% reduction in the oscillating amplitudes of the masses, implying that there is an optimal position of the electromagnet which maximizes the oscillating amplitudes of the masses.

In the physical system, when the electromagnet is positioned furthest away, the amplitude of the pendulum's swing is greatly reduced and M_1 does not oscillate, but jitters about its equilibrium position. Because of friction, this equilibrium position varies, as can be seen in Fig. 2.11(c) where M_1 is approximately oscillating at $x = -0.003$m. The low oscillating amplitude of M_2 also has some jerking motion which cannot be sensed by the resolution of the encoder. Although the motion in M_1 is nearly imperceptible, and M_2 is oscillating at the same frequency as the related test when M_1 is fixed, the allowed motion of M_1 dampens any additive influence of the magnetic force on the motion of M_2.

The variation in the motion of the simulated system responses shown in Fig. 2.12(a) and (b) is attributed to the interaction between the masses in the simulation due to the

46
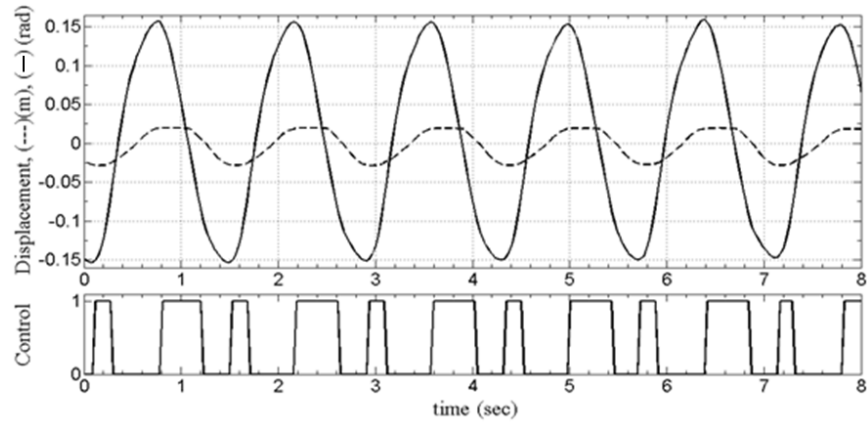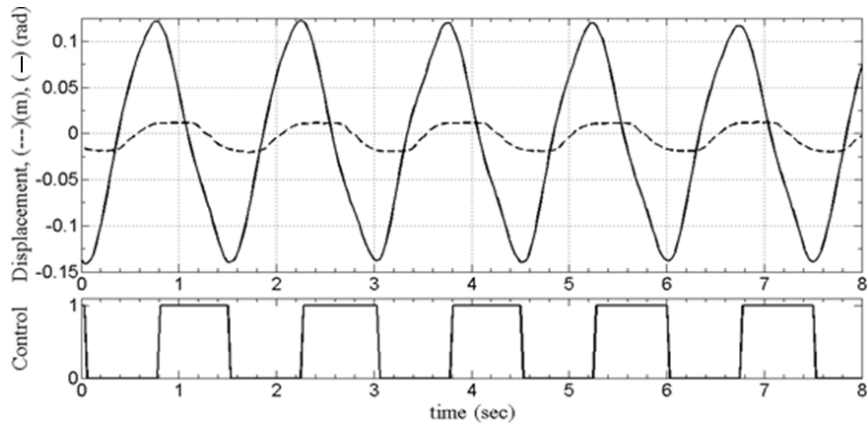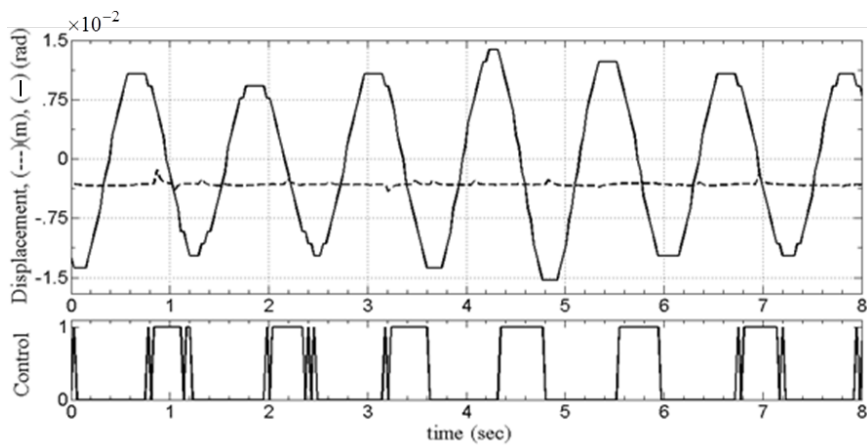
Figure 2.11: Forced response of experimental system of M_1 (- - -) and M_2 (—) and corresponding control logic for x_m equal to (a)-4cm (Test 1), (b)-7.5cm (Test 2), and (c)-11.4cm (Test 3)
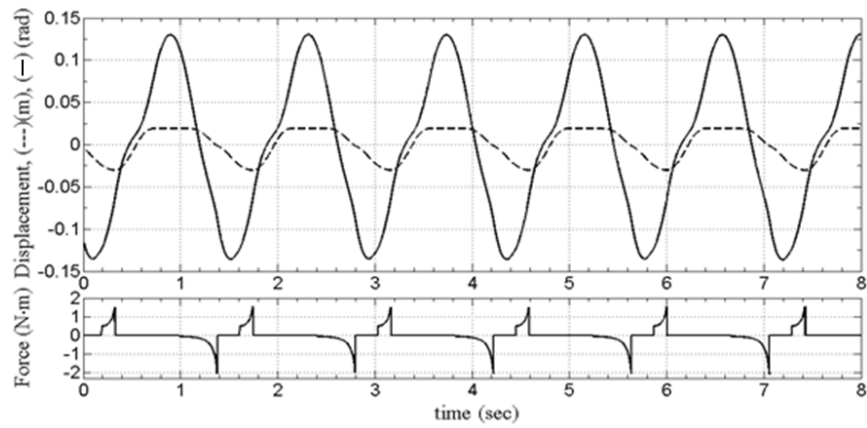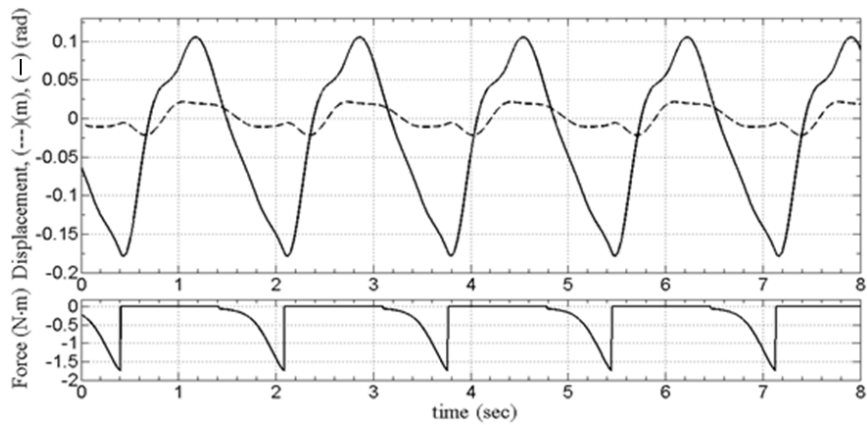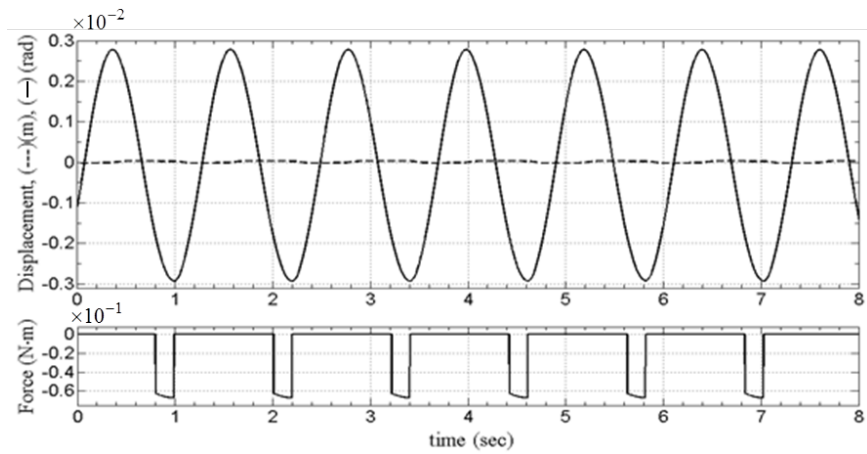
Figure 2.12: Simulated forced system responses of M_1 (- - -) and M_2 (—) and corresponding magnetic force for x_m equal to (a)-4cm (Test 1), (b)-7.5cm (Test 2), and (c)-11.4cm (Test 3)

variable torque applied to M_2. In the simulated response in which M_1 is stationary, the amplitude of M_2 is symmetric and does not exhibit similar variations in its oscillations.

Overall, the simulated system response, characterized by Eq. (2.24) and Eq. (2.25) with torque represented by Eq. (2.31) offers a good representation of the physical system response to the applied magnetic force for the electromagnet positioned within 7.5cm of the system's equilibrium position. In comparing the motion of the physical and simulated systems for both scenarios and all positions of the electromagnet tested, the percent difference between experimental and simulated responses is the greatest for Test 3 with M_1 free to move. The percent differences for this test ranged from 53.1% to 184.9%. This is due to the physical system exhibiting large friction forces for this test which caused the zero position of M_1 to shift and the mass to stick at its maximum amplitudes.

The percent difference in the minimum, maximum, and RMS amplitudes of oscillation for Test 2 with M_1 free to move ranged from 9.2% to 47.0%, with a percent difference of 8% between their oscillating frequencies. For Test 1, the percent difference in the amplitudes of oscillation ranged from 3.7% to 24.5%, with a percent difference of 6.4% between their oscillating frequencies. The lower percent difference between the amplitudes of the masses and their oscillating frequencies for Test 1 then reveals that the simulated response provides the best representation of the physical response for the electromagnet positioned within 4cm of the system's equilibrium position.

Chapter 3

Thermoelectric Generator Using Diesel Engine Exhaust Waste Heat

Thermoelectric generators (TEGs) have consistently demonstrated their usefulness in converting heat into electricity. Their compact size, reliability, and long life are some of the characteristics which contribute to their use in power systems. They are also noted for producing power which can be easily implemented, and the lack of moving parts ensures no dynamic interference of the TEG with the overall system [27].

Large scale applications of thermoelectrics in power generation have gained considerable attention due to an increased emphasis on energy efficiency. This has lead to extensive research in improving the efficiency of thermoelectric (TE) materials, the design of thermoelectric modules, and their application.

3.0.5 Advances in TEG Material

The key to implementing thermoelectric generators as common energy converters is perhaps contingent on increasing the overall efficiency while decreasing the cost of bulk TE materials, such as would be used in commercial power generation. The performance of

50

a TE material compared to different materials at the same temperature application is often expressed by either its figure of merit Z or its dimensionless figure of merit ZT, found by multiplying Z by the operating temperature T. The dimensionless figure of merit for a TE material is defined as

$$ZT = \frac{\alpha^2 \sigma}{\lambda} T \tag{3.1}$$

for the material's temperature dependent Seebeck coefficient α, electrical conductivity σ, absolute operating temperature gradient T, and thermal conductivity λ. The relationship can also be written as

$$ZT = \frac{\alpha^2}{\rho\lambda} T \tag{3.2}$$

since electrical resistivity ρ is the reciprocal of σ. Although a material's ZT value depends on the operating temperature, each material is only useful over a certain temperature range, with most bulk materials having a maximum ZT value less than 2. At room temperature, the most commonly used TE material Bi_2Te_3 has had an approximate figure of merit of 1 for the last decade [28]. Although there is no upper limit for the value of ZT, a limit of $ZT = 4$ has been predicted for bulk materials [29]. At this value it is assumed that a TEG would be able to compete with electric generators in efficiency [28].

Research on improving TE material focuses on developing materials with high electrical but low thermal conductivity, which would increase the temperature gradient across the generator and thereby generate more electrical current. Research in this area includes optimizing structure and composition for the operating temperature, forming micro- and nano-structures, and reducing dimensions based on quantization [28, 30, 31]. As some TE materials are composed of rare earth elements, research is also being conducted on improving the structure of materials composed of more abundant elements and finding new, less

51

expensive materials [32, 33].

3.0.6   Advances in TEG Module Design

Along with research to develop more efficient TE materials, research is also being conducted to develop different module designs for various operating temperatures and heat applications. The most common module design consists of a flat rectangular arrangement of n couples connected electrically in series. A couple simply refers to two semiconducting elements, one n-type and one p-type, placed physically in parallel with an electrically conducting connection on one end. The n couples are then connected thermally in a parallel manner between two ceramic plates which work as thermal conductors. The module has an optimal operating temperature for producing maximum power for the given TE material.

Segmented thermoelectric elements have been proposed for applications with large temperature ranges to take advantage of the maximum ZT values of different materials at different temperatures [34]. Module fabrication has also been investigated to design application specific modules, such as a thin film process tested for producing micro-thermoelectric modules [35]. A high strength module made of a non-toxic, low-cost alloy has been research for effectiveness in low temperature applications requiring a durable TEG [36]. Research in designing modules for different heat configurations is also being conducted, such as a ring structured module fabricated from Bi_2Te_3 alloy pieces for applications with radial heat flow [37].

3.0.7   TEG Applications

The variability in thermoelectric modules and materials has encouraged multiple applications of thermoelectric generation of varying size and operating temperatures. Modules have proven effective since 1961 for long term use in spacecrafts, converting heat from

52

radioactive decay into electricity [27]. The reliable, consistent power supply of a TEG is attractive for human body application for possible use in powering health monitoring devices from micro-machined thermopile chips as small as (4×4)mm^2 [38]. Other TEG applications have been made in biomedicine as pacemakers and muscle stimulators, remote terrestrial environmental monitoring, thermoelectric sensors, and waste heat recovery [34].

With the strong push for energy conservation and reduced fuel consumption, there is a need to increase the overall efficiency of ground vehicles with internal combustion engines. This increase can be realized by increasing the fuel efficiency of the engine, decreasing the energy wasted by decreasing engine inefficiencies, employing more efficient energy sources, and/or increasing the efficient use of the produced energy in the driveline.

In an internal combustion engine, heat loss is primarily due to the engine coolant, the exhaust gases, and radiation from the engine block. In traditional gasoline engines, it is generally estimated that two-thirds of the energy from the burned fuel is rejected as waste heat primarily through the coolant and exhaust gases. Due to the availability of free power in the form of waste heat and the opportunity to increase engine efficiency by increasing the use of an otherwise untapped energy supply, many TEG applications and configurations have been suggested to harvest this thermal energy.

A potential thermoelectric generator for radiator application in a hybrid vehicle is modeled in [39], which predicts 220W output power from 125 thermoelectric modules, yielding a thermoelectric efficiency of 3.4%. A single module is modeled in [40] for both exhaust and radiator waste heat recovery. An output power of 1.24W per module at 0.396% thermoelectric efficiency is calculated for the exhaust with approximate hot side and cold side temperatures of 196°C and 70°C, respectively. Using radiator heat, 0.135W output power is modeled for a single module, producing 0.135% thermoelectric efficiency with approximate thermoelectric hot and cold side temperatures of 90°C and 47.7°C, respec-

tively. A system model using segmented TE elements and a tube and shell heat exchanger on the exhaust produced 20W of power with a full scale generator able to produce 750W power in [41]. For this model, the authors predicted a 10% increase in vehicle fuel efficiency.

To evaluate the increase in vehicle fuel efficiency from thermoelectric waste heat recovery, the negative effects on fuel efficiency must also be considered. The disadvantages include increased engine back pressure from an exhaust heat exchanger and increased vehicle weight which are predicted to limit an improvement in fuel economy from thermoelectric generation to 0.13%–0.36% depending on city or highway driving [42]. Because of the negative affect of TEG weight, class 8 trucks, which have a gross vehicle weight above 14,969kg, are proposed as the most attractive platforms for initial vehicle TEG application, predicting average TEG electrical power of 0.5kW for city driving and 2.0kW for interstate driving. This assumes an efficiency of 5.0% for the overall TEG system [43].

Considering the negative effects, the additional electricity produced still increases the overall efficiency of the system. For applications in which the weight of the TEG system is not an issue, the increase in overall system efficiency is even greater. A stationary diesel or gasoline generator provides an attractive platform for the use of thermoelectric generation from waste heat recovery since the extra weight is not considered.

Thermoelectric generation from the waste heat of a 3-cylinder liquid cooled diesel engine is examined in this paper. For this test, an exhaust thermoelectric waste heat system was designed for heat transfer which would not produce significant engine back pressure. The paper is organized as follows: overview of mathematical models for thermoelectric power generation in Section 3.1, discussion of diesel engine combustion modeling in Section 3.2, description of the experimental system in Section 3.3, numerical and experimental results in Section 3.4, and conclusion in Section 4.

3.1 Thermoelectric Generator Module Mathematical Model

A thermoelectric generator module (TEM) is composed of n couples. Each couple, as shown in Fig. 3.1, is composed of two elements made of different semiconductor materials; referred to as p-type and n-type elements for their different electron transfer properties. The equations for the TEM are derived by expanding the heat transfer dynamics for one element of a couple and then applying them to the entire module. For the analysis, it is assumed (A.1) that each element of constant cross sectional area has both a hot side and a cold side junction in contact with a hot and a cold reservoir respectively. It is also assumed (A.2) that the only heat transfered between the hot and cold reservoirs of temperature T_H and T_C, respectively, is through the TEM with no lateral heat transfer. An electrical current develops in the semiconductor element due to the temperature gradient across the element. This current generates heat within the element. In addition, heat is produced at the junctions of the n-type and p-type semiconductor materials due to the Peltier effect. The rate of heat transfer into the entire module q_H is determined by adding the heat transfer rates due to the Peltier effect, the generated current, and the temperature gradient across the module.
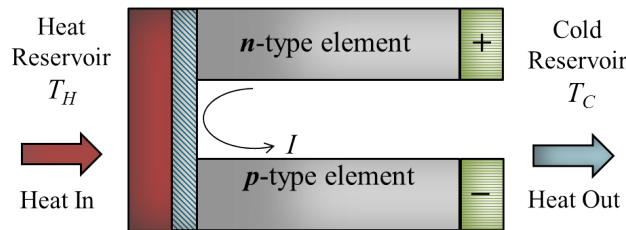
Figure 3.1: A single TEG couple consists of p-type and n-type semiconductor elements in contact with hot, T_H, and cold, T_C, reservoirs where heat is transfered into and out of the couple

3.1.1 Heat Transfer Equations for TE Element

The rate of heat transfer into a TEM can be determined by considering a TE element of length l carrying an electrical current I along its negative temperature gradient $-\frac{dT}{dx}$, as shown in Fig. 3.2. For this analysis, it is assumed (A.3) that the semiconductor properties of the elements, the thermal conductivity λ, electrical resistivity ρ, and Seebeck coefficient α, are independent of temperature.

3.1.1.1 Temperature Distribution of a TE Element

The one-dimensional temperature distribution along the length x of a single element is determined by analyzing the rate of heat transfer into and out of an infinitesimal area of length dx along a one-dimensional element. By Fourier's law of heat conduction, the heat transfer rate q_{in} through the area's left face is the product of the material's cross sectional area A, thermal conductivity λ, and temperature gradient at the left face
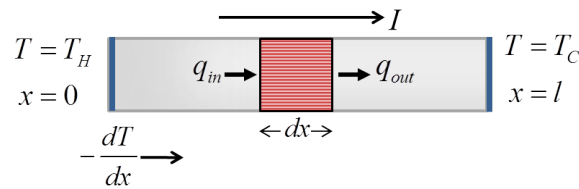
Figure 3.2: Temperature distribution T along a TE element is found by analyzing the rate of heat transfer into, q_{in}, and out of, q_{out}, an infinitesimal area of length dx for a one-dimensional element carrying current I along its negative temperature gradient

$$q_{in} = -A\lambda\frac{dT}{dx} \tag{3.3}$$

where A is equal to 1 for the one-dimensional element. The rate of heat exiting the area's right face q_{out} is also determined by Fourier's law of heat conduction where the temperature gradient at the right face is the sum of the temperature gradient at the left face plus the rate

56

of change in the gradient along the length dx

$$q_{\text{out}} = -\lambda \left[\frac{dT}{dx} + \frac{d}{dx}\left(\frac{dT}{dx}\right) dx \right]. \tag{3.4}$$

The current I passing through the TE element shown in Fig. 3.2 generates Joule heat which is proportional to the square of the current times the material's resistance. For the one dimensional element, the rate of heat transfer due to Joule heat q_J along the length dx is expressed as

$$q_J = J^2 \rho dx \tag{3.5}$$

where $J = \frac{I}{A}$ is defined as current density and $\rho = \frac{1}{\sigma}$ is the material's electrical resistivity.

Assuming (A.4) that the temperatures T_H and T_C in Fig. 3.2 are constant, then the rate of heat transfer at the right face of the area equals the rate of heat transfer at the left face plus the heat generated along the length dx due to Joule heat. This relationship is found by

$$q_{\text{out}} = q_{\text{in}} + q_J \tag{3.6}$$

which simplifies to

$$\lambda \frac{d^2T}{dx^2} + J^2\rho = 0. \tag{3.7}$$

The temperature distribution along the length of the element is found by solving this second order differential equation. Solving using u substitution where $u = \frac{dT}{dx}$ and $\frac{du}{dx} = \frac{d^2T}{dx^2}$, the first indefinite integral is

$$\int du = \int -J^2 \frac{\rho}{\lambda} dx. \tag{3.8}$$

57

This yields the first order differential equation $u = \frac{dT}{dx} = -J^2 \frac{\rho}{\lambda} x + C$ with the constant of integration C. From this differential equation, the indefinite integral

$$\int dT = \int \left(-J^2 \frac{\rho}{\lambda} x + C \right) dx \tag{3.9}$$

yields

$$T = -J^2 \frac{\rho}{2\lambda} x^2 + Cx + D \tag{3.10}$$

with the constant of integration D. Applying the element's boundary conditions $T = T_H$ at $x = 0$ and $T = T_C$ at $x = l$, shown in Fig. 3.2, to Eq. (3.10) gives the integration constants $C = \frac{1}{l} \left(T_C - T_H + J^2 \frac{\rho}{\lambda} l^2 \right)$ and $D = T_H$. The temperature distribution in Eq. (3.10) can then be rewritten as

$$T = \left[T_H - \left(\frac{x}{l} \right) \Delta T \right] + \left[\left(\frac{I}{A} \right)^2 \frac{\rho}{2\lambda} x(l - x) \right] \tag{3.11}$$

where $\Delta T = (T_H - T_C)$ and $J = \frac{I}{A}$. The first term in Eq. (3.11) shows a linear relationship between the temperature and the length x due to the heat transfer between the hot and the cold reservoirs. The second term displays a parabolic relationship between the temperature and the length x due to the current increasing the temperature in the element's interior.

3.1.1.2 Rates of Heat Transfer in a TE Element

The rates of heat transfer q at the hot and cold junctions of a TE element of cross sectional area A and thermal conductivity λ are found by applying Fourier's law of heat conduction, $q = -A\lambda \frac{dT}{dx}$, at each junction [44]. The derivative of Eq. (3.11) with respect

58

to x used in Fourier's law of heat conduction is found to be

$$\frac{dT}{dx} = -\frac{1}{l}\Delta T + \left(\frac{I}{A}\right)^2 \frac{\rho}{2\lambda}[l - 2x]. \tag{3.12}$$

By Fourier's law, at the hot junction where $x = 0$ in Eq. (3.12), the rate of heat transfer q_{H_E} is

$$q_{H_E} = -A\lambda \left(-\frac{1}{l}\Delta T + \left(\frac{I}{A}\right)^2 \frac{\rho}{2\lambda}l \right). \tag{3.13}$$

At the cold junction where $x = l$ in Eq. (3.12), the rate of heat transfer q_{C_E} is

$$q_{C_E} = -A\lambda \left(-\frac{1}{l}\Delta T - \left(\frac{I}{A}\right)^2 \frac{\rho}{2\lambda}l \right) \tag{3.14}$$

by Fourier's law. Letting $\gamma = \frac{A}{l}$, these equations simplify to

$$q_{H_E} = \gamma\lambda\Delta T - \frac{1}{2}I^2\frac{\rho}{\gamma} \tag{3.15}$$

$$q_{C_E} = \gamma\lambda\Delta T + \frac{1}{2}I^2\frac{\rho}{\gamma}. \tag{3.16}$$

As can be seen in Eq. (3.15) and Eq. (3.16), the heat entering the hot junction is reduced by half of the Joule heat which is flowing back to the heat source, while the heat exiting the cold junction is increased by half of the Joule heat.

3.1.2   Heat Transfer Equations for TE Module

The heat transfer equations for a TEM shown in Fig. 3.3 are based on the heat transfer behavior for a couple, as shown in Fig. 3.1. The heat transfer equations for the couple are found by applying Eq. (3.15) and Eq. (3.16) to the n-type and p-type elements in

59

the couple and including the heat transfer due to Peltier heat at the hot and cold junctions. Next, these relationships are scaled by a factor n to account for the number of couples contained in the TEM.

3.1.2.1   Material Properties of a TE Couple

The inclusion of the material properties for a couple's two semiconductor materials in Eq. (3.15) and Eq. (3.16) describes the conductive heat transfer within the couple. These material properties can be expressed in terms of the thermal conductance K which may be defined as the product of a material's thermal conductivity λ and geometry ratio $\gamma = \frac{A}{l}$, and resistance R which may be defined as the ratio of a material's electrical resistivity ρ and geometry ratio γ. For a TE couple, the thermal conductance K_C is the sum of the thermal conductances of both the n- and p-type elements, so that the thermal conductance of the couple is given as

$$K_C = \lambda_n \frac{A_n}{l_n} + \lambda_p \frac{A_p}{l_p} = \lambda_n \gamma_n + \lambda_p \gamma_p, \tag{3.17}$$

with subscripts denoting the n- and p-type materials. The resistance R_C of a couple is the sum of the resistances of each element which gives the couple's resistance as

$$R_C = \frac{\rho_n}{\gamma_n} + \frac{\rho_p}{\gamma_p}. \tag{3.18}$$

3.1.2.2   Heat Transfer Rate due to Peltier Heat

As current generated by the temperature gradient across a TE couple passes through the junction of the n-type and p-type elements, Peltier heat is generated at the junction. From Kelvin's second relation [45], the rates of heat transfer due to Peltier heat for a single
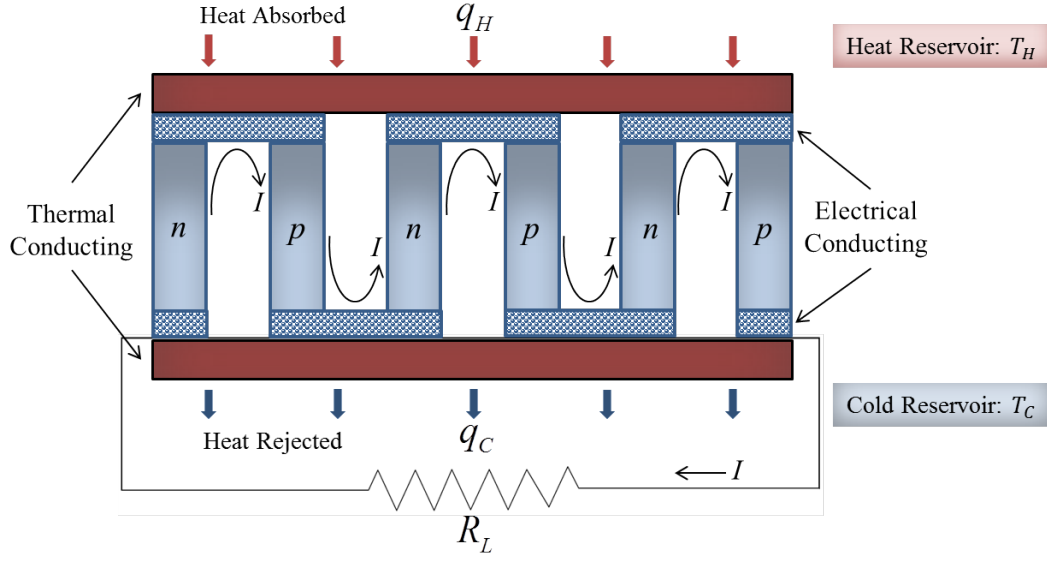
Figure 3.3: Thermoelectric generator module of n n-type and p-type couples with resistive load R_L, generates current I when exposed to a temperature gradient, $\Delta T = T_H - T_C$

couple are

$$q_{P_H} = \alpha T_H I \tag{3.19}$$

and

$$q_{P_C} = \alpha T_C I \tag{3.20}$$

at the hot and cold junctions, respectively, where α is the combined Seebeck coefficient of the n-type and p-type elements of a couple, $\alpha = |\alpha_n| + |\alpha_p|$ [44].

3.1.2.3 Heat Transfer Rates in a TE Couple and a Module

From the material properties of a couple and the generated Peltier heat, the rates of heat transfer for a couple at the hot and cold junctions, q_{H_C} and q_{C_C}, respectively, are

$$q_{H_C} = (\lambda_n \gamma_n + \lambda_p \gamma_p)\Delta T + \alpha T_H I - \frac{1}{2}I^2 \left(\frac{\rho_n}{\gamma_n} + \frac{\rho_p}{\gamma_p}\right) \tag{3.21}$$

61

and

$$q_{C_C} = (\lambda_n\gamma_n + \lambda_p\gamma_p)\Delta T + \alpha T_C I + \frac{1}{2}I^2\left(\frac{\rho_n}{\gamma_n} + \frac{\rho_p}{\gamma_p}\right). \tag{3.22}$$

By writing Eq. (3.21) and Eq. (3.22) in terms of the material properties in Eq. (3.17) and Eq. (3.18), q_{H_C} and q_{C_C} can be rewritten as

$$q_{H_C} = K_C\Delta T + \alpha T_H I - \frac{1}{2}I^2 R_C \tag{3.23}$$

$$q_{C_C} = K_C\Delta T + \alpha T_C I + \frac{1}{2}I^2 R_C. \tag{3.24}$$

The rates of heat transfer for an entire module are then found by multiplying Eq. (3.23) and Eq. (3.24) by the number of couples, n, in a module. From Eq. (3.17) and Eq. (3.18), define the thermal conductance K_M and the electrical resistance R_M for the entire module as

$$K_M = nK_C \tag{3.25}$$

$$R_M = nR_C, \tag{3.26}$$

respectively. The rate of heat transfer at the hot junction of the entire module, q_H, becomes

$$q_H = K_M\Delta T + n\alpha T_H I - \frac{1}{2}I^2 R_M \tag{3.27}$$

and the rate of heat transfer at the cold junction of the entire module, q_C, may be expressed

as

$$q_C = K_M \Delta T + n\alpha T_C I + \frac{1}{2}I^2 R_M. \tag{3.28}$$

3.1.3 Power and Efficiency Equations

The optimal design of a TEM would maximize its output power P_O or thermal efficiency η_t while minimizing its cost. The system level cost of the TEM includes the extra weight the generator adds to the plant as a result of its density and volume as well as the financial cost of the thermoelectric materials. A generator's thermal efficiency

$$\eta_t = \frac{P_O}{q_H} \tag{3.29}$$

is the ratio of the generator's output power to the rate of its input power q_H. From the first law of thermodynamics, the generator's output power can be obtained by finding $P_O = q_H - q_C$ from Eq. (3.27) and Eq. (3.28), giving

$$P_O = n\alpha I \Delta T - I^2 R_M, \tag{3.30}$$

where $n\alpha$ is the Seebeck coefficient of the entire module.

Considering the output power P_O in relation to the output current I and the resistive load R_L of the generator, as shown in the circuit in Fig. 3.3, gives an output power of

$$P_O = I^2 R_L. \tag{3.31}$$

Equating Eq. (3.30) and Eq. (3.31) gives the current produced by the TEM [45]

$$I = \frac{n\alpha \Delta T}{R_M + R_L}. \tag{3.32}$$

63

The numerator in Eq. (3.32) is the open circuit voltage V_0 of the TEM given Ohm's law $V = IR$ or $I = \frac{V}{R}$ so

$$V_0 = n\alpha\Delta T. \tag{3.33}$$

The current from the generator can then be defined as the generator's open circuit voltage divided by the total current resistance, which is the sum of the load resistance R_L and the module's internal resistance R_M.

Substituting Eq. (3.27) and Eq. (3.31), the generator's thermal efficiency in Eq. (3.29) can be written as

$$\eta_t = \frac{I^2 R_L}{K_M \Delta T + n\alpha T_H I - \frac{1}{2} I^2 R_M}. \tag{3.34}$$

This thermal efficiency can be written in terms of the module's figure of merit Z to show the relationship between Z and η_t. A thermoelectric figure of merit can be determined for either a thermoelectric material or a thermoelectric device, such as a TEM. The calculation of Z depending on the

The figure of merit used here is defined for the entire module, unlike the figure of merit in Eq. (3.2) which is defined for comparing thermoelectric properties of different n-type and p-type semiconductor materials at the same operating temperature.

The figure of merit for the entire module is defined as

$$Z = \frac{(n\alpha)^2}{R_M K_M} \tag{3.35}$$

which uses the module's Seebeck coefficient $n\alpha$, and considers the module's geometry in the electrical resistance R_M and thermal conductance K_M, shown in Eq. (3.25) and Eq. (3.26).

The thermal efficiency in Eq. (3.34) can be written in terms of Z by first substituting

64

for I from Eq. (3.32) to give

$$\eta_t = \frac{\frac{n^2\alpha^2\Delta T^2}{(R_M+R_L)^2}R_L}{K_M\Delta T + n\alpha T_H\frac{n\alpha\Delta T}{R_M+R_L} - \frac{1}{2}\frac{n^2\alpha^2\Delta T^2}{(R_M+R_L)^2}R_M} \tag{3.36}$$

which simplifies to

$$\eta_t = \frac{n^2\alpha^2\Delta T^2 R_L}{K_M\Delta T(R_M+R_L)^2 + n^2\alpha^2 T_H\Delta T(R_M+R_L) - \frac{1}{2}n^2\alpha^2\Delta T^2 R_M}. \tag{3.37}$$

The ratio of the load resistance of the TEG to the module's resistance can be designated as $x = \frac{R_L}{R_M}$ which allows for the substitution $R_L = xR_M$ in Eq. (3.37) to give

$$\eta_t = \frac{n^2\alpha^2\Delta T^2 x R_M}{K_M\Delta T R_M^2(1+x)^2 + n^2\alpha^2 T_H\Delta T R_M(1+x) - \frac{1}{2}n^2\alpha^2\Delta T^2 R_M}. \tag{3.38}$$

Dividing all terms by $n^2\alpha^2\Delta T^2 R_M$ gives

$$\eta_t = \frac{x\Delta T}{\frac{K_M R_M}{n^2\alpha^2}(1+x)^2 + T_H(1+x) - \frac{1}{2}\Delta T} \tag{3.39}$$

which can be written as

$$\eta_t = \frac{x\Delta T}{\frac{(1+x)^2}{Z} + T_H(1+x) - \frac{1}{2}\Delta T} \tag{3.40}$$

$$= \frac{Zx\Delta T}{(1+x)^2 + ZT_H(1+x) - \frac{1}{2}Z\Delta T}. \tag{3.41}$$

If the resistance ratio x, the hot side temperature T_H, and the temperature gradient ΔT all remain unchanged in Eq. (3.41), an increase in Z will increase the module's thermal

65

efficiency. From Eq. (3.35) it can be seen that Z increases as the product $R_M K_M$ decreases.

Research in thermoelectric materials seeks to increase Z by decreasing the material properties of electrical resistivity ρ and thermal conductivity λ and by optimizing the geometry of the module's n-type and p-type elements. The expression $R_M K_M$ is defined as

$$R_M K_M = n \left(\frac{\rho_n}{\gamma_n} + \frac{\rho_p}{\gamma_p} \right) + n \left(\lambda_n \gamma_n + \lambda_p \gamma_p \right) \tag{3.42}$$

$$R_M K_M = n^2 \left[\lambda_n \rho_n + \lambda_n \gamma_n \frac{\rho_p}{\gamma_p} + \lambda_p \gamma_p \frac{\rho_n}{\gamma_n} + \lambda_p \rho_p \right]. \tag{3.43}$$

Considering only the geometry of the module, since only limited changes can be made to the material properties ρ and γ, the geometry ratio $\frac{\gamma_n}{\gamma_p}$ can be determined which minimizes $R_M K_M$ for given material properties. The derivative of Eq. (3.43) with respect to $\frac{\gamma_n}{\gamma_p}$ is

$$\frac{d \left(R_M K_M \right)}{d \left(\frac{\gamma_n}{\gamma_p} \right)} = n^2 \left[\gamma_n \rho_p - \gamma_p \rho_n \left(\frac{\gamma_n}{\gamma_p} \right)^{-2} \right] \tag{3.44}$$

which, set equal to zero, gives the geometry ratio minimizing $R_M K_M$ as

$$\frac{\gamma_n}{\gamma_P} = \left(\frac{\lambda_p \rho_n}{\lambda_n \rho_p} \right)^{\frac{1}{2}}. \tag{3.45}$$

Commercially available thermoelectric modules are designed to optimize the geometry of the n-type and p-type elements to give the maximum possible efficiency over a certain temperature range. With the optimum geometry, a TEG can be designed for maximum power depending on the resistance ratio $x = \frac{R_L}{R_M}$.

The conditions necessary for maximizing TEG output power is found by substitut-

66

ing Eq. (3.32) into Eq. (3.31) to get the generator's output power as

$$P_O = \left(\frac{n\alpha\Delta T}{R_M + R_L} \right)^2 R_L. \tag{3.46}$$

In terms of the resistance ratio $x = \frac{R_L}{R_M}$, the output power can be written as

$$P_O = \frac{(n\alpha\Delta T)^2}{\left(1 + \frac{R_L}{R_M}\right)^2} \frac{R_L}{R_M^2} = \frac{(n\alpha\Delta T)^2 \, x}{(1 + x)^2 \, R_M}. \tag{3.47}$$

The resistance ratio which maximizes the output power is found by differentiating Eq. (3.47) with respect to x to get

$$\frac{dP_O}{dx} = \frac{R_M \, (1 + x)^2 \, (n\alpha\Delta T)^2 - 2x R_M \, (1 + x) \, (n\alpha\Delta T)^2}{R_M^2 \, (1 + x)^4}. \tag{3.48}$$

Setting this derivative equal to zero yields

$$R_M \, (1 + x)^2 \, (n\alpha\Delta T)^2 - 2x R_M \, (1 + x) \, (n\alpha\Delta T)^2 = 0 \tag{3.49}$$

which factors into

$$R_M (1 + x) \, (n\alpha\Delta T)^2 \, [1 - x] = 0. \tag{3.50}$$

Solving for x, the ratio of the load resistance to the module resistance which maximizes the power is found to be

$$x = \frac{R_L}{R_M} = 1, \tag{3.51}$$

meaning that maximum power occurs when the load resistance of the system equals the internal resistance of the module, $R_M = R_L$. The thermal efficiency of the module at

maximum power is found by substituting $x = 1$ into Eq. (3.41), which simplifies to

$$\eta_{t(P_{O\max})} = \frac{Z\Delta T}{4 + 2ZT_H - \frac{1}{2}Z\Delta T}. \tag{3.52}$$

By dividing all terms in Eq. (3.52) by ZT_H, the thermal efficiency at maximum power is often given as

$$\eta_{t(P_{O\max})} = \frac{\frac{\Delta T}{T_H}}{\frac{4}{ZT_H} + 2 - \frac{1}{2}\frac{\Delta T}{T_H}}. \tag{3.53}$$

When the module is operating at its maximum power, the current and power can be calculated by using the relationship $R_M = R_L$ from Eq. (3.51). Substituting for R_L in Eq. (3.32) and Eq. (3.46) gives the current $I_{P_{max}}$ at maximum power as

$$I_{P_{max}} = \frac{n\alpha\Delta T}{2R_M} \tag{3.54}$$

and the maximum power P_{max} as

$$P_{max} = \frac{n\alpha\Delta T}{4R_M}. \tag{3.55}$$

3.2   Diesel Engine Waste Heat Recovery

The spark and compression ignition engines are ideal platforms for waste heat recovery especially for stationary installations where weight is not an issue for fuel economy. The mean exhaust temperature in a diesel engine has been stated to be $550°$C as compared to $990°$C in a gasoline engine [46]. This temperature differential is due to the greater expansion of combusted gases in a compression ignition engine which requires larger combustion cylinders. Diesel engines, with their larger compression ratios, are considered to be one of

68

the most efficient types of internal combustion engines. Although the diesel engine is of necessity larger and heavier than a gasoline engine, the lower fuel consumption and larger power stroke of the diesel engine, make it an important power source.

The complex nature of combustion, affected by engine design and varying combustion processes, makes accurate diesel engine modeling an area of ongoing research. A detailed understanding of fluid dynamics during combustion, influenced by the injection type, injector and fuel pump design, combustion chamber design, and intake manifold features typically requires analysis using computational fluid dynamics (CFD). A detailed understanding of the combustion process is then contingent on advanced CFD algorithms.

A less detailed analysis may be performed by a heat release model, classified as a zero-dimensional thermodynamic model, which does not consider fluid dynamics in combustion. This type of model, though simpler, is considered to provide significant combustion process information, although accurate physical engine operating information is needed for the analysis [46].

Application of this heat release model to the diesel engine is considered more straight forward than for a spark ignition (SI) engine because it allows for a single zone model which considers the open system control volume to be the combustion cylinder when both the intake and exhaust valves are closed [47]. Applying the first law of thermodynamics to the control volume shown in Fig. 3.4 gives the equation

$$dU = \delta Q_C - \delta Q_L - \delta W - \Sigma \dot{m}_i h_i \tag{3.56}$$

where the rate of change of internal energy in the system dU equals the rate of heat transfered into the system δQ_C minus the rate of heat transfered out of the system δQ_L, the rate of mechanical work done by the system δW, and the total mass transfer into and out of the control volume at mass flow rate $\dot{m}_i$ and enthalpy h_i, summed over discrete crank-angle

69

increments.
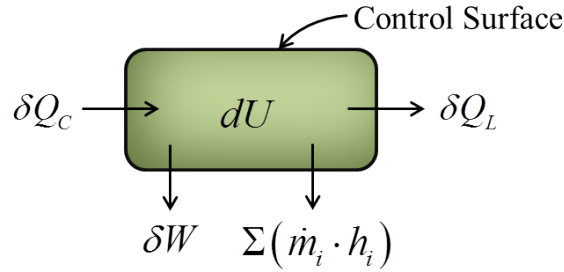
Figure 3.4: A single-zone, zero-dimensional thermodynamic model for a diesel engine applies the first law of thermodynamics to the control volume with internal energy U, work W, mass transfer $\dot{m}_i h_i$, and heat Q (input and losses)

The heat release during combustion δQ_C can be evaluated using Eq. (3.56) by considering combustion to occur at a uniform rate and expressed in terms of crank-angle position. During combustion, the cylinder contents are considered to be a spatially homogeneous mixture of fuel, combustion products, and air with uniform pressure and temperature. The average temperature T in the cylinder can be expressed from the ideal gas law as

$$T = \frac{pV}{mR} \tag{3.57}$$

where V is cylinder volume at the corresponding pressure p, m is the mass of the cylinder charge, and R is the universal gas constant. This approach neglects changes in the liquid fuel due to vaporization. Differentiating Eq. (3.57) to find the temperature change at each instance, the internal energy of the control volume at each instance can be calculated from

$$dU = m_c c_v dT \tag{3.58}$$

for the cylinder mass m_c and specific heat at constant volume c_v [48].

The rate of mechanical work can be determined from physical cylinder pressure

70

engine data and the corresponding cylinder volume in terms of crank-angle degree

$$\delta W = pdV. \tag{3.59}$$

The total enthalpy transfer in the control volume is mainly due to fuel mass entering the system with some additional enthalpy due to piston blow-by. The enthalpy from fuel entering the system may be accounted using physical data for the fuel injection duration, quantity, and temperature. A crevice-flow model is necessary for estimating enthalpy due to piston-blow by [46]. The temperature and composition of the fuel affect the cylinder firing pressure, injection timing and characteristics, emissions, and exhaust temperature to name a few. Accounting for the fuel composition in the combustion analysis may be accomplished using chemical equilibrium programs or by expressing properties in terms of the mole fractions of the fuel components [47].

The heat lost to the cylinder walls is considered difficult to measure due to the unknown distribution of carbon particulate radiation during combustion. For newer diesel engines, radiation is considered to account for only 15% of the total heat transfered to the cylinder walls. A correlation by Woschni [48] is commonly used which includes a radiation term in the convective heat transfer coefficient h_c,

$$q_L = h_c A_c (T - T_w) \tag{3.60}$$

where A_c is the cylinder surface area, T is the mass average gas temperature, and T_w is the temperature of the wall surface area. The expression for h_c, which requires engine and test condition data such as the bore size, displacement volume, average piston speed, and reference values of the cylinder pressure, volume, and temperature at intake valve closing, may be found in a text on combustion engineering [48].

For proper combustion analysis using a zero-dimensional model, all sources state

71

the necessity of accurate experimentally obtained pressure versus crank angle data. Foster stresses the necessity of the data in order to perform a diagnostic combustion analysis as opposed to a predictive analysis, where a 1% error in the pressure measurement can cause approximately 50% error in the resulting heat release [47]. Hsu remarks on many of the difficulties assosicated with obtaining accurate pressure data [46]. It is necessary to have a high frequency response flush mounted pressure transducer, in which the transducer face is directly exposed to the cylinder pressure as opposed to a transducer which is mounted on the other side of an air duct passage drilled in the engine cylinder. The passage mounted transducer is not accurate for rapidly changing pressure measurements and is subject to a pressure wave resonating in the air duct.

A piezoelectric pressure transducer may often be subjected to a phenomenon called "thermoshock" which occurs when the large temperature range in the cylinder can cause the transducer to misread. To correct for this, Hsu suggests mounting two transducers of different makes in the same cylinder [46]. Also to account for drift of the transducer, it is necessary to provide a reference baseline from atmospheric pressure or an average of the inlet and exhaust manifold pressures.

To obtain useful cylinder pressure data for use in combustion analysis for a specific operating condition, many cycles of cylinder pressure must be collected and the pressures of each cycle averaged at corresponding crank-angle positions, referred to as "synchronous averaging" [46].

Since pressure is given in terms of crank-angle position, an accurate, high frequency measure of the crank-angle for each cylinder is required. A single encoder can measure crank shaft rotation if the cylinder timing is known, or encoders may be used to measure each cylinder. To make sure the encoder reading and cylinder position are synchronized, the encoder should be aligned to TDC or BDC of the cylinder. From the known cylinder geometry and the related crank-angle position, the cylinder volume with respect to the

72

crank angle may be determined and related to its corresponding pressure measurement.

3.3   Experimental System

The thermoelectric waste heat system (TWHS) is directly attached to the exhaust line of a diesel engine to minimize the introduction of additional back pressure. The hot side of the temperature gradient, T_H is provided by the heated surface of the TWHS warmed directly by the exhaust gases.

3.3.1   Physical System Characteristics

A Briggs and Stratton Daihatsu four-cycle, three cylinder, 679cc, liquid-cooled diesel engine, model 432447 was used in the experimental test. The engine, pictured in Fig. 3.5, is directly coupled to a Haldex hydraulic gear pump, model 2102727, used in conjunction with a hydraulic brake dynomometer manufactured by International Dyno, model 500. The gear pump has a one-to-one coupling with the engine crankshaft using a heavy duty jaw coupling and rubber spider. Both the engine and the dynomometer are mounted on a heavy duty aluminum cart to allow for the test unit to be moved. Steel supports mounted to a heavy steel plate support the engine while adding weight to the cart to reduce vibration.

The dynomometer and gear pump supply the engine load by providing resistance to the rotation of the engine's crankshaft. Reducing the size of the dynomometer's load valve opening increases the hydraulic fluid pressure, thereby increasing the engine load. A 10% decrease in hydraulic pressure produces an approximate 10% increase in engine speed. A permanent by-pass in the dynomometer ensures that the hydraulic flow cannot be completely shut off. The manufacturers' specifications for the system are listed in Table 3.1.

The TWHS was made of 0.625cm thick steel to securely hold 4 modules manufactured by Tellurex, part G2-56-0375. To ensuring no module motion due to vibration during

73
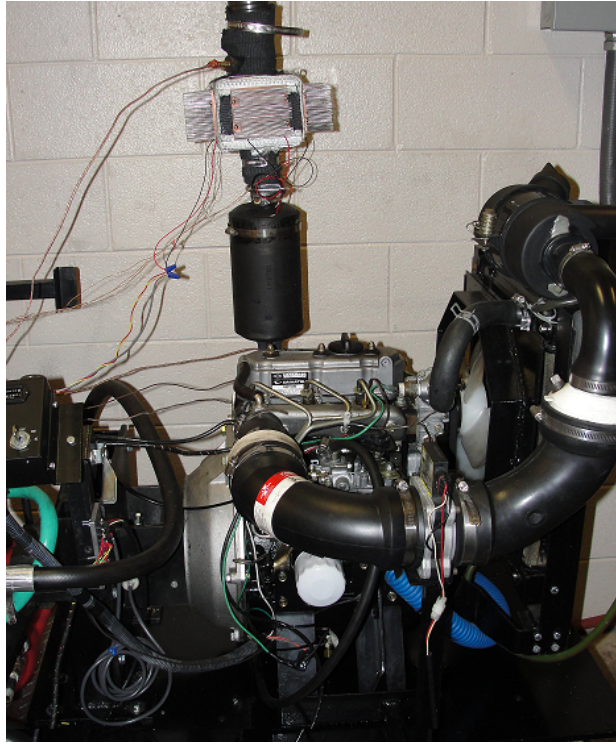
Figure 3.5: Waste heat was generated by a three-cylinder four-cycle Daihatsu diesel engine with the load supplied by an International Dyno dynomometer. The insulated TEG unit with finned heat sinks is attached in line with the engine exhaust after the muffler

| (a) | (b) |
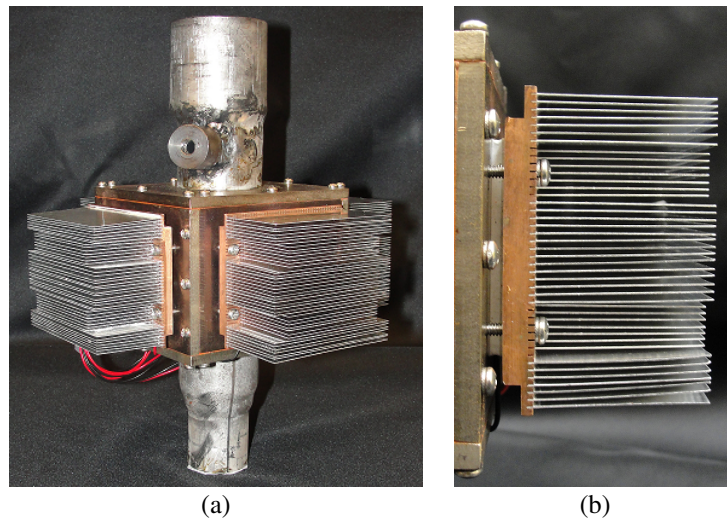
Figure 3.6: The thermoelectric generator is (a) constructed of steel to attach 4 thermo-electric modules with hot side warmed by the diesel engine exhaust, and (b) the cold side attached to individual finned heat sinks

74

testing, the surface of the TWHS was milled out to an approximate 0.826mm depth and module dimensions. The milled out surface was then polished to improve heat transfer.

The modules are produced with a soft thermal interface, but because the thermal coating is easily scratched, thermal paste was applied to both sides. Heat transfer on each module's cold side was aided by a passive aluminum finned copper heat sink, Supermicro SNK-P0007. The TWHS with modules and heat sinks attached is pictured in Fig. 3.6(a) and (b).

During testing it was found that two high speed industrial fans needed to be applied to avoid reaching the module's maximum cold side temperature of $100°C$. Fiberglass exhaust insulation wrap was then used around the modules to maintain the temperature of the entire unit.

3.3.2 Instrumentation

The engine and TWHS is equipped with various sensors to monitor the overall operation. The throttle position on the fuel injector pump is measured by a potentiometer powered by an external 15VDC power supply. An Omron 3-wire proximity switch, part number E2E2-X10C1, powered by the external 15VDC power supply measures the crankshaft speed.

Ten thermocouples, type J and K, measure the system temperatures. The exhaust temperature is recorded approximately 7.6cm and 56.4cm from the exhaust manifold, with the later temperature taken 5.08cm after the TWHS. The ambient temperature is taken approximately 183cm away from the engine block, and the air intake temperature is recorded approximately 127cm from the intake nozzle to the air cleaner and 10.2cm from the intake manifold. The engine coolant temperature is recorded 7.6cm after the engine thermostat and 50.8cm after the radiator outlet (before it enters the engine).

Table 3.1: System Specifications: Diesel Engine, Thermoelectric
Modules, and Heat Sink

Specification	Value or Characteristic
Engine Specifications	
Piston displacement	697cc
Bore $\times$ stroke	68mm $\times$ 64mm
Compression ratio	25.0:1
Gross power at 3600RPM	14,541W
Gross torque at 2400RPM	3.67N·m
Combustion chamber	Swirl type
Injector nozzle	Throttle type
Thermoelectric Waste Heat System Specifications	
Total mass	6.31kg
Total height	29.85cm
Total dimensions (L$\times$W)	$(23.495 \times 22.23)\text{cm}^2$
Thermoelectric Module Specifications	
TE material	Bi-Te based
Dimensions (L$\times$W$\times$H)	$(5.6 \times 5.6 \times 0.43)\text{cm}^3$
Peak continuous temperature	320°C
Maximum heat rejection side temperature	100°C
Specifications at $T_C = 50°\text{C}$ and $T_H = 250°\text{C}$	
Max power output, $P_{\max}$	14.1W
Voltage at max power, $V_{P_{\max}}$	4.2V
Current at max power, $I_{P_{\max}}$	3.4A
Resistance of module, R_M	1.2Ω
Open circuit voltage, V_0	8.4V
Module Seebeck coefficient, $n\alpha$	0.042V/K
Heat Sink Specifications	
Fin material	Aluminum
Number of fins	42
Fin dimensions (L$\times$H)	$(4.32 \times 8.89)\text{cm}^2$
Fin width	0.76mm
Base material	Copper
Base dimensions (L$\times$W)	$(6.35 \times 8.89)\text{cm}^2$
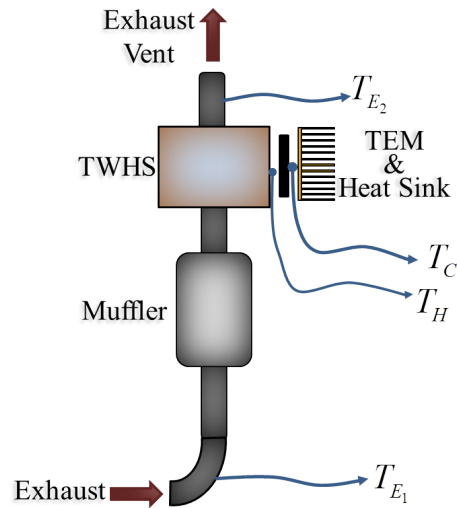
Figure 3.7: Schematic of exhaust and thermoelectric waste heat system (TWHS) with attached thermocouples for measuring system temperatures

Two small gauge thermocouples were used to measure the hot side surface temperature of the TWHS. The average cold side temperature of the thermoelectric modules was found by two small gauge thermocouples mounted between the module's cold side the the attached heat sink. A schematic of the system with location of temperature measurements is given in Fig. 3.7.

The DAQ system is a dSpace controller board DS1103 and a CLP1103 connector panel which works with ControlDesk version 3.2.2 and Matlab/Simulink. The analogue outputs of the throttle position sensor and the proximity switch are connected to the connector panel by BNC connectors. To avoid damaging the DAQ system, a voltage divider steps down the voltage of the proximity switch before connecting the signal to the connector panel.

Each thermocouple is used with a corresponding thermocouple signal conditioner, Omega part numbers OM5-LTC-K2-C and OM5-LTC-J2-C, which are connected to an Omega backplane, part OM5-BP-16. A ribbon cable connects the isolated, linearized, and amplified thermocouple signals to the dSpace connector panel. An Omega high accuracy

77

digital thermometer, model HH-23A, with approximate $(0.1\% \times \text{Reading})^\circ\text{C}$ accuracy, was used to calibrate the thermocouple modules.

The power output of the individual and combined TE modules was determined by recording the output voltage and current. The voltage across the TEG leads was connected to the DAQ connector panel by a BNC connector. The current output of the TEG was first attempted by taking the voltage reading across a $R = 0.01\Omega$ current sense resistor. However, the two voltage readings taken off of the TEG output created a ground loop in the DAQ system. To keep the voltage and current readings independent, the current was recorded externally.

3.4 Numerical and Experimental Results

To determine how well the thermoelectric modules generate power from diesel engine exhaust, the engine exhaust temperatures T_{E_1} and T_{E_2} and thermoelectric hot side temperature T_H were determined for different throttle positions over a range of engine speeds. The open loop (no load) voltage of a single module v_0 and four modules connected in series V_0 were found experimentally over the temperature range and used to determine the module's Seebeck coefficient $n\alpha$ at steady-state operating temperatures. While T_H and T_C were approximately constant, the available power output P_O of the generator was determined by relating voltage V to current I for a range of load resistances R_L applied by a variable resistor. The system temperatures and operating conditions for these tests are listed as Tests 1–5 in Table 3.3, Test 6 in Table 3.4, and Test 7 in Table 3.4.

3.4.1 Engine Values (Tests 1–5)

The ideal engine operating state was determined based on the engine's output temperatures recorded over a range of engine speeds and throttle positions. The exhaust tem-

78

peratures 7.6cm and 56.4cm from the exhaust manifold, T_{E_1} and T_{E_2}, as mentioned in Section 3.3.2 (Instrumentation), were compared to the related coolant temperatures before and after the radiator, T_{R_1} and T_{R_2}, respectively, to ensure that the engine speed was allowing adequate time for the gear driven coolant pump to circulate the coolant through the radiator.

As expected, increasing the throttle position and the engine speed increases the exhaust temperature. It was determined from the engine temperatures, that the best conditions for engine operation with the highest temperatures for waste heat recovery was at throttle positions between wide open throttle (WOT) and 75% of WOT at engine speeds of (1500–1800)RPM. Maximum temperatures at these conditions are listed in Table 3.2 with the average temperatures over steady state operation for the tested engine speeds and throttles given in Table 3.3.

Table 3.2: Maximum Values of Experimental System Data

Parameter	Maximum Value
Exhaust 7.6cm from manifold, T_{E_1}	501.3°C
Exhaust 56.6cm from manifold, T_{E_2}	358.3°C
Hot side of TEG, T_H (without TEMs, heat sink, and forced convection)	203.8°C
Hot side of TEG, T_H (with TEMs, heat sink, and forced convection)	139.3°C
Cold side of TEG, T_C (with TEMs, heat sink, and forced convection)	92.6°C
Temperature gradient, ΔT	60.1°C
Coolant exiting engine, T_{R_1}	73.4°C
Coolant exiting radiator, T_{R_2}	67.1°C
Ambient, T_∞	31.1°C

Data from Tests in Table 3.3 without forced air or attached TEMs or heat sinks, except where noted

Table 3.3: System Operation for Engine Speeds
and Throttle Positions

Test No.	Description	Speed (RPM)	Pressure (PSI)	Pressure (kPa)	T_{E_1} (°C)	T_{E_2} (°C)	T_H (°C)	T_∞ (°C)	T_{R_1} (°C)	T_{R_2} (°C)
25% of WOT (Test run from smaller to larger load)									
1.1	Racing	1714	200	1379	246.0	169.0	101.8	20.6	60.4	23.0
1.2	Racing	1714	225	1551	267.4	183.6	113.2	21.7	60.7	24.0
1.3	Racing	1714	250	1724	282.5	198.5	124.5	22.6	61.5	25.3
1.4	Racing/ Smooth	1667	300	2068	319.0	221.5	136.3	24.1	63.3	28.4
1.5	Smooth	1604	350	2413	345.2	235.1	149.0	24.6	64.7	31.8
1.6	Smooth	1538	375	2586	365.0	244.1	157.3	25.7	65.9	35.0
1.7	Lean/ Smooth	1316	375	2586	353.5	234.2	160.4	26.0	66.7	36.3
1.8	Lean	1000	350	2413	334.1	213.4	153.5	26.9	69.1	36.0
50% of WOT (Test run from smaller to larger load)									
2.1	Racing	1935	425	2930	490.7	345.4	193.9	32.4	71.3	63.2
2.2	Smooth	1714	400	2758	433.1	312.0	208.2	31.8	69.2	54.5
2.3	Smooth	1538	375	2586	383.5	273.7	198.3	31.1	68.2	45.7
2.4	Smooth/ Lean	1304	300	2068	347.3	243.0	181.9	30.8	69.2	44.2
2.5	Lean	1053	300	2068	297.4	206.8	163.4	30.1	69.8	41.1
2.6	Lean	1000	325	2241	331.7	212.3	155.3	30.1	70.9	41.6
50% of WOT (Test run from larger to smaller load)									
3.1	Lean	1000	340	2413	344.5	204.7	119.0	28.5	70.2	38.3
3.2	Lean	1277	360	2413	357.1	225.0	136.1	29.5	69.2	40.5
3.3	Smooth	1556	375	2586	384.2	249.5	153.2	30.1	68.2	42.2
3.4	Smooth	1667	400	2758	414.3	281.7	168.7	31.1	68.3	45.0
3.5	Smooth/ Racing	1818	420	2758	452.7	326.5	187.2	33.2	69.4	51.6
3.6	Racing	1935	400	2758	468.1	344.5	202.8	34.7	72.8	66.2
75% of WOT (Test run from smaller to larger load)									
4.1	Racing	1935	475	3275	494.1	349.2	171.7	35.2	73.2	66.6
4.2	Smooth	1765	400	2758	456.8	324.9	198.1	35.6	73.6	66.6
4.3	Smooth	1538	390	2758	407.7	290.3	197.9	34.5	71.5	60.0
4.4	Lean	1277	350	2413	362.3	253.1	184.0	33.1	70.2	48.8
4.5	Lean	1034	345	2413	342.2	226.1	169.2	32.9	71.4	47.0
WOT (Test run from larger to smaller load)									
5.1	Lean	1034	350	2413	346.4	221.6	158.6	32.4	71.4	46.2
5.2	Lean	1277	375	2586	373.4	240.6	161.2	33.0	71.0	47.2
5.3	Smooth	1500	390	2689	400.9	262.3	173.4	33.9	70.3	49.4
5.4	Smooth	1765	400	2758	456.2	313.5	180.7	34.4	70.1	52.9
5.5	Racing	1935	400	2758	491.2	358.1	205.0	35.9	72.7	66.8

Tested without TE modules, heat sinks, or forced air
Average temperatures given of steady state operation for each test

Exhaust insulation wrap was applied to the exhaust line after the exhaust manifold in attempts to increase the surface temperature T_H of the TWHS. This resulted in an increased T_{E_1} temperature by $20°$C but the increased exhaust temperature did not increase T_H. This is assumed to be due to the increased exhaust flow rate resulting from the increased exhaust temperatures. In testing the TEG power output, only the insulation applied to the TWHS was used.

As can be seen in Table 3.2 by the comparison of T_{E_1} and T_{E_2} which are approximately 48.8cm from each other, a TWHS should be positioned close to the exhaust manifold to avoid heat loss from the exhaust pipe. A significant amount of heat is transferred through the TEG modules, as can be seen by the maximum T_C. This requires positioning the TEG where the heat rejected from the cold side of each TEM will not affect the surroundings. Designs which reject the heat from the cold side to the engine coolant, such as proposed in [39], would have to ensure that the increased coolant temperatures are still sufficient for engine cooling.

3.4.2 Single Module Power (Test 6)

The capabilities of the engine at producing power was first determined by checking the power output of a single module. The module's open circuit voltage v_0 was taken over a time sample in which the engine throttle and speed were increased to approximate steady state values of T_H and T_C at the desired operating conditions. The operating conditions, system temperatures, and the module's open circuit voltage over the time sample are shown in Fig. 3.8. Comparing ΔT and v_0 shows the dependence of the voltage on the temperature gradient which is related in Eq. (3.33).

At steady state, the resistance R_L in a closed loop circuit was varied to determine the maximum power and internal resistance R_M of the module at the operating temperature.

81

The module voltage and current were recorded with the corresponding load resistance. The data points for voltage, current, and calculated power output are shown in Fig. 3.9(a) with the data curve fit. The system operating conditions for tests 6.1 and 6.2 performed with a single module are summarized in Table 3.4.
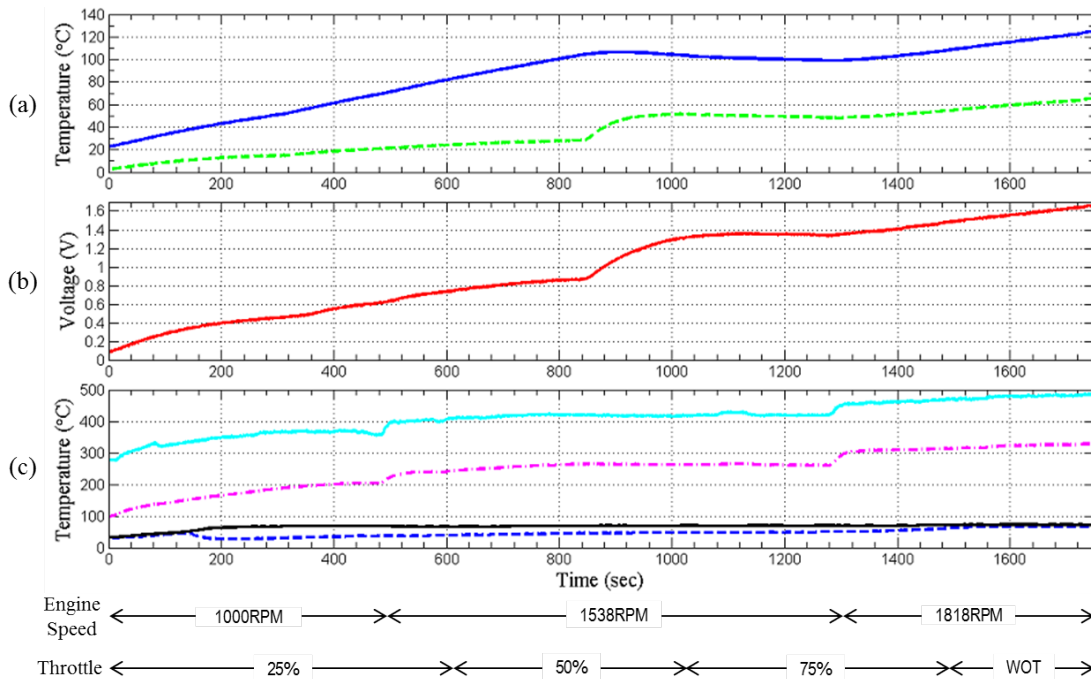
Figure 3.8: The collected data for Test 6.1 on a single module shows the (a) hot side temperature T_H (—), temperature gradient ΔT (- - -) between T_H and T_C, (b) Open circuit voltage v_0, (c) exhaust temperatures T_{E_1} (—) and T_{E_2} (- · -), and radiator inlet T_{R_1} (—) and outlet T_{R_2} (- - -) temperatures versus time

The module's performance curves, provided by the manufacturer, give the module's characteristics for a limited range and combinations of operating conditions. The characteristics of a single module were given for three module cold side temperatures, $T_C = 30°$, $50°$, and $80°$, over a range of T_H. These curves at $T_C = 50°C$ were used to estimate the manufacturer's values for $n\alpha$, v_0, and R_M for T_H close to the experimental system. These values were used to calculate power, current, and voltage from Eq. (3.31), Eq. (3.32), and Ohm's law, respectively, over a range of possible load resistances. The plots of the cal-

82

culations are shown in Fig. 3.9(b) plots (2) and (3). The manufacturer module values and maximum power $P_{\max}$ at current $I_{P_{\max}}$ and voltage $V_{P_{\max}}$ calculated by Eq. (3.54), Eq. (3.55), and Ohm's law are listed in Table 3.6 calculations (2) and (3).

Table 3.4: System Operation for Tests on Single TEG

Test No.	Throttle	Speed (RPM)	T_{E_1} (°C)	T_{E_2} (°C)	T_H (°C)	T_C (°C)	T_∞ (°C)	T_{R_1} (°C)	T_{R_2} (°C)
6.1	Time sample beginning near engine start up for open circuit shown in Fig. 3.8								
6.2*	WOT	1714	453.7	308.9	128.9	62.4	32.7	72.3	65.3
	*Average system temperatures given at constant engine operation.								
	*TEG behavior for various loads recorded in Fig. 3.9(a) and Table 3.5								

The hot side temperature T_H for calculation (2) is close the the hot side temperature for tests run with four modules connected in series in Table 3.8, while T_H for calculation (3) is close to that in the experimental test for the single module in Table 3.5.
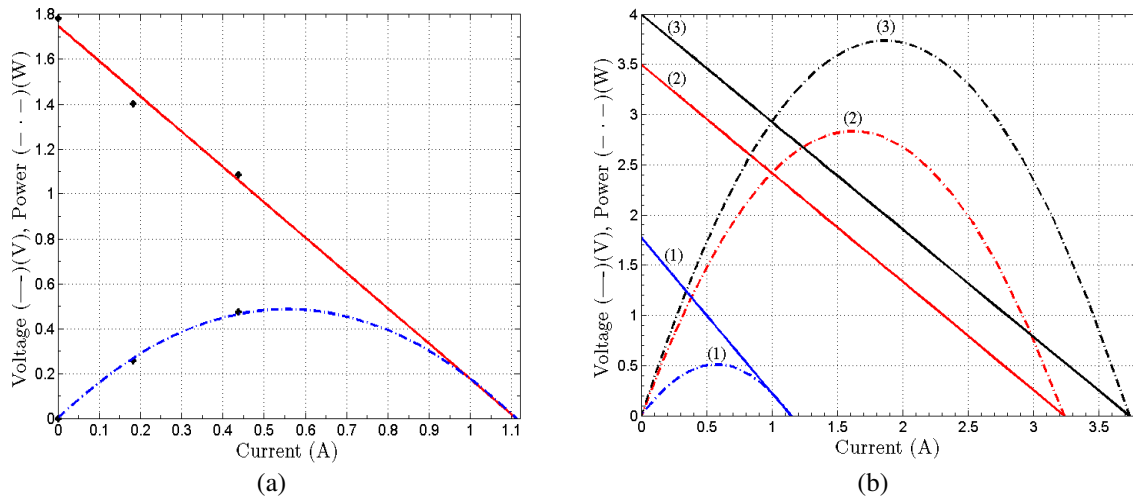
Figure 3.9: Comparison of voltage and power versus current for a single TEM for (a) experimentally determined curves corresponding to data in Table 3.5 and (b) curves numerically derived from experimental data (1) and TE module manufacturer data (2 and 3) using Eq. (3.31) through Eq. (3.33) which correspond to data in Table 3.6

83

Table 3.5: Single Module Experimentally Determined
Maximum Power Values

T_H (°C)	T_C (°C)	ΔT (°C)	$n\alpha$ (V/K)	v_0 (V)	R_M^{**} (Ω)	$V_{P_{\max}}^*$ (V)	$I_{P_{\max}}^*$ (A)	$P_{\max}^*$ (W)
128.9	62.4	66.5	0.0247	1.78	1.55	0.87	0.56	0.49

*Derived from experimental data curve fit

**Calculated from Ohm's law at maximum power

Module characteristics determined experimentally from Test 6.2 in Table 3.4

The experimentally determined Seebeck coefficient $n\alpha$, open loop voltage v_0, and module resistance R_M listed in Table 3.5 were also used in Eq. (3.31), Eq. (3.32), and Ohm's Law to determine the effectiveness of these equations at representing the experimental system. The plots of this power and voltage versus current are shown in Fig. 3.9(b) plot (1). The maximum power calculations based on experimentally determined module data are given in Table 3.6 calculation (1).

Table 3.6: Single Module Numerically Determined
Maximum Power Values

No.	T_H (°C)	T_C (°C)	ΔT (°C)	$n\alpha$ (V/K)	v_0^* (V)	R_M (Ω)	$V_{P_{\max}}^*$ (V)	$I_{P_{\max}}^*$ (A)	$P_{\max}^*$ (W)
(1)	128.9	62.4	66.5	0.0247	1.78	1.55	0.90	0.57	0.52
(2)	125	50	75	0.0470	3.5	1.08	1.77	1.61	2.84
(3)	137.5	50	87.5	0.0457	4.0	1.07	2.03	1.84	3.74

*Calculated using Eq. (3.33), Ohm's law at maximum power, Eq. (3.54), and Eq. (3.55)

(1) Module characteristics from experimentally determined values in Table 3.5

(2) & (3) Module characteristics from manufacturer

At the operating temperatures given in Table 3.5, the module's internal resistance was determined to be 1.55Ω based on the equality of the load resistance and module resistance at maximum power. The maximum power and current measured during experimental

testing were 0.47W and 0.437A while the maximum possible power predicted by the curve fit to the experimental data was 0.49W at 0.56A. Data points at higher current could not be tested due to the physical limitations of lowering the load resistance while still providing enough resistance to measure current.

3.4.3 Series Module Power (Test 7)
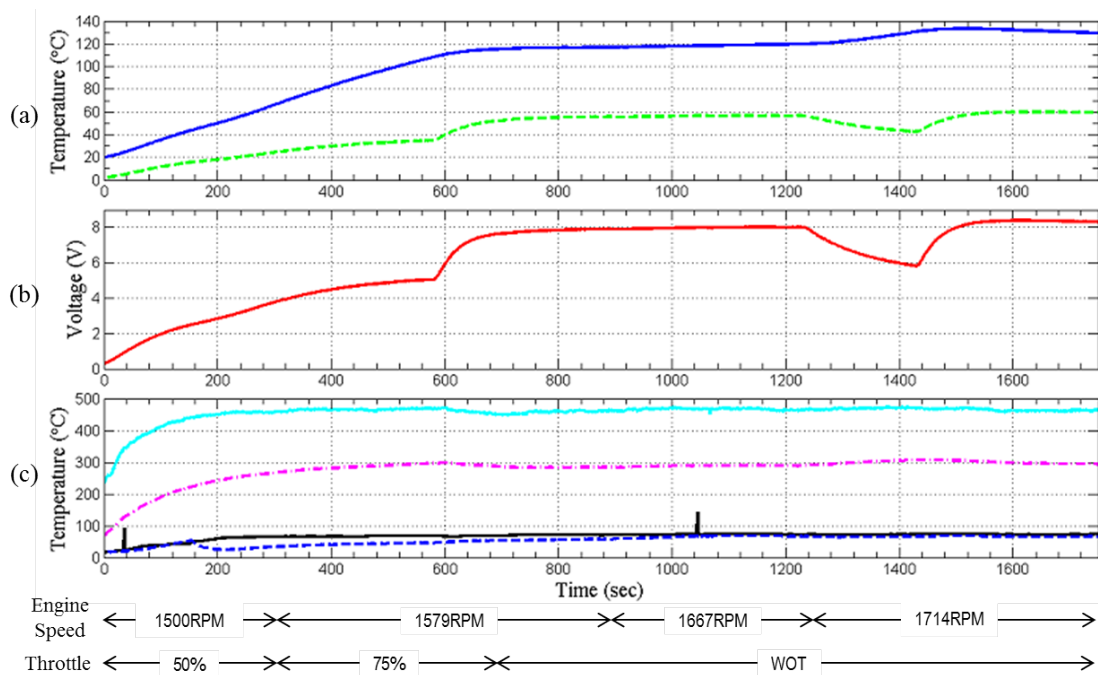
Figure 3.10: The collected data for Test 7.1 on 4 modules connected in series shows the (a) average hot side temperature T_H (—) of the modules, temperature gradient ΔT (- - -) between T_H and T_C, (b) Open circuit voltage V_0, and (c) exhaust temperatures T_{E_1} (—) and T_{E_2} (- · -) and radiator inlet T_{R_1} (—) and outlet T_{R_2} (- - -) temperatures versus time

A series connection was tested for producing maximum power output with use of four modules at the available temperature. The open loop voltage of the modules in series was recorded over a time sample in which the throttle position and engine speed were increased to the desired operating conditions. The temperature data of the engine and TWHS are shown with the related open circuit voltage over the time sample in Fig. 3.10.

85

The system's operating conditions and temperatures for Test 7 on four modules connected in series are listed in Table 3.7.

The maximum power of the series arrangement and its total module resistance were determined by comparing the voltage and current in a closed loop circuit over various load resistances at steady T_H and T_C. The data points and the projected power and voltage curves versus current are shown in Fig. 3.11(a). The maximum power P_{max} at current $I_{P_{max}}$ and voltage $V_{P_{max}}$, derived from the curve fit to the experimental data, is given in Table 3.8.

The maximum power and current obtained during testing were 2.81W and 0.60A at a load resistance of 7.68Ω, while the maximum power projected by the curve fit in Fig. 3.11(a) is 2.91W. This maximum power can be achieved by reconfiguring the circuit to lower the load resistance to the 5.39Ω projected in Table 3.8 for maximum power.

Data from the experimental tests on a single module in Table 3.5 and numerical calculations for the single module with the closest operating conditions in Table 3.6 calculation (2) were applied to the four series connected modules to determine the numerical calculations for the power output of the series connection. For these calculations it was assumed that the Seebeck coefficient for the entire series connections $n\alpha_4$ was four times the Seebeck coefficient of a single module. It was also assumed that the total resistance of the series connection R_{M_4} was four times the resistance of a single module R_M.

The power output, current, voltage, and open circuit voltage V_0 was calculated by Eq. (3.31), Eq. (3.32), Ohm's law, and Eq. (3.33), respectively, over a range of possible load resistances. The plots for the power and voltage versus current are shown in Table 3.11(b). The current at maximum power and the maximum power was calculated by Eq. (3.54) and Eq. (3.55), respectively, for the characteristics estimated for four modules connected in series.

The possibility of using the series connected TEG for charging a battery was tested

86

Table 3.7: System Operation for Tests on Series Connected TEGs

Test No.	Throttle	Speed (RPM)	T_{E_1} (°C)	T_{E_2} (°C)	T_H (°C)	T_C (°C)	T_∞ (°C)	T_{R_1} (°C)	T_{R_2} (°C)
7.1	Time sample beginning near engine start up for open circuit shown in Fig. 3.10								
7.2*	WOT	1714	460.5	299.6	122.6	68.3	30.8	73.7	67.1

*Average system temperatures given at constant engine operation

*TEG behavior for various loads recorded in Fig. 3.11(a) and Table 3.8

(a)　(b)
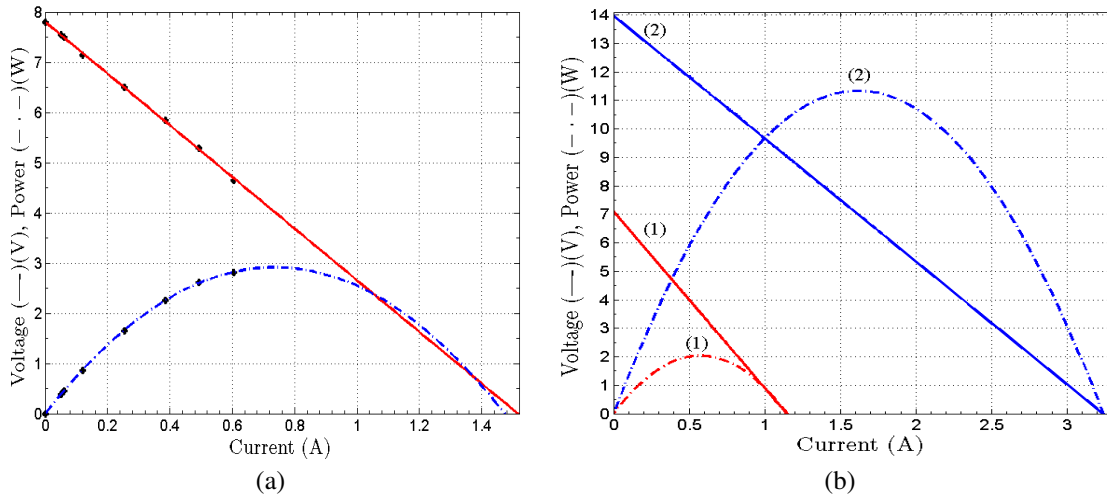
Figure 3.11: Comparison of voltage and power versus current for 4 TE modules connected in series for (a) experimentally determined curves corresponding to data in Table 3.8 and (b) numerically derived curves based on manufacturer data (1) and experimental data from a single module (2) which corresponds to the numerical calculations in Table 3.9

Table 3.8: Four Modules in Series Experimentally Determined
Maximum Power Values

T_H (°C)	T_C (°C)	ΔT (°C)	$n\alpha_4$ (V/K)	V_0 (V)	$R_{M_4}^{**}$ (Ω)	$V_{P_{max}}^*$ (V)	$I_{P_{max}}^*$ (A)	P_{max}^* (W)
122.6	68.3	54.3	0.1477	7.81	5.39	3.99	0.74	2.91

*Derived from experimental data curve fit

**Calculated from Ohm's law at maximum power

Module characteristics determined experimentally from Test 7.2 in Table 3.7

Table 3.9: Four Modules in Series Numerically Determined
Maximum Power Values

No.	T_H (°C)	T_C (°C)	ΔT (°C)	$4 \cdot n\alpha$ (V/K)	V_0^* (V)	$4 \cdot R_M$ (Ω)	$V_{P_{\max}}^*$ (V)	$I_{P_{\max}}^*$ (A)	$P_{\max}^*$ (W)
(1)	128.9	62.4	66.5	0.0988	7.13	6.2	3.75	0.58	2.05
(2)	125	50	75	0.1880	14.1	4.31	7.06	1.63	11.5

*Calculated using Eq. (3.33), Ohm's law at maximum power, Eq. (3.54), and Eq. (3.55)
(1) Module characteristics from experimentally determined values in Table 3.5
(2) Module characteristics from manufacturer in Table 3.6 No. 2

by connecting the power leads to a charge controller connected to a lead acid battery. An LED indication light identified the charging of the battery, however the current and voltage measured over a 44min test sample were found to only range from (0.07–1.36)mA and (1.39–4.95)V, respectively. This was due to the large 53.0kΩ load resistance of the charge controller and the battery, which was not fully charged. Once the battery was charged, the resistance of the charge controller and battery measured an order of magnitude larger at approximately 575kΩ. This larger resistance is due to the circuitry of the charge controller to prevent overcharging a charged battery. To charge a battery at the maximum power output of the thermoelectric module for the hot and cold side operating temperatures requires a charge controller whose resistance equals the internal resistance, R_M, of the TEG.

3.4.4   Variation between Experimental and Numerical Results

The TE materials are considered to be independent of temperature for the derivation of Eq. (3.27) and Eq. (3.28). However, the material properties of thermal conductivity λ, electrical resistivity ρ, and Seebeck coefficient α are dependent on the temperature and the temperature gradient. The temperature dependence of the material properties then requires empirically obtained parameter values for the operating temperatures to calculate power

output of a TEG. This can be seen by comparing the Seebeck coefficients in Table 3.6 for calculation (1) which was determined experimentally and calculation (2) which was estimated from the manufacturers performance curves. The manufacturer's data is 90% greater than the value derived experimentally. Because available TEM performance values are manufacturer specific and considered as maximum possible values [49], the experimentally determined values were repeated over several tests and are considered accurate for this application.

The difference in the experimental data for the series connection in Table 3.8 and the numerical calculation based on the experimental data from the single module in Table 3.9 calculation (1) may be due in part to the varying operating conditions of the diesel engine. The larger Seebeck coefficient for lower operating temperatures and temperature gradient in Table 3.8 implies that using the experimental data of a single module to calculate the power output of a multi-module TEG system will only give an estimate of the true values.

For calculations it was assumed that the TWHS surface temperature is the hot side temperature T_H of the TEM. The thermal contact resistance between the modules and the TWHS faces was not considered. A lower hot side temperature of the TEM due to contact resistance would result in a lower calculated output power. This may account for some of the variation in experimental and calculated values, however thermal paste and pressure applied by the attached heat sink were used to reduce thermal contact resistance.

The thermal conductance of the modules used is not known, therefore the thermoelectric efficiency could not be calculated. In general, manufacturer data on the efficiency of a single TEM composed of BiTe based material is between 3.5–4.5%, which is considered to be a maximum attainable value under strict labratory testing. The actual thermoelectric efficiency is assumed to be much lower. The rate of heat transfer for a single module at the experimental output power of 0.486W for an efficiency of 3.5% would be $q_H = 13.9$W with thermal conductance approximately equal to $K_M = 0.135$W/K.

89

Chapter 4

Conclusion

A mechanical engineering perspective offers the definition of mechatronics to be the integration of electronic, computer, and information technology into dynamic electro-mechanical systems, thereby improving the system's design and allowing the engineer to develop today's integrated technologies [10]. By this definition, knowledge of multiple disciplines is important since it serves to improve the quality of mechanical systems. Many companies take a multi-disciplined approach to engineering in their design of complex integrated systems. This approach then should encourage mechanical engineering academic programs to offer their students hands on experiences in the multiple disciplines included in a basic mechatronics definition.

4.1   Mass–Pendulum System Conclusion

The mass–pendulum laboratory experiment discussed in Chapter 2 provides engineering students an opportunity to model and investigate a coupled dynamics problem while working directly with multiple disciplines in an experimental system. In validating the mathematical model, students gain knowledge simulating non-linear equations, deter-

90

mining physical parameter values, and acquiring and analyzing test data. Use of the electromagnet actuator, provides experience in developing a forcing function to approximate a complex vector field, incorporating the function in a simulation, evaluating the effectiveness of the model, and controlling the actuator. By including a friction force acting on M_1, the derived equations of motion offer a good representation of the physical system for the experimentally determined system parameters. In considering the characteristics of the magnetic field and the physical system, the derived forcing function can be used to simulate the response of the mass-pendulum system actuated by the magnetic field of an electromagnet positioned within 7.5cm of the system's equilibrium position.

Suggestions for Mass-Pendulum Experiment

One of the goals of this interactive bench top laboratory experiment is to promote student investigation into the dynamics and control of the electromagnet excited mass–pendulum system. The physical arrangement of the systems lends itself to several areas of continued research.

- An expansion of the electromagnet control is the development of control logic which incorporates disturbance rejection into the motion of the coupled system. This would increase the complexity of the electromagnet control to identify unacceptable coupled motion and excite the electromagnet to either increase or decrease the motion of M_2. This could be aided by increasing the magnetic strength through a larger number of windings N and current in the electromagnet.

- An increase in the strength of the electromagnet would promote controller development which maintains a chosen maximum amplitude of masses M_1 and/or M_2. This type of controller would be quite complex, possibly basing the control authority on the total kinetic energy of the system rather than the real-time positions of M_1 and

91

M_2. Students would likely be required to control the electromagnet's voltage supply to regulate the strength of the electromagnet by indirectly altering the current. The possibility of this type of control is challenging since isolating the electromagnet's high voltage supply from the DAQ connection panel is necessary to protect the panel.

- The experimental platform can be altered to investigate the effectiveness of a pendulum as both an active and a passive mass damper. This configuration could be achieved by the addition of an actuator to M_1. However, increasing the motion of M_1 may raise the likelihood of damaging the beam load cell used to identify the location of M_1. This possibility could be lowered by adding a second spring attached to the opposite side of M_1 and to the structure. An additional spring would increase the system stiffness and limit the range of motion of M_1 so that it stays within the physical deflection range of the load cell. A slight experimental redesign allowing the weight of M_1 to be altered would promote investigation of the mass ratio relationship between M_1 and M_2 in oscillation damping. The usefulness of the electromagnet in aiding the damping of M_1 could also be studied. For instance, students could be required to analyze the coupled relationship between M_1 and M_2 and incorporate control of the electromagnet into the motion of the system to decrease the motion of M_1.

4.2 Thermoelectric Generator Conclusion

The modern vehicle is the classic example of a mechatronics system with integrated mechanical and electrical systems under computer control. The provision of greater vehicle safety and performance often necessitates an increased electrical demand while improving fuel efficiency. One solution is the production of energy by waste heat recovery using

alternative energy generation. With advances in thermoelectric materials, thermoelectric generators (TEG) offer a potentially effective means for converting waste heat into electric power. The diesel engine is an attractive platform for thermoelectric waste heat recovery since large diesel trucks should be able to handle the added weight of coupled TEG-diesel engine generators plus engines operate at steady-state speed for long periods as they travel the highway.

The temperature dependence of thermoelectric material properties and the published maximum property values specific to different manufacturers should encourage the accompaniment of theoretical analysis of thermoelectric applications with experimental results. The study presented in this thesis determined that useful power can be generated from diesel engine exhaust using a TEG under the right load conditions, although the produced power is lower than the values predicted from manufacturer data.

Suggestions for Waste Heat Recovery by Thermoelectric Generation

The application of thermoelectric generation using waste heat was presented as an initial design for using diesel engine exhaust heat to provide the hot side temperature for TE modules without increasing the energy demands of the overall system. The system design for waste heat recovery using a TEG has several areas open for continuing research.

- The amount of power generated by a TEG is dependent on the hot side temperature of the thermoelectric modules, T_H, and temperature gradient across the modules, ΔT, which should lead to an investigation on increasing these values without decreasing the engine system efficiency. During testing it was found that the temperature T_H of the thermoelectric waste heat system (TWHS) was significantly reduced from the surface temperatures of the exhaust pipes leading into and away from the system. The addition of a baffle in the TWHS would force more hot exhaust gas toward the sides

93

resulting in increased T_H values. The result of this addition on the performance of the engine (i.e., increased exhaust back pressure) should be tested to determine the actual efficiency of this change. The overall efficiency realized by increasing ΔT should also be investigated. The use of an active heat sink may be effective in decreasing the cold side temperature of the modules, T_C, but the power consumption of the heat sink fan would have to be determined. Other heat sinks which do not require power to operate, such as heat pipes as well as those using engine coolant, would be of interest and should be investigated for overall influence on system efficiency.

- The use of four thermoelectric modules connected in series for charging a battery depends on developing an adaptive battery charger which supplies a load resistance equal to the internal resistance of the TEG at the operating temperatures. The charger would have to ensure that the TEG does not see the resistance of the battery since the power output of the TEG depends on the load resistance. The possibility of developing a charge controller which provides a constant resistance of 5.27Ω is unknown at this time.

- Analysis of the output power to the total weight of a thermoelectric generation system needs to be undertaken since the system adds load to the vehicle. The system includes all material added to the vehicle for the operation of the TEG. This analysis would give the net power the TEG supplies to the vehicle.

94

Appendices

Appendix A

Mass–Pendulum Simulink Models

The Simulink models for both the experimental and simulated systems are included below. The corresponding Matlab code is contained in Appendix B. Subsystems are shown after the model they are contained in.

Simulated Forced Response of Coupled System
Mass_Pend_F.mdl
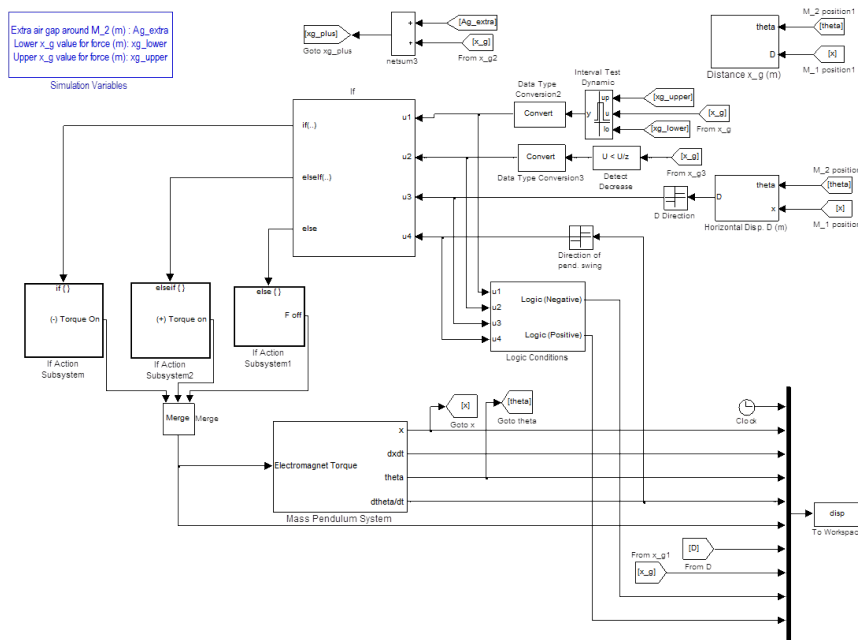
Figure A.1: Simulink code for simulating forced mass–pendulum system response
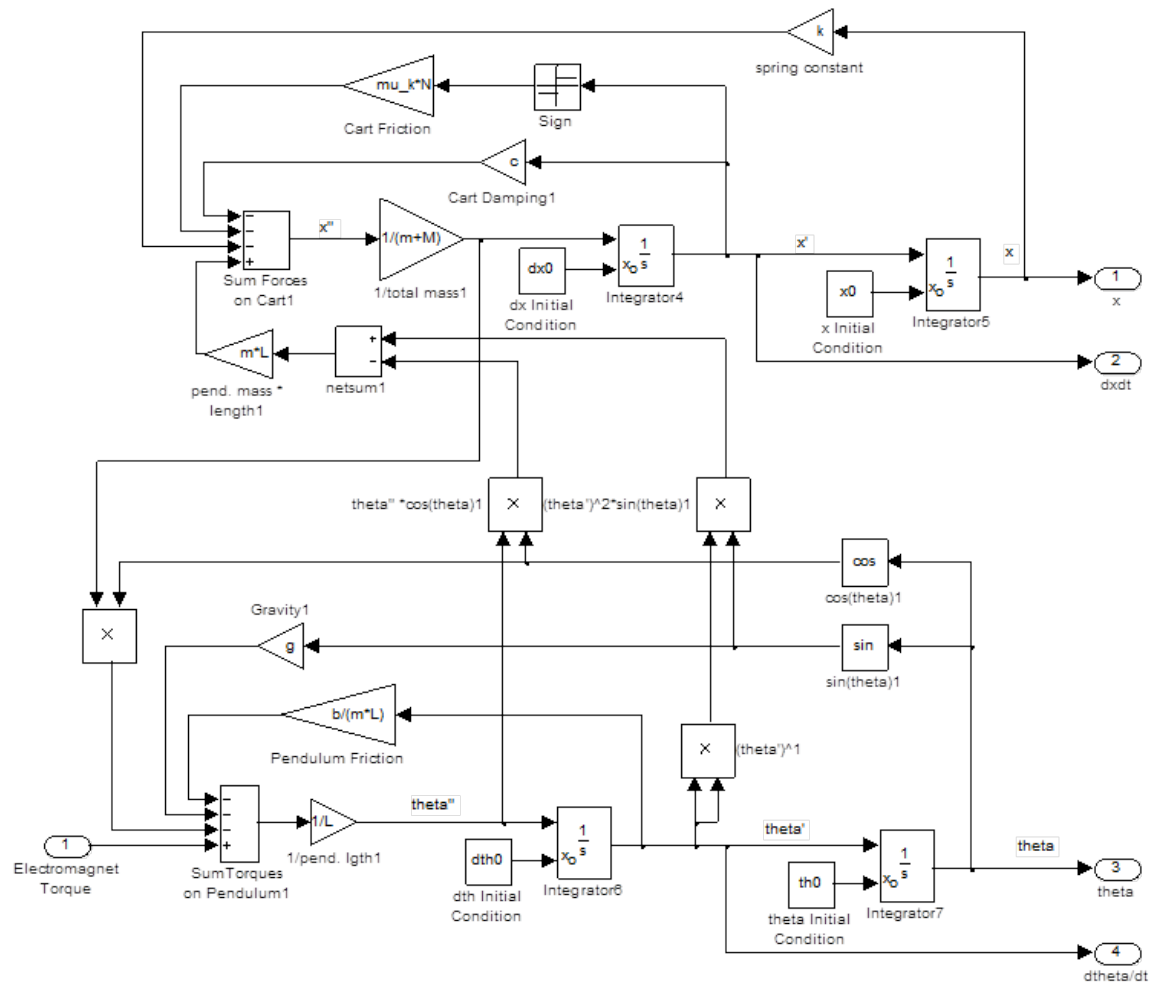
Figure A.2: Mass–pendulum subsystem of coupled equations of motion
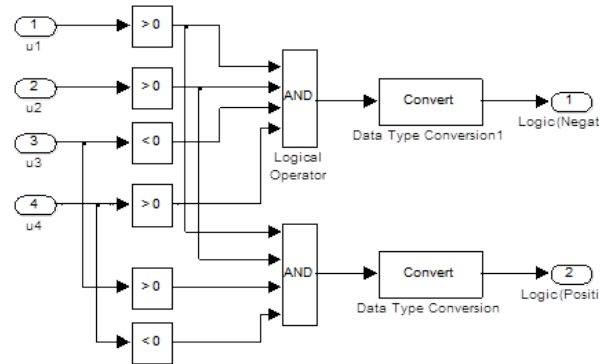
Figure A.3: Control logic subsystem in Mass_Pend_F.mdl

| (a) | (b) |
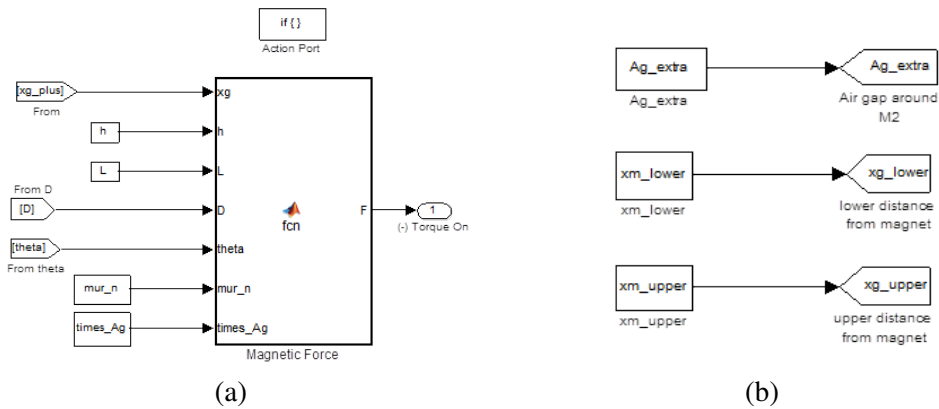
Figure A.4: Mass_Pend_F.mdl (a) if-action subsystem containing embedded Matlab function to calculate magnetic torque and (b) masked subsystem for inserting test parameters

Embedded Matlab functions to calculate negative and positive torque

```
function F = fcn(xg,h,L,D,theta,mur_n,times_Ag)
%Calculations on magnetic torque for mass-pendulum project
%xg is the distance between the pendulum bob and the electromagnet.
%xg must be in meters: xg=(x+Lsin(theta))-xm
%D is the distance between the pendulum bob and the electromagnet.
%D must be in meters: D=(x+Lsin(theta))-xm
%f is the Force of the electromagnet in Newtons
%F is the torque of the electromagnet in N-m
%%%%%%%%%%%%%%%%%%%%%%%%%%%%%%%%%%%%%%%%%%%%%%%%%%%%%%%%%%%%%%%%%%%%%%%%%%%
phi=atan(D/(L-L*cos(theta)));     %Angle phi of system calculated
mu0=4*pi*10^(-7);     %H/m
L1=0.2032;            %Magnetic Path of Electtromagnet, m
L2=0.0571;           %Diameter of Pendulum Bob, m
Ac=5.067e-4;         %Cross sectional Area of Core, m^2
Al=0.0449*h;         %Average load cross sectional area, m^2
%For 22-AWG wire
NA=864;              %Turns on electromagnet
IA=2.67;             %Current, Amps
%Neglecting Fringing
```

98

(a)   (b)

Figure A.5: Subsystems of Mass_Pend_F.mdl for calculating (a) distance D and (b) displacement x_g

```
Ag=times_Ag*Ac;          %Cross sectional area of air gap
R_N=L1/(mu0*mur_n*Ac)+(2*xg)/(mu0*Ag)+L2/(mu0*mur_n*Al); %Reluctance
dRdx_N=2/(mu0*Ag);                 %Deriv. of reluctance w.r.t x
flux=NA*IA/R_N;                    %Magnetic flux
fmech_N=abs(-0.5*flux^2*dRdx_N);   %Magnetic force (Negative), N
F=-fmech_N*L*sin(phi+theta);       %Negative Torque, N-m


function F = fcn(xg,h,L,D,theta,mur_p,times_Ag)
%Calculations on magnetic torque for mass-pendulum project
%xg is the distance between the pendulum bob and the electromagnet.
%xg must be in meters: xg=(x+Lsin(theta))-xm
%D is the distance between the pendulum bob and the electromagnet.
%D must be in meters: D=(x+Lsin(theta))-xm
%f is the Force of the electromagnet in Newtons
%F is the torque of the electromagnet in N-m
%%%%%%%%%%%%%%%%%%%%%%%%%%%%%%%%%%%%%%%%%%%%%%%%%%%%%%%%%%%%%%%%%%%%%%%
phi=atan(D/(L-L*cos(theta)));      %Angle phi of system calculated
mu0=4*pi*10^(-7);      %H/m
L1=0.2032;             %Magnetic Path of Electromagnet, m
L2=0.0571;             %Diameter of Pendulum Bob, m
Ac=5.067e-4;           %Cross sectional Area of Core, m^2
Al=0.0449*h;           %Average load cross sectional area, m^2
%For 22-AWG wire
NA=864;                %Turns on electromagnet
IA=2.67;               %Current, Amps
%Neglecting Fringing
Ag=times_Ag*Ac;        %Cross sectional area of air gap
R_N=L1/(mu0*mur_p*Ac)+(2*xg)/(mu0*Ag)+L2/(mu0*mur_p*Al); %Reluctance
dRdx_N=2/(mu0*Ag);                 %Deriv. of reluctance w.r.t x
flux=NA*IA/R_N;                    %Magnetic flux, Wb
fmech_N=abs(0.5*flux^2*dRdx_N);    %Magnetic force (positive), N
f=0.8*fmech_N;                     %Scaled magnetic force
F=-L*f*sin(theta+phi);             %Positive torque
```

99

Experimental Simulink Code Used with dSpace

Mass_Pend_dspace.mdl
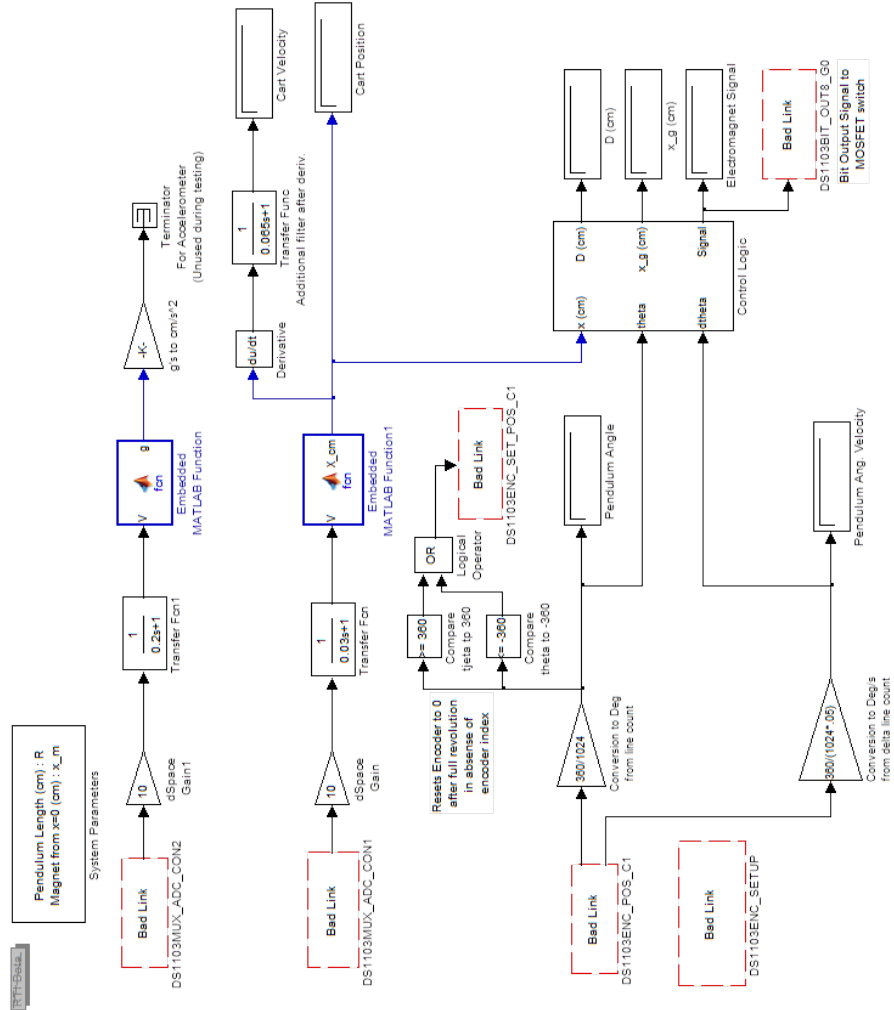
Figure A.6: Matlab Simulink code used with dSpace and ControlDesk for data acquisition
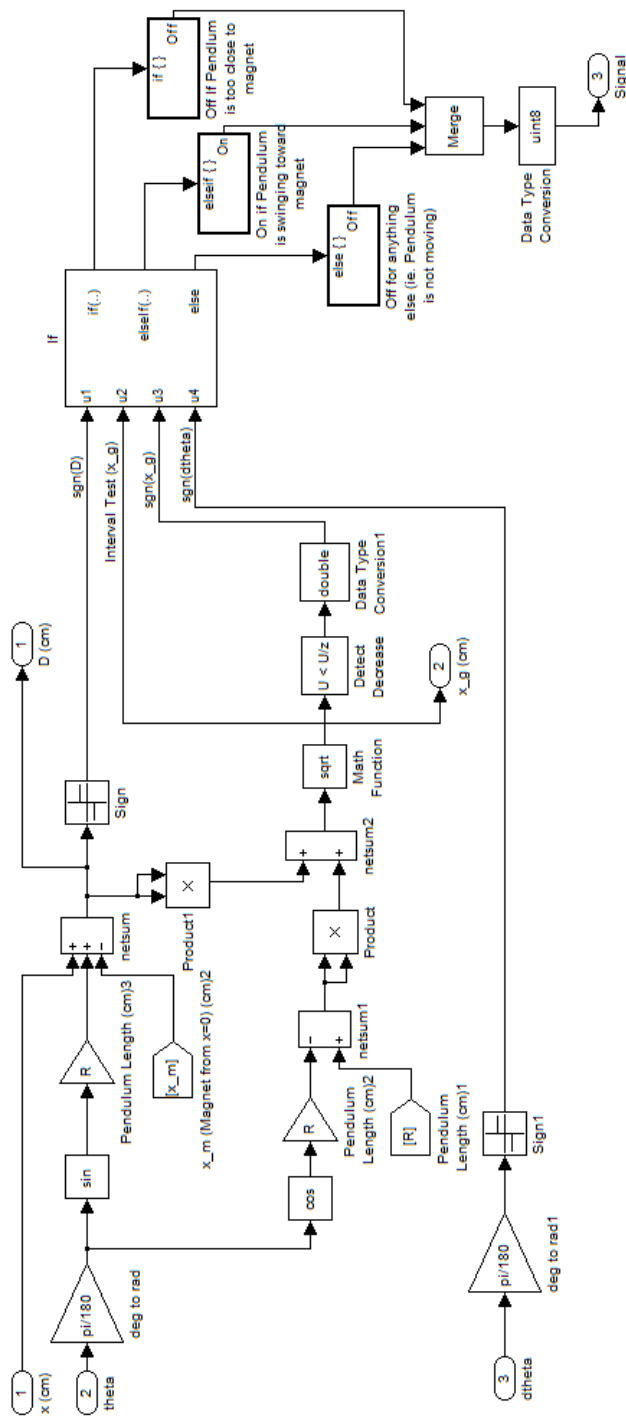
Figure A.7: Control Logic subsystem of Mass_Pend_dspace.mdl

101

Simulated Forced Response with M_1 Constrained

Pend_Only_F.mdl
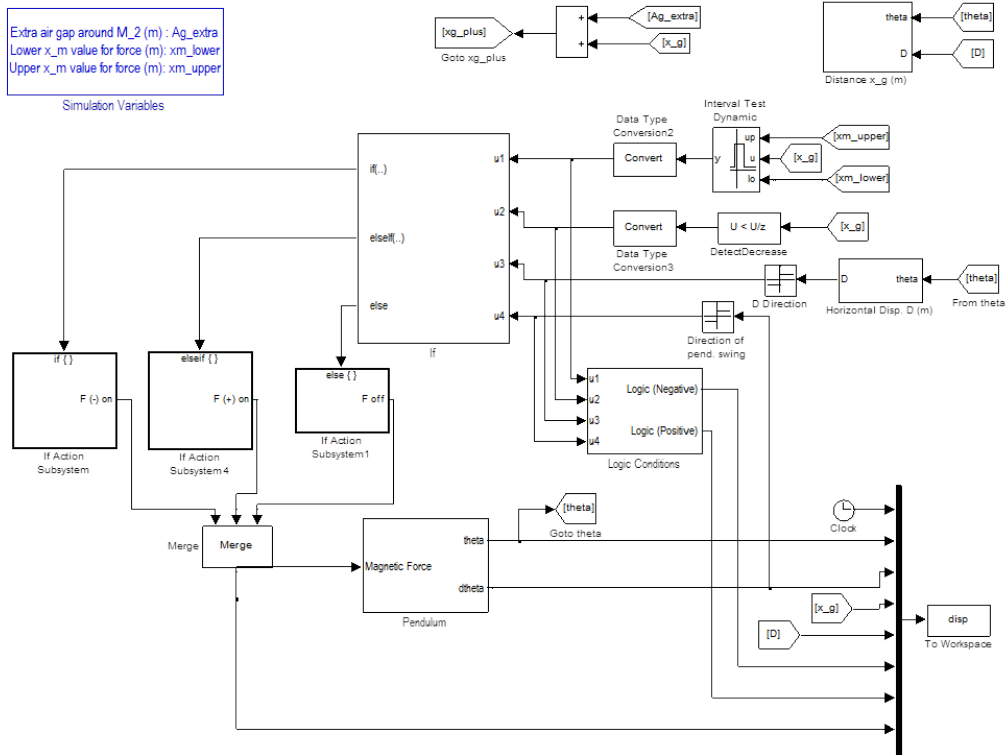
Figure A.8: Simulink code for simulating forced response of pendulum with M_1 fixed
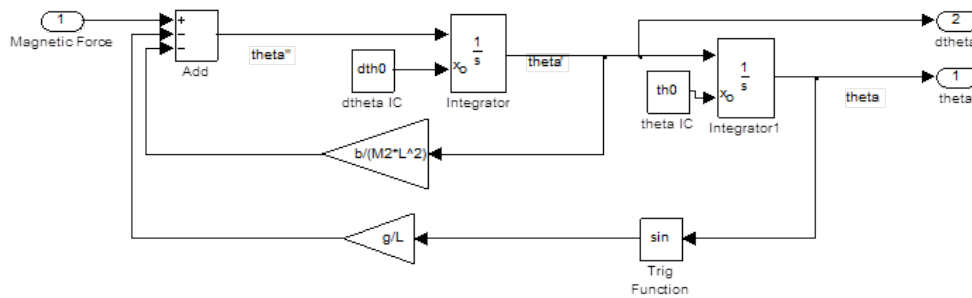
Figure A.9: 'Pendulum' subsystem equation of motion
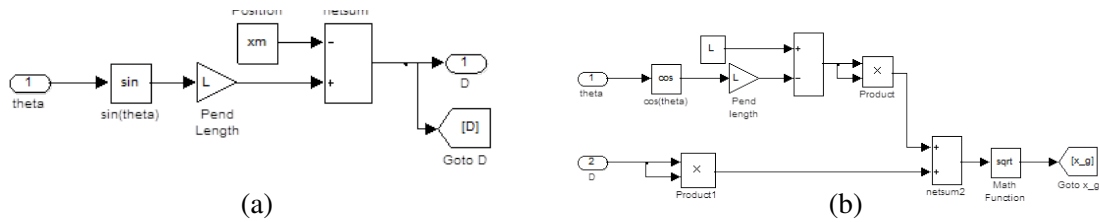
Figure A.10: Subsystems of Pend_Only_F.mdl for calculating (a) distance D and (b) displacement x_g
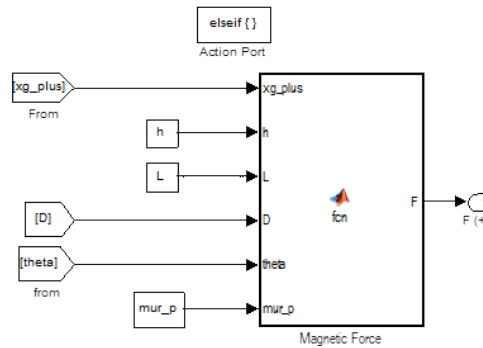
Figure A.11: Pend_Only_F.mdl if-action subsystem containing embedded Matlab function to calculate magnetic torque on pendulum

Embedded Matlab functions to calculate negative and positive torque for forced pendulum

```
function F = fcn(xg_plus,h,L,D,theta,mur_n)
%Calculations of negative magnetic torque for mass-pendulum project
%xg=distance between the pendulum bob and the electromagnet.
%xg_plus (m) includes an additional air gap around the electromagnet
%D=horizontal distance between pendulum bob and electromagnet.
%Distances must be in meters
%%%%%%%%%%%%%%%%%%%%%%%%%%%%%%%%%%%%%%%%%%%%%%%%%%%%%%%%%%%%%%%%%%%%%%%%%%%
phi=atan(D/(L-L*cos(theta)));    %Angle phi in system calculated
mu0=4*pi*10^(-7);      %H/m
L1=0.2032;             %Magnetic path of electtromagnet, m
L2=0.0571;             %Diameter of pendulum bob, m
Ac=5.067e-4;           %Cross sectional area of aore, m^2
Al=0.0449*h;           %Average load cross sectional area, m^2
%For 22-AWG wire
NA=864;                %Turns on electromagnet
IA=2.67;               %Current, Amps
%Neglecting Fringing
Ag=2.5*Ac;             %Cross sectional area of air gap
%Ag=(Ac+Al)/2;
%Ag=Al;
R_N=L1/(mu0*mur_n*Ac)+(2*xg_plus)/(mu0*Ag)+L2/(mu0*mur_n*Al);
    %Reluctance
dRdx_N=2/(mu0*Ag);     %Deriv. of reluctance w.r.t x
flux=NA*IA/R_N;        %Magnetic flux
fmech_N=abs(-0.5*flux^2*dRdx_N);   %Magnetic force, N
```

103

```
F=-fmech_N*L*sin(phi+theta);        %Torque (in negative direction), N-m

function F = fcn(xg_plus,h,L,D,theta,mur_p)
%Calculations of positive magnetic torque for mass-pendulum project
%D=horizontal distance between pendulum bob and electromagnet.
%D must be in meters
%F is force of the electromagnet in N-m
%%%%%%%%%%%%%%%%%%%%%%%%%%%%%%%%%%%%%%%%%%%%%%%%%%%%%%%%%%%%%%%%%%%%%%%%%
phi=atan(D/(L-L*cos(theta)));    %Angle phi of system calculated
mu0=4*pi*10^(-7);           %H/m
L1=0.2032;                  %Magnetic path of electromagnet, m
L2=0.0571;                  %Diameter of pendulum bob, m
Ac=5.067e-4;                %Cross sectional area of core, m^2
Al=0.0449*h;                %Avg. load cross sectional area, m^2
%For 22-AWG wire
NA=864;                     %Turns
IA=2.67;                    %Current, Amps
%Neglecting Fringing
Ag=2.5*Ac;                  %Cross sectional area of air gap
R_N=L1/(mu0*mur_p*Ac)+(2*xg_plus)/(mu0*Ag)+L2/(mu0*mur_p*Al);
    %Reluctance
dRdx_N=2/(mu0*Ag);          %Deriv. of reluctance w.r.t x
flux=NA*IA/R_N;             %Magnetic flux, Wb
fmech_N=abs(0.5*flux^2*dRdx_N);
f=0.8*fmech_N;              %Force directed toward positive direction, N
F=-L*f*sin(theta+phi);     %Positive torque
```
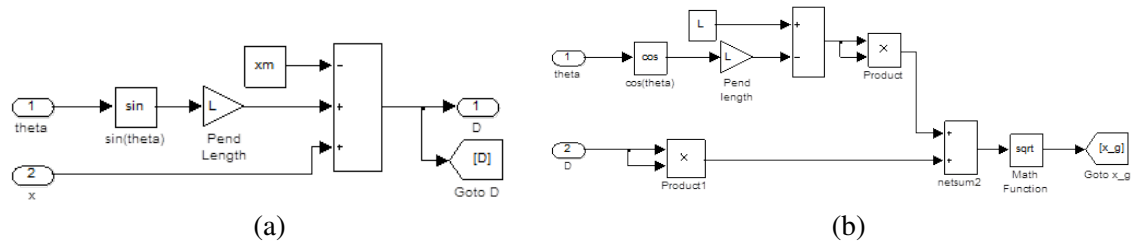
Simulated Free Response Uncoupled System

Uncoupled_Masses_FR.mdl
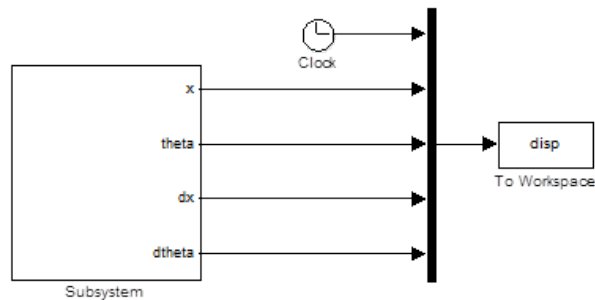
Figure A.12: Simulink code for simulating free response of uncoupled M_1 and M_2
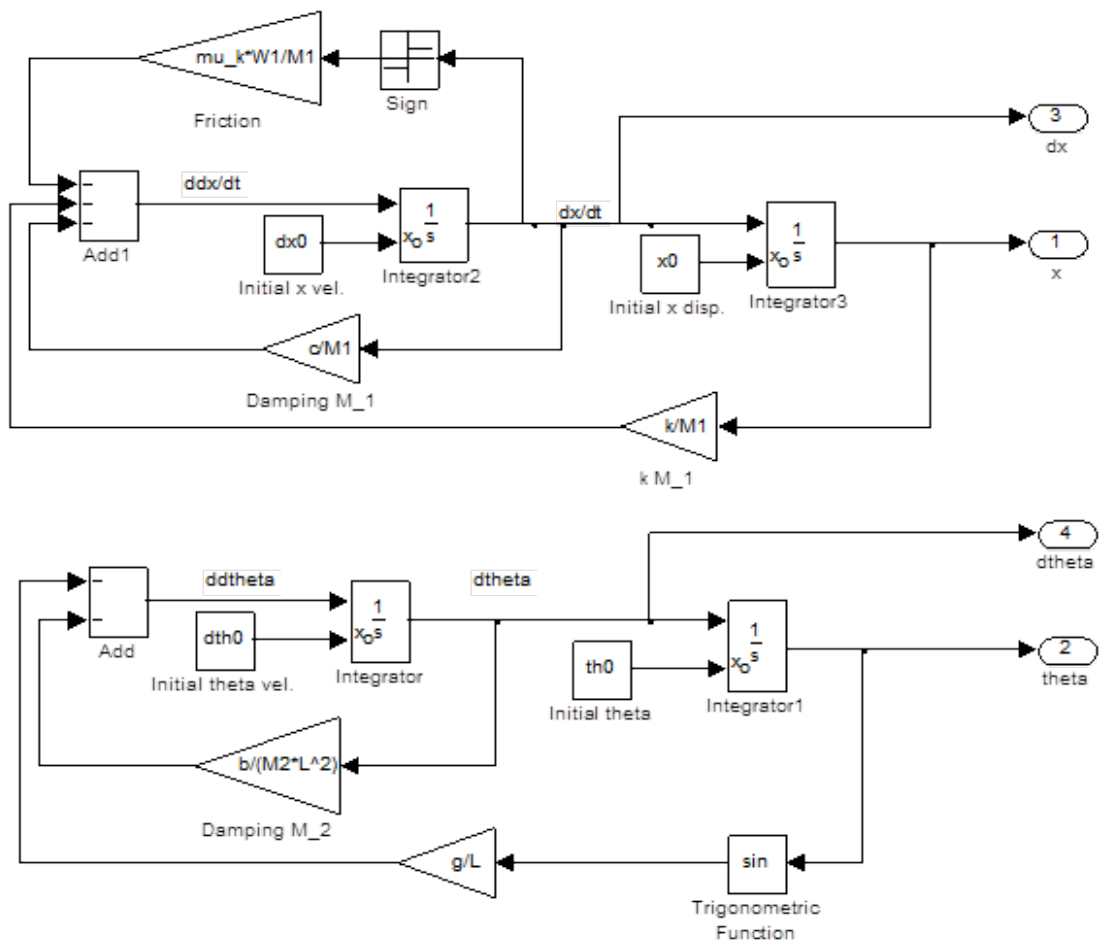
Figure A.13: Uncoupled_Masses_FR.mdl subsystem of uncoupled equations of motion

Appendix B

Mass–Pendulum Matlab Code

The Matlab code for the mass–pendulum bench top laboratory experiment is included below. Code for the two cases of forced response were M_1 is constrained and free to move are grouped together as are the files for free response. Code for the magnetic force and miscellaneous code follow.

Forced Response Code
PendrunCC_MKS_Paper_Plots.m

```
%Runs simulink model PendCC_4_MKS.mdl with subsystem
%PendulumCart_CC.mdl which simulates the response to the mass-pendulum
%system in which the pendulum is subject to an attractive force from
%an electromagnet positioned xm centimeters from the equilibrium
%position of the masses.
%%%%%%%%%%%%%%%%%%%%%%%%%%%%%%%%%%%%%%%%%%%%%%%%%%%%%%%%%%%%%%%%%%%%%%%%%%
sz=0.001;           %Step Size
SF=1/sz;            %Sampling frequency
xm=-10.6/100;       %Distance of magnet from equilibrium point, m
mur_n=60;           %Relative Permeability in negative torque
mur_p=50;           %Relative Permeability in positive torque
times_Ag=2.5;       %Multiple to get air gap cross sectional area
c=1.54;             %Damping in Cart, N*s/m
g=9.81;             %Gravity, m/s^2
k=84.5;             %Spring Constant, N/m
M=0.95;             %Mass of M_1, kg
mR=0.1776;          %Mass of Pendulum Rod, kg
LT=0.3715;          %R length (center of rotation to pend base), m
b=3.84*10^(-4);     %Damping in Pendulum due to Mass B, N*m*s/rad
h=0.0293+0.0316;    %Height of pendulum bob, m
```

106

```
L=LT-h/2;             %R length(point of rotation to center), m
m=1.1854+mR;          %Mass of M_2, kg
mu_k=0.015;           %Coefficient of friction
N=g*(M+m);            %Friction force, N
%Initial Conditions
th0=-2.4*(pi/180);          %Initial theta of pendulum, rad
x0=th0;                     %Initial displacement of M_1, m
dth0=-0.02;                 %Initial angular velocity of M_2, rad/s
dx0=-0.001;                 %Initial velocity of M_1, m/s

sim Mass_Pend_F

%Data from Simulink model
time=disp(:,1);
x_m=disp(:,2);              %x displacement, m
theta=disp(:,4);            %theta, rad
Force=disp(:,6);            %Torque from Magnetic Force
D_m=disp(:,7);              %D(horizontal disp of M2 from magnet), m
xg_m=disp(:,8);             %Displacement xg, m
logic_pos_F=disp(:,10);     %Logic for (+)F
logic_neg_F=disp(:,9);      %Logic for (-)F
x_cm=x_m*100;               %x displacement, cm
xg_cm=xg_m*100;             %Displacement of M_2, cm
%%%%%%%%%%%%%%%%%%%%%%%%%%%%%%%%%%%%%%%%%%%%%%%%%%%%%%%%%%%%%%%%%%%%%
%50 to 70 sec sample
tB=time((50*(1/sz)+1):(60*(1/sz)+1));
xB=x_m((50*(1/sz)+1):(60*(1/sz)+1));
thetaB=theta((50*(1/sz)+1):(60*(1/sz)+1));
min_xB=min(xB);
max_xB=max(xB);
min_thB=min(thetaB);
max_thB=max(thetaB);
RMS_xB=sqrt(sum(xB.^2)/length(xB));
RMS_thB=sqrt(sum(thetaB.^2)/length(thetaB));
Test_2=[min_xB,max_xB,RMS_xB,min_thB,max_thB,RMS_thB]
%%%%%%%%%%%%%%%%%%%%%%%%%%%%%%%%%%%%%%%%%%%%%%%%%%%%%%%%%%%%%%%%%%%%%%%%
%%%%%%%%%%%%%%%%%%%%%%%%%%% plots for paper %%%%%%%%%%%%%%%%%%%%%%%%%%%%
figure(2)
figure2=figure(2);
%Plot of x and theta
%for xm=-4cm %%%%%%%%%%%%%
xtick_2h=[49.5,50.5,51.5,52.5,53.5,54.5,55.5,56.5,57.5];
xlim_2h=[49.5 57.5];
%xtick_2h_a=[49,50,51,52,53,54,55,56,57];
ytick_2h_a=[-0.15,-0.10,-0.05,0,0.05,0.10,0.15];
ylim_2h_a=[-0.15 0.15];
%for xm=-7.5cm %%%%%%%%%%%%
xtick_2i=[50,51,52,53,54,55,56,57,58];
xlim_2i=[50 58];
ytick_2i_a=[-0.20,-0.15,-0.10,-0.05,0,0.05,0.10];
ylim_2i_a=[-0.2 0.13];
```

107

```
%for xm=-11.4cm %%%%%%%%%%
xtick_2k=[50.5,51.5,52.5,53.5,54.5,55.5,56.5,57.5,58.5];
xlim_2k=[50.5 58.5];
ytick_2k_a=[-0.03,-0.02,-0.01,0,0.01,0.02,0.03];
ylim_2k_a=[-0.031 0.03];
ytick_label_2k={-0.3,-0.2,-0.1,0,0.1,0.2,0.3};
axes5 = axes('Parent',figure2,...
    'YTick',ytick_2k_a,...
    'YTickLabel',ytick_label_2k,...
    'YMinorTick','on',...
    'XTick',xtick_2k,...
    'XTickLabel',{0,1,2,3,4,5,6,7,8},...
    'XMinorTick','on',...
    'Position',[0.15 0.35 0.78 0.38],...
    'FontSize',18);
xlim(axes5,xlim_2k);                 %x limit of axes
ylim(axes5,ylim_2k_a);               %y limit of axes
box(axes5,'on');
grid(axes5,'on');
hold(axes5,'all');
%Create plot
plot2 = plot(time,x_m,'--k',time,theta,'-k','Parent',axes5,
'LineWidth',2,'Color',[0 0 0]);
ylabel('Displacement, (---)(m), (   ) (rad)','FontSize',20,
'FontName','Times');

%Plot of Electromagnetic torque
%for xm=-4cm
ytick_2h_b=[-2.0,-1.0,0,1.0,2.0];
ylim_2h_b=[-2.3 2];
%for xm=-7.5cm
ytick_2i_b=[-2.0,-1.5,-1,-0.5,0];
ylim_2i_b=[-2 0.2];
%for xm=-11.4cm
ytick_2k_b=[-0.08,-0.06,-0.04,-0.02,0];
ylim_2k_b=[-0.075 0.008];
ytick_label_2k_b=[-0.8,-0.6,-0.4,-0.2,0];
axes6 = axes('Parent',figure2,'YTick',ytick_2k_b,...
    'YTickLabel',ytick_label_2k_b,...
    'XTick',xtick_2k,...
    'XTickLabel',{0,1,2,3,4,5,6,7,8},...
    'XMinorTick','on',...
    'Position',[0.15 0.17 0.78 0.12],...
    'FontSize',18);
xlim(axes6,xlim_2k);                 %x limit of axes
ylim(axes6,ylim_2k_b);               %y limit of axes
box(axes6,'on');
grid(axes6,'on');
hold(axes6,'all');
%Create plot
plot(time,Force,'Parent',axes6,'LineWidth',2,'Color',[0 0 0]);
```

108

```
xlabel('time sample (sec)','FontSize',20,'FontName','Times');
ylabel('Force (N\cdotm)','FontSize',20,'FontName','Times');
```

PendulumOnly_F.m

```
%Compares forced response of experimental and simulated systems for M_1
%constrained from tested positions on the electromagnet
%Runs Pend_only_C.mdl: simulink model of pendulum subject to
%electromagnet force
%%%%%%%%%%%%%%%%%%%%%%%%%%%%%%%%%%%%%%%%%%%%%%%%%%%%%%%%%%%%%%%%%%%%%%%%%%%
%Experimental data
%Test 1h xm=-3.8cm
FC_1h=load('C:\...\Data_9_12\fc_1h_ab912');
t_1h=FC_1h.fc_1h_ab912.X.Data;
x_1h=FC_1h.fc_1h_ab912.Y(1).Data;           %x in cm
x_1h_m=x_1h/100;                            %x in m
th_1h=FC_1h.fc_1h_ab912.Y(4).Data;          %theta in deg
th_1h_rad=th_1h*pi/180;                     %theta in rad
dth_1h=FC_1h.fc_1h_ab912.Y(3).Data;         %dtheta/dt
logic_1h=FC_1h.fc_1h_ab912.Y(2).Data;       %Control logic
xg_1h=FC_1h.fc_1h_ab912.Y(5).Data/100;      %xg in m
%Selecting data from the point that test 1h starts oscillating
%(at 2.91sec)
ST_e=t_1h(2)-t_1h(1);         %Sampling rate in exp system
IC_h=int32(2.91/ST_e+1);      %Sample number at IC of test h
th_1h_rad_a=th_1h_rad(IC_h:length(th_1h_rad));
t_1h_a=t_1h(1:length(th_1h_rad_a));
RMS_th_1h=sqrt(sum(th_1h_rad_a.^2)/length(th_1h_rad_a));
Test_1h=[min(th_1h_rad_a),max(th_1h_rad_a),RMS_th_1h]
%%%%%%%%%%%%%%%%%%%%%%%%%%%%%%%%%%%%%%%%%%%%%%%%%%%%%%%%%%%%%%%%%%%%%%%%%%%
%Test 1i xm=-7.6cm
FC_1i=load('C:\...\Data_9_12\fc_1i_ab912');
t_1i=FC_1i.fc_1i_ab912.X.Data;
x_1i=FC_1i.fc_1i_ab912.Y(1).Data;           %x in cm
x_1i_m=x_1i/100;                            %x in m
th_1i=FC_1i.fc_1i_ab912.Y(4).Data;          %theta in deg
th_1i_rad=th_1i*pi/180;                     %theta in rad
dth_1i=FC_1i.fc_1i_ab912.Y(3).Data;         %dtheta/dt
logic_1i=FC_1i.fc_1i_ab912.Y(2).Data;       %Control logic
xg_1i=FC_1i.fc_1i_ab912.Y(5).Data/100;      %xg in m
%Selecting data from the point that test 1h starts oscillating
%(at 2.94sec)
IC_i=int32(2.94/ST_e+1);      %Sample number at IC of test
th_1i_rad_a=th_1i_rad(IC_i:length(th_1i_rad));
t_1i_a=t_1i(1:length(th_1i_rad_a));
RMS_th_1i=sqrt(sum(th_1i_rad_a.^2)/length(th_1i_rad_a));
Test_1i=[min(th_1i_rad_a),max(th_1i_rad_a),RMS_th_1i]
%%%%%%%%%%%%%%%%%%%%%%%%%%%%%%%%%%%%%%%%%%%%%%%%%%%%%%%%%%%%%%%%%%%%%%%%%%%
%Test 1k xm=-11.4cm
FC_1k=load('C:\...\Data_9_12\fc_1k_ab912');
t_1k=FC_1k.fc_1k_ab912.X.Data;
x_1k=FC_1k.fc_1k_ab912.Y(1).Data;           %x in cm
```

109

```
x_1k_m=x_1k/100;                              %x in m
th_1k=FC_1k.fc_1k_ab912.Y(4).Data;           %Theta in deg
th_1k_rad=th_1k*pi/180;                       %Theta in rad
dth_1k=FC_1k.fc_1k_ab912.Y(3).Data;          %dtheta/dt
logic_1k=FC_1k.fc_1k_ab912.Y(2).Data;        %Control logic
xg_1k=FC_1k.fc_1k_ab912.Y(5).Data/100;       %xg in m
%Selecting data from the point that test 1h starts oscillating
%(at 1.38sec)
IC_k=int32(1.38/ST_e+1);        %Sample number at IC of test
th_1k_rad_a=th_1k_rad(IC_k:length(th_1k_rad));
t_1k_a=t_1k(1:length(th_1k_rad_a));
RMS_th_1k=sqrt(sum(th_1k_rad_a.^2)/length(th_1k_rad_a));
Test_1k=[min(th_1k_rad_a),max(th_1k_rad_a),RMS_th_1k]
%%%%%%%%%%%%%%%%%%%%%%%%%%%%%%%%%%%%%%%%%%%%%%%%%%%%%%%%%%%%%%%%%%%%%%%%%
%Test 1k xm=-11.4cm
%for 0-300 sec
FC_1k_X=load('C:\...\Forced Response Mass AB\fc_1k_ab914');
t_1k_X=FC_1k_X.fc_1k_ab914.X.Data;
x_1k_X=FC_1k_X.fc_1k_ab914.Y(1).Data;        %x in cm
x_1k_m_X=x_1k_X/100;                          %x in m
th_1k_X=FC_1k_X.fc_1k_ab914.Y(4).Data;       %Theta in deg
th_1k_rad_X=th_1k_X*pi/180;                   %Theta in rad
dth_1k_X=FC_1k_X.fc_1k_ab914.Y(3).Data;      %dtheta/dt
logic_1k_X=FC_1k_X.fc_1k_ab914.Y(2).Data;    %Control logic
xg_1k_X=FC_1k_X.fc_1k_ab914.Y(5).Data/100;   %xg in m
%Selecting data from the point that test 1h starts oscillating
%(at 0.42sec)
IC_k_X=int32(0.42/ST_e+1);       %Sample number at IC of test
th_1k_rad_a_X=th_1k_rad_X(IC_k_X:length(th_1k_rad_X));
t_1k_a_X=t_1k_X(1:length(th_1k_rad_a_X));
RMS_th_1k_a_X=sqrt(sum(th_1k_rad_a.^2)/length(th_1k_rad_a));
Test_1k_a_X=[min(th_1k_rad_a),max(th_1k_rad_a),RMS_th_1k]
%%%%%%%%%%%%%%%%%%%%%%%%%%%%%%%%%%%%%%%%%%%%%%%%%%%%%%%%%%%%%%%%%%%%%%%%%
%Equilibrium position of experimental sys
%Position M1 is fixed at, to account for equilibrium exactly at 0
E_1h=(sum(x_1h)/length(x_1h))/100;
E_1i=(sum(x_1i)/length(x_1i))/100;
E_1k=(sum(x_1k)/length(x_1k))/100;
E_1k_X=(sum(x_1k_X)/length(x_1k_X))/100;
%%%%%%%%%%%%%%%%%%%%%%%%%%%%%%%%%%%%%%%%%%%%%%%%%%%%%%%%%%%%%%%%%%%%%%%%%
ST=0.001;              %Sample Time Step
SF=1/ST;               %Sampling Frequency
%x_m from equilibrium position (accounting for fixed position of M1)
%xm=-3.8/100-E_1h;      %Test_1h:
%th0=0;                 %Initial position of M_2, rad
%dth0=0.1;              %Inivial velocity of M_2, rad/s
xm=-6.8/100-E_1i;       %Test_1i:
th0=0.005;             %IC for Test_1i
dth0=.25;
%xm=-11.4/100-E_1k;     %Test_1k:
%th0=0;                 %IC for Test_1k
```

110

```
%dth0=-0.9;
%xm=-10.5/100-E_1k_X;    %Test_1k_X
%th0=-0.003;             %IC for Test_1k_X
%dth0=-0.13;
mur_n=60;                %mu_r for negative torque
mur_p=50;                %mu_r for positive torque
g=9.81;                  %Gravity, m/s^2
mR=0.1776;               %Mass of Pendulum Rod, kg
RT=0.3715;               %R length(rotation center to pend base), m
b=3.84*10^(-4);          %Damping in M2 due to Mass B, N*m*s/rad
h=0.0293+0.0316;         %Height of pendulum bob, m
L=RT-h/2;                %Length pend rod (to center of gravity), m
M2=1.1854+mR;            %Mass of M_2 for Mass B, kg

sim Pend_Only_F

time=disp(:,1);
theta=disp(:,2);               %Rad
d_theta=disp(:,3);             %Angular velocity, rad/s
D_m=disp(:,4);                 %D in meters
xg_m=disp(:,5);                %Displacement of M_2 from electromagnet
logic_pos_F=disp(:,7);         %Logic for (+)F
logic_neg_F=disp(:,6);         %Logic for (-)F
Fmag=disp(:,8);                %Torque from magnetic force, N*m
%%%%%%%%%%%%%%%%%%%%%%%%%%%%%%%%%%%%%%%%%%%%%%%%%%%%%%%%%%%%%%%%%%%%%%%
%Selecting simulated data to run for same amount of time as exp.
figure(1)
%%Test 1h
time_end_h=int32(t_1h_a(end)/ST+1);
time_1h_a=time(1:time_end_h);
theta_1h_a=theta(1:length(time_1h_a));
RMS_theta_1h=sqrt(sum(theta_1h_a.^2)/length(theta_1h_a));
Simulation_1h=[min(theta_1h_a),max(theta_1h_a),RMS_theta_1h_a]
%Plot Test 1h vs. Simulated for exp data starting at initial motion
plot(t_1h_a,th_1h_rad_a,'-b',time_1h_a,theta_1h_a,'-g','LineWidth',2)
title('Forced Pendulum')
legend('Exp. Data','Sim. Data')
xlabel('time (sec)')
ylabel('theta (deg)')
%%%%%%Test 1i
time_end_i=int32(t_1i_a(end)/ST+1);
time_1i_a=time(1:time_end_i);
theta_1i_a=theta(1:length(time_1i_a));
RMS_theta_1i=sqrt(sum(theta_1i_a.^2)/length(theta_1i_a));
Simulation_1i=[min(theta_1i_a),max(theta_1i_a),RMS_theta_1i]
%Plot Test 1h vs. Simulated for exp data starting at initial motion
plot(t_1i_a,th_1i_rad_a,'-b',time_1i_a,theta_1i_a,'-g','LineWidth',2)
title('Forced Pendulum')
legend('Exp. Data','Sim. Data')
xlabel('time (sec)')
ylabel('theta (deg)')
```

111

```
%%%%%Test 1k
time_end_k=int32(t_1k_a(end)/ST+1);
time_1k_a=time(1:time_end_k);
theta_1k_a=theta(1:length(time_1k_a));
RMS_theta_1k=sqrt(sum(theta_1k_a.^2)/length(theta_1k_a));
Simulation_1k=[min(theta_1k_a),max(theta_1k_a),RMS_theta_1k]
%Plot Test 1h vs. Simulated for exp data starting at initial motion
plot(t_1k_a,th_1k_rad_a,'-b',time_1k_a,theta_1k_a,'-g','LineWidth',2)
title('Forced Pendulum')
legend('Exp. Data','Sim. Data')
xlabel('time (sec)')
ylabel('theta (deg)')
%%%%%Test 1k_X
time_end_k=int32(t_1k_a(end)/ST+1);
time_1k_a=time(1:time_end_k);
theta_1k_a=theta(1:length(time_1k_a));
%Plot Test 1h vs. Simulated for exp data starting at initial motion
plot(t_1k_a_X,th_1k_rad_a_X,'-b',time,theta,'g','LineWidth',2)
title('Forced Pendulum')
legend('Exp. Data','Sim. Data')
xlabel('time (sec)')
ylabel('theta (deg)')
```

Compare_Sim_Exp_Test1.m

```
%Approximate percent difference between experimental and simulated
%forced response for M_1 held stationary from polynomial fit to selected
%amplitude data: Percent approximately over 1st 100sec of motion
t=0:0.001:100;
%%%%%%%%%%%%%%%%%%%%%%%%%%%%%%%%%%%%%%%%%%%%%%%%%%%%%%%%%%%%%%%%%%%%%%%%%%%%%
%Test 1h
%Curve fit of Experimental Data
exp_1h_a=-1e-8.*t.^4+3e-6.*t.^3-0.0003.*t.^2+0.0222.*t-0.0067;
exp_1h=-8e-5*t.^2+0.0151*t+0.0355;
%Curve fit of Simulated Data
sim_1h_a=-1e-8.*t.^4+3e-6.*t.^3-0.0003.*t.^2+0.0216.*t+0.0052;
sim_1h=-6e-5*t.^2+0.0136*t+0.0535;
%%%%%%%%%%%%%%%%%%%%%%%%%%%%%%
%Average percent difference over 0-100sec time sample
diff_1h=abs(exp_1h-sim_1h);
avg_1h=0.5*(exp_1h+sim_1h);
p_diff_1h=diff_1h./avg_1h;
avg_p_diff_1h=sum(p_diff_1h)/length(p_diff_1h)
%%%%%%%%%%%%%%%%%%%%%%%%%%%%%
diff_1h_a=abs(exp_1h_a-sim_1h_a);
avg_1h_a=0.5*(exp_1h_a+sim_1h_a);
p_diff_1h_a=diff_1h_a./avg_1h_a;
avg_p_diff_1h_a=sum(p_diff_1h_a)/length(p_diff_1h_a)
%%%%%%%%%%%%%%%%%%%%%%%%%%%%%%%%%%%%%%%%%%%%%%%%%%%%%%%%%%%%%%%%%%%%%%%%%%%%%
%Test 1i
%Curve Fit of Experimental Data
exp_1i=-8e-5*t.^2+0.0152*t+0.0255;
```

112

```
%Curve fit Simulated Data
sim_1i=-4e-5*t.^2+0.0117*t+0.0319;
%%%%%%%%%%%%%%%%%%%%%%%%%%%%%
diff_1i=abs(exp_1i-sim_1i);
avg_1i=0.5*(exp_1i+sim_1i);
p_diff_1i=diff_1i./avg_1i;
avg_p_diff_1i=sum(p_diff_1i)/length(p_diff_1i)
%%%%%%%%%%%%%%%%%%%%%%%%%%%%%%%%%%%%%%%%%%%%%%%%%%%%%%%%%%%%%%%%%%%%%%%%
%Test_1k
%Curve fit of expirimental Data
exp_1k=3e-5*t.^2+0.0009*t+0.1595;
%Curve fit for simulated Data
sim_1k=1e-5*t.^2+0.0024*t+0.1624;
%%%%%%%%%%%%%%%%%%%%%%%%%%%%%
diff_1k=abs(exp_1k-sim_1k);
avg_1k=0.5*(exp_1k+sim_1k);
p_diff_1k=diff_1k./avg_1k;
avg_p_diff_1k=sum(p_diff_1k)/length(p_diff_1k)
%%%%%%%%%%%%%%%%%%%%%%%%%%%%%%%%%%%%%%%%%%%%%%%%%%%%%%%%%%%%%%%%%%%%%%%%
%Test 1k_X  for [85-250]sec
tk_X=85:0.001:250;
%Curve fit of expirimental Data
exp_1k_X=-3e-5*tk_X.^2+0.0128*tk_X-0.7644;
%Curve fit for simulated Data
sim_1k_X=-9e-6*tk_X.^2+0.0074*tk_X-0.4112;
%%%%%%%%%%%%%%%%%%%%%%%%%%%%%
diff_1k_X=abs(exp_1k_X-sim_1k_X);
avg_1k_X=0.5*(exp_1k_X+sim_1k_X);
p_diff_1k_X=diff_1k_X./avg_1k_X;
avg_p_diff_1k_X=sum(p_diff_1k_X)/length(p_diff_1k_X)
```

Exp_Test_2_Plots.m

```
%Plots of experimental data of forced response of M1 and M2 where M1 is
%free to move
%Oscillating frequency is determined by fft analysis
%%%%%%%%%%%%%%%%%%%%%%%%%%%%%%%%%%%%%%%%%%%%%%%%%%%%%%%%%%%%%%%%%%%%%%%%%%
fc2h=load('C:\...\Forced Response Mass AB\fc_2h_ab2');
fc2i=load('C:\...\Forced Response Mass AB\fc_2i_ab1');
fc2k=load('C:\...\Forced Response Mass AB\fc_2k_ab2');
%M1 free to move
%Test 2h
t2h=fc2h.fc_2h_ab2.X.Data;                  %Time
EMF2h=fc2h.fc_2h_ab2.Y(2).Data;             %Electromagnet Signal
x2h=fc2h.fc_2h_ab2.Y(1).Data/100;           %x
th2h=fc2h.fc_2h_ab2.Y(4).Data*pi/180;       %theta
%Test 2i
t2i=fc2i.fc_2i_ab1.X.Data;                  %Time
EMF2i=fc2i.fc_2i_ab1.Y(2).Data;             %Electromagnet Signal
x2i=fc2i.fc_2i_ab1.Y(1).Data/100;           %x
th2i=fc2i.fc_2i_ab1.Y(4).Data*pi/180;       %theta
%Test 2k
```

113

```
t2k=fc2k.fc_2k_ab2.X.Data;                      %Time
EMF2k=fc2k.fc_2k_ab2.Y(2).Data;                 %Electromagnet Signal
x2k=fc2k.fc_2k_ab2.Y(1).Data/100;               %x
th2k=fc2k.fc_2k_ab2.Y(4).Data*pi/180;           %theta
%%%%%%%%%%%%%%%%%%%%%%%%%%%%%%%%%%%%%%%%%%%%%%%%%%%%%%%%%%%%%%%%%%%%%%%%%%
%Figures for Paper
%10 sec sample
%test xm=-3.8
ST_2h=t2h(2)-t2h(1);            %Sample Time Step - Experimental Sys
t2h_B=0:ST_2h:11;
x2h_B=x2h(fix(10.29/ST_2h):(t2h_B(length(t2h_B))/
    ST_2h+fix(10.29/ST_2h)));
th2h_B=th2h(fix(10.29/ST_2h):(t2h_B(length(t2h_B))/
    ST_2h+fix(10.29/ST_2h)));
EMF2h_B=EMF2h(fix(10.29/ST_2h):(t2h_B(length(t2h_B))/
    ST_2h+fix(10.29/ST_2h)));
%test xm=-7.6cm
ST_2i=t2i(2)-t2i(1);           %Sample Time Step - Experimental Sys
t2i_B=0:ST_2i:11;
x2i_B=x2i(fix(11.52/ST_2i):(t2i_B(length(t2i_B))/
    ST_2i+fix(11.52/ST_2i)));
th2i_B=th2i(fix(11.52/ST_2i):(t2i_B(length(t2i_B))/
    ST_2i+fix(11.52/ST_2i)));
EMF2i_B=EMF2i(fix(11.52/ST_2i):(t2i_B(length(t2i_B))/
    ST_2i+fix(11.52/ST_2i)));
%test xm=-11.4cm
ST_2k=t2k(2)-t2k(1);           %Sample Time Step - Experimental Sys
t2k_B=0:ST_2k:11;
x2k_B=x2k(fix(10.68/ST_2k):(t2k_B(length(t2k_B))/
    ST_2k+fix(10.68/ST_2k)));
th2k_B=th2k(fix(10.68/ST_2k):(t2k_B(length(t2k_B))/
    ST_2k+fix(10.68/ST_2k)));
EMF2k_B=EMF2k(fix(10.68/ST_2k):(t2k_B(length(t2k_B))/
    ST_2k+fix(10.68/ST_2k)));
%%%%%%%%%%%%%%%%%%%%%%%%%%%%%%%%%%%%%%%%%%%%%%%%%%%%%%%%%%%%%%%%%%%%%%%%%%
%Plots for Paper
figure(1)
figure1=figure(1);
%plot 2h
%Create axes
axes1 = axes('Parent',figure1,
    'YTick',[-0.15 -0.1 -0.05 0 0.05 0.1 0.15],...
    'YMinorTick','on',...
    'XTick',[0 1 2 3 4 5 6 7 8],...
    'XMinorTick','on',...
    'Position',[0.15 0.35 0.78 0.38],...
    'FontSize',18);
xlim(axes1,[0 8]);
ylim(axes1,[-.16,.165]);
box(axes1,'on');
grid(axes1,'on');
```

114

```
hold(axes1,'all');
%Create plot
plot1 = plot(t2h_B,x2h_B,'--g',t2h_B,th2h_B,'-b','Parent',
    axes1,'LineWidth',2);
ylabel('Displacement, (---)(m), (   ) (rad)','FontSize',20,
    'FontName','Times');
%%%%%%%%%%%%%%%%%%%%%%%%%%%%%%%%%%%%%%%%%%%%%%%%%%%%%%%%%%%%%%%%%%%%%%
axes2 = axes('Parent',figure1,'YTick',[0 1],
    'XTick',[0 1 2 3 4 5 6 7 8],...
    'XMinorTick','on',...
    'Position',[0.15 0.19 0.78 0.12],...
    'FontSize',18);
xlim(axes2,[0 8]);
ylim(axes2,[0 1.1]);
box(axes2,'on');
hold(axes2,'all');
plot(t2h_B,EMF2h_B,'Parent',axes2,'LineWidth',2,'Color',[.9 0.2 1]);
xlabel('time sample (sec)','FontSize',20,'FontName','Times');
ylabel('Control','FontSize',20,'FontName','Times');
%%%%%%%%%%%%%%%%%%%%%%%%%%%%%%%%%%%%%%%%%%%%%%%%%%%%%%%%%%%%%%%%%%%%%%
%Plot Test 2i
figure(2)
figure2=figure(2);
% Create axes
axes3 = axes('Parent',figure2,
    'YTick',[-0.15,-0.10,-0.05,0,.05,.1,.15],...
    'YMinorTick','on',...
    'XTick',[0 1 2 3 4 5 6 7 8],...
    'XMinorTick','on',...
    'Position',[0.15 0.35 0.78 0.38],...
    'FontSize',18);
xlim(axes3,[0 8]);
ylim(axes3,[-.15,.125]);
box(axes3,'on');
grid(axes3,'on');
hold(axes3,'all');
% Create plot
plot2 = plot(t2i_B,x2i_B,'--g',t2i_B,th2i_B,'-b','Parent',
    axes3,'LineWidth',2);
ylabel('Displacement, (---)(m), (   ) (rad)','FontSize',20,
    'FontName','Times');
%%%%%%%%%%%%%%%%%%%%%%%%%%%%%%%%%%%%%%%%%%%%%%%%%%%%%%%%%%%%%%%%%%%%%%
axes4 = axes('Parent',figure2,'YTick',[0 1],
    'XTick',[0 1 2 3 4 5 6 7 8],...
    'XMinorTick','on',...
    'Position',[0.15 0.19 0.78 0.12],...
    'FontSize',18);
xlim(axes4,[0 8]);
ylim(axes4,[0 1.1]);
box(axes4,'on');
hold(axes4,'all');
```

```matlab
% Create plot
%plot(t2i_B,EMF2i_B,'Parent',axes4,'LineWidth',2,'Color',[0 0 0]);
plot(t2i_B,EMF2i_B,'Parent',axes4,'LineWidth',2,'Color',[.9 0.2 1]);
xlabel('time sample (sec)','FontSize',20,'FontName','Times');
ylabel('Control','FontSize',20,'FontName','Times');
%%%%%%%%%%%%%%%%%%%%%%%%%%%%%%%%%%%%%%%%%%%%%%%%%%%%%%%%%%%%%%%%%%%%%%%
%plot Test 2k
figure(3)
figure3=figure(3);
% Create axes
axes5 = axes('Parent',figure3,
    'YTickLabel',{'-1.5','-.75','0','.75','1.5'},...
    'YTick',[-0.015,-0.0075,0,0.0075,0.015],...
    'YMinorTick','on',...
    'XTick',[0 1 2 3 4 5 6 7 8],...
    'XMinorTick','on',...
    'Position',[0.15 0.35 0.78 0.38],...
    'FontSize',18);
xlim(axes5,[0 8]);
ylim(axes5,[-0.017,.015]);
box(axes5,'on');
grid(axes5,'on');
hold(axes5,'all');
% Create plot
plot3 = plot(t2k_B,x2k_B,'--g',t2k_B,th2k_B,'-b','Parent',axes5,
    'LineWidth',2);
ylabel('Displacement, (---)(m), (   ) (rad)','FontSize',20,
    'FontName','Times');
%%%%%%%%%%%%%%%%%%%%%%%%%%%%%%%%%%%%%%%%%%%%%%%%%%%%%%%%%%%%%%%%%%%%%%%
axes6 = axes('Parent',figure3,'YTick',[0 1],
    'XTick',[0 1 2 3 4 5 6 7 8],...
    'XMinorTick','on',...
    'Position',[0.15 0.19 0.78 0.12],...
    'FontSize',18);
xlim(axes6,[0 8]);
ylim(axes6,[0 1.1]);
box(axes6,'on');
hold(axes6,'all');
% Create plot
%plot(t2k_B,EMF2k_B,'Parent',axes6,'LineWidth',2,'Color',[0 0 0]);
plot(t2k_B,EMF2k_B,'Parent',axes6,'LineWidth',2,'Color',[.9 0.2 1]);
xlabel('time sample (sec)','FontSize',20,'FontName','Times');
ylabel('Control','FontSize',20,'FontName','Times');
%%%%%%%%%%%%%%%%%%%%%%%%%%%%%%%%%%%%%%%%%%%%%%%%%%%%%%%%%%%%%%%%%%%%%%%
%Frequency Plots
%Test 2h
ST_2h=t2h(2)-t2h(1);                %Sample Time Step
SF_2h=1/ST_2h;                      %Sampling Frequency
L_2h=length(t2h);                   %Number of samples
NFFT_2h = 2^nextpow2(L_2h);         %Next power of 2
Y_2h_theta = fft(th2h,NFFT_2h)/L_2h;   %fft of theta
```

116

```
Y_2h_x = fft(x2h,NFFT_2h)/L_2h;          %fft of x
f_2h= SF_2h/2*linspace(0,1,NFFT_2h/2+1);
%Test 2i
ST_2i=t2i(2)-t2i(1);                     %Sample Time Step
SF_2i=1/ST_2i;                           %Sampling Frequency
L_2i=length(t2i);                        %Number of samples
NFFT_2i = 2^nextpow2(L_2i);              %Next power of 2
Y_2i_theta = fft(th2i,NFFT_2i)/L_2i;     %fft of theta
Y_2i_x = fft(x2i,NFFT_2i)/L_2i;          %fft of x
f_2i= SF_2i/2*linspace(0,1,NFFT_2i/2+1);
%Test 2k
ST_2k=t2k(2)-t2k(1);                     %Sample Time Step
SF_2k=1/ST_2k;                           %Sampling Frequency
L_2k=length(t2k);                        %Number of samples
NFFT_2k = 2^nextpow2(L_2k);              %Next power of 2
Y_2k_theta = fft(th2k,NFFT_2k)/L_2k;     %fft of theta
Y_2k_x = fft(x2k,NFFT_2k)/L_2k;          %fft of x
f_2k= SF_2k/2*linspace(0,1,NFFT_2k/2+1);
%%%%%%%%%%%%%%%%%%%%%%%%%%%%%%%%%%%%%%%%%%%%%%%%%%%%%%%%%%%%%%%%%%%%%%%%%%%%%
%Min, max, and RMS test values
%%%%%Test 2h
figure(4)
subplot(3,1,1)
plot(f_2h,2*abs(Y_2h_theta(1:NFFT_2h/2+1)),'-',
    f_2h,2*abs(Y_2h_x(1:NFFT_2h/2+1)),'--')
title('Single-Sided Amplitude Spectrum Test 2h: xm=-3.8cm')
xlabel('Frequency (Hz)')
ylabel('|Y(f)|')
axis([0,1,0,0.11])
x_values_2h=[max(x2h),min(x2h),sqrt(sum(x2h.^2)/size(x2h,2))];
th_values_2h=[max(th2h),min(th2h),sqrt(sum(th2h.^2)/size(th2h,2))];
%%%%%Test 2i
subplot(3,1,2)
plot(f_2i,2*abs(Y_2i_theta(1:NFFT_2i/2+1)),'-',
    f_2i,2*abs(Y_2i_x(1:NFFT_2i/2+1)),'--')
title('Single-Sided Amplitude Spectrum Test 2i: xm=-7.6cm')
xlabel('Frequency (Hz)')
ylabel('|Y(f)|')
axis([0,1,0,0.11])
x_values_2i=[max(x2i),min(x2i),sqrt(sum(x2i.^2)/size(x2i,2))];
th_values_2i=[max(th2i),min(th2i),sqrt(sum(th2i.^2)/size(th2i,2))];
%%%%%Test 2k
subplot(3,1,3)
plot(f_2k,2*abs(Y_2k_theta(1:NFFT_2k/2+1)),'-',
    f_2k,2*abs(Y_2k_x(1:NFFT_2k/2+1)),'--')
title('Single-Sided Amplitude Spectrum Test 2h: xm=-11.4cm')
xlabel('Frequency (Hz)')
ylabel('|Y(f)|')
axis([0,1,0,0.015])
x_values_2k=[max(x2k),min(x2k),sqrt(sum(x2k.^2)/size(x2k,2))];
th_values_2k=[max(th2k),min(th2k),sqrt(sum(th2k.^2)/size(th2k,2))];
```

117

Free Response Code
Exp_Vs_Sim_FR_819.m

```
%Experimental versus Simulated Free response runs Pend_FR.mdl with
%subsystem PendulumCart_FR.mdl to simulate the free response the
%coupled system due to an initial displacement of the cart and/or
%pendulum. Oscillating frequency is also calculated.
%%%%%%%%%%%%%%%%%%%%%%%%%%%%%%%%%%%%%%%%%%%%%%%%%%%%%%%%%%%%%%%%%%%%%%%%
%Experimental Data collected 8/19/11 after adding resistor in series
%with  load cell signal and recalibrating
%%%%%%%%%%%%%%%%%%%%%%%%%%%%%%%%%%%%%%%%%%%%%%%%%%%%%%%%%%%%%%%%%%%%%%%%
%Free Response 1
FR1=load('C:\...\fr_1ab_819.mat');
t1B=FR1.fr_1ab_819.X.Data;
x1B=FR1.fr_1ab_819.Y(1).Data/100;            %M1 displacement in meters
th1B=FR1.fr_1ab_819.Y(4).Data*pi/180;        %theta in radians
dth1B=FR1.fr_1ab_819.Y(3).Data*pi/180;
dx1B=FR1.fr_1ab_819.Y(6).Data/100;
%IC starts at t1B=0.69sec Which is t1B(24)
%Run for 15 sec
t1B_a=(0:0.03:15);
x1B_a=x1B(33:(t1B_a(length(t1B_a))/0.03+33));
th1B_a=th1B(29:(t1B_a(end)/.03+29));
dx1B_a=dx1B(33:(t1B_a(end)/.03+33));
dth1B_a=dth1B(29:(t1B_a(end)/.03+29));
%For phase plot
th1B_p=th1B(29:(t1B_a(end)/.03+29));
%%%%%%%%%%%%%%%%%%%%%%%%%%%%%%%%%%%%%%%%%%%%%%%%%%%%%%%%%%%%%%%%%%%%%%%%
%Free Response 2
FR2=load('C:\...\fr_2ab_819.mat');
t2B=FR2.fr_2ab_819.X.Data;
x2B=FR2.fr_2ab_819.Y(1).Data/100;            %x in meters
th2B=FR2.fr_2ab_819.Y(4).Data*pi/180;        %theta in radians
dx2B=FR2.fr_2ab_819.Y(6).Data/100;
dth2B=FR2.fr_2ab_819.Y(3).Data*pi/180;
%IC starts at t2B=0.9 sec which is t2B(101)
%Run for 15 sec
t2B_a=(0:0.03:15);
x2B_a=x2B(110:(t2B_a(end)/.03+110));
th2B_a=th2B(105:(t2B_a(end)/.03+105));
dx2B_a=dx2B(110:(t2B_a(end)/.03+110));
dth2B_a=dth2B(105:(t2B_a(end)/.03+105));
%For phase plot
th2B_p=th2B(108:(t2B_a(end)/.03+108));
%%%%%%%%%%%%%%%%%%%%%%%%%%%%%%%%%%%%%%%%%%%%%%%%%%%%%%%%%%%%%%%%%%%%%%%%
%Free Response 3
FR3=load('C:\...\fr_3ab_819.mat');
t3B=FR3.fr_3ab_819.X.Data;
x3B=FR3.fr_3ab_819.Y(1).Data/100;
th3B=FR3.fr_3ab_819.Y(4).Data*pi/180;
dx3B=FR3.fr_3ab_819.Y(6).Data/100;
dth3B=FR3.fr_3ab_819.Y(3).Data*pi/180;
```

118

```
%IC starts at t3B=1.65 sec which is t3B(29)
%Run for 15 sec
t3B_a=(0:0.03:15);
x3B_a=x3B(32:(t3B_a(end)/.03+32));
th3B_a=th3B(29:(t3B_a(end)/.03+29));
dx3B_a=dx3B(32:(t3B_a(end)/.03+32));
dth3B_a=dth3B(29:(t3B_a(end)/.03+29));
%%%%%%%%%%%%%%%%%%%%%%%%%%%%%%%%%%%%%%%%%%%%%%%%%%%%%%%%%%%%%%%%%%%%%%%%
%Free Response 4
FR4=load('C:\...\Free Response Mass AB 8_19\fr_4ab_819.mat');
t4B=FR4.fr_4ab_819.X.Data;
x4B=FR4.fr_4ab_819.Y(1).Data/100;
th4B=FR4.fr_4ab_819.Y(4).Data*pi/180;
dx4B=FR4.fr_4ab_819.Y(6).Data/100;
dth4B=FR4.fr_4ab_819.Y(3).Data*pi/180;
%IC starts at t2B=0.81 sec which is t4B(29)
%Run for 15 sec
t4B_a=(0:0.03:15);
x4B_a=x4B(36:(t4B_a(end)/.03+36));
th4B_a=th4B(31:(t4B_a(end)/.03+31));
dx4B_a=dx4B(36:(t4B_a(end)/.03+36));
dth4B_a=dth4B(31:(t4B_a(end)/.03+31));
%For Phase Plot
th4B_p=th4B(34:(t4B_a(end)/.03+34));
%%%%%%%%%%%%%%%%%%%%%%%%%%%%%%%%%%%%%%%%%%%%%%%%%%%%%%%%%%%%%%%%%%%%%%%%%%%
%%%%%%%%%%%%%%%%%%%%%%%%%%%%%%%%%%%%%%%%%%%%%%%%%%%%%%%%%%%%%%%%%%%%%%%%%%%
%Simulated Parameters
M=0.95;                  %Mass of M_1, kg
c=1.54;                  %Damping in Cart, N*s/m
g=9.81;                  %Gravity, m/s^2
k=84;                    %Spring Constant, N/m
mR=0.1776;               %Mass of Pendulum Rod, kg
LT=0.3715;               %Rod length from center of rotation to bob
%Mass B
b=3.1826*10^(-4);        %Damping in M2 due to Mass B, N*m*s/rad
h=0.0293+0.0316;         %Height of pendulum bob, m
L=LT-h/2;                %R from C.O.R to center of pendulum
m=1.1854+mR;             %Mass of M_2 for Mass B, kg
%Friction acting on M1
mu_k=0.015;
N=g*(M+m);
%Initial Conditions
i=1:4;
x0=[x1B_a(1),x2B_a(1),x3B_a(1),x4B_a(1)];
th0=[th1B_a(1),th2B_a(1),th3B_a(1),th4B_a(1)];
dx0=[dx1B_a(1),dx2B_a(1),dx3B_a(1),dx4B_a(1)];
dth0=[dth1B_a(1),dth2B_a(1),dth3B_a(1),dth4B_a(1)];

sim Mass_Pend_FR
%Free Response model uses Mass_Pend_F.mdl subsystem of coupled EOM
```

119

```matlab
%simulated Responses
ts=disp(:,1);
xs1=disp(:,2);
xs2=disp(:,3);
xs3=disp(:,4);
xs4=disp(:,5);
ths1=disp(:,6);
ths2=disp(:,7);
ths3=disp(:,8);
ths4=disp(:,9);
%%%%%%%%%%%%%%%%%%%%%%%%%%%%%%%%%%%%%%%%%%%%%%%%%%%%%%%%%%%%%%%%%%%%%%%%%%%%
%Determine Oscillating Frequency
%Experimental System
%Test_1B
ST_1=t1B_a(2)-t1B_a(1);               %Sample Time Step - Exp Sys
SF_1=1/ST_1;                          %Sampling Freq - Exp Sys
L_1=length(t1B_a);                    %Number of samples
NFFT_1 = 2^nextpow2(L_1);             %Next power of 2
Y_1_theta = fft(th1B_a,NFFT_1)/L_1;   %theta
Y_1_x = fft(x1B_a,NFFT_1)/L_1;        %x
f_1= SF_1/2*linspace(0,1,NFFT_1/2+1);
%Test_2B
ST_2=t2B_a(2)-t2B_a(1);               %Sample Time Step - Exp Sys
SF_2=1/ST_2;                          %Sampling Freq - Exp Sys
L_2=length(t2B_a);                    %Number of samples
NFFT_2 = 2^nextpow2(L_2);             %Next power of 2
Y_2_theta = fft(th2B_a,NFFT_2)/L_2;   %theta
Y_2_x = fft(x2B_a,NFFT_2)/L_2;        %x
f_2= SF_2/2*linspace(0,1,NFFT_2/2+1);
%Simulated Sytstem
%Test 1
ST_s=ts(2)-ts(1);                     %Sample Time Step - Sim Sys
SF_s=1/ST_s;                          %Sampling Frequency - Sim Sys
L_s=length(ts);                       %Number of samples
NFFT_s = 2^nextpow2(L_s);             %Next power of 2
Y_1_ths1 = fft(ths1,NFFT_s)/L_s;      %theta
Y_1_xs1 = fft(xs1,NFFT_s)/L_s;        %x
f_s= SF_s/2*linspace(0,1,NFFT_s/2+1);
%Test 2
Y_2_ths2 = fft(ths2,NFFT_s)/L_s;      %theta
Y_2_xs2 = fft(xs2,NFFT_s)/L_s;        %x
%%%%%%%%%%%%%%%%%%%%%%%%%%%%%%%%%%%%%%%%%%%%%%%%%%%%%%%%%%%%%%%%%%%%%%%%%%%%
%Frequency plots
figure(7)
subplot(2,2,1)
plot(f_1,2*abs(Y_1_theta(1:NFFT_1/2+1)),'-',
f_1,2*abs(Y_1_x(1:NFFT_1/2+1)),'--')
title('Single-Sided Amplitude Spectrum FR Test 1: Experimental System')
xlabel('Frequency (Hz)')
ylabel('|Y(f)|')
axis([0,1,0,0.2])
```

120

```
subplot(2,2,3)
plot(f_2,2*abs(Y_2_theta(1:NFFT_2/2+1)),'-',
f_2,2*abs(Y_2_x(1:NFFT_2/2+1)),'--')
title('Single-Sided Amplitude Spectrum FR Test 2: Experimental System')
xlabel('Frequency (Hz)')
ylabel('|Y(f)|')
axis([0,1,0,0.2])

subplot(2,2,2)
plot(f_s,2*abs(Y_1_ths1(1:NFFT_s/2+1)),'-',
f_s,2*abs(Y_1_xs1(1:NFFT_s/2+1)),'--')
title('Single-Sided Amplitude Spectrum FR Test 1: Simulated System')
xlabel('Frequency (Hz)')
ylabel('|Y(f)|')
axis([0,1,0,0.2])

subplot(2,2,4)
plot(f_s,2*abs(Y_2_ths2(1:NFFT_s/2+1)),'-',
f_s,2*abs(Y_2_xs2(1:NFFT_s/2+1)),'--')
title('Single-Sided Amplitude Spectrum FR Test 2: Simulated System')
xlabel('Frequency (Hz)')
ylabel('|Y(f)|')
axis([0,1,0,0.2])
%%%%%%%%%%%%%%%%%%%%%%%%%%%%%%%%%%%%%%%%%%%%%%%%%%%%%%%%%%%%%%%%%%%%%%%%%%%
%Plots comparing simulated and experimental responses for each mass
figure(2)
subplot(2,2,1)
plot(t3B_a,x3B_a,'-',ts,xs3,'--','LineWidth',2)
legend('Experimental x','Simulated x')
xlabel('time(sec)')
ylabel('m')
title('Free Response Simulation: Test 3')

subplot(2,2,2)
plot(t3B_a,th3B_a,'-',ts,ths3,'--','LineWidth',2)
legend('Experimental theta','Simulated theta')
xlabel('time(sec)')
ylabel('Radians')
title('Free Response Simulation: Test 3')
%%%%%%%%%%%%%%%%%%%%%%%%%%%%%%%%%%%%%%%%%%%%%%%%%%%%%%%%%%%%%%%%%%%%%%%%%%%%%%
%%%%%%%%%%%%%%%%%%%%%%%%%%%%%%%%%%%%%%%%%%%%%%%%%%%%%%%%%%%%%%%%%%%%%%%%%%%%
%Plot for Paper
%Test 1
figure(4)
subplot(2,1,1)
plot(t1B_a,x1B_a,'-b',ts,xs1,'--g','LineWidth',2)
xlabel('time (sec)','FontName','Times','FontSize',18)
ylabel('M_1 Displacement, x (m)','FontName','Times','FontSize',18)
set(gca,'XTick',[0,1,2,3,4,5,6,7,8],'FontSize',16)
set(gca,'YTick',[-0.08,-0.06,-0.04,-0.02,0,0.02,0.04,0.06,0.08],
```

121

```
'FontSize',16)
axis([0,6,-0.095,0.09]);
grid on
subplot(2,1,2)
plot(t1B_a,th1B_a,'-b',ts,ths1,'--g','LineWidth',2)
xlabel('time (sec)','FontName','Times','FontSize',18)
ylabel('M_2 Displacement, \theta (rad)','FontName','Times',
'FontSize',18)
set(gca,'XTick',[0,1,2,3,4,5,6],'FontSize',16)
set(gca,'YTick',[-0.4,-0.3,-0.2,-0.1,0,0.1,0.2,0.3,0.4],
'FontSize',16)
axis([0,6,-0.4,0.4]);
grid on
figure(5)
subplot(2,2,1)
plot(x1B_a,th1B_a,'-b','LineWidth',1.5)
xlabel('x (m)','FontName','Times','FontSize',20)
ylabel('\theta (rad)','FontName','Times','FontSize',20)
axis([-.095,0.08,-.31,.4]);
set(gca,'XTick',[-.08,-.06,-.04,-.02,0,.02,.04,.06,.08],'FontSize',15)
set(gca,'YTick',[-0.3,-0.2,-0.1,0,0.1,0.2,0.3,0.4],'FontSize',16)
grid on
subplot(2,2,2)
plot(xs1,ths1,'--g','LineWidth',1.5)
xlabel('x (m)','FontName','Times','FontSize',20)
ylabel('\theta (rad)','FontName','Times','FontSize',20)
axis([-.095,.09,-.31,0.4]);
set(gca,'XTick',[-.08,-.06,-.04,-.02,0,.02,.04,.06,.08],'FontSize',15)
set(gca,'YTick',[-0.3,-0.2,-0.1,0,0.1,0.2,0.3,0.4],'FontSize',16)
grid on
%Code for plotting Test 2 omitted for space
%Code for plotting Test 4 Omitted for space
```

Uncoupled_FR.m

```
%Compared experimental and simulated response of uncoupled masses runs
%Uncoupled_Mass_FR.mdl and compares it to Experimental Data to simulate
%free response of the uncoupled masses due to  initial conditions (IC)
%Runs fft analysis on experimental and simulated data and plots
%frequency plots
%%%%%%%%%%%%%%%%%%%%%%%%%%%%%%%%%%%%%%%%%%%%%%%%%%%%%%%%%%%%%%%%%%%%%%%%%%%
%Experimental Data
FRM2=load('C:\...\Free Response Mass AB & M1\fr_ab_only.mat');
FR_M1=load('C:\...\Data_9_12\m1_onlya_9_12.mat');
%%%%Free Response Data M2
tab=FRM2.fr_ab_only.X.Data;
thab=FRM2.fr_ab_only.Y(4).Data;
dthab=FRM2.fr_ab_only.Y(3).Data;
%IC starts at tab=2.16sec Which is tab(73)
%Run for 15 sec
tab_a=(0:0.03:15);
thab_a=thab(73:(tab_a(length(tab_a))/0.03+73));
```

122

```
dthab_a=dthab(73:(tab_a(length(tab_a))/0.03+73));
%%%%Free Response Data M1
tM1=FR_M1.m1_onlya_9_12.X.Data;
xM1=FR_M1.m1_onlya_9_12.Y(1).Data;
dxM1=FR_M1.m1_onlya_9_12.Y(6).Data;
%Test a: IC starts at tab=0.72sec
IC=0.72;
M1_IC=IC/ST_M1+1;
tM1_a=(0:ST_M1:tM1(end)-IC);
xM1_a=xM1(M1_IC:(tM1_a(length(tM1_a))/ST_M1+M1_IC));
dxM1_a=dxM1(M1_IC:(tM1_a(length(tM1_a))/ST_M1+M1_IC));
%%%%%%%%%%%%%%%%%%%%%%%%%%%%%%%%%%%%%%%%%%%%%%%%%%%%%%%%%%%%%%%%%%%%%%%%%%%
%Simulated Response
c=2;                %Damping in Cart, N*s/m
g=9.81;             %Gravity, m/s^2
k=84.7;             %Spring Constant, N/m
M1=0.95;            %Mass of M_1, kg
mR=0.1776;          %Mass of Pendulum Rod, kg
LT=0.3715;          %R length (rotation center to pend base), m
mu_k=0.02;
W1=g*M1;
b=3.844*10^(-4);    %Damping in Pendulum due to Mass B, N*m*s/rad
h=0.0293+0.0316;    %Height of pendulum bob, m
L=LT-h/2;           %Pend rod length (to center of gravity), m
M2=1.1854+mR;       %Mass of M_2 for Mass B, kg
%Initial Conditions of Mass M1
x0=xM1_a(1)/100;              %IC of M_1 equal to experimental, m
dx0=dxM1_a(1)/100;           %Initial Velocity of M_1, m/s
%Initial Conditions of Mass M2
th0=thab_a(1)*(pi/180);      %IC of M_2 equal to experimental, rad
dth0=dthab_a(1)*(pi/180);    %Initial angular velocity, rad/s

sim Uncoupled_Masses_FR

time=disp(:,1);
x=disp(:,2)*100;            %Converting output to cm
theta=disp(:,3)*180/pi;     %Converting output to degrees
x_prime=disp(:,4);          %dx/dt
theta_prime=disp(:,5);      %dtheta/dt
%%%%%%%%%%%%%%%%%%%%%%%%%%%%%%%%%%%%%%%%%%%%%%%%%%%%%%%%%%%%%%%%%%%%%%%%%%%
figure(1)
subplot(2,1,1)
plot(tM1_a,xM1_a,'-',time,x,'--','LineWidth',2)
legend('Exp.Data','Sim. Data')
xlabel('time(sec)')
ylabel('Displacement (cm)')
title('Free Response of Uncoupled Mass M1')

subplot(2,1,2)
plot(tab_a,thab_a,'-',time,theta,'--','LineWidth',2)
legend('Exp.Data','Sim. Data')
```

123

```
xlabel('time(sec)')
ylabel('Displacement (deg)')
title('Free Response of Uncoupled Mass M2')
%%%%%%%%%%%%%%%%%%%%%%%%%%%%%%%%%%%%%%%%%%%%%%%%%%%%%%%%%%%%%%%%%%%%%%%%
%Finding Oscillating Frequency
%M1_Experimental Data
ST_M1=tM1_a(2)-tM1_a(1);          %Sample Time Step - Exp. Sys
SF_M1=1/ST_M1;                    %Sampling Frequency - Exp. Sys
L_M1=length(xM1_a);              %Number of samples
NFFT_M1 = 2^nextpow2(L_M1);       %Next power of 2
Y_M1 = fft(xM1_a,NFFT_M1)/L_M1;   %fft calculation
f_M1= SF_M1/2*linspace(0,1,NFFT_M1/2+1);
%M2 Experimental Data
ST_M2=tab_a(2)-tab_a(1);          %Sample Time Step - Exp. Sys
SF_M2=1/ST_M2;                    %Sampling Frequency - Exp. Sys
L_M2=length(thab_a);             %Number of samples
NFFT_M2 = 2^nextpow2(L_M2);       %Next power of 2
Y_M2 = fft(thab_a,NFFT_M2)/L_M2;  %fft calculation
f_M2= SF_M2/2*linspace(0,1,NFFT_M2/2+1);
%M1_Simulated Data
ST_x=time(2)-time(1);             %Sample Time Step - Exp. Sys
SF_x=1/ST_x;                      %Sampling Frequency - Exp. Sys
L_x=length(x);                   %Number of samples
NFFT_x = 2^nextpow2(L_x);         %Next power of 2
Y_x = fft(x,NFFT_x)/L_x;          %fft calculation
f_x= SF_x/2*linspace(0,1,NFFT_x/2+1);
%M2 Experimental Data
ST_th=time(2)-time(1);            %Sample Time Step - Exp. Sys
SF_th=1/ST_th;                    %Sampling Frequency - Exp. Sys
L_th=length(theta);              %Number of samples
NFFT_th = 2^nextpow2(L_th);       %Next power of 2
Y_th = fft(theta,NFFT_th)/L_th;   %fft calculation
f_th= SF_th/2*linspace(0,1,NFFT_th/2+1);
% Plot single-sided amplitude spectrum.
figure(4)
%M1 Free response, Experimental: frequency plots
subplot(2,2,1)
plot(f_M1,2*abs(Y_M1(1:NFFT_M1/2+1)))
title('Single-Sided Amplitude Spectrum of M1 Experimental Data')
xlabel('Frequency (Hz)')
ylabel('|Y(f)|')
axis([0,10,0,6])
%M2 Free Response, Experimental
subplot(2,2,2)
plot(f_M2,2*abs(Y_M2(1:NFFT_M2/2+1)))
title('Single-Sided Amplitude Spectrum of M2 Experimental Data')
xlabel('Frequency (Hz)')
ylabel('|Y(f)|')
axis([0,10,0,35])
%M1 Free Response, Simulated
subplot(2,2,3)
```

124

```
plot(f_x,2*abs(Y_x(1:NFFT_x/2+1)))
title('Single-Sided Amplitude Spectrum of M1 Simulated Data')
xlabel('Frequency (Hz)')
ylabel('|Y(f)|')
axis([0,10,0,6])
%M2 Free Response, Simulated
subplot(2,2,4)
plot(f_th,2*abs(Y_th(1:NFFT_th/2+1)))
title('Single-Sided Amplitude Spectrum of M2 Simulated Data')
xlabel('Frequency (Hz)')
ylabel('|Y(f)|')
axis([0,10,0,35])
```

Uncoupled_Masses.m

```
%Analysis of experimental data of free response of uncoupled masses to
%determine parameter values;
%fft analysis to determine damped natural frequency
%%%%%%%%%%%%%%%%%%%%%%%%%%%%%%%%%%%%%%%%%%%%%%%%%%%%%%%%%%%%%%%%%%%%%%%%%%%
%Experimental Data
FR_M2=load('C:\...\Data_9_12\m2_onlya_9_12');    %M2 data
FR_M1=load('C:\...\Data_9_12\m1_onlya_9_12');    %M1 data
%Free Response Data M2
tab=FR_M2.m2_onlya_9_12.X.Data;              %Time
thab=FR_M2.m2_onlya_9_12.Y(4).Data;          %Theta
dthab=FR_M2.m2_onlya_9_12.Y(3).Data;         %dTheta/dt
%Free Response Data M1
tM1=FR_M1.m1_onlya_9_12.X.Data;              %Time
xM1=FR_M1.m1_onlya_9_12.Y(1).Data;           %x
dxM1=FR_M1.m1_onlya_9_12.Y(6).Data;          %dx/dt
ST_M1=tM1(2)-tM1(1);                          %Sample Time Step
SF_M1=1/ST_M1;                               %Sampling Frequency
%Test a: Initial Condition (IC) starts at time tab=0.72sec
IC=0.72;
M1_IC=IC/ST_M1+1;
tM1_a=(0:ST_M1:tM1(end)-IC);
xM1_a=xM1(M1_IC:(tM1_a(length(tM1_a))/ST_M1+M1_IC));
dxM1_a=dxM1(M1_IC:(tM1_a(length(tM1_a))/ST_M1+M1_IC));
%%%%%%%%%%%%%%%%%%%%%%%%%%%%%%%%%%%%%%%%%%%%%%%%%%%%%%%%%%%%%%%%%%%%%%%%%%%
figure(1)
subplot(2,1,1)
plot(tM1,xM1,'-','LineWidth',2)
xlabel('time(sec)')
ylabel('Displacement (cm)')
title('Free Response of Uncoupled Mass M1')
%%%%%%%%%%%%%%%%%%%%%%%%%%%%%%%%%%%%%%%%%%%%%%%%%%%%%%%%%%%%%%%%%%%%%%%%%%%
subplot(2,1,2)
plot(tab,thab,'-','LineWidth',2)
xlabel('time(sec)')
ylabel('Displacement (deg)')
title('Free Response of Uncoupled Mass M2')
%%%%%%%%%%%%%%%%%%%%%%%%%%%%%%%%%%%%%%%%%%%%%%%%%%%%%%%%%%%%%%%%%%%%%%%%%%%
```

125

```
figure(2)
a=0;
plot(tM1_a,xM1_a,'-',tM1_a,dxM1_a,'--',tM1_a,a,'-k','LineWidth',2)
legend('M1 displacement','M1 Velocity')
title('Experimental Data')
%%%%%%%%%%%%%%%%%%%%%%%%%%%%%%%%%%%%%%%%%%%%%%%%%%%%%%%%%%%%%%%%%%%%%%%%
%Finding Oscillating Frequency
%M1_Experimental Data
L_M1=length(xM1_a);                 %Number of samples
NFFT_M1 = 2^nextpow2(L_M1);         %Next power of 2
Y_M1 = fft(xM1_a,NFFT_M1)/L_M1;
f_M1= SF_M1/2*linspace(0,1,NFFT_M1/2+1);
%M2 Experimental Data
ST_M2=tab(2)-tab(1);                %Sample Time Step
SF_M2=1/ST_M2;                      %Sampling Frequency
L_M2=length(thab);                  %Number of samples
NFFT_M2 = 2^nextpow2(L_M2);         %Next power of 2 from
Y_M2 = fft(thab,NFFT_M2)/L_M2;      %Fast fourier transform
```

Magnetic Force Code
Electromagnet_Force.m

```
%Calculations on magnetic force for Mass-Pendulum project.
%Comparing holding force of two masses of different cross sections
%Comparing holding force of mass B with various air gap cross sectional
%areas
%%%%%%%%%%%%%%%%%%%%%%%%%%%%%%%%%%%%%%%%%%%%%%%%%%%%%%%%%%%%%%%%%%%%%%%%
mu0=4*pi*10^(-7);      %Permability of free space, H/m
mur=70;                %Relative permeability of steel
L1E=8;                 %Magnetic Path of Electromagnet, in
L1=L1E*0.0254;         %m
L2E=2.25;              %Magnetic path through Pendulum, in
L2=L2E*0.0254;         %m
AcE=pi*0.5^2;          %Cross sectional Area of Core, in^2
Ac=AcE*(0.0254)^2;     %m^2
%For 22-AWG wire
NA=432*2;              %Turns
IA=2.67;               %Current, Amps
xg_Eng=0:0.001:4;      %Air gap length, Dist. b/t magnet and pend, in
xg=xg_Eng*(2.54/100);  %m
%%%%%%%%%%%%%%%%%%%%%%%%%%%%%%%%%%%%%%%%%%%%%%%%%%%%%%%%%%%%%%%%%%%%%%%%
%Pendulum Mass A
h_A=1.155;                          %Height M_2A, in
AlE_A=(pi*(2.25/2)^2*h_A)/2.25;     %Avg cross sectional area, in^2
Al_A=AlE_A*(0.0254)^2;              %Avg cross sectional area, m^2

%Neglecting Fringing
Ag_A=Ac;                            %Air gap cross sectional area
R_NA=L1/(mu0*mur*Ac)+(2*xg)./(mu0*Ag_A)+L2/(mu0*mur*Al_A);
dRdx_NA=2/(mu0*Ag_A);                         %dR/dx
fmech_NA=0.5*(NA*IA)^2./(R_NA.^2).*dRdx_NA;  %Magnetic force, N
```

126

```matlab
fmech_N_EngA=fmech_NA/4.448;                    %Magnetic force, Lbs
%Acounting for Fringing
AgF_A=(sqrt(Ag_A)+xg).^2;
R_FA=L1/(mu0*mur*Ac)+(2*xg)./(mu0*AgF_A)+L2/(mu0*mur*Al_A);
dRdx_FA=(-2*(xg-sqrt(Ag_A)))./(mu0*(sqrt(Ag_A)+xg).^3);
fmech_FA=0.5*(NA*IA)^2./R_FA.^2.*dRdx_FA;       %Magnetic force, N
fmech_F_EngA=abs(fmech_FA)/4.448;               %Magnetic force, Lbs
Fhold_A=fmech_FA(1);                            %Holding force, N
Fhold_Eng_A=fmech_F_EngA(1);                    %Holding force, lb
%%%%%%%%%%%%%%%%%%%%%%%%%%%%%%%%%%%%%%%%%%%%%%%%%%%%%%%%%%%%%%%%%%%%%%
%Pendulum Mass B
hB=2.4;                         %Height M_2B, in
AlE_B=(pi*(2.25/2)^2*hB)/2.25;  %Avg cross sectional area, in^2
Al_B=AlE_B*(0.0254)^2;          %Avg cross sectional area, m^2

%Neglecting Fringing
Ag_B=Ac;                        %Air gap cross sectional area equal to core
R_NB=L1/(mu0*mur*Ac)+(2*xg)./(mu0*Ag_B)+L2/(mu0*mur*Al_B);%Reluctance
dRdx_NB=2/(mu0*Ag_B);                           %dR/dx
fmech_NB=0.5*(NA*IA)^2./(R_NB.^2).*dRdx_NB;     %Magnetic force, N
fmech_N_EngB=fmech_NB/4.448;                    %Magnetic force, Lbs
%Acounting for Fringing
AgF_B=(sqrt(Ag_B)+xg).^2;
R_FB=L1/(mu0*mur*Ac)+(2*xg)./(mu0*AgF_B)+L2/(mu0*mur*Al_B);
dRdx_FB=(-2*(xg-sqrt(Ag_B)))./(mu0*(sqrt(Ag_B)+xg).^3);
fmech_FB=0.5*(NA*IA)^2./R_FB.^2.*dRdx_FB;
fmech_F_EngB=abs(fmech_FB)/4.448;               %Converting to lbs
Fhold_B=fmech_FB(1);                            %Holding force, N
Fhold_Eng_B=fmech_F_EngB(1);                    %Holding force, lb
%%%%%%%%%%%%%%%%%%%%%%%%%%%%%%%%%%%%%%%%%%%%%%%%%%%%%%%%%%%%%%%%%%%%%%%%%%
%%%%%%%%%%%%%%%%%%%%%%%%%%%%%%%%%%%%%%%%%%%%%%%%%%%%%%%%%%%%%%%%%%%%%%%%%%
%Checking influence of Ag (Air gap cross sectional area) for Mass B
Ag_B2=(Ac+Al_B)/2;      %Air gap cross sectional area as avg
Ag_B3=2.5*Ac;           %Air gap cross sectional area as 2.5 of Ac

%Neglecting Fringing
R_NB2=L1/(mu0*mur*Ac)+(2*xg)./(mu0*Ag_B2)+L2/(mu0*mur*Al_B);
dRdx_NB2=2/(mu0*Ag_B2);                         %dR/dx
fmech_NB2=0.5*(NA*IA)^2./(R_NB2.^2).*dRdx_NB2; %Magnetic force, N
fmech_N_EngB2=fmech_NB2/4.448;                  %Magnetic force, Lbs
%Acounting for Fringing
AgF_B2=(sqrt(Ag_B2)+xg).^2;
R_FB2=L1/(mu0*mur*Ac)+(2*xg)./(mu0*AgF_B2)+L2/(mu0*mur*Al_B);
dRdx_FB2=(-2*(xg-sqrt(Ag_B2)))./(mu0*(sqrt(Ag_B2)+xg).^3);
fmech_FB2=0.5*(NA*IA)^2./R_FB2.^2.*dRdx_FB2;    %Magnetic force, N
fmech_F_EngB2=abs(fmech_FB2)/4.448;             %Lbs

%Neglecting Fringing
R_NB3=L1/(mu0*mur*Ac)+(2*xg)./(mu0*Ag_B3)+L2/(mu0*mur*Al_B);
dRdx_NB3=2/(mu0*Ag_B3);                         %dR/dx
fmech_NB3=0.5*(NA*IA)^2./(R_NB3.^2).*dRdx_NB3; %Magnetic force, N
```

127

```
fmech_N_EngB3=fmech_NB3/4.448;                    %Lbs
%Acounting for Fringing
AgF_B3=(sqrt(Ag_B3)+xg).^2;
R_FB3=L1/(mu0*mur*Ac)+(2*xg)./(mu0*AgF_B3)+L2/(mu0*mur*Al_B);
dRdx_FB3=(-2*(xg-sqrt(Ag_B3)))./(mu0*(sqrt(Ag_B3)+xg).^3);%dR/dx
fmech_FB3=0.5*(NA*IA)^2./R_FB3.^2.*dRdx_FB3;   %Magnetic force, N
fmech_F_EngB3=abs(fmech_FB3)/4.448;               %Lbs
Fhold_B2=fmech_FB2(1);                %Holding force air gap Ag_B2, N
Fhold_Eng_B2=fmech_F_EngB2(1);      %Lbs
Fhold_B3=fmech_FB3(1);                %Holding force air gap Ag_B3, N
Fhold_Eng_B3=fmech_F_EngB3(1);      %Lbs
%%%%%%%%%%%%%%%%%%%%%%%%%%%%%%%%%%%%%%%%%%%%%%%%%%%%%%%%%%%%%%%%%%%%%
%Holding Forces
fprintf('mu_r=70\n')
fprintf('\n')
fprintf('Holding Force on Mass A: (Ag=Ac) N, Lb')
F_Hold_M2A=[Fhold_A,Fhold_Eng_A]
fprintf('Holding Force on Mass B: (Ag=Ac) N, Lb and')
fpringf('(Ag=(Ac+AL)/2) N,Lb')
F_Hold_M2B=[Fhold_B,Fhold_Eng_B,Fhold_B2,Fhold_Eng_B2]
fprintf('Holding Force on Mass B: (Ag=Al) N, Lb')
F_Hold_M2B_3=[Fhold_B3,Fhold_Eng_B3]
%%%%%%%%%%%%%%%%%%%%%%%%%%%%%%%%%%%%%%%%%%%%%%%%%%%%%%%%%%%%%%%%%%%%%%%%
%%%%%%%%%%%%%%%%%%%%%%%%%%%%%%%%%%%%%%%%%%%%%%%%%%%%%%%%%%%%%%%%%%%%%%%%
%Checking influence of relative permeability, mu_r,
%on Mass B, for Ag_B=Ac
mur2=50;                %Relative permeability of core and load
R_NBmu2=L1/(mu0*mur2*Ac)+(2*xg)./(mu0*Ag_B)+L2/(mu0*mur2*Al_B);
dRdx_NBmu2=2/(mu0*Ag_B);                      %dR/dx
fmech_NBmu2=0.5*(NA*IA)^2./(R_NBmu2.^2).*dRdx_NBmu2; %magnet force, N
fmech_N_EngBmu2=fmech_NBmu2/4.448;         %Lbs
Fhold_mu2=fmech_NBmu2(1);                   %Holding force, N

mur3=60;                %Relative permeability or core and load
R_NBmu3=L1/(mu0*mur3*Ac)+(2*xg)./(mu0*Ag_B)+L2/(mu0*mur3*Al_B);
dRdx_NBmu3=2/(mu0*Ag_B);                      %dR/dx
fmech_NBmu3=0.5*(NA*IA)^2./(R_NBmu3.^2).*dRdx_NBmu3; %Magnet force, N
fmech_N_EngBmu3=fmech_NBmu3/4.448;         %Lbs
Fhold_mu3=fmech_NBmu3(1);                   %Holding force, N

mur4=80;                %Relative permeability of core and load
R_NBmu4=L1/(mu0*mur4*Ac)+(2*xg)./(mu0*Ag_B)+L2/(mu0*mur4*Al_B);
dRdx_NBmu4=2/(mu0*Ag_B);                      %dR/dx
fmech_NBmu4=0.5*(NA*IA)^2./(R_NBmu4.^2).*dRdx_NBmu4; %Magnet force, N
fmech_N_EngBmu4=fmech_NBmu4/4.448;         %Lbs
Fhold_mu4=fmech_NBmu4(1);                   %Holding force, N

murC=80;                %Relative permeability of core
murL=30;                %Relative permeability of load
R_NBmu_D=L1/(mu0*murC*Ac)+(2*xg)./(mu0*Ag_B)+L2/(mu0*murL*Al_B);
dRdx_NBmu_D=2/(mu0*Ag_B);                     %dR/dx
```

128

```matlab
fmech_NBmu_D=0.5*(NA*IA)^2./(R_NBmu_D.^2).*dRdx_NBmu_D;%Magnet-force, N
fmech_N_EngBmu_D=fmech_NBmu_D/4.448;          %Lbs
Fhold_mu_D=fmech_NBmu_D(1);                    %Holding force, N
%%%%%%%%%%%%%%%%%%%%%%%%%%%%%%%%%%%%%%%%%%%%%%%%%%%%%%%%%%%%%%%%%%%%%%%%%
%Holding Forces
fprintf('Holding Force on Mass B (Ag=Ac): mu_r=50, 60, 70, 80,')
fprintf{'and mu_rC=80 and mu_rL=30 \n')
fprintf('Force is in Newtons')
F_Hold_B_mu=[Fhold_mu2,Fhold_mu3,Fhold_B,Fhold_mu4,Fhold_mu_D]
%%%%%%%%%%%%%%%%%%%%%%%%%%%%%%%%%%%%%%%%%%%%%%%%%%%%%%%%%%%%%%%%%%%%%%%%%
%Plot for Paper Mass A and Mass B in metric units
%Neglecting fringing and considering fringing
figure(1)
y=0;
plot(xg,fmech_NA,'-r',xg,fmech_FA,'--r',xg,fmech_NB,'-b',
    xg,fmech_FB,'--b',xg,y,'-k','LineWidth',1.5)
xlabel('Air Gap, x_g, (m)','FontName','Times','FontSize',13)
ylabel('Magnetic Force (N)','FontName','Times','FontSize',13)
legend('M_A Neglecting Fringing','M_A Considering Fringing',
    'M_B Neglecting Fringing','M_B Considering Fringing')
set(gca,'XTick',[0,0.005,0.01,0.015,0.02,0.025],'FontSize',11)
axis([0,0.03,-1,50]);
grid on
%%%%%%%%%%%%%%%%%%%%%%%%%%%%%%%%%%%%%%%%%%%%%%%%%%%%%%%%%%%%%%%%%%%%%%%%%
figure(2)
%Effect of mu_r value
plot(xg,fmech_NBmu2,'-g',xg,fmech_NBmu3,'r',xg,fmech_NB,'-k',
    xg,fmech_NBmu4,'-b',xg,fmech_NBmu_D,'-m',xg,y,'-k','LineWidth',2)
xlabel('Air Gap, x_g, (m)','FontName','Times','FontSize',13)
ylabel('Magnetic Force (N)','FontName','Times','FontSize',13)
legend('mu_r=50','mu_r=60','mu_r=70','mu_r=80','mu_rC=80, mu_rL=30')
title('Magnetic Force, Mass B for Air Gap A_g=A_C Neglecting Fringing')
set(gca,'XTick',[0,0.01,0.015,0.02,0.025,0.03],'FontSize',11)
set(gca,'YTick',[0,1,2,3,4,5,6,7],'FontSize',11)
axis([0.01,0.03,0.7,7]);
grid on
%%%%%%%%%%%%%%%%%%%%%%%%%%%%%%%%%%%%%%%%%%%%%%%%%%%%%%%%%%%%%%%%%%%%%%%%%
%Plot for paper comparing different air gap lengths w/ and w/o fringing
figure(3)
subplot(1,1,1)
y=0;
plot(xg,fmech_NB,'-k',xg,fmech_FB,':k',xg,fmech_NB2,'--k',
    xg,fmech_FB2,'-.k',xg,y,'-k','LineWidth',2.2)
xlabel('Air Gap, x_g, (m)','FontName','Times','FontSize',13)
ylabel('Magnetic Force (N)','FontName','Times','FontSize',13)
set(gca,'XTick',[0,0.005,0.01,0.015,0.02,0.025,0.03],'FontSize',11)
axis([0,0.03,-1,70]);
grid on
```

Magnetic_Force_Symbolic.m
```matlab
%Calculating symbolic equation for magnetic force
```

129

```
%%%%%%%%%%%%%%%%%%%%%%%%%%%%%%%%%%%%%%%%%%%%%%%%%%%%%%%%%%%%%%%%%%%%%%%%%
syms mu0 mur L1 L2 N I xg Ac Al Ag
%mu0=4*pi*10^(-7);            %Permability of free space, H/m
%mur=80;                      %Relative permeability of steel
%Neglecting Fringing
R_NB=(L1/(mu0*mur*Ac))+((2*xg)/(mu0*Ag))+ (L2/(mu0*mur*Al));%Reluctance
dRdx_NB=2/(mu0*Ag);                          %Deriv. of reluctance w.r.t x
fmech_NB=0.5*(N*I)^2/(R_NB^2)*dRdx_NB;  %Magnetic force in Newtons
pretty(fmech_NB)
%Acounting for Fringing
AgF_B=(sqrt(Ag)+xg)^2;
R_FB=L1/(mu0*mur*Ac)+(2*xg)/(mu0*AgF_B)+L2/(mu0*mur*Al);
dRdx_FB=(-2*(xg-sqrt(Ag)))/(mu0*(sqrt(Ag)+xg)^3);
fmech_FB=0.5*(N*I)^2/R_FB^2*dRdx_FB;
pretty(fmech_FB)
```

Magnetic_f_paper.m

```
%Calculations of magnetic force functions in terms of variable x_g
%%%%%%%%%%%%%%%%%%%%%%%%%%%%%%%%%%%%%%%%%%%%%%%%%%%%%%%%%%%%%%%%%%%%%%%%%
syms xg
mu0=4*pi*10^(-7);          %Permeability of free space, H/m
mur=70;                    %Relative permeability of steel
L1E=8;                     %Magnetic Path of Electromagnet, in
L2E=2.25;                  %Magnetic path through Pendulum
    %(diameter of pendulum Bob, in)
AcE=pi*0.5^2;              %Cross sectional Area of Core, in^2
%Converted to metric
Ac=AcE*(0.0254)^2;         %Cross sectional Area of Core, m^2
L1=L1E*0.0254;             %m
L2=L2E*0.0254;             %m
%For 22-AWG wire
NA=432*2;                  %Turns
IA=2.67;                   %Current, Amps
%Mass M_2B
hB=2.4;                              %Height of pendulum M_2B, in
AlE_B=(pi*(2.25/2)^2*hB)/2.25;   %M2 avg cross sectional area, in^2
%Convert to Metric
Al_B=AlE_B*(0.0254)^2;           %m^2
%%%%%%%%%%%%%%%%%%%%%%%%%%%%%%%%%%%%%%%%%%%%%%%%%%%%%%%%%%%%%%%%%%%%%%%%%
%Neglecting Fringing
%Ag_B=Ag;                         %Cross sectional area of air gap
%Ag_B=(Ac+Al_B)/2;
Ag_B=2.5*Ac;
R_NB=simple(L1/(mu0*mur*Ac)+(2*xg)/(mu0*Ag_B)+L2/(mu0*mur*Al_B));
dRdx_NB=2/(mu0*Ag_B);            %dR/dx
phi=(NA*IA)/(R_NB);              %Magnetic flux
fmech_NB=0.5*phi^2*dRdx_NB;      %Magnetic force in Newtons
fmech_NC=simple(fmech_NB);       %Simplify function
fprintf('Magnetic Forcing Function, Neglecting Fringing')
pretty(fmech_NC)
%%%%%%%%%%%%%%%%%%%%%%%%%%%%%%%%%%%%%%%%%%%%%%%%%%%%%%%%%%%%%%%%%%%%%%%%%
```

130

```
%Acounting for Fringing
AgF_B=(sqrt(Ag_B)+xg)^2;
R_FB=simple(L1/(mu0*mur*Ac)+(2*xg)/(mu0*AgF_B)+L2/(mu0*mur*Al_B));
dRdx_FB=simple((-2*(xg-sqrt(Ag_B)))/(mu0*(sqrt(Ag_B)+xg)^3));
phi_F=simple((NA*IA)/R_FB);
fmech_FB=0.5*phi_F^2*dRdx_FB;
fprintf('Magnetic Forcing Function, Considering Fringing')
pretty(fmech_FB)
```

Miscellaneous Code
M1_M2_Uncertainty.m

```
%Calculate uncertainty of the system parameters
%Calculating system parameters from experimentally measured log
%decrement and w_d for uncoupled M1 and M2
%Calculating propagated error to find uncertainty in system parameters
%M_1 Experimentally determined values
%%%%%%%%%%%%%%%%%%%%%%%%%%%%%%%%%%%%%%%%%%%%%%%%%%%%%%%%%%%%%%%%%%%%%%%%%%
M1=0.950;               %M1 mass, kg
u_M1=0.124;             %M1 uncertainty
del_c=0.5705;           %Log decrement
u_del_c=0.2367;         %Log decrement uncertainty
wd_c=9.698;             %Damped natural Frequency (rad/s)
u_wd_c=0.346;           %Uncertainty in Frequency
%%%%%%%%%%%%%%%%%%%%%%%%%%%%%%%%%%%%%%%%%%%%%%%%%%%%%%%%%%%%%%%%%%%%%%%%%%

%M_1 Calculated Parameters
zeta_c=del_c/sqrt(4*pi^2+del_c^2);  %Damping ratio
wn_c=wd_c/sqrt(1-zeta_c^2);         %Natural Freq, rad/s
k=wn_c^2*M1;                        %Spring Constant, N*m
c=2*zeta_c*wn_c*M1;                 %Damping coeffieicnt N*s/m
%M_1 Uncertainty
u_zeta_c=abs(-0.5*del_c*(4*pi^2+del_c)^(-3/2)+(4*pi^2+del_c)^(-1/2)*
u_del_c);
u_wn_c=sqrt(((1-zeta_c^2)^(-1/2)*u_wd_c)^2+((wd_c*zeta_c)*
(1-zeta_c^2)^(-3/2)*u_zeta_c)^2);
u_k=sqrt((2*wn_c*M1*u_wn_c)^2+(wn_c^2*u_M1)^2);
u_c=sqrt((2*wn_c*M1*u_zeta_c)^2+(2*wn_c*zeta_c*u_M1)^2+(2*zeta_c*
M1*u_wn_c)^2);
fprintf('M_1 Calculated Parameters \n')
fprintf('zeta_c, u_zeta_c, wn_c, u_wn, k, u_k, c, u_c')
M1_Parameters=[zeta_c, u_zeta_c, wn_c, u_wn_c, k, u_k, c, u_c]
%%%%%%%%%%%%%%%%%%%%%%%%%%%%%%%%%%%%%%%%%%%%%%%%%%%%%%%%%%%%%%%%%%%%%%%%%%
%M_2 Experimentally determined values
R=0.3410;                           %Rod length, m
M2=1.363;                           %M2 mass, kg
u_M2=0.1239;                        %Uncertainty in M2 mass
del_p=1.186e-3;                     %Log decrement
u_del_p=5.77e-4;                    %Uncertainty in log decrement
wd_p=5.3192;                        %Damped natural feq
u_wd_p=6.98e-3;                     %Uncertainty
```

131

```
%M_2 Calculated parameters
zeta_p=del_p/sqrt(4*pi^2+del_p^2);   %Damping ratio
wn_p=wd_p/sqrt(1-zeta_p^2);          %Natural frequency
b=2*zeta_p*wn_p*M2*R^2;              %Damping coefficient
%M_2 Uncertainty
u_zeta_p=abs(-0.5*del_p*(4*pi^2+del_p)^(-3/2)+(4*pi^2+del_p)^(-1/2)*
u_del_p);
u_wn_p=sqrt(((1-zeta_p^2)^(-1/2)*u_wd_p)^2+(wd_p*zeta_p*
(1-zeta_p)^(-3/2))^2);
u_b=sqrt((2*wn_p*M2*R^2*u_zeta_p)^2+(2*zeta_p*M2*R^2*u_wn_p)^2+
(2*zeta_p*wn_p*R^2*u_M2)^2);
fpringf('M_2 Calculated Parameters \n')
fprintf('zeta_p, u_zeta_p, wn_p, u_wn_p, b, u_b')
M2_Parameters=[zeta_p, u_zeta_p, wn_p, u_wn_p, b, u_b]
```

Appendix C

Mass–Pendulum AutoCAD Drawings

The AutoCAD drawings for the mass–pendulum experimental system are shown with a brief description offered in the caption. The system material is given. Unless otherwise noted, units are in inches.
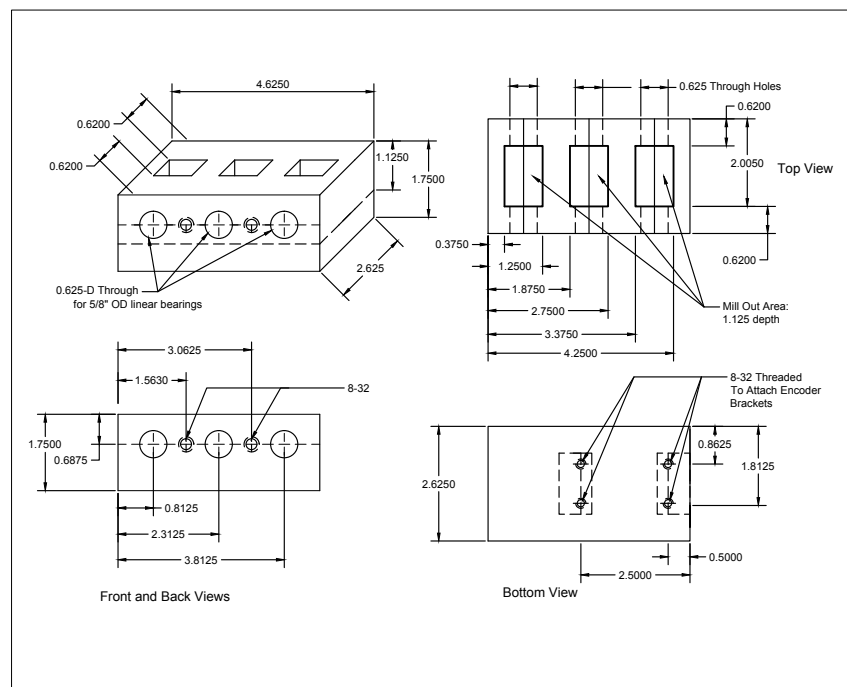
Figure C.1: Mass M_1 made of aluminum, designed to hold 6 linear ball bearings, support the pendulum, and attach the spring
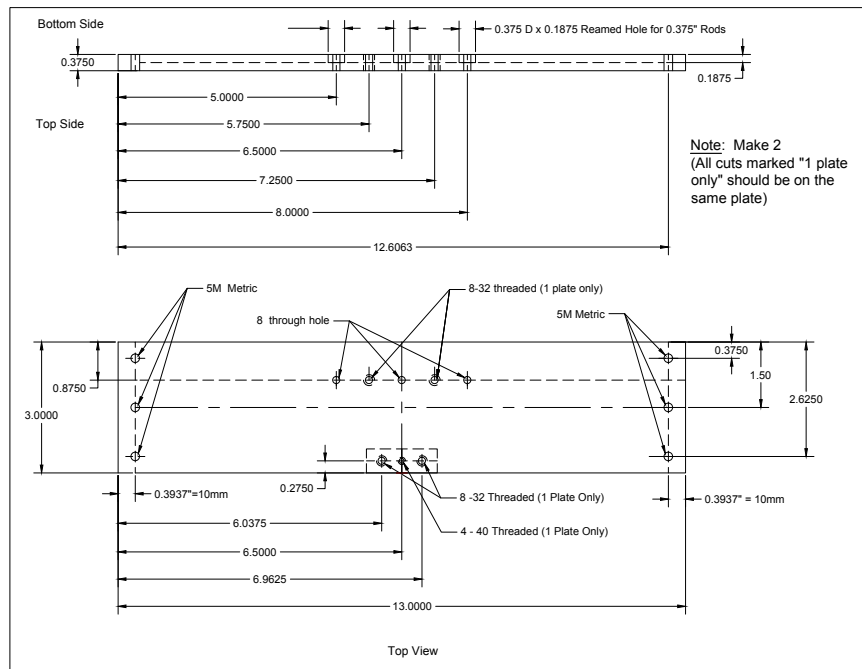
Figure C.2: Aluminum, structure end plates to support parallel rods and connector brackets of the beam load cell
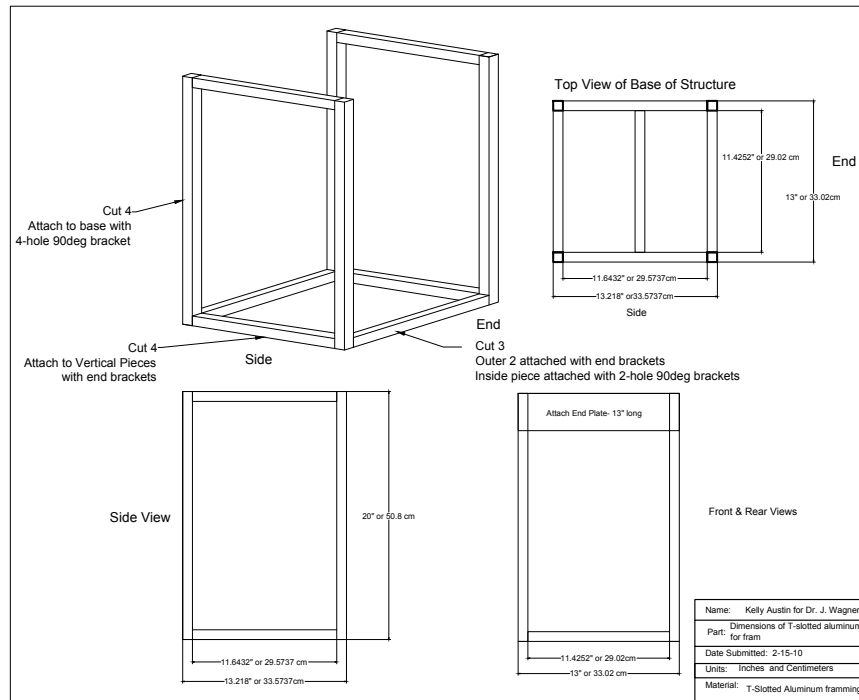
Figure C.3: Dimensions of structure made from 20mm extruded aluminum
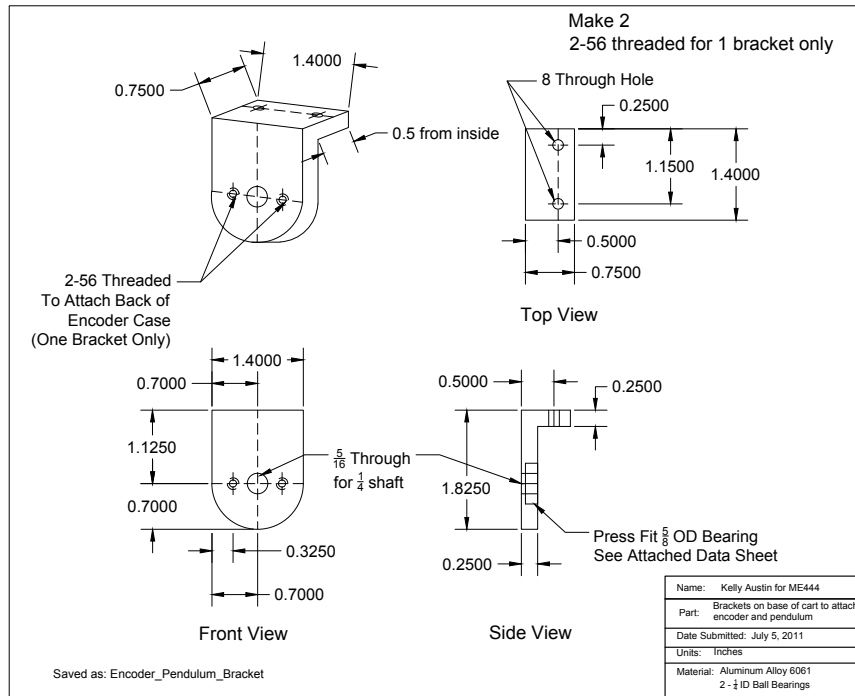
Figure C.4: Aluminum brackets supporting the encoder casing and a 6.35mm diameter pendulum support rod
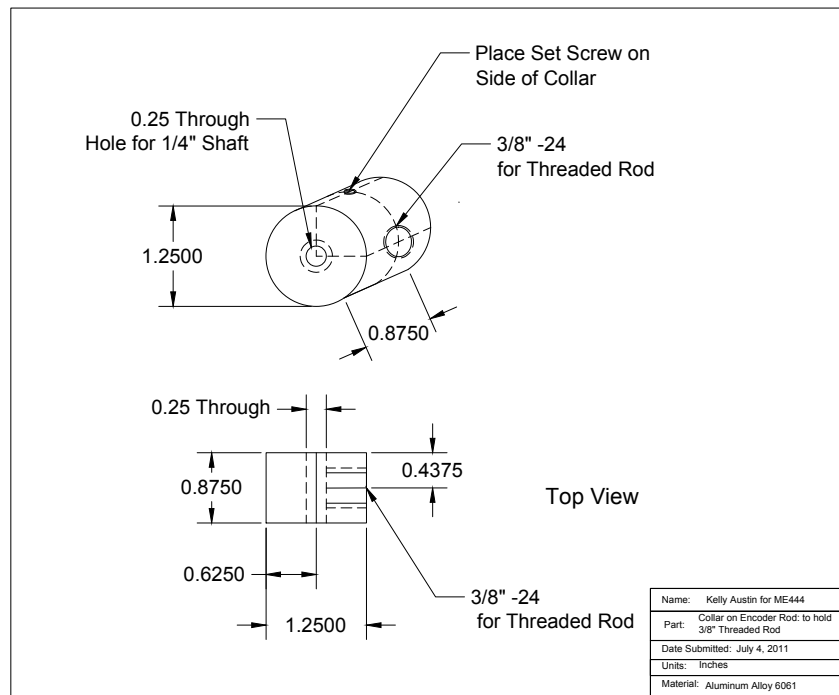
Figure C.5: Aluminum collar attached over a 6.35mm diameter rod, providing a threaded attachment for the pendulum rod

135
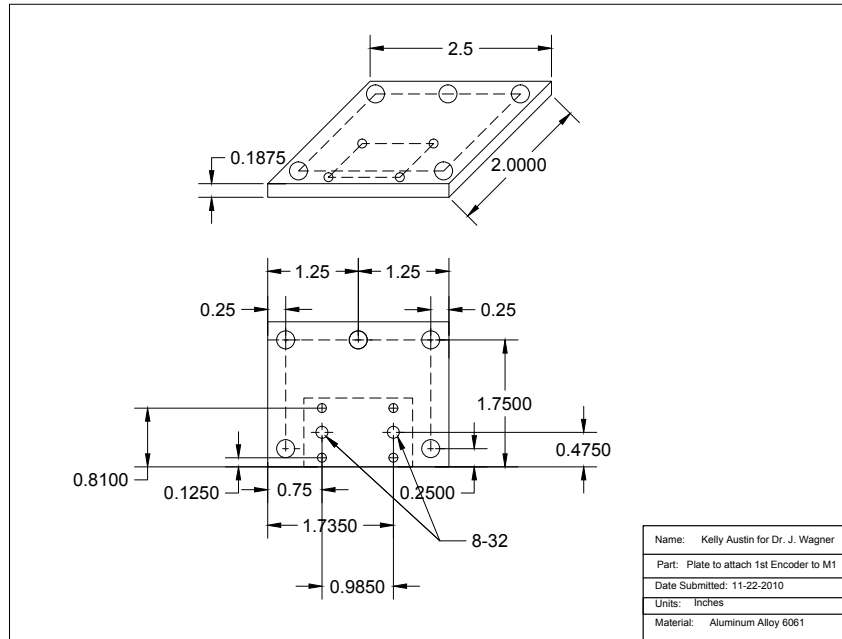
Figure C.6: Aluminum plate for securely attaching encoder bracket to the base of M_1
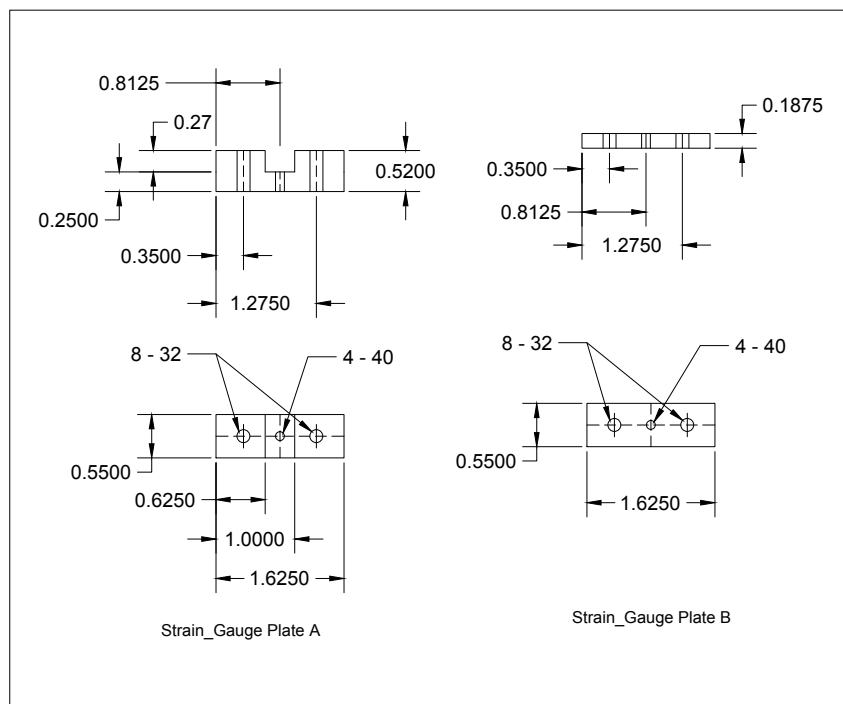
Figure C.7: Upper and lower beam load cell aluminum connectors which attach to structure end plates while providing correct load cell bending

136
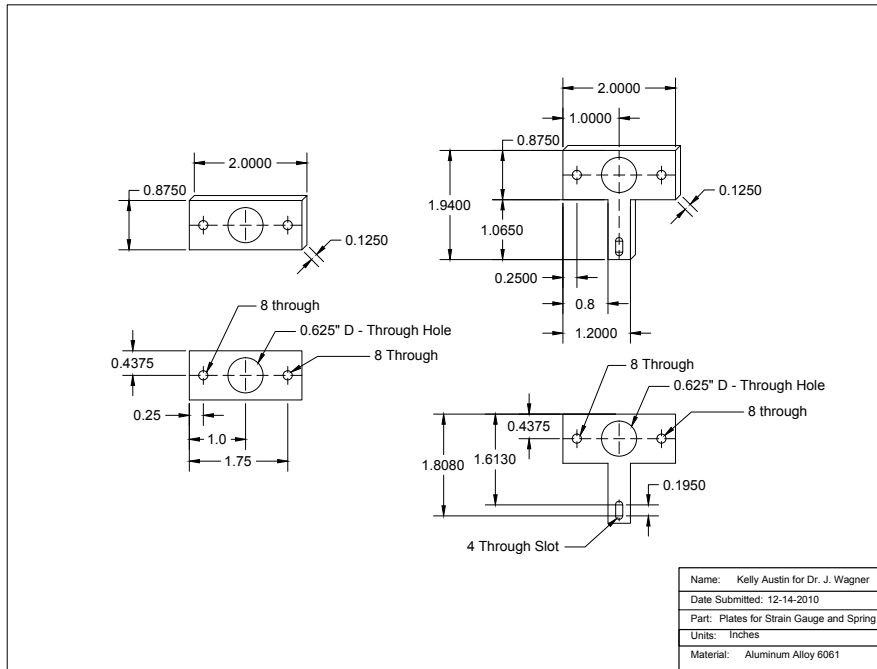
Figure C.8: Two separate connectors for attaching the spring to the beam load cell and M_1
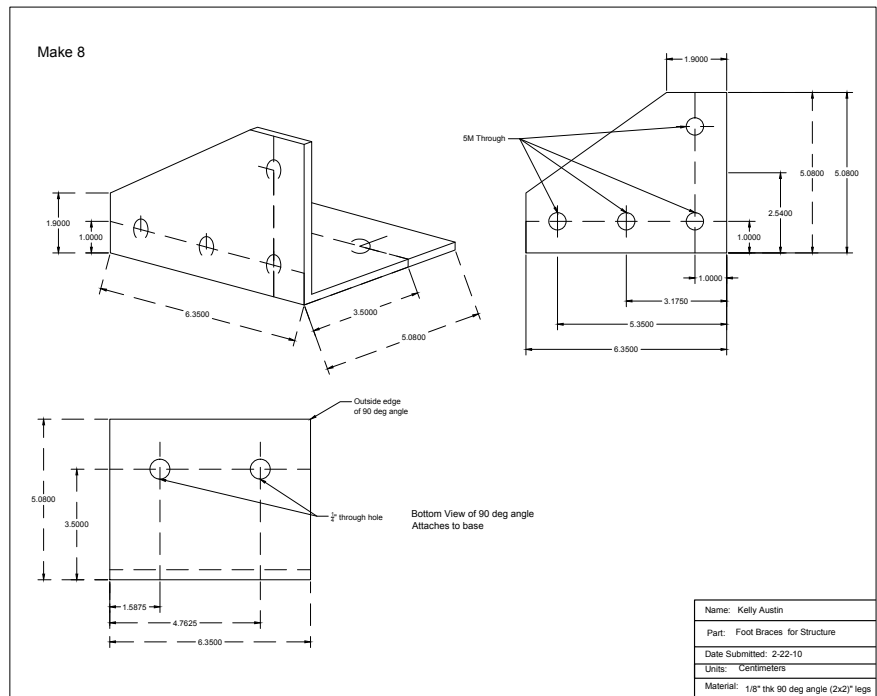
Figure C.9: Stability brackets attaching to the base of the extruded aluminum structure
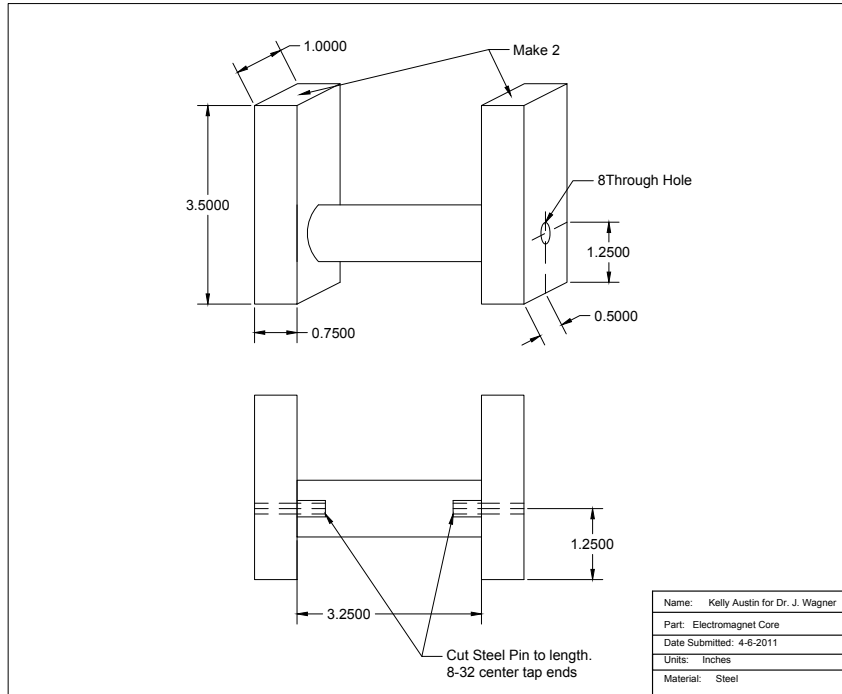
Figure C.10: Steel electromagnet core composed of three pieces
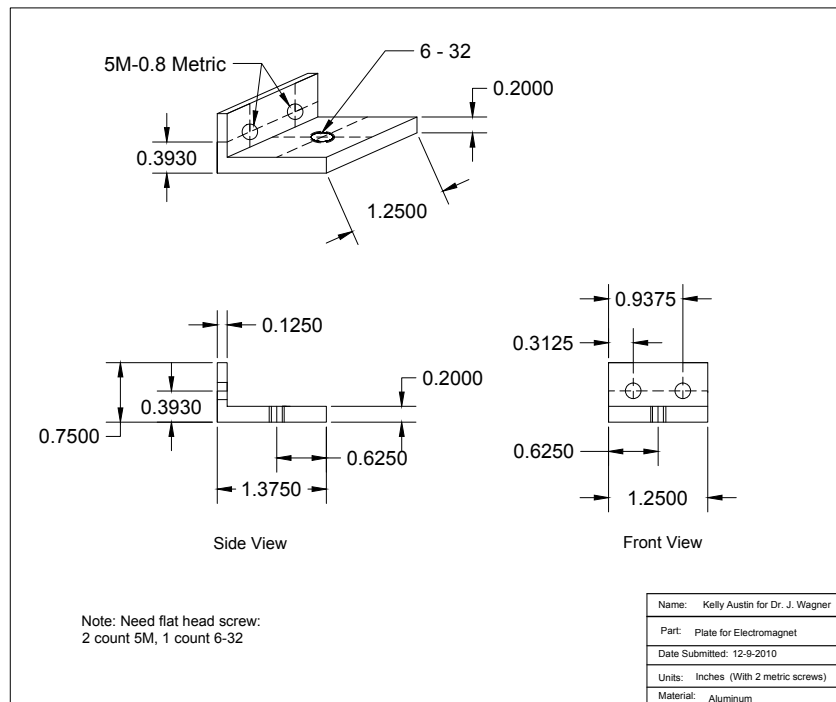
Figure C.11: Bracket to connect to base of structure and supply heat sink and support to a previously tested electromagnet
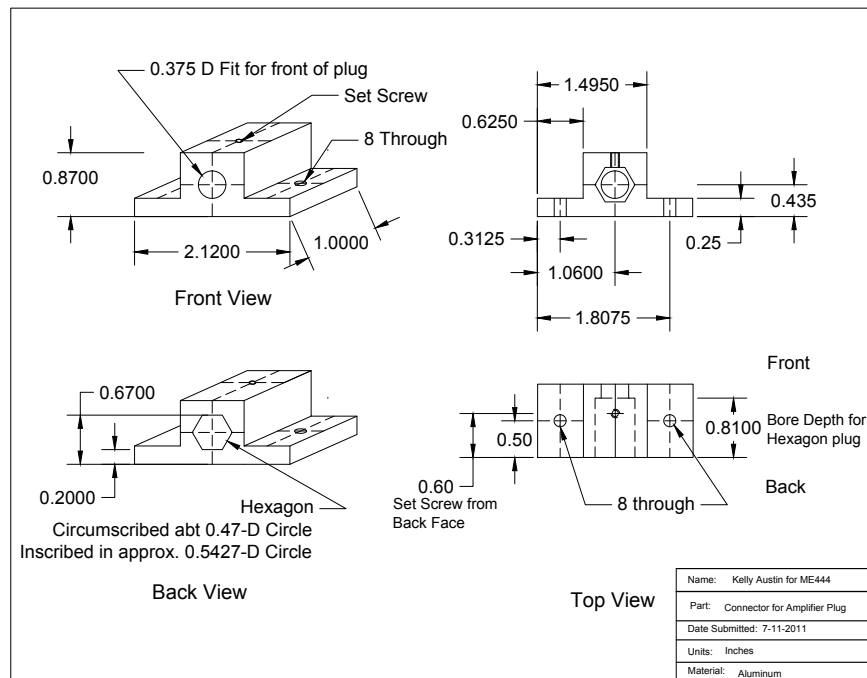
Figure C.12: Support collar for pig-tail electrical connection for lab amplifiers used with beam load cells

Appendix D

Mass–Pendulum Additional Data

The forced responses of the experimental and simulated systems for which M_1 was constrained are shown below in Fig. D.1 through Fig. D.3. The plots for the three tested positions of the electromagnet are displayed.
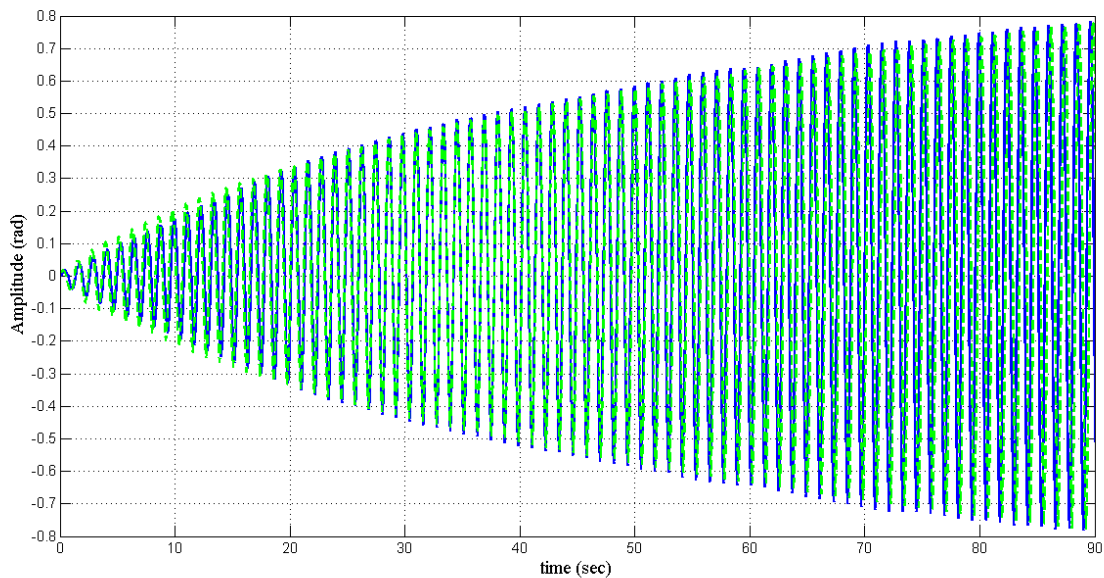
Figure D.1: Comparison of experimental (—) and simulated (- - -) forced responses for $x_m = -4$cm and M_1 fixed
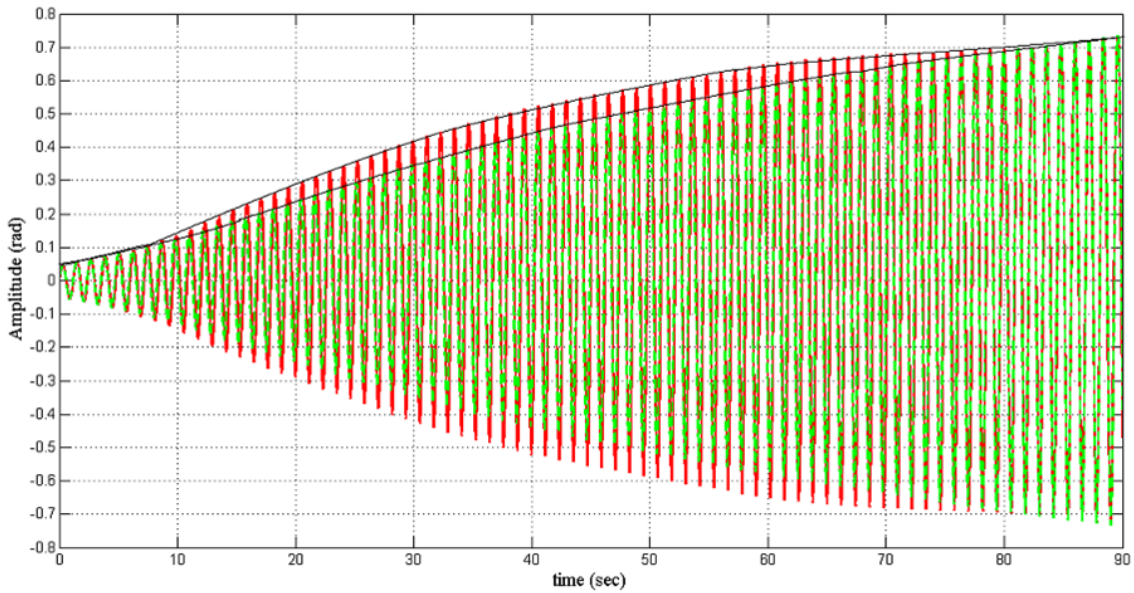
Figure D.2: Comparison of experimental (—) (outside curve) and simulated (- - -) (inside curve) forced responses for $x_m = -7.5$cm and M_1 fixed
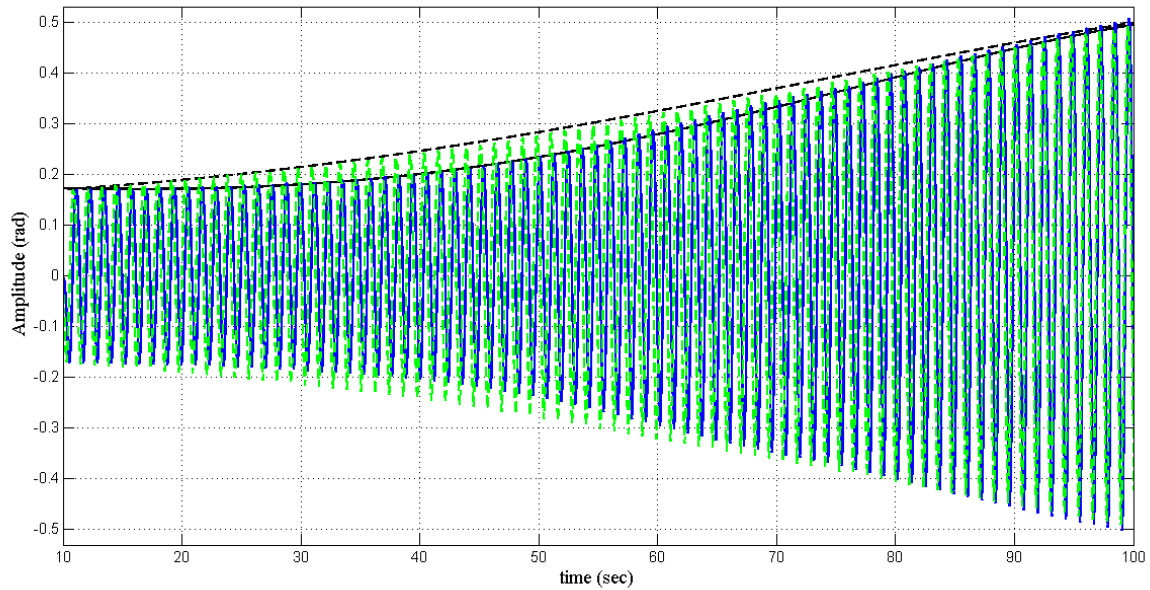
Figure D.3: Comparison of experimental (—) (inside curve) and simulated (- - -) (outside curve) forced responses for $x_m = -11.4$cm and M_1 fixed

141

A comparison of the influence of different pendulum masses M_2 on the coupled free response is shown in Fig. D.4. The comparison of the experimental and simulated free responses in which friction in M_1 is not included in the simulation is shown in Fig. D.5.
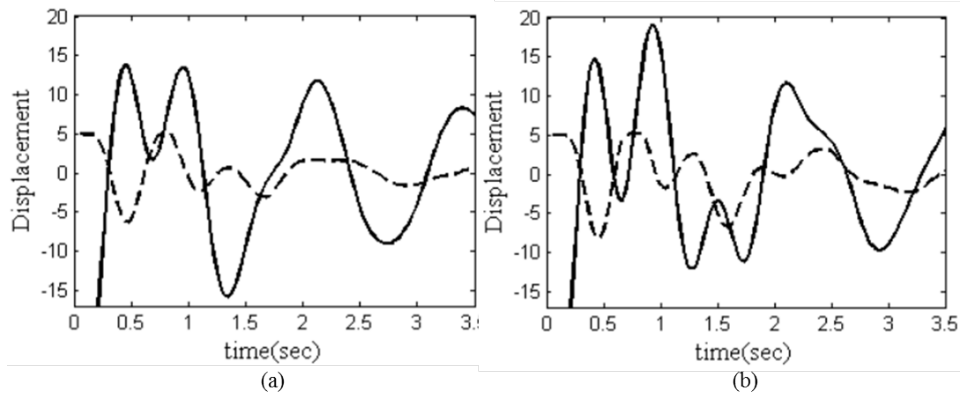
Figure D.4: Experimental data comparing free response relationship between M_1 (- - -)(cm) and M_2 (—)(deg) for (a) $M_2 = 0.75$ kg and (b) $M_2 = 1.36$ kg for similar initial conditions
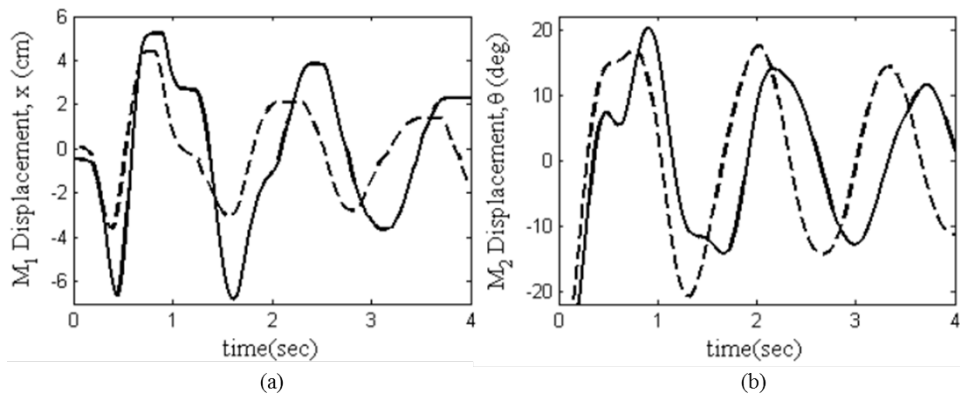
Figure D.5: Free response comparison of experimental(- - -) and simulated (—) data of M_1 and M_2 for initial conditions $x = 0$ cm and $\theta = -30°$deg, neglecting friction as a simulation parameter

Appendix E

TEG Simulink Models

The Simulink model used with dSpace and ControlDesk in the experimental system is shown below. The subsystems appear below with the equations for J- and K-type thermocouple calibrations contained in the Appendix H.
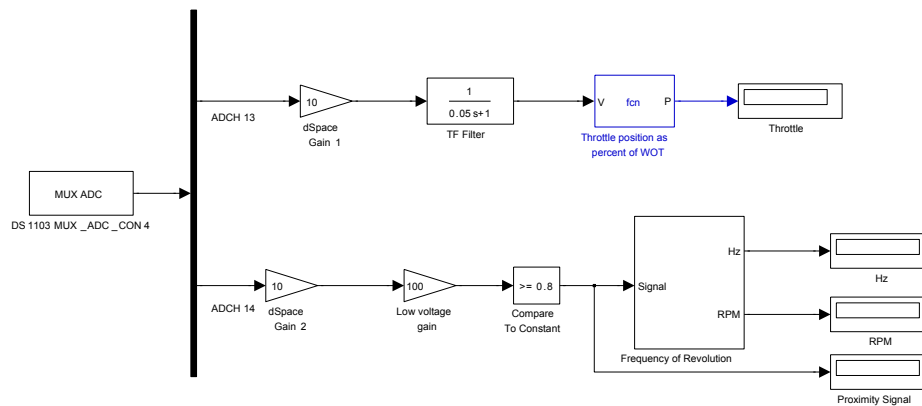
Figure E.1: TEG_dSpace.mdl subsystem used with dSpace and ControlDesk to calibrate and record throttle position and proximity sensors

143
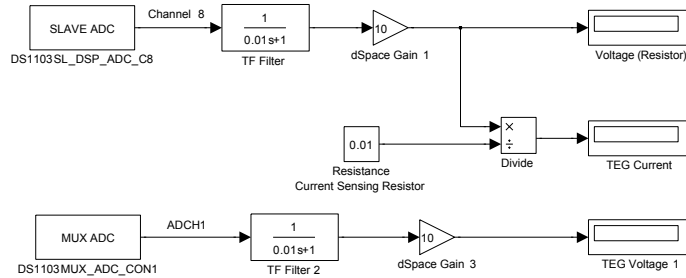
Figure E.2: TEG_dSpace.mdl subsystem used with dSpace and ControlDesk to record voltage and current from thermoelectric modules (During testing Channel 8 was unused because it was found to create a ground loop)
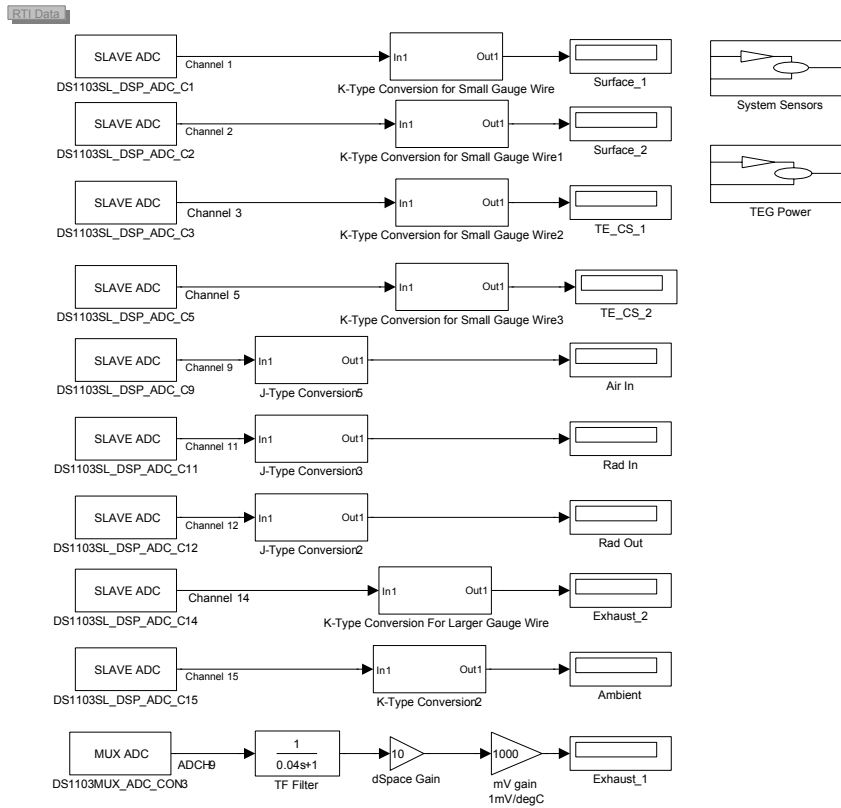
Figure E.3: TEG_dSpace.mdl Simulink model used with dSpace and ControlDesk identifies signal connections and calibrates input signals

144

Appendix F

TEG Matlab Code

The Matlab code used to plot and analyze experimental data and perform numerical calculations is contained below. The code used for all experimental data sets and engine settings is not included due to space and the use of identical commands for compiling data. Differences in code are due to different file names and corresponding variable names.

Code Analyzing and Compiling Experimental Data
TEG_4_Series.m: Experimental data from 4 modules connected in series

```
%4 Modules connected in Series
%Open circuit voltage, Seebeck coeff.
%Voltage at max temp with variable resistive load
%Calculated current for test is recorded in
%Parameters_System_and_Test.xlsx under Series_Data tab
V_4_open=load('C:\...\teg_4_open.mat');
t_V4=V_4_open.teg_4_open.X.Data;
%Temperature Data for open circuit over temp range
Ambient_V4=V_4_open.teg_4_open.Y(2).Data;        %Ambient Air
Exh1_V4=V_4_open.teg_4_open.Y(3).Data;           %Exhaust 1
Exh2_V4=V_4_open.teg_4_open.Y(4).Data;           %Exhaust 2
Surf1_V4=V_4_open.teg_4_open.Y(7).Data;          %Hot Side 1
Surf2_V4=V_4_open.teg_4_open.Y(8).Data;          %Hot Side 2
TEG_V4=V_4_open.teg_4_open.Y(12).Data;           %TEG Voltage no load
TE_CS_1_V4=V_4_open.teg_4_open.Y(13).Data;       %TEG Cold Side 1
TE_CS_2_V4=V_4_open.teg_4_open.Y(14).Data;       %TEG Cold Side 2
Avg_HS_V4=(Surf1_V4+Surf2_V4)/2;                 %Avg hot side temp
Avg_CS_V4=(TE_CS_1_V4+TE_CS_2_V4)/2;             %Avg Cold side Temp
DeltaT_4=Avg_HS_V4-Avg_CS_V4;                    %Avg Temp gradient
Alpha_4=TEG_V4./DeltaT_4;        %Seebeck coefficient over temp range
```

145

```
%%%%%%%%%%%%%%%%%%%%%%%%%%%%%%%%%%%%%%%%%%%%%%%%%%%%%%%%%%%%%%%%%%%%%%%%%%%%
RPM_V4=V_4_open.teg_4_open.Y(9).Data;
throttle_V4=V_4_open.teg_4_open.Y(10).Data*100;
Rad1_V4=V_4_open.teg_4_open.Y(5).Data;
Rad2_V4=V_4_open.teg_4_open.Y(6).Data;
%plots for V_4_open
figure(1)
figure1=figure(1);
%Plot of T_hot and Delta T
xtick_1=0:200:1800;
xlim_1=[0 1750];
ytick_1=0:20:140;
ylim_1=[0 140];
axes1 = axes('Parent',figure1,...
    'YTick',ytick_1,...
    'YMinorTick','on',...
    'XTick',xtick_1,...
    'XMinorTick','on',...
    'Position',[0.15 0.72 0.78 0.26],...
    'FontSize',12);
xlim(axes1,xlim_1);
ylim(axes1,ylim_1);
box(axes1,'on');
grid(axes1,'on');
hold(axes1,'all');
plot1 = plot(t_V4,Avg_HS_V4,'-b',t_V4,DeltaT_4,'--g','Parent',...
    axes1,'LineWidth',2.5);
ylabel('Temperature (\circC)','FontSize',16,'FontName','Times');
%Plot of Open Loop voltage
xtick_2=0:200:1800;
xlim_2=[0 1750];
ytick_2=0:2:10;
ylim_2=[0 9];
axes2 = axes('Parent',figure1,'YTick',ytick_2,...
    'XTick',xtick_2,...
    'XMinorTick','on',...
    'Position',[0.15 0.41 0.78 0.26],...
    'FontSize',12);
xlim(axes2,xlim_2);
ylim(axes2,ylim_2);
box(axes2,'on');
grid(axes2,'on');
hold(axes2,'all');
plot2=plot(t_V4,TEG_V4,'-r','Parent',axes2,'LineWidth',2.5);
ylabel('Voltage (V)','FontSize',16,'FontName','Times');
%Plot of Exhaust Temps
xtick_3=0:200:1800;
xlim_3=[0 1750];
ytick_3=0:100:500;
ylim_3=[0 500];
axes3 = axes('Parent',figure1,'YTick',ytick_3,...
```

146

```
        'XTick',xtick_3,...
        'XMinorTick','on',...
        'Position',[0.15 0.10 0.78 0.26],...
        'FontSize',12);
xlim(axes3,xlim_3);
ylim(axes3,ylim_3);
box(axes3,'on');
grid(axes3,'on');
hold(axes3,'all');
plot3=plot(t_V4,Exh1_V4,'-c',t_V4,Exh2_V4,'-.m',t_V4,Rad1_V4,...
    '-k',t_V4,Rad2_V4,'--b','Parent',axes3,'LineWidth',2.5);
xlabel('Time (sec)','FontSize',16,'FontName','Times');
ylabel('Temperature (\circC)','FontSize',16,'FontName','Times');
%%%%%%%%%%%%%%%%%%%%%%%%%%%%%%%%%%%%%%%%%%%%%%%%%%%%%%%%%%%%%%%%%%%%%%%%%%
figure(2)
figure2=figure(2);
%Plot Seebeck vs. Temp Gradient
xtick_4=0:10:70;
xlim_4=[0 60.2];
ytick_4=0:.01:0.2;
ylim_4=[0.13 0.2];
axes4 = axes('Parent',figure2,...
    'YTick',ytick_4,...
    'YMinorTick','on',...
    'XTick',xtick_4,...
    'XMinorTick','on',...
    'FontSize',12);
xlim(axes4,xlim_4);
ylim(axes4,ylim_4);
box(axes4,'on');
grid(axes4,'on');
hold(axes4,'all');
plot4=scatter(DeltaT_4,Alpha_4,'.b','Parent',axes4);
xlabel('Temperature Gradient (\circC)','FontSize',16,...
    'FontName','Times');
ylabel('Seebeck Coeffient (V/\circC)','FontSize',16,...
    'FontName','Times');
%Plot of Seebeck Coeff over time sample
figure(3)
figure3=figure(3);
xtick_5=0:200:1800;
xlim_5=[0 1750];
ytick_5=0:.01:0.2;
ylim_5=[0.13 0.2];
axes5 = axes('Parent',figure3,...
    'YTick',ytick_5,...
    'YMinorTick','on',...
    'XTick',xtick_5,...
    'XMinorTick','on',...
    'FontSize',12);
xlim(axes5,xlim_5);
```

147

```matlab
ylim(axes5,ylim_5);
box(axes5,'on');
grid(axes5,'on');
hold(axes5,'all');
plot5=scatter(t_V4,Alpha_4,'.m','Parent',axes5);
ylabel('Seebeck Coeffient (V/\circC)','FontSize',16,'FontName',...
    'Times');
xlabel('time (sec)','FontSize',16,'FontName','Times');
%%%%%%%Plot of open circuit RPM and Throttle
figure(4)
subplot(4,1,1)
plot(t_V4,RPM_V4,'LineWidth',2)
axis([0,t_V4(end),1000,2000])
xlabel('Time (sec)')
ylabel('Engine Speed (RPM)')
title('Engine Speed and Throttle for Open Circuit Series Connection')
subplot(4,1,2)
plot(t_V4,throttle_V4,'LineWidth',2)
axis([0,t_V4(end),10,105])
%%%%%%%%%%%%%%%%%%
%Tabulate Engine Speed [(0-480),(530-1270),(1340-1560),(1560-end)]sec
ST_V4=t_V4(2)-t_V4(1);      %sample time step
RPM_V4_1=tabulate(round(RPM_V4(1:fix(200/ST_V4))));
RPM_V4_2=tabulate(round(RPM_V4(fix(200/ST_V4)+1:fix(300/ST_V4))));
RPM_V4_3=tabulate(round(RPM_V4(fix(300/ST_V4)+1:fix(910/ST_V4))));
RPM_V4_4=tabulate(round(RPM_V4(fix(930/ST_V4)+1:fix(1270/ST_V4))));
RPM_V4_5=tabulate(round(RPM_V4(fix(1280/ST_V4)+1:...
    fix(t_V4(end)/ST_V4))));
%1st column of tabulate output is the value 2nd column is the count
RPM_V4_val_1=RPM_V4_1(:,1); RPM_V4_cnt_1=RPM_V4_1(:,2);
RPM_V4_val_2=RPM_V4_2(:,1); RPM_V4_cnt_2=RPM_V4_2(:,2);
RPM_V4_val_3=RPM_V4_3(:,1); RPM_V4_cnt_3=RPM_V4_3(:,2);
RPM_V4_val_4=RPM_V4_4(:,1); RPM_V4_cnt_4=RPM_V4_4(:,2);
RPM_V4_val_5=RPM_V4_5(:,1); RPM_V4_cnt_5=RPM_V4_5(:,2);
%figure(2)
subplot(4,3,7)
plot(RPM_V4_val_1(1200:end),RPM_V4_cnt_1(1200:end),'LineWidth',2)
title('RPM (0-200)sec')
subplot(4,3,8)
plot(RPM_V4_val_2(1450:end),RPM_V4_cnt_2(1450:end),'LineWidth',2)
title('RPM (200-300sec')
subplot(4,3,9)
plot(RPM_V4_val_3(1500:1700),RPM_V4_cnt_3(1500:1700),'LineWidth',2)
title('RPM (300-910sec')
subplot(4,3,10)
plot(RPM_V4_val_4(1600:end),RPM_V4_cnt_4(1600:end),'LineWidth',2)
title('RPM (930-1270)sec')
subplot(4,3,11)
plot(RPM_V4_val_5(1600:end),RPM_V4_cnt_5(1600:end),'LineWidth',2)
title('RPM (1280-end)sec')
%%%%%%%%%%%%%%%%%%%%%%%%%%%%%%%%%%%%%%%%%%%%%%%%%%%%%%%%%%%%%%%%%%%%%%%%%%
```

148

```matlab
%Data for Max temp at variable resistances
V_4a=load('C:\...\teg_4a.mat');
V_4b=load('C:\...\teg_4b.mat');
V_4c=load('C:\...\teg_4c.mat');
V_4d=load('C:\...\teg_d.mat');
V_4e=load('C:\...\teg_e.mat');
V_4f=load('C:\...\teg_f.mat');
V_4g=load('C:\...\teg_g.mat');
%Data, Test 4a
Air_V4a=V_4a.teg_4a.Y(2).Data;                  %Ambient Temp
Avg_Air_V4a=sum(Air_V4a)/length(Air_V4a);
Exh1_V4a=V_4a.teg_4a.Y(3).Data;                 %Exh 1
Avg_Exh1_V4a=sum(Exh1_V4a)/length(Exh1_V4a);
Exh2_V4a=V_4a.teg_4a.Y(4).Data;                 %Exh 2
Avg_Exh2_V4a=sum(Exh2_V4a)/length(Exh2_V4a);
Rad1_V4a=V_4a.teg_4a.Y(5).Data;                 %Rad Inlet
Avg_Rad1_V4a=sum(Rad1_V4a)/length(Rad1_V4a);
Rad2_V4a=V_4a.teg_4a.Y(6).Data;                 %Rad Outlet
Avg_Rad2_V4a=sum(Rad2_V4a)/length(Rad2_V4a);
Surf1_V4a=V_4a.teg_4a.Y(7).Data;                %Hot Side 1
Surf2_V4a=V_4a.teg_4a.Y(8).Data;                %Hot Side 2
TEG_V4a=V_4a.teg_4a.Y(12).Data;                 %TEG Voltage no load
TE_CS_1_V4a=V_4a.teg_4a.Y(13).Data;             %TEG Cold Side 1
TE_CS_2_V4a=V_4a.teg_4a.Y(14).Data;             %TEG Cold Side 2
Avg_HS_V4a=(Surf1_V4a+Surf2_V4a)/2;             %Avg hot side temp
Avg_CS_V4a=(TE_CS_1_V4a+TE_CS_2_V4a)/2;         %Avg Cold side Temp
HSavg_V4a=sum(Avg_HS_V4a)/length(Avg_HS_V4a);   %Single Avg HS temp
CSavg_V4a=sum(Avg_CS_V4a)/length(Avg_CS_V4a);   %Single Avg CS temp
DeltaT_4a=HSavg_V4a-CSavg_V4a;                  %Single Avg Temp gradient
Vavg_V4a=sum(TEG_V4a)/length(TEG_V4a);          %Single Voltage avg
RPM_V4a=V_4a.teg_4a.Y(9).Data;                  %RPM
throttle_V4a=V_4a.teg_4a.Y(10).Data;            %throttle
Avg_throttle_V4a=sum(throttle_V4a)/length(throttle_V4a);
fprintf('Average values Test 4a \n')
fprintf('T_E1 \n T_E2 \n T_R1 \n  T_R2 \n  T_H \n T_C \n')
fprintf('Delta_T  \n T_Air  \n')
Avg_V4a=[Avg_Exh1_V4a; Avg_Exh2_V4a; Avg_Rad1_V4a; Avg_Rad2_V4a; ...
         HSavg_V4a; CSavg_V4a;DeltaT_4a; Avg_Air_V4a]
%%%%%%%%%%%%%%%%%%%%%%%%%%%%%%%%%%%%%%%%%%%%%%%%%%%%%%%%%%%%%%%%%%%%%%%%%
%Data, Test 4b
Air_V4b=V_4b.teg_4b.Y(2).Data;                  %Ambient Temp
Avg_Air_V4b=sum(Air_V4b)/length(Air_V4b);
Exh1_V4b=V_4b.teg_4b.Y(3).Data;                 %Exh 1
Avg_Exh1_V4b=sum(Exh1_V4b)/length(Exh1_V4b);
Exh2_V4b=V_4b.teg_4b.Y(4).Data;                 %Exh 2
Avg_Exh2_V4b=sum(Exh2_V4b)/length(Exh2_V4b);
Rad1_V4b=V_4b.teg_4b.Y(5).Data;                 %Rad Inlet
Avg_Rad1_V4b=sum(Rad1_V4b)/length(Rad1_V4b);
Rad2_V4b=V_4b.teg_4b.Y(6).Data;                 %Rad Outlet
Avg_Rad2_V4b=sum(Rad2_V4b)/length(Rad2_V4b);
Surf1_V4b=V_4b.teg_4b.Y(7).Data;                %Hot Side 1
```

149

```matlab
Surf2_V4b=V_4b.teg_4b.Y(8).Data;                    %Hot Side 2
TEG_V4b=V_4b.teg_4b.Y(12).Data;                     %TEG Voltage no load
TE_CS_1_V4b=V_4b.teg_4b.Y(13).Data;                 %TEG Cold Side 1
TE_CS_2_V4b=V_4b.teg_4b.Y(14).Data;                 %TEG Cold Side 2
Avg_HS_V4b=(Surf1_V4b+Surf2_V4b)/2;                 %Avg hot side temp
Avg_CS_V4b=(TE_CS_1_V4b+TE_CS_2_V4b)/2;             %Avg Cold side Temp
HSavg_V4b=sum(Avg_HS_V4b)/length(Avg_HS_V4b);   %Single Avg HS temp
CSavg_V4b=sum(Avg_CS_V4b)/length(Avg_CS_V4b);   %single Avg HS temp
DeltaT_4b=HSavg_V4b-CSavg_V4b;                      %Single Avg Temp gradient
Vavg_V4b=sum(TEG_V4b)/length(TEG_V4b);          %Single Voltage avg
RPM_V4b=V_4b.teg_4b.Y(9).Data;                      %RPM
throttle_V4b=V_4b.teg_4b.Y(10).Data;            %throttle
Avg_throttle_V4b=sum(throttle_V4b)/length(throttle_V4b);
fprintf('Average values Test 4b \n')
Avg_V4b=[Avg_Exh1_V4b; Avg_Exh2_V4b; Avg_Rad1_V4b; Avg_Rad2_V4b; ...
        HSavg_V4b; CSavg_V4b;DeltaT_4b; Avg_Air_V4b]
%Data, Test 4c
Air_V4c=V_4c.teg_4c.Y(2).Data;                      %Ambient Temp
Avg_Air_V4c=sum(Air_V4c)/length(Air_V4c);
Exh1_V4c=V_4c.teg_4c.Y(3).Data;                     %Exh 1
Avg_Exh1_V4c=sum(Exh1_V4c)/length(Exh1_V4c);
Exh2_V4c=V_4c.teg_4c.Y(4).Data;                     %Exh 2
Avg_Exh2_V4c=sum(Exh2_V4c)/length(Exh2_V4c);
Rad1_V4c=V_4c.teg_4c.Y(5).Data;                     %Rad Inlet
Avg_Rad1_V4c=sum(Rad1_V4c)/length(Rad1_V4c);
Rad2_V4c=V_4c.teg_4c.Y(6).Data;                     %Rad Outlet
Avg_Rad2_V4c=sum(Rad2_V4c)/length(Rad2_V4c);
Surf1_V4c=V_4c.teg_4c.Y(7).Data;                    %Hot Side 1
Surf2_V4c=V_4c.teg_4c.Y(8).Data;                    %Hot Side 2
TEG_V4c=V_4c.teg_4c.Y(12).Data;                     %TEG Voltage no load
TE_CS_1_V4c=V_4c.teg_4c.Y(13).Data;                 %TEG Cold Side 1
TE_CS_2_V4c=V_4c.teg_4c.Y(14).Data;                 %TEG Cold Side 2
Avg_HS_V4c=(Surf1_V4c+Surf2_V4c)/2;                 %Avg hot side temp
Avg_CS_V4c=(TE_CS_1_V4c+TE_CS_2_V4c)/2;             %Avg Cold side Temp
HSavg_V4c=sum(Avg_HS_V4c)/length(Avg_HS_V4c);   %Single Avg HS temp
CSavg_V4c=sum(Avg_CS_V4c)/length(Avg_CS_V4c);   %single Avg HS temp
DeltaT_4c=HSavg_V4c-CSavg_V4c;                      %Single Avg Temp gradient
Vavg_V4c=sum(TEG_V4c)/length(TEG_V4c);          %Single Voltage avg
RPM_V4c=V_4c.teg_4c.Y(9).Data;                      %RPM
throttle_V4c=V_4c.teg_4c.Y(10).Data;            %throttle
Avg_throttle_V4c=sum(throttle_V4c)/length(throttle_V4c);
fprintf('Average values Test 4c \n')
Avg_V4c=[Avg_Exh1_V4c; Avg_Exh2_V4c; Avg_Rad1_V4c; Avg_Rad2_V4c; ...
        HSavg_V4c; CSavg_V4c;DeltaT_4c; Avg_Air_V4c]
%Data, Test 4d
Air_V4d=V_4d.teg_d.Y(2).Data;                       %Ambient Temp
Avg_Air_V4d=sum(Air_V4d)/length(Air_V4d);
Exh1_V4d=V_4d.teg_d.Y(3).Data;                      %Exh 1
Avg_Exh1_V4d=sum(Exh1_V4d)/length(Exh1_V4d);
Exh2_V4d=V_4d.teg_d.Y(4).Data;                      %Exh 2
Avg_Exh2_V4d=sum(Exh2_V4d)/length(Exh2_V4d);
```

150

```matlab
Rad1_V4d=V_4d.teg_d.Y(5).Data;                        %Rad Inlet
Avg_Rad1_V4d=sum(Rad1_V4d)/length(Rad1_V4d);
Rad2_V4d=V_4d.teg_d.Y(6).Data;                        %Rad Outlet
Avg_Rad2_V4d=sum(Rad2_V4d)/length(Rad2_V4d);
Surf1_V4d=V_4d.teg_d.Y(7).Data;                       %Hot Side 1
Surf2_V4d=V_4d.teg_d.Y(8).Data;                       %Hot Side 2
TEG_V4d=V_4d.teg_d.Y(12).Data;                        %TEG Voltage no load
TE_CS_1_V4d=V_4d.teg_d.Y(13).Data;                    %TEG Cold Side 1
TE_CS_2_V4d=V_4d.teg_d.Y(14).Data;                    %TEG Cold Side 2
Avg_HS_V4d=(Surf1_V4d+Surf2_V4d)/2;                   %Avg hot side temp
Avg_CS_V4d=(TE_CS_1_V4d+TE_CS_2_V4d)/2;               %Avg Cold side Temp
HSavg_V4d=sum(Avg_HS_V4d)/length(Avg_HS_V4d);   %Single Avg HS temp
CSavg_V4d=sum(Avg_CS_V4d)/length(Avg_CS_V4d);   %single Avg HS temp
DeltaT_4d=HSavg_V4d-CSavg_V4d;                        %Single Avg Temp gradient
Vavg_V4d=sum(TEG_V4d)/length(TEG_V4d);         %Single Voltage avg
RPM_V4d=V_4d.teg_d.Y(9).Data;                    %RPM
throttle_V4d=V_4d.teg_d.Y(10).Data;              %throttle
Avg_throttle_V4d=sum(throttle_V4d)/length(throttle_V4d);
fprintf('Average values Test 4d \n')
Avg_V4d=[Avg_Exh1_V4d; Avg_Exh2_V4d; Avg_Rad1_V4d; Avg_Rad2_V4d; ...
        HSavg_V4d; CSavg_V4d;DeltaT_4d; Avg_Air_V4d]
%Data, Test 4e
Air_V4e=V_4e.teg_e.Y(2).Data;                         %Ambient Temp
Avg_Air_V4e=sum(Air_V4e)/length(Air_V4e);
Exh1_V4e=V_4e.teg_e.Y(3).Data;                        %Exh 1
Avg_Exh1_V4e=sum(Exh1_V4e)/length(Exh1_V4e);
Exh2_V4e=V_4e.teg_e.Y(4).Data;                        %Exh 2
Avg_Exh2_V4e=sum(Exh2_V4e)/length(Exh2_V4e);
Rad1_V4e=V_4e.teg_e.Y(5).Data;                        %Rad Inlet
Avg_Rad1_V4e=sum(Rad1_V4e)/length(Rad1_V4e);
Rad2_V4e=V_4e.teg_e.Y(6).Data;                        %Rad Outlet
Avg_Rad2_V4e=sum(Rad2_V4e)/length(Rad2_V4e);
Surf1_V4e=V_4e.teg_e.Y(7).Data;                       %Hot Side 1
Surf2_V4e=V_4e.teg_e.Y(8).Data;                       %Hot Side 2
TEG_V4e=V_4e.teg_e.Y(12).Data;                        %TEG Voltage no load
TE_CS_1_V4e=V_4e.teg_e.Y(13).Data;                    %TEG Cold Side 1
TE_CS_2_V4e=V_4e.teg_e.Y(14).Data;                    %TEG Cold Side 2
Avg_HS_V4e=(Surf1_V4e+Surf2_V4e)/2;                   %Avg hot side temp
Avg_CS_V4e=(TE_CS_1_V4e+TE_CS_2_V4e)/2;               %Avg Cold side Temp
HSavg_V4e=sum(Avg_HS_V4e)/length(Avg_HS_V4e);   %Single Avg HS temp
CSavg_V4e=sum(Avg_CS_V4e)/length(Avg_CS_V4e);   %single Avg HS temp
DeltaT_4e=HSavg_V4e-CSavg_V4e;                        %Single Avg Temp gradient
Vavg_V4e=sum(TEG_V4e)/length(TEG_V4e);         %Single Voltage avg
RPM_V4e=V_4e.teg_e.Y(9).Data;                    %RPM
throttle_V4e=V_4e.teg_e.Y(10).Data;              %throttle
Avg_throttle_V4e=sum(throttle_V4e)/length(throttle_V4e);
fprintf('Average values Test 4e \n')
Avg_V4e=[Avg_Exh1_V4e; Avg_Exh2_V4e; Avg_Rad1_V4e; Avg_Rad2_V4e; ...
        HSavg_V4e; CSavg_V4e;DeltaT_4e; Avg_Air_V4e]
%Data, Test 4f
Air_V4f=V_4f.teg_f.Y(2).Data;                         %Ambient Temp
```

151

```matlab
Avg_Air_V4f=sum(Air_V4f)/length(Air_V4f);
Exh1_V4f=V_4f.teg_f.Y(3).Data;                    %Exh 1
Avg_Exh1_V4f=sum(Exh1_V4f)/length(Exh1_V4f);
Exh2_V4f=V_4f.teg_f.Y(4).Data;                    %Exh 2
Avg_Exh2_V4f=sum(Exh2_V4f)/length(Exh2_V4f);
Rad1_V4f=V_4f.teg_f.Y(5).Data;                    %Rad Inlet
Avg_Rad1_V4f=sum(Rad1_V4f)/length(Rad1_V4f);
Rad2_V4f=V_4f.teg_f.Y(6).Data;                    %Rad Outlet
Avg_Rad2_V4f=sum(Rad2_V4f)/length(Rad2_V4f);
Surf1_V4f=V_4f.teg_f.Y(7).Data;                   %Hot Side 1
Surf2_V4f=V_4f.teg_f.Y(8).Data;                   %Hot Side 2
TEG_V4f=V_4f.teg_f.Y(12).Data;                    %TEG Voltage no load
TE_CS_1_V4f=V_4f.teg_f.Y(13).Data;                %TEG Cold Side 1
TE_CS_2_V4f=V_4f.teg_f.Y(14).Data;                %TEG Cold Side 2
Avg_HS_V4f=(Surf1_V4f+Surf2_V4f)/2;               %Avg hot side temp
Avg_CS_V4f=(TE_CS_1_V4f+TE_CS_2_V4f)/2;           %Avg Cold side Temp
HSavg_V4f=sum(Avg_HS_V4f)/length(Avg_HS_V4f);     %Single Avg HS temp
CSavg_V4f=sum(Avg_CS_V4f)/length(Avg_CS_V4f);     %single Avg HS temp
DeltaT_4f=HSavg_V4f-CSavg_V4f;                    %Single Avg Temp gradient
Vavg_V4f=sum(TEG_V4f)/length(TEG_V4f);            %Single Voltage avg
RPM_V4f=V_4f.teg_f.Y(9).Data;                     %RPM
throttle_V4f=V_4f.teg_f.Y(10).Data;               %throttle
Avg_throttle_V4f=sum(throttle_V4f)/length(throttle_V4f);
fprintf('Average values Test 4f \n')
Avg_V4f=[Avg_Exh1_V4f; Avg_Exh2_V4f; Avg_Rad1_V4f; Avg_Rad2_V4f; ...
        HSavg_V4f; CSavg_V4f;DeltaT_4f; Avg_Air_V4f]
%Data, Test 4g
Air_V4g=V_4g.teg_g.Y(2).Data;                     %Ambient Temp
Avg_Air_V4g=sum(Air_V4g)/length(Air_V4g);
Exh1_V4g=V_4g.teg_g.Y(3).Data;                    %Exh 1
Avg_Exh1_V4g=sum(Exh1_V4g)/length(Exh1_V4g);
Exh2_V4g=V_4g.teg_g.Y(4).Data;                    %Exh 2
Avg_Exh2_V4g=sum(Exh2_V4g)/length(Exh2_V4g);
Rad1_V4g=V_4g.teg_g.Y(5).Data;                    %Rad Inlet
Avg_Rad1_V4g=sum(Rad1_V4g)/length(Rad1_V4g);
Rad2_V4g=V_4g.teg_g.Y(6).Data;                    %Rad Outlet
Avg_Rad2_V4g=sum(Rad2_V4g)/length(Rad2_V4g);
Surf1_V4g=V_4g.teg_g.Y(7).Data;                   %Hot Side 1
Surf2_V4g=V_4g.teg_g.Y(8).Data;                   %Hot Side 2
TEG_V4g=V_4g.teg_g.Y(12).Data;                    %TEG Voltage no load
TE_CS_1_V4g=V_4g.teg_g.Y(13).Data;                %TEG Cold Side 1
TE_CS_2_V4g=V_4g.teg_g.Y(14).Data;                %TEG Cold Side 2
Avg_HS_V4g=(Surf1_V4g+Surf2_V4g)/2;               %Avg hot side temp
Avg_CS_V4g=(TE_CS_1_V4g+TE_CS_2_V4g)/2;           %Avg Cold side Temp
HSavg_V4g=sum(Avg_HS_V4g)/length(Avg_HS_V4g);     %Single Avg HS temp
CSavg_V4g=sum(Avg_CS_V4g)/length(Avg_CS_V4g);     %single Avg HS temp
DeltaT_4g=HSavg_V4g-CSavg_V4g;                    %Single Avg Temp gradient
Vavg_V4g=sum(TEG_V4g)/length(TEG_V4g);            %Single Voltage avg
RPM_V4g=V_4g.teg_g.Y(9).Data;                     %RPM
throttle_V4g=V_4g.teg_g.Y(10).Data;               %throttle
Avg_throttle_V4g=sum(throttle_V4g)/length(throttle_V4g);
```

```
fprintf('Average values Test 4g \n')
Avg_V4g=[Avg_Exh1_V4g; Avg_Exh2_V4g; Avg_Rad1_V4g; Avg_Rad2_V4g; ...
        HSavg_V4g; CSavg_V4g;DeltaT_4g; Avg_Air_V4g]
%Average values for Data samples a-g
Resistances=[2.2,10.4,14.7,25.3,58.8,124,150.1];
fprintf('Average Values of Series Tests a-g for Max Temp at Given R\n')
fprintf('R, V, T_hot, T_cold, deltaT \n')
%%%%%%%%%%%%%%%%%%%%%%%%%%%%%%%%%%%%%%%%%%%%%%%%%%%%%%%%%%%%%%%%%%%%%%%%%
Test_Avgs=[Resistances;
    Vavg_V4a,Vavg_V4b,Vavg_V4c,Vavg_V4d,Vavg_V4e,Vavg_V4f,Vavg_V4g;
    HSavg_V4a,HSavg_V4b,HSavg_V4c,HSavg_V4d,HSavg_V4e,HSavg_V4f,...
        HSavg_V4g;
    CSavg_V4a,CSavg_V4b,CSavg_V4c,CSavg_V4d,CSavg_V4e,CSavg_V4f,...
        CSavg_V4g;
    DeltaT_4a,DeltaT_4b,DeltaT_4c,DeltaT_4d,DeltaT_4e,DeltaT_4f,...
        DeltaT_4g]'
%%%%%%%%%%%%%%%%%%%%%%%%%%%%%%%%%%%%%%%%%%%%%%%%%%%%%%%%%%%%%%%%%%%%%%%%%
%Overall Temperature Averages
Exh1=[Exh1_V4a Exh1_V4b Exh1_V4c Exh1_V4d Exh1_V4e Exh1_V4f Exh1_V4g];
Exh2=[Exh2_V4a Exh2_V4b Exh2_V4c Exh2_V4d Exh2_V4e Exh2_V4f Exh2_V4g];
TH=[Avg_HS_V4a Avg_HS_V4b Avg_HS_V4c Avg_HS_V4d Avg_HS_V4e ...
    Avg_HS_V4f Avg_HS_V4g];
TC=[Avg_CS_V4a Avg_CS_V4b Avg_CS_V4c Avg_CS_V4d Avg_CS_V4e ...
    Avg_CS_V4f Avg_CS_V4g];
Air=[Air_V4a Air_V4b Air_V4c Air_V4d Air_V4e Air_V4f Air_V4g];
Rad1=[Rad1_V4a Rad1_V4b Rad1_V4c Rad1_V4d Rad1_V4e Rad1_V4f Rad1_V4g];
Rad2=[Rad2_V4a Rad2_V4b Rad2_V4c Rad2_V4d Rad2_V4e Rad2_V4f Rad2_V4g];

Avg_Exh1=sum(Exh1)/length(Exh1);        %Average
std_Exh1=std(Exh1);                     %Standard Deviation in Measure
Avg_Exh2=sum(Exh2)/length(Exh2);
std_Exh2=std(Exh2);
Avg_TH=sum(TH)/length(TH);
std_TH=std(TH);
Avg_TC=sum(TC)/length(TC);
std_TC=std(TC);
Avg_Air=sum(Air)/length(Air);
std_Air=std(Air);
Avg_Rad1=sum(Rad1)/length(Rad1);
std_Rad1=std(Rad1);
Avg_Rad2=sum(Rad2)/length(Rad2);
std_Rad2=std(Rad2);
fprintf('Overall Average Temperatures \n')
fprintf('T_E1 \n T_E2 \n T_H \n T_C \n T_Air \n T_R1 \n T_R2 \n')
Overall_Temps=[Avg_Exh1; Avg_Exh2; Avg_TH; Avg_TC; Avg_Air;...
    Avg_Rad1; Avg_Rad2]
Std_dev=[std_Exh1; std_Exh2; std_TH; std_TC; std_Air; std_Rad1; ...
    std_Rad2]
%%%%%%%%%%%%%%%%%%%%%%%%%%%%%%%%%%%%%%%%%%%%%%%%%%%%%%%%%%%%%%%%%%%%%%%%%
%Tabulate Engine Speed test b and c
RPM_V4a_t=tabulate(round(RPM_V4a));
```

153

```
RPM_V4b_t=tabulate(round(RPM_V4b));
RPM_V4c_t=tabulate(round(RPM_V4c));
RPM_V4d_t=tabulate(round(RPM_V4d));
RPM_V4e_t=tabulate(round(RPM_V4e));
RPM_V4f_t=tabulate(round(RPM_V4f));
RPM_V4g_t=tabulate(round(RPM_V4g));
%1st column of tabulate output is the value 2nd column is the count
RPM_V4a_val=RPM_V4a_t(:,1); RPM_V4a_cnt=RPM_V4a_t(:,2);
RPM_V4b_val=RPM_V4b_t(:,1); RPM_V4b_cnt=RPM_V4b_t(:,2);
RPM_V4c_val=RPM_V4c_t(:,1); RPM_V4c_cnt=RPM_V4c_t(:,2);
RPM_V4d_val=RPM_V4d_t(:,1); RPM_V4d_cnt=RPM_V4d_t(:,2);
RPM_V4e_val=RPM_V4e_t(:,1); RPM_V4e_cnt=RPM_V4e_t(:,2);
RPM_V4f_val=RPM_V4f_t(:,1); RPM_V4f_cnt=RPM_V4f_t(:,2);
RPM_V4g_val=RPM_V4g_t(:,1); RPM_V4g_cnt=RPM_V4g_t(:,2);
figure(5)
subplot(3,3,1)
plot(RPM_V4a_val(1600:end),RPM_V4a_cnt(1600:end),'LineWidth',2)
title('RPM Test 4a')
subplot(3,3,2)
plot(RPM_V4b_val(1600:end),RPM_V4b_cnt(1600:end),'LineWidth',2)
title('RPM Test 4b')
subplot(3,3,3)
plot(RPM_V4c_val(1600:end),RPM_V4c_cnt(1600:end),'LineWidth',2)
title('RPM Test 4c')
subplot(3,3,4)
plot(RPM_V4d_val(1600:end),RPM_V4d_cnt(1600:end),'LineWidth',2)
title('RPM Test 4d')
subplot(3,3,5)
plot(RPM_V4e_val(1600:end),RPM_V4e_cnt(1600:end),'LineWidth',2)
title('RPM Test 4e')
subplot(3,3,6)
plot(RPM_V4f_val(1600:end),RPM_V4f_cnt(1600:end),'LineWidth',2)
title('RPM Test 4f')
subplot(3,3,7)
plot(RPM_V4g_val(1600:end),RPM_V4g_cnt(1600:end),'LineWidth',2)
title('RPM Test 4g')
Throttle=[Avg_throttle_V4a; Avg_throttle_V4b; Avg_throttle_V4c;...
    Avg_throttle_V4d; Avg_throttle_V4e; Avg_throttle_V4f;...
    Avg_throttle_V4g]
```

TEG_Single.m: Experimental data from 1 module

```
%Tests for 1 module open circuit and circuit w/ variable resistance
%File teg_v_open.mat records data for open circuit voltage for
%1 module for set resistance over range of exhaust and surface temps.
%Calculated current for test is recorded in
%Parameters_System_and_Test.xlsx under Single_Module tab
%Single module was on surface 2 (Surf2)
%%%%%%%%%%%%%%%%%%%%%%%%%%%%%%%%%%%%%%%%%%%%%%%%%%%%%%%%%%%%%%%%%%%%%%
V_1_open=load('C:\...\teg_v_open.mat');
t_V1O=V_1_open.teg_v_open.X.Data;
%Temperature Data for open circuit over temp range
```

154

```
%Single Module was located on surface 2 of TEWHS
Ambient_V1O=V_1_open.teg_v_open.Y(2).Data;        %Ambient Air
Exh1_V1O=V_1_open.teg_v_open.Y(3).Data;           %Exhaust 1
Exh2_V1O=V_1_open.teg_v_open.Y(4).Data;           %Exhaust 2
Rad1_V1O=V_1_open.teg_v_open.Y(5).Data;           %Coolant inlet
Rad2_V1O=V_1_open.teg_v_open.Y(6).Data;           %Coolant outlet
Surf2_V1O=V_1_open.teg_v_open.Y(8).Data;          %Hot Side 2
TEG_V1O=V_1_open.teg_v_open.Y(12).Data;           %TEG Voltage no load
TECS2_V1O=V_1_open.teg_v_open.Y(14).Data;         %TEG Cold Side 2
DeltaT2=Surf2_V1O-TECS2_V1O;                      %Temp gradient side 2
Alpha_1=TEG_V1O./DeltaT2;    %Seebeck coefficient over temp range
RPM_V1O=V_1_open.teg_v_open.Y(9).Data;
throttle_V1O=V_1_open.teg_v_open.Y(10).Data;
%%%%%%%%%%%%%%%%%%%%%%%%%%%%%%%%%%%%%%%%%%%%%%%%%%%%%%%%%%%%%%%%%%%%%%
%plots for V_1_open
figure(1)
figure1=figure(1);
%Plot of T_hot and Delta T
xtick_1=0:200:1800;
xlim_1=[0 1750];
ytick_1=0:20:140;
ylim_1=[0 140];
axes1 = axes('Parent',figure1,...
    'YTick',ytick_1,...
    'YMinorTick','on',...
    'XTick',xtick_1,...
    'XMinorTick','on',...
    'Position',[0.15 0.72 0.78 0.26],...
    'FontSize',12);
xlim(axes1,xlim_1);
ylim(axes1,ylim_1);
box(axes1,'on');
grid(axes1,'on');
hold(axes1,'all');
plot1 = plot(t_V1O,Surf2_V1O,'-b',t_V1O,DeltaT2,'--g','Parent',...
    axes1,'LineWidth',2.5);
ylabel('Temperature (\circC)','FontSize',16,'FontName','Times');
%Plot of Open Loop voltage
xtick_2=0:200:1800;
xlim_2=[0 1750];
ytick_2=0:0.2:1.7;
ylim_2=[0 1.7];
axes2 = axes('Parent',figure1,'YTick',ytick_2,...
    'XTick',xtick_2,...
    'XMinorTick','on',...
    'Position',[0.15 0.41 0.78 0.26],...
    'FontSize',12);
xlim(axes2,xlim_2);
ylim(axes2,ylim_2);
box(axes2,'on');
grid(axes2,'on');
```

155

```
hold(axes2,'all');
plot2=plot(t_V1O,TEG_V1O,'-r','Parent',axes2,'LineWidth',2.5);
ylabel('Voltage (V)','FontSize',16,'FontName','Times');
%Plot of Exhaust Temps
xtick_3=0:200:1800;
xlim_3=[0 1750];
ytick_3=0:100:500;
ylim_3=[0 500];
axes3 = axes('Parent',figure1,'YTick',ytick_3,...
    'XTick',xtick_3,...
    'XMinorTick','on',...
    'Position',[0.15 0.10 0.78 0.26],...
    'FontSize',12);
xlim(axes3,xlim_3);
ylim(axes3,ylim_3);
box(axes3,'on');
grid(axes3,'on');
hold(axes3,'all');
plot3=plot(t_V1O,Exh1_V1O,'-c',t_V1O,Exh2_V1O,'-.m',t_V1O,...
    Rad2_V1O,'--b',t_V1O,Rad1_V1O,'-k','Parent',axes3,...
    'LineWidth',2.5);
xlabel('Time (sec)','FontSize',16,'FontName','Times');
ylabel('Temperature (\circC)','FontSize',16,'FontName','Times');
%Plots of RPM and Throttle over sample time for V_1_open
figure(2)
subplot(3,1,1)
plot(t_V1O,RPM_V1O,'LineWidth',2)
axis([0,t_V1O(end),1000,2000])
xlabel('Time (sec)')
ylabel('Engine Speed (RPM)')
title('Engine Speed and Throttle for Open Circuit for Single Module')
subplot(3,1,2)
plot(t_V1O,throttle_V1O,'LineWidth',2)
axis([0,t_V1O(end),0,1.5])
%%%%%%%%%%%%%%%%%%%%%%%%%%%%%%%%%%%%%%%%%%%%%%%%%%%%%%%%%%%%%%%%%%%%%%%%
%Tabulate Engine Speed [(0-480),(530-1270),(1340-1560),(1560-end)]sec
ST_V1O=t_V1O(2)-t_V1O(1);      %sample time step
RPM_V1O_1=tabulate(round(RPM_V1O(1:fix(480/ST_V1O))));
RPM_V1O_2=tabulate(round(RPM_V1O(fix(530/ST_V1O)+1:...
    fix(1270/ST_V1O))));
RPM_V1O_3=tabulate(round(RPM_V1O(fix(1340/ST_V1O)+1:...
    fix(1560/ST_V1O))));
RPM_V1O_4=tabulate(round(RPM_V1O(fix(1560/ST_V1O)+1:...
    fix(t_V1O(end)/ST_V1O))));
%1st column of tabulate output is the value 2nd column is the count
RPM_V1O_val_1=RPM_V1O_1(:,1); RPM_V1O_cnt_1=RPM_V1O_1(:,2);
RPM_V1O_val_2=RPM_V1O_2(:,1); RPM_V1O_cnt_2=RPM_V1O_2(:,2);
RPM_V1O_val_3=RPM_V1O_3(:,1); RPM_V1O_cnt_3=RPM_V1O_3(:,2);
RPM_V1O_val_4=RPM_V1O_4(:,1); RPM_V1O_cnt_4=RPM_V1O_4(:,2);
%figure(2)
subplot(3,4,9)
```

156

```
plot(RPM_V1O_val_1(500:end),RPM_V1O_cnt_1(500:end),'LineWidth',2)
title('RPM (0-480)sec')
subplot(3,4,10)
plot(RPM_V1O_val_2(1450:end),RPM_V1O_cnt_2(1450:end),'LineWidth',2)
title('RPM (530-1270sec')
subplot(3,4,11)
plot(RPM_V1O_val_3(1750:end),RPM_V1O_cnt_3(1750:end),'LineWidth',2)
title('RPM (1340-1560)sec')
subplot(3,4,12)
plot(RPM_V1O_val_4(1750:end),RPM_V1O_cnt_4(1750:end),'LineWidth',2)
title('RPM (1560-end)sec')
%%%%%%%%%%%%%%%%%%%%%%%%%%%%%%%%%%%%%%%%%%%%%%%%%%%%%%%%%%%%%%%%%%%%%%%%%
%%%%%%%%%%%%%%%%%%%%%%%%%%%%%%%%%%%%%%%%%%%%%%%%%%%%%%%%%%%%%%%%%%%%%%%%
V_1a=load('C:\...\teg_v_closed_single.mat');
V_1b=load('C:\...\teg_single_1.mat');
V_1c=load('C:\...\teg_single_2.mat');
%Data for V_1a
%1.6Ohm load on TEM, 1840sec sample,
%Approx (1-1000)sec: throttle=25,50,75, RPM=1500
%Approx (1000-1840)sec: throttle=75,100, RPM=1800
%Current recorded independently though rejected for not fitting trend
t_V1a=V_1a.teg_v_closed_single.X.Data;              %Time
Amb_V1a=V_1a.teg_v_closed_single.Y(2).Data;
Exh1_V1a=V_1a.teg_v_closed_single.Y(3).Data;        %Exhaust 1
Exh2_V1a=V_1a.teg_v_closed_single.Y(4).Data;        %Exhaust 2
Rad1_V1a=V_1a.teg_v_closed_single.Y(5).Data;        %Radiator Inlet
Rad2_V1a=V_1a.teg_v_closed_single.Y(6).Data;        %Radiator Outlet
Surf2_V1a=V_1a.teg_v_closed_single.Y(8).Data;       %Hot side 2
TEG_V1a=V_1a.teg_v_closed_single.Y(12).Data;        %TEG voltage
TE_CS2_V1a=V_1a.teg_v_closed_single.Y(14).Data;     %Cold side 2
RPM_V1a=V_1a.teg_v_closed_single.Y(9).Data;
throttle_V1a=V_1a.teg_v_closed_single.Y(10).Data;
%%%%%%%%%%%%%%%%%%%%%%%%%%%%%%%%%%
%Plots of Test V1a
figure(3)
subplot(3,1,1)
plot(t_V1a,Exh1_V1a,'-g',t_V1a,Exh2_V1a,'-.b',t_V1a,Rad1_V1a,'--r',...
t_V1a,Rad2_V1a,':k','LineWidth',2)
title('Temperature Data for Test 1a with Single Module')
xlabel('time')
ylabel('Temperature (C)')
subplot(3,1,2)
plot(t_V1a,Surf2_V1a,'-g',t_V1a,TE_CS2_V1a,'--b',t_V1a,Amb_V1a,...
':k','LineWidth',2)
title('Temperature Data Test 1a with Single Module')
legend('T_H','T_C','T_Air')
xlabel('time')
ylabel('Temperature (C)')
subplot(3,1,3)
plot(t_V1a,TEG_V1a)
title('Closed Circuit Voltage')
```

157

```
xlabel('time')
ylabel('Voltage')
figure(4)
subplot(2,1,1)
plot(t_V1a,RPM_V1a,'LineWidth',2)
axis([0,t_V1a(end),950,2000])
xlabel('Time (sec)')
ylabel('Engine Speed (RPM)')
title('Engine Speed and Throttle for Test 1a single Module')
subplot(2,1,2)
plot(t_V1a,throttle_V1a,'LineWidth',2)
axis([0,t_V1O(end),0.10,1.5])
xlabel('time (sec)')
ylabel('trottle')
%%%%%%%%%%%%%%%%%%%%%%%%%%%%%%%%%%%%%%%%%%%%%%%%%%%%%%%%%%%%%%%%%%%%%%%%%%
%Data for V_1b============================
%Tests V_1b and V_1c at approx speed:(1714+1764)/2 at WOT
t_V1b=V_1b.teg_single_1.X.Data; %Time
Air_V1b=V_1b.teg_single_1.Y(2).Data;
Avg_Air_V1b=sum(Air_V1b)/length(Air_V1b);
Exh1_V1b=V_1b.teg_single_1.Y(3).Data;               %Exhaust 1
AvgExh1_V1b=sum(Exh1_V1b)/length(Exh1_V1b);
Exh2_V1b=V_1b.teg_single_1.Y(4).Data;               %Exhaust 2
Avg_Exh2_V1b=sum(Exh2_V1b)/length(Exh2_V1b);
Rad1_V1b=V_1b.teg_single_1.Y(5).Data;               %Radiator Inlet
Avg_Rad1_V1b=sum(Rad1_V1b)/length(Rad1_V1b);
Rad2_V1b=V_1b.teg_single_1.Y(6).Data;               %Radiator Out
Avg_Rad2_V1b=sum(Rad2_V1b)/length(Rad2_V1b);
Surf2_V1b=V_1b.teg_single_1.Y(8).Data;              %Hot side 2
Avg_Surf2_V1b=sum(Surf2_V1b)/length(Surf2_V1b);
TEG_V1b=V_1b.teg_single_1.Y(12).Data;               %TEG voltage
TECS2_V1b=V_1b.teg_single_1.Y(14).Data;             %Cold side 2
Avg_TECS2_V1b=sum(TECS2_V1b)/length(TECS2_V1b);
RPM_V1b=V_1b.teg_single_1.Y(9).Data;
throttle_V1b=V_1b.teg_single_1.Y(10).Data;
fprintf('Average values Test 1b \n')
fprintf('T_E1 \n T_E2 \n T_R1 \n  T_R2 \n  T_H \n T_C \n T_Air  \n')
Avg_V1b=[AvgExh1_V1b; Avg_Exh2_V1b; Avg_Rad1_V1b; Avg_Rad2_V1b; ...
        Avg_Surf2_V1b; Avg_TECS2_V1b;Avg_Air_V1b]
%Data for V_1c============================
t_V1c=V_1c.teg_single_2.X.Data;                     %Time
Air_V1c=V_1c.teg_single_2.Y(2).Data;                %Ambient
Avg_Air_V1c=sum(Air_V1c)/length(Air_V1c);
Exh1_V1c=V_1c.teg_single_2.Y(3).Data;               %Exhaust 1
Avg_Exh1_V1c=sum(Exh1_V1c)/length(Exh1_V1c);
Exh2_V1c=V_1c.teg_single_2.Y(4).Data;               %Exhuast 2
Avg_Exh2_V1c=sum(Exh2_V1c)/length(Exh2_V1c);
Rad1_V1c=V_1c.teg_single_2.Y(5).Data;               %Radiator Inlet
Avg_Rad1_V1c=sum(Rad1_V1c)/length(Rad1_V1c);
Rad2_V1c=V_1c.teg_single_2.Y(6).Data;               %Radiator Out
Avg_Rad2_V1c=sum(Rad2_V1c)/length(Rad2_V1c);
```

158

```matlab
Surf2_V1c=V_1c.teg_single_2.Y(8).Data;              %Hot side 2
Avg_Surf2_V1c=sum(Surf2_V1c)/length(Surf2_V1c);
TEG_V1c=V_1c.teg_single_2.Y(12).Data;               %TEG voltage
TECS2_V1c=V_1c.teg_single_2.Y(14).Data;             %Cold side2
Avg_TECS2_V1c=sum(TECS2_V1c)/length(TECS2_V1c);
RPM_V1c=V_1c.teg_single_2.Y(9).Data;
throttle_V1c=V_1c.teg_single_2.Y(10).Data;
fprintf('Average values Test 1c \n')
Avg_V1c=[Avg_Exh1_V1c; Avg_Exh2_V1c; Avg_Rad1_V1c; Avg_Rad2_V1c; ...
        Avg_Surf2_V1c; Avg_TECS2_V1c;Avg_Air_V1c]
%Calculating Overall Average of Test b-c
Avg_Exh1=(sum(Exh1_V1b)+sum(Exh1_V1c))/(length(Exh1_V1b)+...
    length(Exh1_V1c));
Avg_Exh2=(sum(Exh2_V1b)+sum(Exh2_V1c))/(length(Exh2_V1b)+...
    length(Exh2_V1c));
Avg_Rad1=(sum(Rad1_V1b)+sum(Rad1_V1c))/(length(Rad1_V1b)+...
    length(Rad1_V1c));
Avg_Rad2=(sum(Rad2_V1b)+sum(Rad2_V1c))/(length(Rad2_V1b)+...
    length(Rad2_V1c));
Avg_Surf2=(sum(Surf2_V1b)+sum(Surf2_V1c))/(length(Surf2_V1b)+...
    length(Surf2_V1c));
Avg_TECS2=(sum(TECS2_V1b)+sum(TECS2_V1c))/(length(TECS2_V1b)+...
    length(TECS2_V1c));
Avg_Air=(sum(Air_V1b)+sum(Air_V1c))/(length(Air_V1b)+length(Air_V1c));
fprintf('Overall Average Temperatures')
Overall_Avg=[Avg_Exh1; Avg_Exh2; Avg_Rad1; Avg_Rad2; Avg_Surf2;
                Avg_TECS2; Avg_Air]
%%%%%%%%%%%%%%%%%%%%%%%%%%%%%%%%%%%%%%%%%%%%%%%%%%%%%%%%%%%%%%%%%%%%%%%%%
%Compiling test data corresponding to measured current data
%Data in Power_Test is in 30sec intervals to correspond with current
%data which was recorded at 30sec sample time step
%Test V_1a:
ST_V1a=t_V1a(2)-t_V1a(1);                      %Sample time step
TS_V1a=30:30:(30*60);                          %30 min Sample time
TV_V1a=TS_V1a./ST_V1a+1;                        %Sample number
S_TEG_V1a=TEG_V1a(round(TV_V1a(1:end)));        %V for Sample number
S_Surf2_V1a=Surf2_V1a(round(TV_V1a(1:end)));    %Thot corresponding
S_TE_CS2_V1a=TE_CS2_V1a(round(TV_V1a(1:end)));  %Tcold corresponding
fprintf('Open Power_Test_ah in variable editor to see\n')
fprintf('Voltage of 1 modules; T_hot; T_cold for test V_1a\n')
Power_Test_aH=[S_TEG_V1a;S_Surf2_V1a;S_TE_CS2_V1a]';  %Data Vectors
%Test V_1b:
ST_V1b=t_V1b(2)-t_V1b(1);                      %Sample time step
TS_V1b=30:30:360;                              %30 min Sample time
TV_b=TS_V1b./ST_V1b+1;                          %Sample number
S_TEG_V1b=TEG_V1b(round(TV_b(1:end)));          %V for Sample number
S_Surf2_V1b=Surf2_V1b(round(TV_b(1:end)));      %Thot corresponding
S_TE_CS2_V1b=TECS2_V1b(round(TV_b(1:end)));     %Tcold corresponding
%Recorded Current Sample in mA
S_Amp_V1b=[449.6,446,441.2,438.1,436,434.3,432.6,435,433,435.2,...
    429.7,430.5].*(10^-3);
```

159

```matlab
fprintf('Data for 3.0 Ohm load \n')
fprintf('Current; Voltage; Thot; Tcold at max temp\n')
Power_Test_b=[S_Amp_V1b;S_TEG_V1b;S_Surf2_V1b;S_TE_CS2_V1b]
%Test V_1c:
ST_V1c=t_V1c(2)-t_V1c(1);                        %Sample time step
TS_V1c=30:30:300;                                %30 min Sample time
TV_V1c=TS_V1c./ST_V1c+1;                          %Sample number
S_TEG_V1c=TEG_V1c(round(TV_V1c(1:end)));         %V for Sample number
S_Surf2_V1c=Surf2_V1c(round(TV_V1c(1:end)));     %Thot corresponding
S_TE_CS2_V1c=TECS2_V1c(round(TV_V1c(1:end)));    %Tcold corresponding
%Recorded Current Sample in mA
S_Amp_V1c=[185,186,185.4,184.5,183.2,183.5,183,182,181.3,...
    180.7].*(10^-3);
fprintf('Data for 8.0 ohm load \n')
fprintf('Current; Voltage; Thot; Tcold at max temp\n')
Power_Test_c=[S_Amp_V1c;S_TEG_V1c;S_Surf2_V1c;S_TE_CS2_V1c]
%%%%%%%%%%%%%%%%%%%%%%%%%%%%%%%%%%%%%%%%%%%%%%%%%%%%%%%%%%%%%%%%%%%%%%%
%%%%%%%%%%%%%%%%%%%%%%%%%%%%%%%%%%%%%%%%%%%%%%%%%%%%%%%%%%%%%%%%%%%%%%%
%Plots for V_1b and V_1c
figure(5)
subplot(2,1,1)
plot(t_V1b,Surf2_V1b,t_V1b,TECS2_V1b,'LineWidth',2)
title('Hot and Cold side Temps test 1b: 1 module w/ Resistive Load')
xlabel('time (sec)')
ylabel('temp (C)')
subplot(2,1,2)
plot(t_V1c,Surf2_V1c,t_V1c,TECS2_V1c,'LineWidth',2)
title('Hot and Cold side Temps test 1c: 1 module w/ Resistive Load')
xlabel('time (sec)')
ylabel('temp (C)')
%%%%%%%%%%%%%%%
figure(6)
subplot(2,1,1)
plot(t_V1b,TEG_V1b,'LineWidth',2)
title('Voltage (Test 1b) 1 Module for 3Ohm load')%xlabel('time (sec)')
ylabel('Voltage (V)')
subplot(2,1,2)
plot(t_V1c,TEG_V1c,'LineWidth',2)
title('Voltage (Test 1c) 1 Module at 8Ohm load')
xlabel('time (sec)')
ylabel('Voltage (V)')
%%%%%%%%%%%%%%%
figure(7)
subplot(3,1,1)
plot(t_V1b,RPM_V1b,'-b',t_V1c,RPM_V1c,'-g')
axis([0,t_V1b(end),1500,1900])
title('Engine speed tests b and c Single Module')
legend('b','c')
subplot(3,1,2)
plot(t_V1b,throttle_V1b,'-b',t_V1c,throttle_V1c,'-g')
axis([0,t_V1b(end),0.4,1.1])
```

160

```
title('Engine throttle tests b and c Single Module')
legend('b','c')
%%%%%%%%%%%%%%%%%%%%%%%%%%%%%%%%%%%%%%%%%%%%%%%%%%%%%%%%%%%%%%%%%%%%%%%%%%%%
%Tabulate Engine Speed test b and c
RPM_V1b_t=tabulate(round(RPM_V1b));
RPM_V1c_t=tabulate(round(RPM_V1c));
%1st column of tabulate output is the value 2nd column is the count
RPM_V1b_val=RPM_V1b_t(:,1); RPM_V1b_cnt=RPM_V1b_t(:,2);
RPM_V1c_val=RPM_V1c_t(:,1); RPM_V1c_cnt=RPM_V1c_t(:,2);
%figure(2)
subplot(3,2,5)
plot(RPM_V1b_val(1600:end),RPM_V1b_cnt(1600:end),'LineWidth',2)
title('RPM 1b')
subplot(3,2,6)
plot(RPM_V1c_val(1600:2000),RPM_V1c_cnt(1600:2000),'LineWidth',2)
title('RPM test 1c')
```

RPM_Throttle_Chk.m: Code to check throttle and RPM of time samples within a larger data set. Only code for WOT is shown.

```
%Data 12/19/11 at 25, 50, 75, 100% of WOT at various engine speeds
%Engine revolutions noted by proximity sensor with RPM calculated in
%Simulink program used in conjunction with DAQ hardware
%See EXCEL file \TEG_Research\Parameter_System_and Test for test sample
%times for differnet loads
thrtl_100=load('C:\...\100_throttle_12_19.mat');
%%%%%%%%%%%%%%%%%%%%%%%%%%%%%%%%%%%%%%%%%%%%%%%%%%%%%%%%%%%%%%%%%%%%%%%%%%%%
%Data for 100% throttle
t_100=thrtl_100.throttle_12_19.X.Data;
RPM_100=thrtl_100.throttle_12_19.Y(9).Data;
Throttle_100=thrtl_100.throttle_12_19.Y(10).Data;
avg_thrtl_100=sum(Throttle_100)/length(Throttle_100)
ST_100=t_100(2)-t_100(1); %Sample Time
RPM_100_1=tabulate(round(RPM_100(1:fix(360/ST_100))));
RPM_100_2=tabulate(round(RPM_100(fix(384/ST_100)+1:fix(672/ST_100))));
RPM_100_3=tabulate(round(RPM_100(fix(696/ST_100)+1:fix(984/ST_100))));
RPM_100_4=tabulate(round(RPM_100(fix(1008/ST_100)+1:fix(1320/ST_100))))
RPM_100_5=tabulate(round(RPM_100(fix(1368/ST_100)+1:fix(1608/ST_100))))
RPM_100_val_1=RPM_100_1(:,1); RPM_100_cnt_1=RPM_100_1(:,2);
RPM_100_val_2=RPM_100_2(:,1); RPM_100_cnt_2=RPM_100_2(:,2);
RPM_100_val_3=RPM_100_3(:,1); RPM_100_cnt_3=RPM_100_3(:,2);
RPM_100_val_4=RPM_100_4(:,1); RPM_100_cnt_4=RPM_100_4(:,2);
RPM_100_val_5=RPM_100_5(:,1); RPM_100_cnt_5=RPM_100_5(:,2);
figure(5)
subplot(2,3,1)
plot(RPM_100_val_1(900:2500),RPM_100_cnt_1(900:2500),'LineWidth',2)
title('RPM at load 1 100% throttle')
subplot(2,3,2)
plot(RPM_100_val_2(900:1765),RPM_100_cnt_2(900:1765),'LineWidth',2)
title('RPM at load 2 100% throttle')
subplot(2,3,3)
plot(RPM_100_val_3(900:2000),RPM_100_cnt_3(900:2000),'LineWidth',2)
```

161

```
title('RPM at load 3 100% throttle')
subplot(2,3,4)
plot(RPM_100_val_4(900:2000),RPM_100_cnt_4(900:2000),'LineWidth',2)
title('RPM at load 4 100% throttle')
subplot(2,3,5)
plot(RPM_100_val_5(900:2000),RPM_100_cnt_5(900:2000),'LineWidth',2)
title('RPM at load 5 100% throttle')
```

Data_12_19_Temp_Data.m: Code to analyze system data for time samples of a larger data set. The larger data set was taken at different throttle positions with the time samples within each set taken at different engine speeds. Only code for WOT is shown. The data is presented in Table 3.3 in Appendix H.

```
%3600sec of data on 12/19/11 at 25, 50, 75, 100% of WOT at various RPMs
%Average temperaturs are calculated for the last (20-100)sec of
%sample time. Values determined from steady state in data plots.
%Corresponding data plots are given in Data_12_19_11_Temp_Plots.m
%See EXCEL file \TEG_Research\Parameter_System_and Test for parameters
%RPM data for different loads is given in Data_12_19_11_RPM_throttle.m
thrtl_100=load('C:\...\TEG_Test_Data\Engine
%%%%%%%%%%%%%%%%%%%%%%%%%%%%%%%%%%%%%%%%%%%%%%%%%%%%%%%%%%%%%%%%%%%%%%%%
%%%%%%%%%%%%%%%%%%%%%%%%%%%%%%%%%%%%%%%%%%%%%%%%%%%%%%%%%%%%%%%%%%%%%%%%
%Data for 100% throttle
t_100=thrtl_100.throttle_12_19.X.Data;
Ambient_100=thrtl_100.throttle_12_19.Y(2).Data;
Exh1_100=thrtl_100.throttle_12_19.Y(3).Data;
Exh2_100=thrtl_100.throttle_12_19.Y(4).Data;
RadIn_100=thrtl_100.throttle_12_19.Y(5).Data;
RadOut_100=thrtl_100.throttle_12_19.Y(6).Data;
Surf1_100=thrtl_100.throttle_12_19.Y(7).Data;
Surf2_100=thrtl_100.throttle_12_19.Y(8).Data;
ST_100=t_100(2)-t_100(1);    %Sample Step
%%%%%%%%%%%%%%%%%%%%%%%%%%%%%%%%%%%%%%%%%%%%%%%%%%%%%%%%%%%%%%%%%%%%%%%%
%Test 5.1: Load 1 at 100% WOT 0-360sec 1034 RPM
%Avg over 320-360sec
Ambient_100_1=Ambient_100(round(320/ST_100)+1:round(360/ST_100)+1);
Avg_Amb_100_1=sum(Ambient_100_1)/length(Ambient_100_1);
Exh1_100_1=Exh1_100(round(320/ST_100)+1:round(360/ST_100)+1);
Avg_Exh1_100_1=sum(Exh1_100_1)/length(Exh1_100_1);
Exh2_100_1=Exh2_100(round(320/ST_100)+1:round(360/ST_100)+1);
Avg_Exh2_100_1=sum(Exh2_100_1)/length(Exh2_100_1);
RadIn_100_1=RadIn_100(round(320/ST_100)+1:round(360/ST_100)+1);
Avg_RadIn_100_1=sum(RadIn_100_1)/length(RadIn_100_1);
RadOut_100_1=RadOut_100(round(320/ST_100)+1:round(360/ST_100)+1);
Avg_RadOut_100_1=sum(RadOut_100_1)/length(RadOut_100_1);
Surf1_100_1=Surf1_100(round(320/ST_100)+1:round(360/ST_100)+1);
Surf2_100_1=Surf2_100(round(320/ST_100)+1:round(360/ST_100)+1);
TH_100_1=sum((Surf1_100_1+Surf2_100_1)/2)/length(Surf2_100_1);
%%%%%%%%%%%%%%%%%%%%%%%%%%%%%%%%%%%%%%%%%%%%%%%%%%%%%%%%%%%%%%%%%%%%%%%%
%Test 5.2: Load 2 at 100% WOT 384-672sec 1277RPM
%Avg over 625-672sec
Ambient_100_2=Ambient_100(round(625/ST_100):round(672/ST_100)+1);
```

162

```
Avg_Amb_100_2=sum(Ambient_100_2)/length(Ambient_100_2);
Exh1_100_2=Exh1_100(round(625/ST_100):round(672/ST_100)+1);
Avg_Exh1_100_2=sum(Exh1_100_2)/length(Exh1_100_2);
Exh2_100_2=Exh2_100(round(625/ST_100):round(672/ST_100)+1);
Avg_Exh2_100_2=sum(Exh2_100_2)/length(Exh2_100_2);
RadIn_100_2=RadIn_100(round(625/ST_100):round(672/ST_100)+1);
Avg_RadIn_100_2=sum(RadIn_100_2)/length(RadIn_100_2);
RadOut_100_2=RadOut_100(round(625/ST_100):round(672/ST_100)+1);
Avg_RadOut_100_2=sum(RadOut_100_2)/length(RadOut_100_2);
Surf1_100_2=Surf1_100(round(625/ST_100):round(672/ST_100)+1);
Surf2_100_2=Surf2_100(round(625/ST_100):round(672/ST_100)+1);
TH_100_2=sum((Surf1_100_2+Surf2_100_2)/2)/length(Surf2_100_2);
%%%%%%%%%%%%%%%%%%%%%%%%%%%%%%%%%%%%%%%%%%%%%%%%%%%%%%%%%%%%%%%%%%%%
%Test 5.3: Load 3 at 100% WOT 696-984sec 1500 RPM
%Avg over 950-984sec
Ambient_100_3=Ambient_100(round(950/ST_100):round(984/ST_100)+1);
Avg_Amb_100_3=sum(Ambient_100_3)/length(Ambient_100_3);
Exh1_100_3=Exh1_100(round(950/ST_100):round(984/ST_100)+1);
Avg_Exh1_100_3=sum(Exh1_100_3)/length(Exh1_100_3);
Exh2_100_3=Exh2_100(round(950/ST_100):round(984/ST_100)+1);
Avg_Exh2_100_3=sum(Exh2_100_3)/length(Exh2_100_3);
RadIn_100_3=RadIn_100(round(950/ST_100):round(984/ST_100)+1);
Avg_RadIn_100_3=sum(RadIn_100_3)/length(RadIn_100_3);
RadOut_100_3=RadOut_100(round(950/ST_100):round(984/ST_100)+1);
Avg_RadOut_100_3=sum(RadOut_100_3)/length(RadOut_100_3);
Surf1_100_3=Surf1_100(round(950/ST_100):round(984/ST_100)+1);
Surf2_100_3=Surf2_100(round(950/ST_100):round(984/ST_100)+1);
TH_100_3=sum((Surf1_100_3+Surf1_100_3)/2)/length(Surf2_100_3);
%%%%%%%%%%%%%%%
fprintf('Ambient \n Exh_1 \n Exh_2 \n Rad_In \n Rad_Out \n T_H \n')
fprintf('Test 5.1;   Test 5.2;   Test 5.3;   \n')
Test_100_A=[Avg_Amb_100_1,   Avg_Amb_100_2,       Avg_Amb_100_3;
        Avg_Exh1_100_1,      Avg_Exh1_100_2,      Avg_Exh1_100_3;
        Avg_Exh2_100_1,      Avg_Exh2_100_2,      Avg_Exh2_100_3;
        Avg_RadIn_100_1,     Avg_RadIn_100_2,     Avg_RadIn_100_3;
        Avg_RadOut_100_1,    Avg_RadOut_100_2,    Avg_RadOut_100_3;
        TH_100_1,            TH_100_2,            TH_100_3]
%%%%%%%%%%%%%%%%%%%%%%%%%%%%%%%%%%%%%%%%%%%%%%%%%%%%%%%%%%%%%%%%%%%%%%%
%Test 5.4: Load 4 at 100% WOT 1008-1320sec 1765RPM
%Avg over 1290-1320sec
Ambient_100_4=Ambient_100(round((1008+CT)/ST_100):...
    round(1320/ST_100)+1);
Avg_Amb_100_4=sum(Ambient_100_4)/length(Ambient_100_4);
Exh1_100_4=Exh1_100(round((1008+CT)/ST_100):round(1320/ST_100)+1);
Avg_Exh1_100_4=sum(Exh1_100_4)/length(Exh1_100_4);
Exh2_100_4=Exh2_100(round((1008+CT)/ST_100):round(1320/ST_100)+1);
Avg_Exh2_100_4=sum(Exh2_100_4)/length(Exh2_100_4);
RadIn_100_4=RadIn_100(round((1008+CT)/ST_100):round(1320/ST_100)+1);
Avg_RadIn_100_4=sum(RadIn_100_4)/length(RadIn_100_4);
RadOut_100_4=RadOut_100(round((1008+CT)/ST_100):round(1320/ST_100)+1);
Avg_RadOut_100_4=sum(RadOut_100_4)/length(RadOut_100_4);
```

163

```matlab
Surf1_100_4=Surf1_100(round((1008+CT)/ST_100):round(1320/ST_100)+1);
Surf2_100_4=Surf2_100(round((1008+CT)/ST_100):round(1320/ST_100)+1);
TH_100_4=sum((Surf1_100_4+Surf2_100_4)/2)/length(Surf2_100_4);
%%%%%%%%%%%%%%%%%%%%%%%%%%%%%%%%%%%%%%%%%%%%%%%%%%%%%%%%%%%%%%%%%%%%%
%Test 5.5: Load 5 at 100% WOT 1368-1608sec 1906RPM
%Avg over 1575-1608sec
Ambient_100_5=Ambient_100(round(1575/ST_100):round(1608/ST_100)+1);
Avg_Amb_100_5=sum(Ambient_100_5)/length(Ambient_100_5);
Exh1_100_5=Exh1_100(round(1575/ST_100):round(1608/ST_100)+1);
Avg_Exh1_100_5=sum(Exh1_100_5)/length(Exh1_100_5);
Exh2_100_5=Exh2_100(round(1575/ST_100):round(1608/ST_100)+1);
Avg_Exh2_100_5=sum(Exh2_100_5)/length(Exh2_100_5);
RadIn_100_5=RadIn_100(round(1575/ST_100):round(1608/ST_100)+1);
Avg_RadIn_100_5=sum(RadIn_100_5)/length(RadIn_100_5);
RadOut_100_5=RadOut_100(round(1575/ST_100):round(1608/ST_100)+1);
Avg_RadOut_100_5=sum(RadOut_100_5)/length(RadOut_100_5);
Surf1_100_5=Surf1_100(round(1575/ST_100):round(1608/ST_100)+1);
Surf2_100_5=Surf2_100(round(1575/ST_100):round(1608/ST_100)+1);
TH_100_5=sum((Surf1_100_5+Surf2_100_5)/2)/length(Surf2_100_5);
%%%%%%%%%%%%%%%
fprintf('Test 5.4;   Test 5.5;    \n')
Test_100_B=[Avg_Amb_100_4,  Avg_Amb_100_5;
        Avg_Exh1_100_4,    Avg_Exh1_100_5;
        Avg_Exh2_100_4,    Avg_Exh2_100_5;
        Avg_RadIn_100_4,    Avg_RadIn_100_5;
        Avg_RadOut_100_4,  Avg_RadOut_100_5;
        TH_100_4,          TH_100_5]
```

Code for Numerical Calculations on Thermoelectric Power Generation
Single_Module_Calcs.m:

```matlab
%Power calculations for a single TE module from experimental data
%Check possible TE efficiency and K_M values
%%%%%%%%%%%%%%%%%%%%%%%%%%%%%%%%%%%%%%%%%%%%%%%%%%%%%%%%%%%%%%%%%%%%%
I_S=0:0.01:1.6;          %Projected Current
V_S=-1.5749*I_S+1.7493;  %Calculated Voltage function
P_S=I_S.*V_S;            %Calculated Power
Max_Power_S=max(P_S)     %Calcualted Maximum Power
%Data Points
I_S_Points=[0.183,0.437,0];
V_S_Points=[1.402,1.086,1.783];
P_S_Points=[0.2573,0.474,0];
%Calculations for TE efficiency
Th=135.3;
Tc=63.1;
DT=Th-Tc;
R_m=0.774;              %Module resistanc, Ohm
K_m=0.135;              %Increasing K_m increased Eta
n_alpha=0.0247;
q_h=DT.*K_m+n_alpha*Th.*I_S-0.5.*I_S.^2*R_m;
```

164

```
Eta=P_S./q_h;
%%%%%%%%%%%%%%%%%%%%%%%%%%%%%%%%%%%%%%%%%%%%%%%%%%%%%%%%%%%%%%%%%%%%%
figure(1)
figure1=figure(1);
xtick_S=0:0.1:1.1;
xlim_S=[0 1.12];
ytick_SV=0:0.2:1.8;
ylim_S=[0 1.8];
axes1 = axes('Parent',figure1,...
    'YTick',ytick_SV,...
    'YMinorTick','on',...
    'XTick',xtick_S,...
    'XMinorTick','on',...
    'FontSize',14);
xlim(axes1,xlim_S);
ylim(axes1,ylim_S);
box(axes1,'on');
grid(axes1,'on');
hold(axes1,'all');
plot1 = plot(I_S,Eta,I_S_Points,V_S_Points,'*k',I_S_Points,P_S_Points,
'*k',I_S,V_S,':g',I_S,P_S,'-.b','Parent', axes1,'LineWidth',2.6);
ylabel('Voltage (...)(V),   Power (-.-)(W)','FontSize',20,
'FontName','Times');
xlabel('Current (A)','FontSize',20,'FontName','Times');
```

Series_Module_Calcs.m:

```
%Calculations for 4 Modules Connected in Series
%Determining voltage and power curve fits from experimental data
%%%%%%%%%%%%%%%%%%%%%%%%%%%%%%%%%%%%%%%%%%%%%%%%%%%%%%%%%%%%%%%%%%%%%
%Data Points
I_4S_Points=[0.6045,0.4939,0.3862,0.2542,0.1196,0.0603,0.05018,0];
V_4S_Points=[4.642,5.294,5.840,6.492,7.145,7.494,7.543,7.8];
P_4S_Points=I_4S_Points.*V_4S_Points;
%Best Fit Calculations
I_4S=0:0.01:2;                   %Projected Current
V_4SF=polyfit(I_4S_Points,V_4S_Points,1); %I vs. V fit
V_4S=V_4SF(1).*I_4S+V_4SF(2);
P_4SF=polyfit(I_4S_Points,P_4S_Points,2); %I vs. P fit
P_4S=P_4SF(1).*I_4S.^2+P_4SF(2).*I_4S+P_4SF(3);
Max_Power_S=max(P_4S)            %Calcualted Maximum Power
%Calculations for efficiency
K_M=0.14; %Thermal Conductance, W/K
q_h=Km*DT+n_alpha*Th*Imax-0.5*Imax^2*Rm;
eta=Pmax/q_h;
%%%%%%%%%%%%%%%%%%%%%%%%%%%%%%%%%%%%%%%%%%%%%%%%%%%%%%%%%%%%%%%%%%%%%
figure(1)
figure1=figure(1);
xtick_4S=0:.2:1.6;
xlim_4S=[0 1.52];
ytick_4S=0:1:8;
ylim_4S=[0 8];
```

```matlab
axes1 = axes('Parent',figure1,...
    'YTick',ytick_4S,...
    'YMinorTick','on',...
    'XTick',xtick_4S,...
    'XMinorTick','on',...
    'FontSize',14);
xlim(axes1,xlim_4S);
ylim(axes1,ylim_4S);
box(axes1,'on');
grid(axes1,'on');
hold(axes1,'all');
plot1 = plot(I_4S_Points,V_4S_Points,'*k',I_4S,V_4S,':b',I_4S_Points,
P_4S_Points,'*k',I_4S,P_4S,'-.m','Parent',axes1,'LineWidth',2.7);
ylabel('Voltage (...)(V),Power (-.-)(W)', 'FontSize',20, 'FontName',
'Times');
xlabel('Current (A)','FontSize',20,'FontName','Times');
```

Theoretical_Calcs.m:

```matlab
%Calculations of Power, Current, Voltage of a single module
%1st and 2nd Calculations based on manufacture's Data
%3rd Calculation uses experimental data
%%%%%%%%%%%%%%%%%%%%%%%%%%%%%%%%%%%%%%%%%%%%%%%%%%%%%%%%%%%%%%%%%%%%%%%%
Th=[125,135,135];          %Hot Side Temp, C
Tc=[50,50,63];             %Cold Side Temp, C
DT=Th-Tc;                  %Delta T, C
V_o=[3.5,4.0,1.8];         %Open Ciruit Voltage, V
R_M=[1.077,1.07,0.774];    %Module Resistance at Temp
R_L=0:0.1:3000;            %Range of Load resistances
fprintf('1st and 2nd Calculations based on manufacture data \n')
fprintf('3rd Calculation used experimental data\n')
n_alpha=V_o./DT;           %Seebeck Coeff, V/C
I_1=V_o(1)./(R_M(:,1)+R_L); %Calculated Current
I_2=V_o(2)./(R_M(:,2)+R_L);
I_3=V_o(3)./(R_M(:,3)+R_L);
P_1=I_1.^2.*R_L;           %Calculated Power
P_2=I_2.^2.*R_L;
P_3=I_3.^2.*R_L;
V_1=I_1.*R_L;              %Calculated Voltage
V_2=I_2.*R_L;
V_3=I_3.*R_L;
Max_Current=[max(I_1),max(I_2),max(I_3)]
Max_Power=[max(P_1),max(P_2),max(P_3)]
%%%%%%%%%%%%%%%%%%%%%%%%%%%%%%%%%%%%%%%%%%%%%%%%%%%%%%%%%%%%%%%%%%%%%%%%%%%
figure(1)
figure1=figure(1);
% Create axes
xtick_S=0:0.5:4;
xlim_S=[0 3.8];
ytick_SV=0:0.5:4;
ylim_S=[0 4];
axes1 = axes('Parent',figure1,...
```

166

```
    'YTick',ytick_SV,...
    'YMinorTick','on',...
    'XTick',xtick_S,...
    'XMinorTick','on',...
    'FontSize',14);
xlim(axes1,xlim_S);            %x limit of axes
ylim(axes1,ylim_S);            %y limit of axes
box(axes1,'on');
grid(axes1,'on');
hold(axes1,'all');
plot1 = plot(I_1,P_1,'-.r',I_1,V_1,'-r',I_2,P_2,'-.k',I_2,V_2,'-k',...
    I_3,P_3,'-.b',I_3,V_3,'-b','Parent',axes1,'LineWidth',2.6);
ylabel('Voltage (----)(V),   Power ($-\cdot-$)(W)','FontSize',20,...
    'FontName','Times','interpreter','latex','FontWeight','b');
xlabel('Current (A)','FontSize',20,'FontName','Times',...
    'interpreter','latex','FontWeight','b');
text(1.8,3.88,'(1)','FontSize',16,'FontName','Times')
text(1.55,2.97,'(2)','FontSize',16,'FontName','Times')
text(1.1,1.19,'(3)','FontSize',16,'FontName','Times')
text(0.2,3.87,'(1)','FontSize',16,'FontName','Times')
text(0.2,3.36,'(2)','FontSize',16,'FontName','Times')
text(0.2,1.75,'(3)','FontSize',16,'FontName','Times')
%%%%%%%%%%%%%%%%%%%%%%%%%%%%%%%%%%%%%%%%%%%%%%%%%%%%%%%%%%%%%%%%%%%%%%%%%%%
%%%%%%%%%%%%%%%%%%%%%%%%%%%%%%%%%%%%%%%%%%%%%%%%%%%%%%%%%%%%%%%%%%%%%%%%%%%
%Calculations for 4 Modules connected in series
%Based on Manufacturer data for similar temps (1st temp data above)
R_M4S=R_M(1)*4;           %Approx resistance
n_alpha_4S=n_alpha(1)*4;  %Approx alpha
V_o4S=n_alpha_4S*DT(1);   %Estimated open ciruit voltage
I_4S=V_o4S./(R_M4S+R_L);  %Estimated current
P_4S=I_4S.^2.*R_L;        %Esitmated Power
V_4S=P_4S./I_4S;          %Estimated Power
fprintf('Estimated Values for 4 Modules in Series\n')
fprintf('R, alpha, V_open, I_max, P_max\n')
values_4S=[R_M4S,n_alpha_4S,V_o4S,max(I_4S),max(P_4S)]
%Calculations based on Experimental Values of 1 modules
R_M4SE=R_M(3)*4;            %Approx resistance
n_alpha_4SE=n_alpha(3)*4;   %Approx alpha
V_o4SE=n_alpha_4SE*DT(3);   %Estimated open ciruit voltage
I_4SE=V_o4SE./(R_M4SE+R_L); %Estimated current
P_4SE=I_4SE.^2.*R_L;        %Esitmated Power
V_4SE=P_4SE./I_4SE;         %Estimated Power
fprintf('Estimated Values for 4 Modules in Series\n')
fprintf('R, alpha, V_open, I_max, P_max\n')
values_4S=[R_M4SE,n_alpha_4SE,V_o4SE,max(I_4SE),max(P_4SE)]
%%%%%%%%%%%%%%%%%%%%%%%%%%%%%%%%%%%%%%%%%%%%%%%%%%%%%%%%%%%%%%%%%%%%%%%%
figure(2)
figure2=figure(2);
% Create axes
xtick_4=0:0.5:7;
xlim_4=[0 3.3];
```

```
ytick_4=0:1.0:16;
ylim_4=[0 14.1];
axes2 = axes('Parent',figure2,...
    'YTick',ytick_4,...
    'YMinorTick','on',...
    'XTick',xtick_4,...
    'XMinorTick','on',...
    'FontSize',14);
xlim(axes2,xlim_4);
ylim(axes2,ylim_4);
box(axes2,'on');
grid(axes2,'on');
hold(axes2,'all');
% Create plot
plot2 = plot(I_4S,P_4S,'-.b',I_4S,V_4S,'-b',I_4SE,P_4SE,'-.r',...
    I_4SE,V_4SE,'-r','Parent',axes2,'LineWidth',2.7);
ylabel('Voltage (----)(V),   Power ($-\cdot-$)(W)','FontSize',20,...
    'FontName','Times','interpreter','latex','FontWeight','b');
xlabel('Current (A)','FontSize',20,'FontName','Times',...
    'interpreter','latex','FontWeight','b');
text(1.55,11.9,'(1)','FontSize',16,'FontName','Times')
text(1.1,4.7,'(2)','FontSize',16,'FontName','Times')
text(0.2,13.5,'(1)','FontSize',16,'FontName','Times')
text(0.2,7,'(2)','FontSize',16,'FontName','Time
```

Appendix G

TEG AutoCAD Drawings

The AutoCAD drawings for the TEG exhaust system are shown below. The part consisted of four pieces with steel exhaust pipes welded to the top and bottom pieces to connect to the engine and the exhaust vent. Permatex Ultra Copper high temperature RTV silicone with a maximum temperature rating of 371°C was applied to the part joints before fastening the pieces together. Units are in inches.
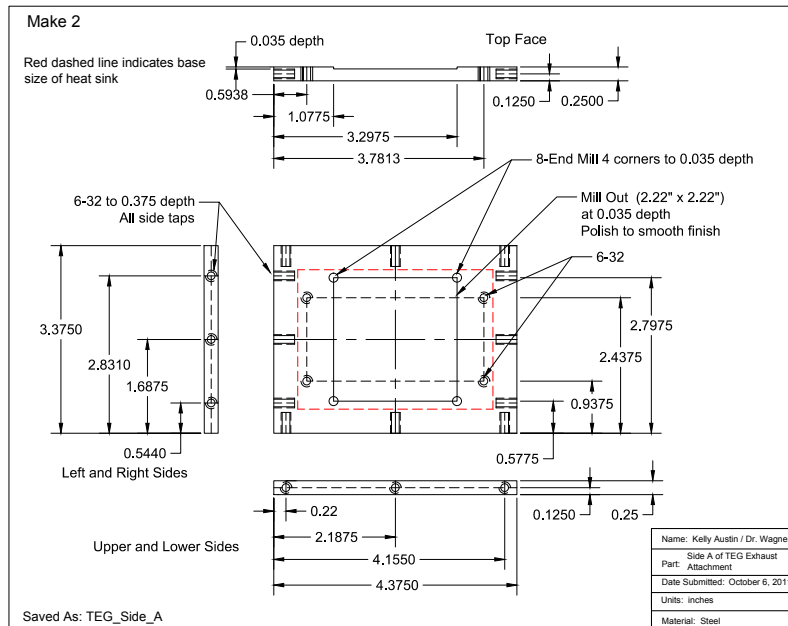

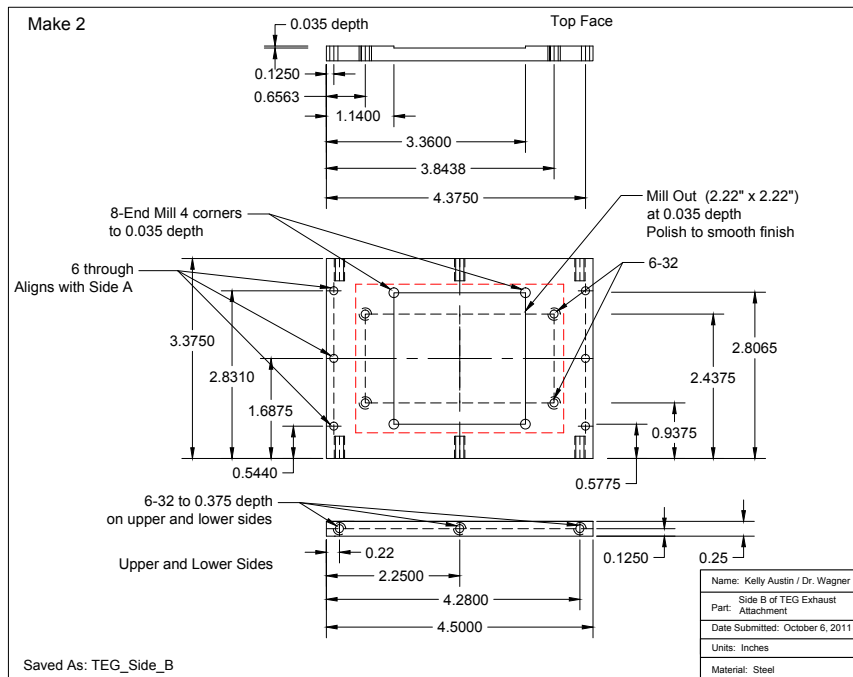Figure G.1: Thermoelectric exhaust system Side A

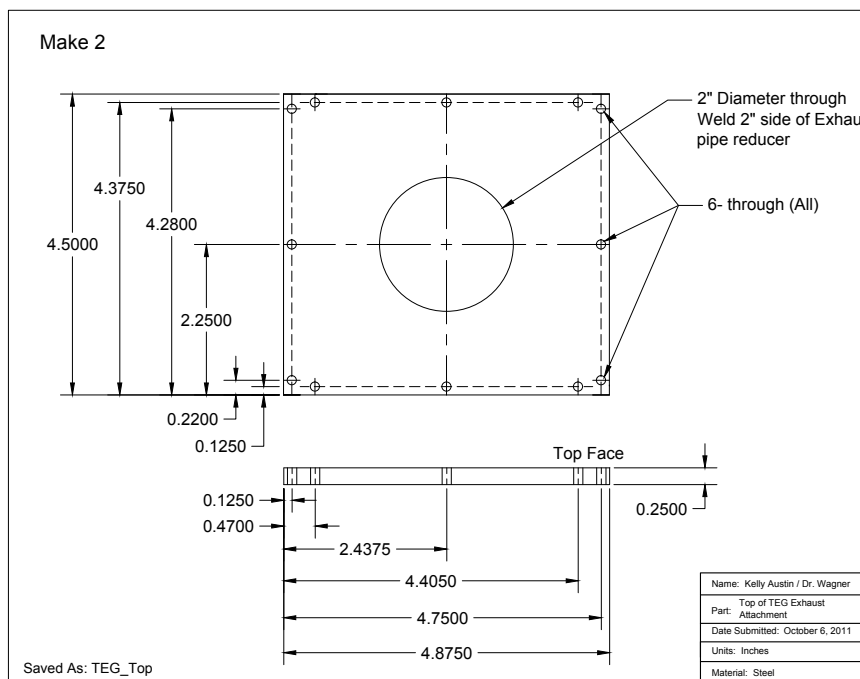169

Figure G.2: Thermoelectric exhaust system Side B

Figure G.3: Top and bottom of thermoelectric exhaust system which weld to steel exhaust pipes

Appendix H

TEG Additional Material

The temperatures of the exhaust T_{E_1} and T_{E_2} and the hot engine coolant T_{R_1} for wide open throttle (WOT) and 75% WOT are shown in Fig. H.1 and Fig. H.2, respectively. The difference in the temperature profiles is due to the mode of engine warm up. The initial engine speed was low and then increased in Fig. H.1; whereas the engine was run from a higher to a lower speed in Fig. H.2. The engine speed tabulated over a time sample is shown in Fig. H.3(a) and the calibration curves used in Fig. E.3 are shown in Fig. H.3(b).
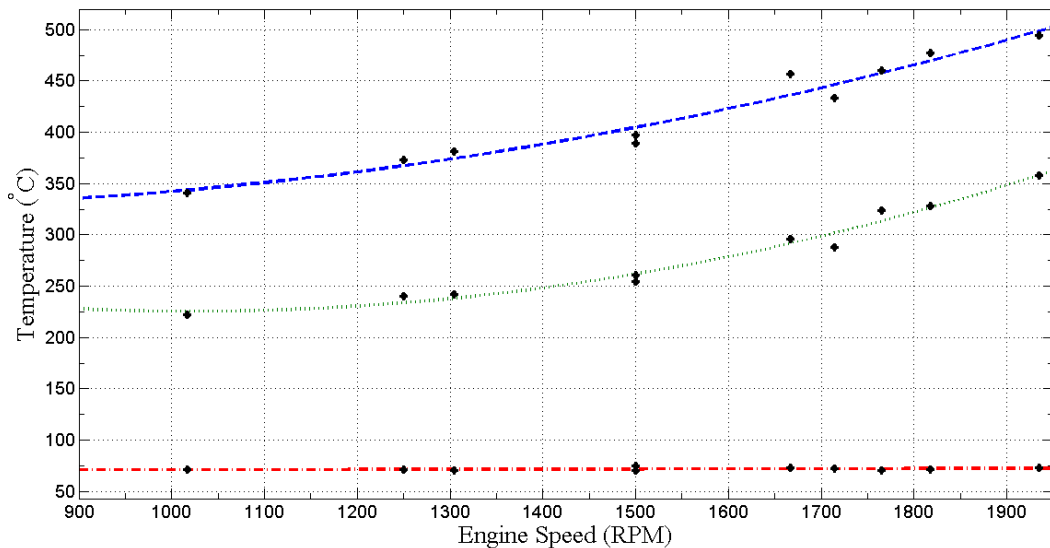

Figure H.1: Temperatures T_{E_1} (- - -), T_{E_2} ($\cdots$), and T_{R_1} ($- \cdot -$) for WOT over a range of RPM
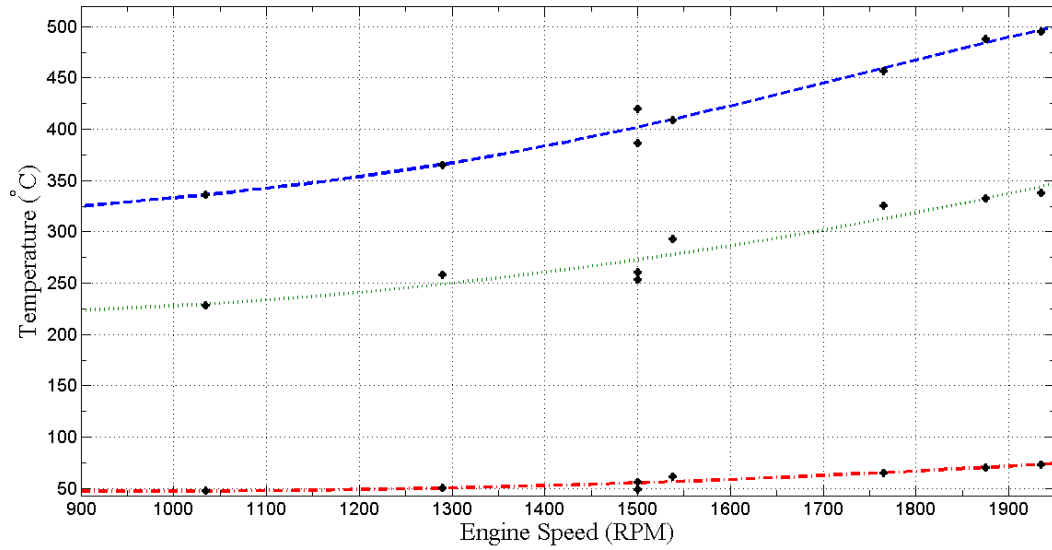
Figure H.2: Temperatures T_{E_1} (- - -), T_{E_2} ($\cdots$), and T_{R_1} ($- \cdot -$) for 75% of WOT over a range of RPM
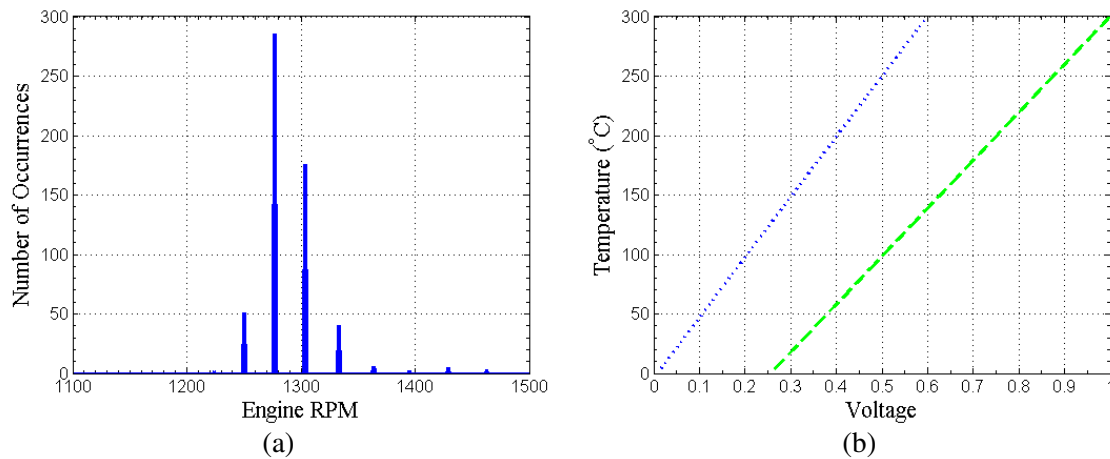

(a)   (b)

Figure H.3: (a) Example of tabulated RPM data from a time sample shows an RPM of 1277 and (b) calibration curves for J-type (- - -) and K-type ($\cdots$) thermocouples

172

Bibliography

[1] Colorado State University, http://mechatronics.colostate.edu/definitions.html, accessed 1/09/2012.

[2] A. S. Brown, "Who owns mechatronics," *Mechanical Engineering Magazine*, vol. 130, no. 6, pp. 24–29, June 2008.

[3] D. Bradley, "Mechatronics more questions than answers," *Mechatronics*, vol. 20, no. 8, pp. 827–841, 2010.

[4] A. M. Mazid, "Philosophy of mechatronics course development," in *IEEE International Conference Industrial Technology*, vol. 2, Bankok, Thailand, Dec. 2002, pp. 1337–1341.

[5] M. K. Habib, "Human adaptive and friendly mechatronics (HAFM)," in *Mechatronics and Automation, 2008. ICMA 2008. IEEE International Conference*, Takamatsu, Japan, Aug. 2008, pp. 61–65.

[6] M. K. Habib, "Mechatronics engineering the evolution, the needs and the challenges," in *IEEE Industrial Electronics–32nd Annual Conference*, Paris, France, Nov. 2006, pp. 4510–4515.

[7] W. Bolton, *Mechatronics: a multidisciplinary approach*, 4th ed. New Jersey: Prentice Hall, Inc., 2008.

[8] C. Stockmans-Daou, A. Cruz-Martin, and J. Fernandez-Madrigal, "A heterogeneity-enabled development system for educational mechatronics," in *Mechatronics, 2009. ICM 2009. IEEE International Conference*, Malaga, Spain, April 2009, pp. 1–6.

[9] R. Rabb, J. Rogers, and D. Chang, "Course development in interdisciplinary controls and mechatronics," in *Frontiers in Education Conference, 2008. FIE 2008. 38th Annual*, Saratoga Springs, NY, Oct. 2008, pp. T3F–11–T3F–15.

[10] M. Kutz, *Mechanical Engineers' Handbook: Instrumentation, Systems, Controls, and MEMS*, 3rd ed. New Jersey: John Wiley & Sons, 2006.

[11] M. Lindner and T. Tille, "Design of highly integrated mechatronic gear selector levers for automotive shift-by-wire systems," *IEEE/ASME Transactions on Mechatronics*, vol. 15, no. 6, pp. 961–968, 2010.

[12] K. Sakurama, S. Hara, and K. Nagano, "Swing–up and stabilization control of a cart-pendulum system via energy control and controlled lagrangian methods," *Electrical Engineering in Japan*, vol. 160, no. 4, pp. 24–31, 2007.

[13] H. Yu, Y. Liu, and T. Yang, "Closed-loop tracking control of a pendulum-driven cart-pole underactuated system," in *Proceedings of the Institution of Mechanical Engineers, Part I: Journal of Systems and Control Engineering*, vol. 222, no. 2, March 2008, pp. 109–125.

[14] E. Matta and A. De Stefano, "Seismic performance of pendulum and translational roof-garden TMDs," *Mechanical Systems and Signal Processing*, vol. 23, no. 3, pp. 908–921, 2009.

[15] N. Abe, "Passive and active switching vibration control with pendulum type damper," in *Proceedings of 2004 IEEE Conference on Control Applications*, vol. 2, Taipei, Taiwan, 2004, pp. 1037–1042.

[16] Y. Song, H. Sato, Y. Iwata, and T. Komatsuzaki, "The response of a dynamic vibration absorber system with a parametrically excited pendulum," *Journal of Sound and Vibration*, vol. 259, no. 4, pp. 747–759, 2003.

[17] W. J. Palm III, *System Dynamics*. New York: McGraw-Hill, 2005.

[18] D. T. Greenwood, *Principles of Dynamics*. New Jersey: Prentice Hall, 1988.

[19] J. H. Williams, Jr., *Fundamentals of Applied Dynamics*. New York: John Wiley and Sons, 1996.

[20] G. Rizzoni, *Principles and Applications of Electrical Engineering*, 5th ed. New York: McGraw-Hill, 2007.

[21] D. G. Fink and H. W. Beaty, *Standard Handbook for Electrical Engineers*, 13th ed. New York: McGraw-Hill, 1993.

[22] D. G. Zill and M. R. Cullen, *Advanced Engineering Mathematics*, 2nd ed. Boston: Jones and Bartlett Publishers, 2000.

[23] R. H. Cannon, Jr., *Dynamics of Physical Systems*. New York: McGraw-Hill, 1967.

[24] Omega Engineering, Inc., http://www.omega.com/Pressure/pdf/LCL.pdf, accessed 8/1/2011.

[25] P. A. Tipler and G. Mosca, *Physics for Scientists and Engineers*, 5th ed. New York: W.H. Freeman and Company, 2004.

[26] L. Meirovitch, *Elements of Vibration Analysis*. New York: McGraw-Hill, 1975.

[27] R. D. Abelson, "Space missions and applications," in *Thermoelectrics Handbook: Macro to Nano*, D. M. Rowe, Ed. CRC Press, 2006, pp. 56.1–56.29.

[28] A. V. Dmitriev and I. P. Zvyagin, "Current trends in the physics of thermoelectric materials," *Physics–Uspekhi Fizicheskikh Nauk, Russian Academy of Sciences*, vol. 53, no. 8, pp. 789–803, 2010.

[29] H. J. Goldsmid, "A new upper limit to the thermoelectric figure of merit," in *Thermoelectrics Handbook: Macro to Nano*, D. M. Rowe, Ed. CRC Press, 2006, pp. 10.1–10.10.

[30] Ø. Prytz, A. E. Gunnæs, O. B. Karlsen, T. H. Breivik, E. S. Toberer, G. Jeffrey Snyder, and J. Taftø, "Nanoscale inclusions in the phonon glass thermoelectric material Zn_4Sb_3," *Philosophical Magazine Letters*, vol. 89, no. 6, pp. 362–369, 2009.

[31] M. C. Robert and R. Saravanan, "Triple phase structure and electron density analysis of the thermoelectric material $Bi_{80}Sb_{20}$," *Powder Technology*, vol. 197, no. 3, pp. 159–164, 2010.

[32] S. K. Bux, R. G. Blair, P. K. Gogna, H. Lee, G. Chen, M. S. Dresselhaus, R. B. Kaner, and J. Fleurial, "Nanostructured bulk silicon as an effective thermoelectric material," *Advanced Functional Materials*, vol. 19, no. 15, pp. 2445–2452, 2009.

[33] A. Zevalkink, E. S. Toberer, W. G. Zeier, E. Flage-Larsen, and G. J. Snyder, "Ca_3AlSb_3: an inexpensive, non-toxic thermoelectric material for waste heat recovery," *Energy And Environmental Science*, vol. 4, no. 2, pp. 510–518, 2011.

[34] M. S. El-Genk and H. H. Saber, "A modeling and optimization of segmented thermoelectric generators for terrestrial and space applications," in *Thermoelectrics Handbook: Macro to Nano*, D. M. Rowe, Ed.   CRC Press, 2006, pp. 43.1–43.13.

[35] T. Huesgen, P. Woias, and N. Kockmann, "Design and fabrication of MEMS thermoelectric generators with high temperature efficiency," *Sensors and Actuators A: Physical*, vol. 145,146, pp. 423–429, 2008.

[36] M. Mikami, K. Kobayashi, T. Kawada, K. Kubo, and N. Uchiyama, "Development and evaluation of high-strength Fe_2VAl thermoelectric module," *Japanese Journal of Applied Physics*, vol. 47, no. 3, pp. 1512–1516, 2008.

[37] G. Min and D. M. Rowe, "Ring–structured thermoelectric module," *Semiconductor Science and Technology*, vol. 22, no. 8, pp. 880–883, 2007.

[38] Z. Wang, V. Leonov, P. Fiorini, and C. V. Hoof, "Realization of a wearable miniaturized thermoelectric generator for human body applications," *Sensors and Actuators A: Physical*, vol. 156, no. 1, pp. 95–102, 2009.

[39] L. Headings, V. Marano, C. Jaworski, Y. Guezennec, G. Washington, J. Heremans, and G. Rizzoni, "Opportunities for thermoelectric energy conversion in hybrid vehicles," in *Proceedings of 2006 ASME International Mechanical Engineering Congress and Exposition*, Chicago, IL, Nov. 2006, pp. 405–414.

[40] Y. Hsiao, W. Chang, and S. Chen, "A mathematic model of thermoelectric module with applications on waste heat recovery from automobile engine," *Energy*, vol. 35, no. 3, pp. 1447–1454, 2010.

[41] J. LaGrandeur, D. Crane, S. Hung, B. Mazar, and A. Eder, "Automotive waste heat conversion to electric power using skutterudite, TAGS, PbTe and BiTe," in *25th International Conference on Thermoelectrics*, Vienna, Austria, Aug 2006, pp. 343–348.

[42] M. Mori, T. Yamagami, N. Oda, M. Hattori, M. Sorazawa, and T. Haraguchi, "Current possibilities of thermoelectric technology relative to fuel economy," in *Proceedings of SAE World Congress*, Detroit, MI, April 2009.

[43] K. Smith and M. Thornton, "Feasibility of thermoelectrics for waste heat recovery in conventional vehicles,"
http://www.nrel.gov/docs/fy09osti/44247.pdf, 2009.

[44] S. W. Angrist, *Direct Energy Conversion*, 3rd ed.   Boston: Allyn and Bacon, 1976.

[45] B. D. Wood, *Applications of Thermodynamics*, 2nd ed.   Boston: Addison-Wesley, 1982.

175

[46] B. D. Hsu, *Practical Diesel-Engine Combustion Analysis*. Pennsylvania: Society of Automotive Engineers, Inc., 2002.

[47] D. E. Foster, "An overview of zero-dimensional thermodynamic models for IC engine data analysis," in *Proceedings of International Fuels and Lubricants Meeting and Exposition*, Tulsa, OK, Oct. 1985.

[48] G. L. Borman and K. W. Ragland, *Combustion Engineering*. Boston: WCB/McGraw Hill, 1998.

[49] Tellurex Corp., "G2-56-0375 thermoelectric module specifications," http://www.tellurex.com/pdf/G2-56-0375-Specifications.pdf, 2010.

176